Università degli Studi di Parma

Ph.D. in
Science and Technology of Innovative Materials

Cavitand receptors for environmental monitoring

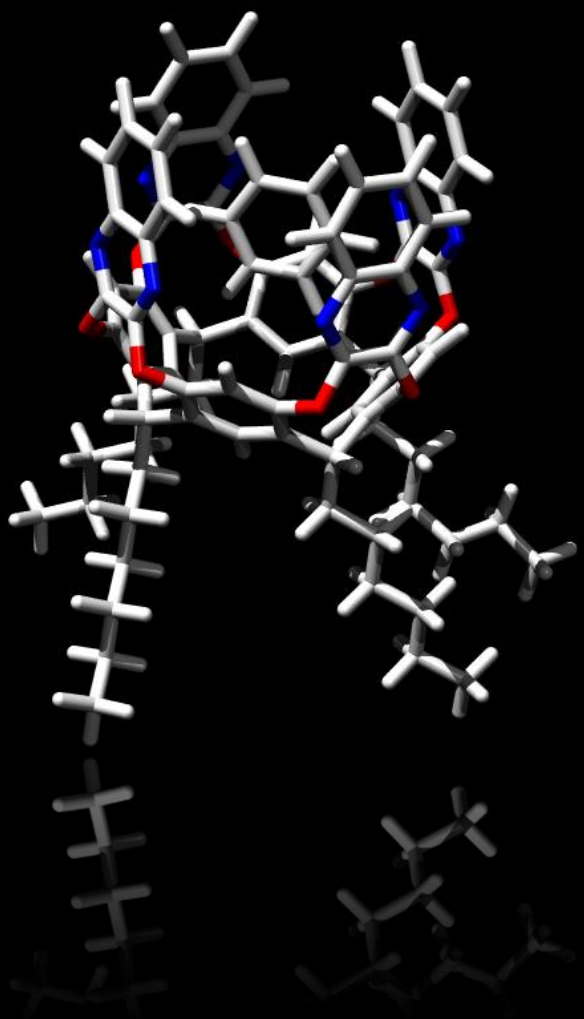

Betti Paolo

This Ph.D. thesis is dedicated to my family, who always supported me in my academic undertakings.

Dipartimento di Chimica Organica ed Industriale

Università degli Studi di Parma

Cavitand receptors for environmental monitoring

Paolo Betti

Ph.D. in Science and Technology of Innovative Materials

XX° Cycle (2005-2007)

Coordinator: prof. Manfredo Manfredi

Supervisor: prof. Enrico Dalcanale

Author: Paolo Betti

“Copy from one, it’s plagiarism; copy form two, it’s research.”

Wilson Mizner, 1876-1933.

Contents

CHAPTER 1

CAVITAND BASED SUPRAMOLECULAR SENSORS

1.1 Introduction..... 1
1.1.1 Overview of the transducers used in supramolecular gas sensing..... 2
1.1.2 Cavitand as molecular receptors..... 5
1.1.3 Issues related to vapor sensing with molecular receptors..... 9
1.1.4 Location of the adsorbed analytes in the receptor layers..... 11
1.1.5 Rational design of supramolecular receptors for vapour sensing: The cavitand case..... 13
1.1.6 SPR supramolecular sensors..... 17
1.1.7 Differential versus specific binding in sensor arrays..... 20
1.2 Conclusions and Outlook..... 20
1.3 References and Notes..... 22

CHAPTER 2

A SUPRAMOLECULAR APPROACH TO SUB-PPB AROMATIC VOCS DETECTION IN AIR

2.1 Introduction..... 25
2.2 Results and discussion..... 28
2.2.1 Molecular receptor..... 29
2.2.2 Specific vs unspecific interaction..... 36
2.2.3 Fluidodynamic of the trap..... 39
2.2.4 Kinetics of adsorption and desorption..... 41
2.2.5 Miniaturization of the system..... 44
2.2.6 Prototype testing..... 48

2.2.7 Real world measurements..... 50
2.2.8 Deeper and more rigid cavities..... 52
2.2.9 OaCav measurements..... 55
2.3 Conclusions..... 59
2.4 Acknowledgements..... 60
2.5 Experimental section..... 61
2.6 References and Notes..... 66

CHAPTER 3

CAVITAND BASED SOL-GEL COATINGS FOR SOLID PHASE MICROEXTRACTION

3.1 Introduction..... 67
3.2 Results and discussion..... 73
3.2.1 Molecular receptor..... 73
3.2.2 The sol-gel..... 77
3.2.2.1 QxCav sol gel with plasticizer..... 77
3.2.2.2 QxCav sol-gel..... 83
3.2.3 Fiber characterization..... 90
3.2.4 Study of the extraction capabilities of fibers with plasticizer..... 92
3.2.5 Performances of fibers without plasticizer..... 96
3.2.6 Extraction capabilities towards other aromatic compounds..... 97
3.3 Conclusions..... 99
3.4 Experimental section..... 100
3.5 References and notes..... 106

CHAPTER 4

SUPRAMOLECULAR FLUORESCENT SENSORS

4.1 Introduction..... 109
4.2 Results and discussion..... 115
4.2.1 The fluorescent receptor..... 115
4.2.2 Synthesis of the fluorescent bridging group **7**..... 116
4.2.3 Synthesis of fluorescent cavitand **8**..... 119
4.2.4 Solution testing of **8**..... 120
4.2.5 Design of a new florescent receptor..... 122
4.2.6 Solution measurements of **14-in**..... 127
4.2.7 Gas-solid interface apparatus..... 130
4.2.8 Sensor measurements..... 133
4.2.9 Synthesis of cavitand **18-in**..... 139
4.2.10 Solution measurement of **18-in**..... 142
4.3 Conclusions..... 144
4.4 Acknowledgements..... 144
4.5 Experimental section..... 145
4.6 References and notes..... 161

CHAPTER 5

HOST-GUEST COMPLEXATION ON SI(100) SURFACE

5.1 Introduction..... 163
5.2 Results and discussion..... 165
5.2.1 Molecular receptors..... 165
5.2.2 Grafting on silicon..... 167
5.2.3 XPS evidence of complexation of QxCav@Trifluorotoluene..... 171
5.2.4 Preliminary XPS study of complexation of AcCav@DMMP..... 172
5.3 Conclusions..... 173
5.4 Experimental section..... 174
5.5 References and notes..... 176

CHAPTER 6

SYNTHESIS OF PARTIALLY-BRIDGED PHOSPHONATE AND THIOPHOSPHONATE RESORCINARENES

6.1 Introduction..... 177
6.2 Results and discussion..... 179
6.2.1 Synthesis of resorcinarenes bearing two and three P=X (X=S,O) bridges at the upper rim..... 179
6.2.2 X-ray crystallographic investigation..... 182
6.3 Conclusions..... 184
6.4 Acknowledgments..... 184
6.5 Experimental section..... 185
6.6 References and notes..... 189

CHAPTER 7

CRYSTALLOGRAPHIC DESCRIPTION OF SOLVENT INCLUSION IN CAVITANDS VIA CH-π INTERACTIONS

7.1 Introduction..... 191
7.2 Results and discussion..... 192
7.2.1 Crystal structure of compounds **1** and **2**..... 192
7.3 Conclusions..... 194
7.4 Acknowledgments..... 194
7.5 Experimental Section..... 195
7.6 References and notes..... 198

Cavitand based supramolecular sensors

1

1.1 Introduction

Nature has provided many examples of exquisitely specific binding interactions like enzyme-substrate, antigen-antibody and complementary DNA annealing. To achieve this specificity, biological systems exploit molecular recognition between two species that complement one another in size, shape and functionality. In the last three decades these so called “lock and key” interactions, have been widely exploited by supramolecular chemists for the design and synthesis of molecular receptors which are useful to understand and mimic nature’s specific interactions. As for biological systems, the concepts of shape recognition and binding site complementarity are central for effective molecular recognition in artificial host-guest systems. This selectivity mechanism is particularly useful in the development of chemical sensors, whereas the recognition process can be translated into an analytical signal.[1] The vast majority of chemical sensors contain a chemically sensitive layer for analytes detection coupled with a transducer which transforms this interaction in a readable signal (Figure 1.1). All chemical receptors for gas and vapour sensing are used in the solid state, either in the form of organized films or amorphous layers. The lock and key approach, so successful in the liquid phase, cannot be automatically transferred to vapour and gas sensing due to

two major hurdles: (i) in moving from the vapour to the condensed phase the analyte experiences a dramatic increase in nonspecific dispersion interactions, negligible in liquid to solid transfer;[2](ii) the entropic cost for binding to the receptor is not alleviated by solvent release in the bulk liquid phase.[3]
For these reasons achieving effective molecular recognition at the gas-solid interface is a demanding task, which requires a fresh approach, both in terms of receptor design and characterization tools. Another essential feature is the reversibility of the responses, which requires recourse to weak interactions, since the formation of covalent or ionic bonds would result in an irreversible saturation of the layer.[4]

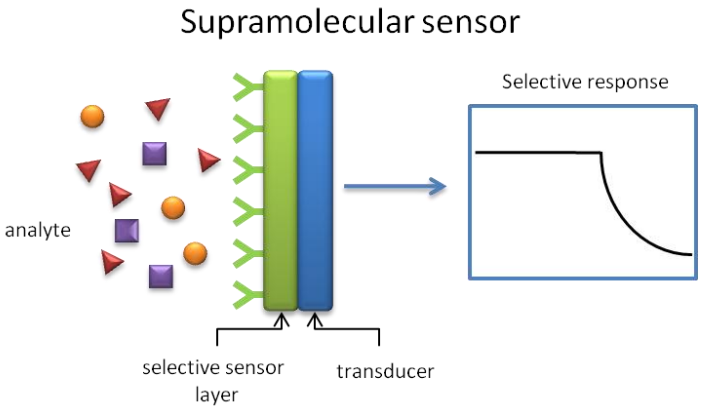

Figure 1.1. Working principle of supramolecular sensors.

1.1.1 Overview of the transducers used in supramolecular gas sensing

Acoustic wave (AW) transducers are the workhorse of supramolecular sensors for gases, because they do not require receptor derivatization for their operation modes, like fluorescent probes for optical sensing. They measure the mass uptake of a sensing layer when exposed to vapours. Usually AW sensors consist of a piezoelectric quartz crystal with electrodes affixed to each side of the plate. When an oscillating potential is applied at a frequency near the resonant frequency of the piezoelectric crystal, a stable oscillating circuit is formed. The key feature of AW sensors is that the frequency and the amplitude of the acoustic wave is affected by a mass change of the system.

The Sauerbrey equation describes the resonant frequency shift of an acoustic resonator upon mass increase on its surface.[2]

$$\Delta f = -2 f_0^2 \cdot \Delta m \cdot A^{-1} \cdot \sqrt{c/\rho}$$

In the equation f_0 (Hz) is the fundamental frequency of the quartz crystal, Δf (Hz) is the frequency shift proportional to the deposited mass Δm (g), A (m^2) is the area of quartz plate or electrode surface, c ($s^2 m\ g^{-1}$) is the elastic coefficient of the system and ρ (g m^{-3}) represents the crystal density. The more widely applied mass sensors based on this principle are quartz crystal microbalance (QCM) and surface acoustic wave (SAW) resonators (Figure 1.2). In the former one, the acoustic wave propagates through the bulk of the system in a direction normal to the surface. Therefore thickness and permeability of the layer are critical features. The acoustic wave produces surface particle displacements that are parallel to the surface. In the SAW device, motion occurs only at the surface, penetrating to a depth of approximately one acoustic wavelength into the crystal; here the direction of propagation is parallel to the surface itself. The waves generated are Rayleigh waves. These have one particle displacement component that is normal to the surface, in contrast with QCM devices. Since in SAW resonators the acoustic energy is trapped near the surface, they are potentially much more sensitive than bulk wave devices. On the other hand the influence of small temperature fluctuations and mechanical stresses is higher, and therefore their handling and interpretation of experimental results is not as straightforward as the case of QCM.

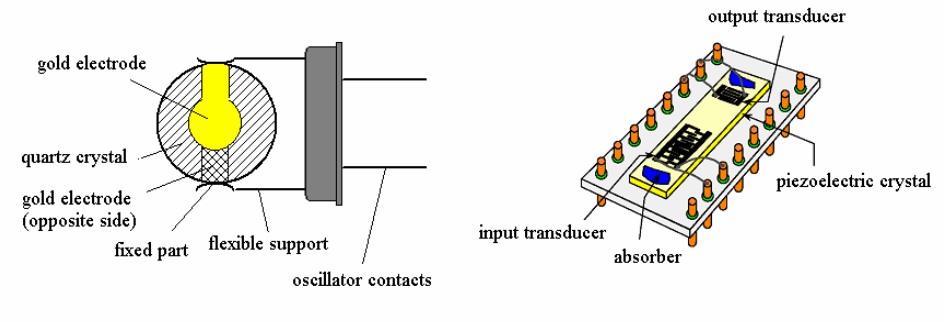

Figure 1.2. QCM (left) and SAW (right) transducers.

By integrating an AW measurement platform with a selective sensing layer, a chemical sensor is constructed, in which molecular recognition events are converted into an electric signal. An important feature of AW sensors is that mass transduction disregards the electronic properties of the sensing layer since the electric read-out does not rely on the conductivity of the organic material but only on the frequency shift of the piezoelectric crystal. This allows to overcome the limitation due to the restricted number of conductive organic materials, making it possible to exploit each molecule endowed with molecular recognition as sensing material.

Recently optical sensing techniques based on the phenomenon of surface plasmon resonance (SPR) have received considerable attention as a transduction scheme for the detection of organic vapour at low level concentration.[5] These optical systems can provide a safe, remote, non-destructive means of sensing and have already been used for gas sensing, biosensing, immuno-sensing and electrochemical studies. In the Kretschmann configuration shown in Figure 1.3 a sensing layer is deposited on one side of a gold film which is 40-50 nm thick and a prism is placed on the other side.

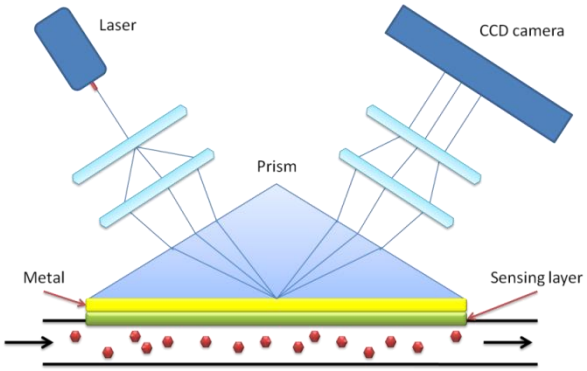

Figure 1.3. The Kretschmann configuration of SPR transducer.

The gold surface is illuminated from the prism side with monochromatic light and the reflection intensity is measured as a function of the incidence angle. Surface plasmon resonance is a strong coupling phenomenon between the light and plasmon waves formed by free electrons on the gold surface and it results in a loss of energy and therefore a reduction in the intensity of the reflected light which is measured by a CCD chip. An evanescent electrical field associated with the plasma wave travels for a short distance (~300 nm) into the medium from the metallic film. Consequently the SP (surface plasmon) is

sensitive to changes in the environment near the interface. Hence, when a sensing layer of receptors deposited on the gold film is exposed to a gaseous analyte in a flow cell (Figure 1.3), the molecular recognition process induces a change in the refractive index providing a selective signal for the receptor-analyte interaction.

1.1.2 CAVITAND AS MOLECULAR RECEPTORS

The name "cavitand" was given in 1982 by Cram[6] to the class of synthetic organic compounds that contain an enforced concave cavity sufficiently large to accommodate other molecules or ion. The concave surface permits the positioning of different functional groups that coverage on the substrate binding site that is usually located inside the cavity.[7]

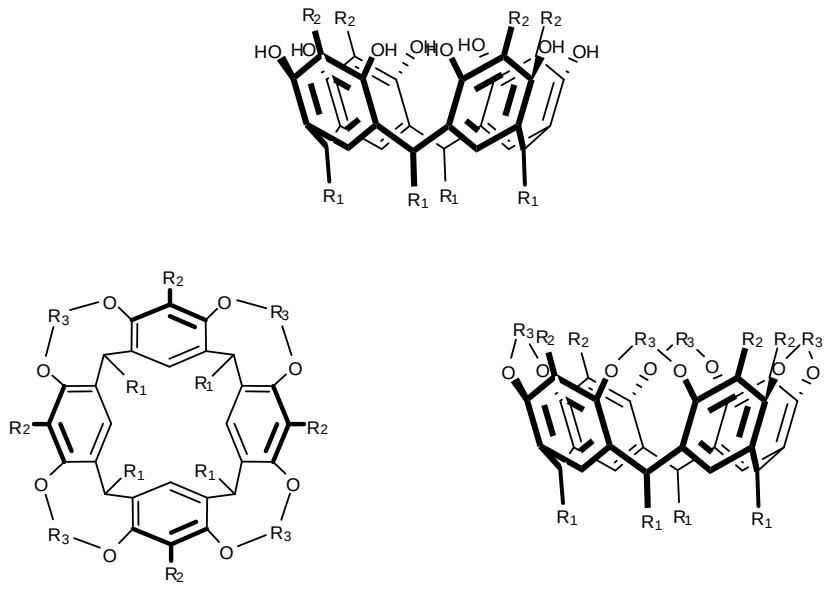

Figure 1.4. Structure of a resorcinarene (up) and of a cavitand top (left) and side (right) views.

Cavitands are generally synthesized by covalent linkage of neighboring phenolic hydroxyl groups in the corresponding octols. They are particularly attractive because the rim of the bowls can be varied by different R_2 substituent and bridging groups R_3 for deepening the bowl cavity and for introducing potentially cooperating functional groups to act as molecular receptors.[8] Moreover the R1 substituent can be use for manipulating the solubility or the morphology in the solid state.

Alkylenedioxyl-bridged cavitands. The first synthesis of a cavitand was reported in 1982.[9] Treat of a resorcinarene with excess CH_2BrCl and base in a mixture of DMSO and DMF gave a tetramethylene bridged cavitand Figure 1.5.

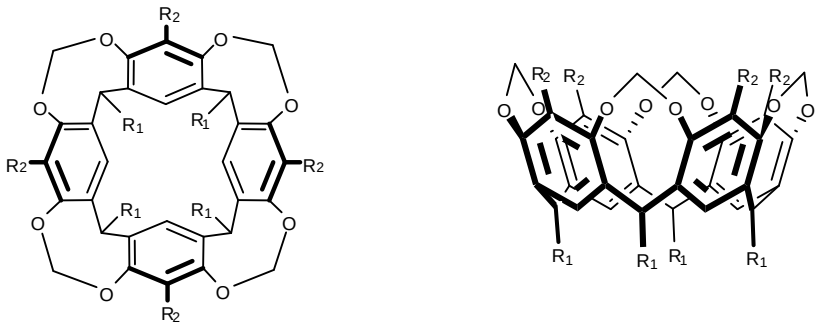

Figure 1.5. Structure of a tetramethylene bridged cavitand.

Compared to the parent resorcinarenes, cavitands are extremely rigid molecules. They adopt a crown-like conformation with C_{4v} symmetry in the solid state and only slightly derivate from this structure in solution.[9] The complexation proprieties of cavitands have been studied both in the solid state and in solution.[10] Most cavitands crystallize as thermally stable solvates from a variety of solvents. Complementarity is high with guests like CH_3CN, $C_6H_5CH_3$, CH_2Cl_2 and $CHCl_3$, but low with C_6H_6 and cyclohexane. All of these are inclusion complexes, but some contain solvent molecules packed between the inclusion complexes. Most complexes (cavitand@guests) could be freed from solvent by heating under vacuum.

Heterophenylene-bridged cavitands. The cavity of resorcinarenes can be largely extended by bridging phenolic hydroxyl groups with aromatic spacers.[11] The quinoxailne spacers can occupy either axial (*a*) or equatorial (*e*) positions.

In the vase (*aaaa*) conformer (Figure 1.6), the spacers touch each other via their α-hydrogens while forming a box like cavity with C_{4V} symmetry which is approximately 7 Å wide and 8 Å deep.[12] The cavity is open at the top and closed at the bottom by the cavitand itself. In the kite (*eeee*) conformer, the spacers are more or less in the same plane.

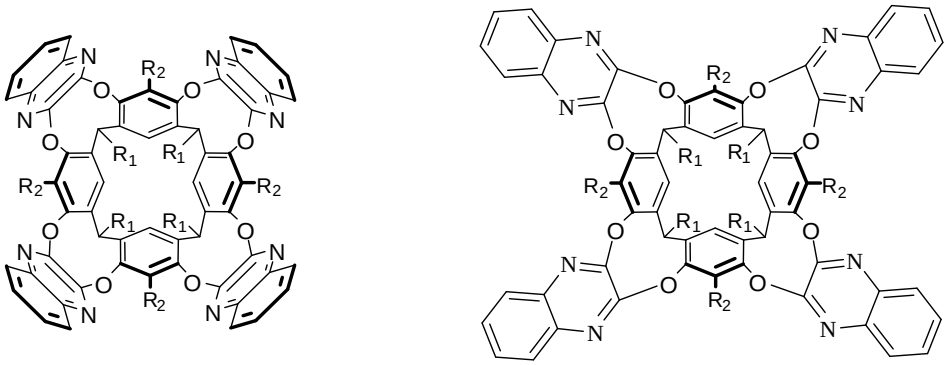

Figure 1.6. Structure of Quinoxaline cavitand *aaaa* conformer (left) and *eeee* conformer (right).

Quinoxaline cavitand (QxCav, R_1=C_6H_{13}, R_2=H), which exists exclusively in the vase conformation above 5°C, forms inclusion complexes in the solid state with neutral molecules like acetone and dichloromethane, but preferentially binds aromatic guests, with binding constants up to 200 M^{-1} for 4-(dimethylamino)nitrobenzene in acetone. This value is considerably higher than those observed for other aromatic guests, like benzene and toluene, because of strong dipole-dipole interaction between host and opposite-directed guest in addition to π-π interaction.

Phosphorous bridged cavitands. The P=O phosphoryl group has strong binding proprieties toward cationic guests and it is a good hydrogen-bond acceptor. Therefore, incorporation of the phosphoryl unit at the upper rim of a resorcinarene preorganized structure can provide powerful receptors for the recognition of cations and hydrogen bond donor molecules.[13] However the presence of four stereogenic centers in the tetrabridged phosphocavitands gives rise to six possible diasteromeric cavitands. The inward (in or *i*) and

outward (out or *o*) configurations are defined relative to the endo and exo orientation of the P=O bonds.[14]

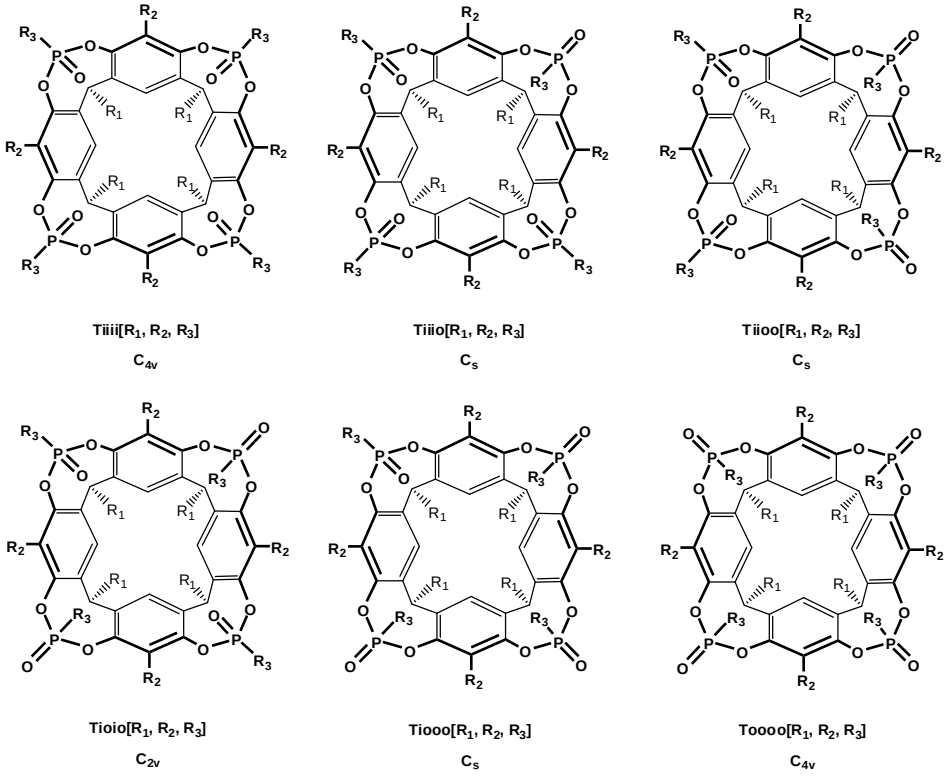

Figure 1.7. Six possible diasteromeric isomers of tetrabridged phosphocavitands

To ensure strong binding, the cavity should containing binding sites preorganized for the interaction with the guests and the iiii (4i) stereoisomer appears to be a prerequisite for a good recognition proprieties.

1.1.3 ISSUES RELATED TO VAPOR SENSING WITH MOLECULAR RECEPTORS

The sorption behaviour of an amorphous sorbent layer towards different analytes can be inferred using the linear sorption energy relationship equation (LSER).[15] According to this model and under the hypothesis of weak non-covalent interactions, the logarithm of the coefficient partition of a sorbent layer with respect to a given volatile species is the linear combination of five terms expressing the intensity of five basic interaction mechanisms: polarizability, dipolarity, H-bond acidity and basicity and the solubility term related to dispersion interactions.
The relation can be written as follows:

$$\log K_p = c + r \cdot R_2 + s \cdot \pi_2^H + a \cdot \alpha_2^H + b \cdot \beta_2^H + l \cdot \log L^{16}$$

where K_p is the layer coefficient partition and R_2, π_2^H , α_2^H , β_2^H and $\log L^{16}$ are the solute parameters of the volatile compounds and *r*, *s*, *a*, *b*, and *l* are coefficients relative to the absorbing material.
For molecular receptors the last term $\log L^{16}$ must be minimized or, even better, eliminated to fully exploit its complexation properties. In other words, one or more of the material coefficients relative to specific binding modes (*r, s, a, b*) must be maximized with respect to the *l* coefficient, expression of dispersion interactions.
Before delving into the subject, two critical issues must be discussed: (i) the cavity effect and (ii) the influence of layer morphology and permeability. Contrary to expectations, the mere presence of a cavity in the molecules which form the sensitive layer does not guarantee sensing selectivity. This fact has been clearly demonstrated by Grate, Abraham and co-workers some years ago by comparing the selectivity patterns of polymers with those of cavitands, cyclodextrins and cyclophanes towards a set of analytes.[16] In all cases the selectivity patterns were similar, which indicates that general dispersion interactions rather than shape complementarity determine selectivity. It must be underlined that the considered receptors presented only preorganized cavities without a functional group decoration for specific interactions. Upon entering the solid layer the analyte can position itself not only into the cavity but also between the host structures, having a higher probability in the last case because of the absence of energetically favourable interactions. The extra versus intracavity positioning of the guest is often exacerbated by the presence of long alkyl chains in peripheral positions of the receptors, necessary for quick

and reversible responses of the receptor layer. For this reason, the receptors are functionalized with alkyl chains that are expected to contribute to the total sensitivity, increasing the dispersion interactions, and to the response time, increasing the permeability of the layer to the analytes. The drawback is that as the length of these chains increases, the relative amount of dispersion interactions tends to override specific complexation phenomena.
Layer morphology is also highly influenced by the presence of alkyl chains, as shown in Figure 1.8. Sensitive layers of cavitands having the same cavity with or without alkyl chains at the lower rim have been coated on a QCM. AFM analysis of the coating surface showed an amorphous layer in the first case and a layer dotted with microcrystalline zones in the second case. Accordingly, the sensor responses to acetonitrile were fast and reversible for the amorphous layer (red trace), whilst very slow and basically irreversible for the partially crystalline one (blue trace) (Figure 1.8).[17]

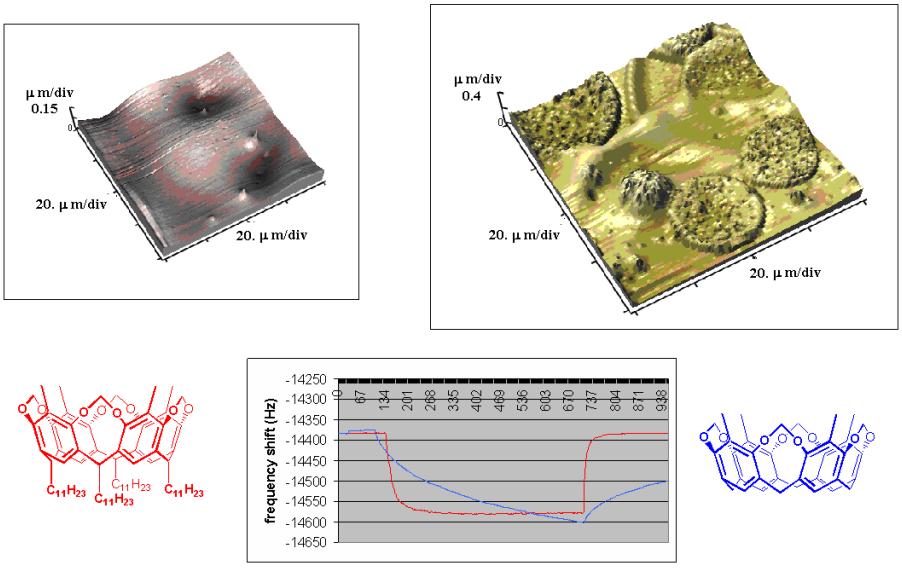

Figure 1.8. Layer morphology (3D AFM image 80x80 μm^2 scan) and QCM responses to acetonitrile (1500 ppm) of MeCav-$C_{11}H_{23}$ (red) and MeCav-H (blue) coated on 10 MHz quartzes, via spray coating.

Considering the above mentioned issues, the direct translation of the molecular recognition properties of a given receptor from solution to the solid-gas interface is not trivial, since non-specific interactions and material properties come into play.

1.1.4 LOCATION OF THE ADSORBED ANALYTES IN THE RECEPTOR LAYERS

The key problem of assessing intracavity complexation versus extracavity adsorption in solid receptor layers has been addressed using two different techniques, namely adsorption isotherms and FT-IR spectroscopy.[18] The former is the diagnostic method, since it can be applied to any coating/analyte couple by plotting the sensor responses versus analyte concentration. FT-IR can be considered a support technique, to be used in connection with the former in the case where host and guest diagnostic bands do not overlap.[4]

Linear adsorption isotherms are typical of nonspecific physisorption processes, following Henry's law; Langmuir-type isotherms, which deviate significantly from linearity, indicate specific, preferential analyte/layer interactions, particularly at low concentrations.[19] Reliable measurements require the comparison of the acquired isotherms with the ones relative to those of known nonspecific layers in the presence of the same analytes and/or with those relative to the same receptor layer exposed to unsuitable guests.

A typical example is shown in Figure 1.9.[20] Five different cavitand layers having the same thickness coated on 10 MHz QCM transducers were exposed to different concentrations of ethanol (Figure 1.9a) and n-pentane (Figure 1.9b). **Mi** cavitands **1** and **3** are selective for alcohols (see later), whilst the other three are unselective. Langmuir-type isotherms are observed only for the compounds **1** and **3** exposed to ethanol, whilst the other three cavitand coatings show linear responses under the same conditions (Figure 1.9a). The exponential trend at low vapour concentrations is the result of the complexation between the analyte and the cavitand receptor. As the receptor layer tends to be saturated, the isotherm flattens assuming a linear course. In the case of pentane, an analyte unable of H-bonding interactions, all sensors respond in a linear fashion (Figure 1.9b). The overall trend can be rationalized assuming a dual mode interaction: the energetically more favourable cavity binding dominates at low analyte concentration, whereas nonspecific extracavity absorption is preponderant at high analyte concentration. As a consequence, when the exponential trend is absent, the molecular recognition events are either absent or negligible.

Reliable adsorption isotherms proving complexation in the solid matrix are reported in literature for a limited number of receptors/analytes: cyclophanes/chloroform,[21] modified cyclodextrins/(R)- and (S)-methyl lactate,[22] and phosphonate cavitands/short chain alcohols.[10]

Metalloporphyrins and related macrocycles, as well as metallophtalocyanines are special cases, in which the specific sensing mode is given either by π

stacking of the analyte into organized layers of the flat macrocycles or by analyte coordination to the metal centre, with no cavity inclusion involved. Also in these cases, adsorption isotherms proved the π stacking and the coordination to the metal centre as an energetically favoured site respectively for flat aromatic compounds and for coordinating molecules.[23,24]

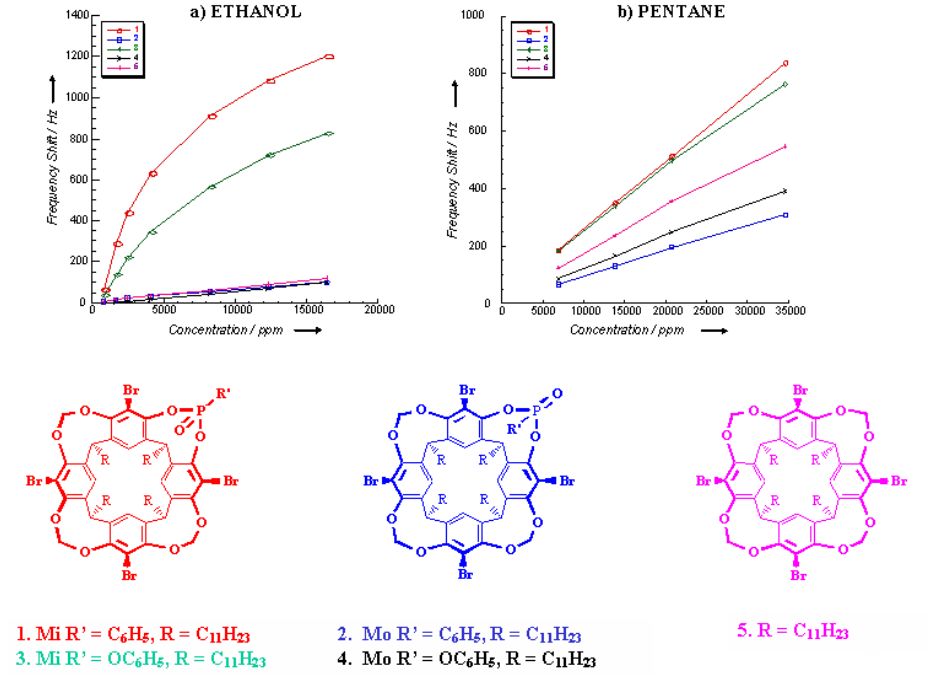

Figure 1.9. Experimental isotherms for cavitand-coated QCM sensors **1**-**5** in the presence of ethanol (a) and pentane (b).

1.1.5 Rational design of supramolecular receptors for vapour sensing: The cavitand case

The design of supramolecular receptors for vapour sensing requires as the first step the appropriate choice of the weak interactions to be implemented in function to the analytes to be detected. The second step, considering the constraints previously described, requires the mastering of the weak interactions between receptor and analyte at the gas-solid interface.
Both topics will be addressed taking the example of the phosphonate cavitands/alcohol case. The molecular structures of the cavitands employed as sensing materials are shown in Figure 1.10. The focus is on phosphonate cavitands because of their better H-bonding acceptor ability with respect to the corresponding phosphates.[25] The presence of four long alkyl chains at the lower rim is needed to obtain highly permeable amorphous layers, that allow easier access of the analytes to the bulk of the layer (see Figure 1.10).

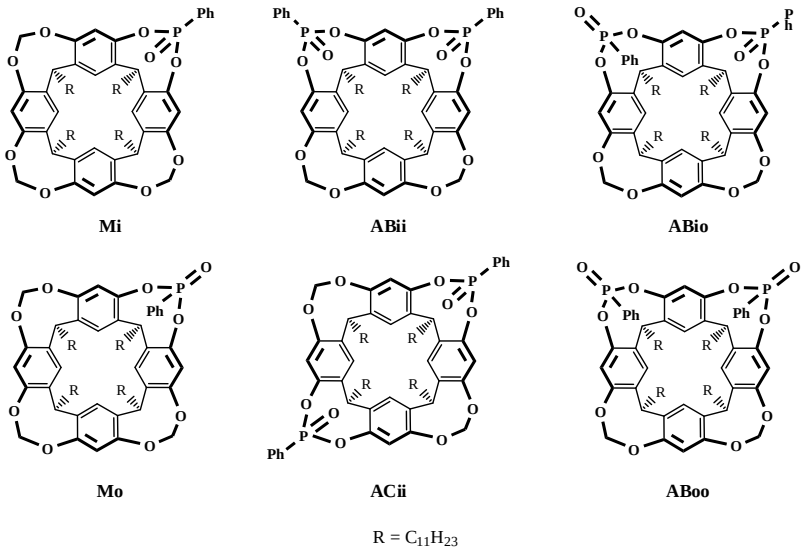

Figure 1.10. Cavitands employed as sensing material discussed in the present introduction.

A synergistic two point interaction was initially selected for alcohol detection.[26] The introduction of a single P=O unit as bridging group at the upper rim of a rigid methylene-bridged cavitand (**Mi** and **Mo** cavitands of Figure 1.10) allows

the cooperative formation of an H-bond between the P=O and the alcoholic OH and CH-π interactions between the alkyl residue of the alcohol and the π-basic cavity beneath. The well-defined spatial orientation of the P=O group with respect to the cavity determines the complexation properties of these cavitands. The two-point interaction with alcohol is possible only for the **Mi** cavitand, whilst in the **Mo** isomer the two interactions are disconnected. Furthermore, in the **Mo** cavitand the phenyl residue on the phosphorus occludes the cavity, excluding the possibility of CH-π interactions with the guest. The importance of cooperativity between H-bonding and CH-π interactions for complexation is reflected in the different behaviour of the two cavitands towards linear alcohols as sensing layers coated on QCM transducers. The responses of the **Mi** cavitand layer are by far much larger than those of the **Mo** one across the entire alcohol series (Figure 1.11). The general enhancement of the responses of all sensors, associated with increasing chain length of the alcohols, is due to the greater number of dispersion interactions experienced by the analyte, as shown by the similar behaviour of nonspecific polymer coatings like PECH (polyepichlorohydrin) and PIB (polyisobutylene). The overall effect is the undesired dilution of the specific cavity responses in the **Mi** layer, which are comparable for each alcohol in the series.

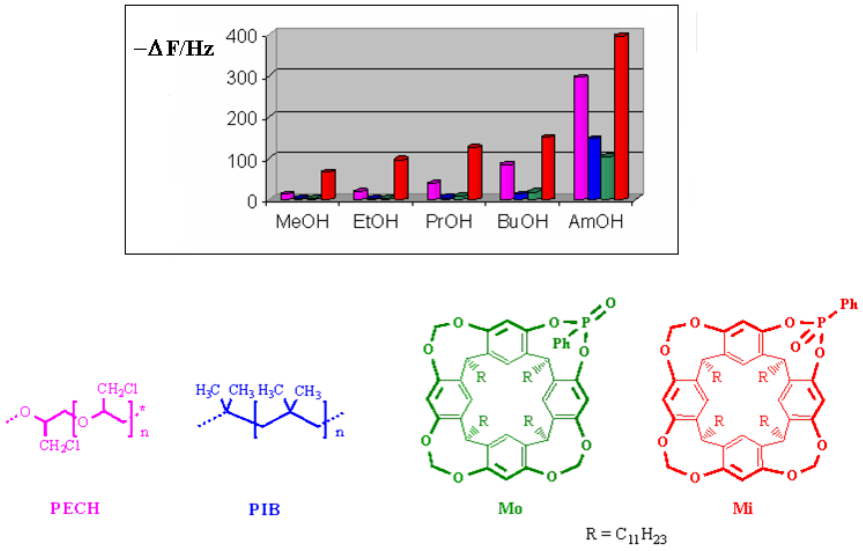

Figure 1.11. Selectivity patterns of Mi and Mo cavitands, PIB and PECH towards linear C_1-C_5 alcohols (3000 ppm each).

The role of the cavity is not limited to CH-π interactions, however, as indicated by the inefficient H-bonding ability of the outward facing P=O in the **Mo** isomer. A possible explanation can be related to the different environment experienced by the P=O groups in the two isomeric cavitands. For the **Mi** isomer the presence of a rigid, preorganized cavity embracing the P=O group eliminates the necessity to generate a void in the lattice for the incoming analyte. On the other hand, the P=O group in **Mo** is on the exterior surface of the receptor, in close contact to other molecules. The analyte must carve out a space to H-bond with the P=O in **Mo**, which is energetically demanding.[2] Therefore, we propose that the cavity has a double role: it is the site for CH-π interactions and, more important, it provides a permanent free volume for the analyte around the inward facing P=O group, pivotal for effective H-bonding. (Figure 1.12).

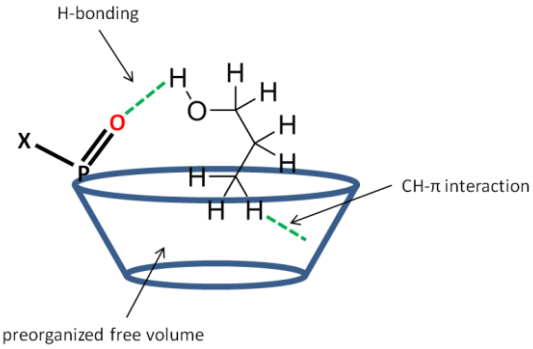

Figure 1.12. Sketch of the binding mode of Mi cavitands towards alcohol.

The next question which arose was: how can we increase selectivity, given the constraint of layer permeability? Following the "lock-and-key" approach, the best solution is an increase of the number of interactions available to the guest upon complexation. In the specific case treated here, this can be achieved in two ways: (i) strengthening a single binding mode via multiple interactions (enthalpic gain); (ii) increasing the number of energetically equivalent binding options available to the guest in a single receptor (entropic gain). AB and AC-diphosphonate-bridged cavitands were prepared to test which of the two options was suitable for alcohol sensing. The expected binding modes for **ABii** and **ACii** cavitands toward alcohols are sketched in Figure 1.13. For the **ABii** isomer, the distance between the two inward facing P=O groups is sufficient to allow the formation of a three-centre H-bond,[27] which, at least in theory,

should be stronger than a two-centre one (the enthalpic gain mode).[28] In the case of the **ACii** cavitand the only possibility for the guest is H-bonding alternatively to one or the other P=O, since the distance between the two P=O is too long for a three-centre H-bond (the entropic gain mode). All the other stereoisomers (**ABio, ACio, ABoo, ACoo**) should not bind alcohols, in analogy with the **Mo** case.

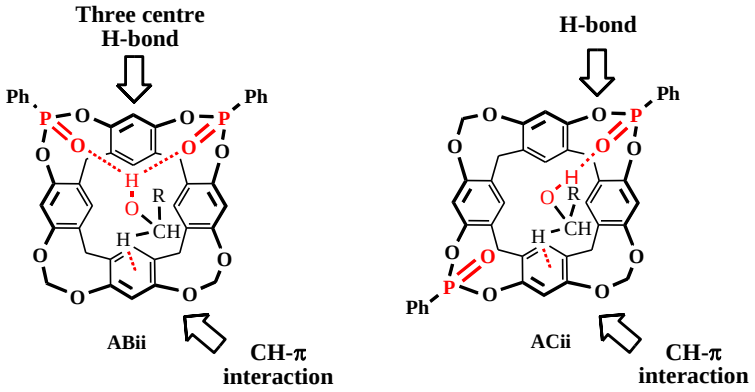

Figure 1.13. Sketch of the different binding mode of **ABii** and **ACii** cavitands towards alcohols.

Cavitands **ACii**, **ABii**, **ABio**, **ABoo**, **Mi** and **Mo** and reference polymer PECH were coated on QCM. Figure 1.14a reports the selectivity patterns of the seven layers toward methanol. The observed responses follows the order: **ACii ≈ ABii > Mi > ABio > Mo ≈ ABoo ≈ PECH**.[21] The introduction of a second P=O group in the inward configuration leads to relevant improvements both in selectivity and sensitivity with respect to the **Mi** counterpart. The relative position of the two P=O groups (**ACii** vs **ABii**) is not determinant, suggesting that the entropic stabilization of the complex via a second energetically equivalent H-bond is the preferred option (see later for structural proofs). Even more compelling are the responses of **ABio** and **ABoo** isomers. These are progressively reduced by the presence of one/two phenyl groups filling the cavity and by the diverging orientation of the P=O groups. Figure 1.14b reports the responses of **ABii** and **Mi** to linear C_1-C_5 alcohols. The responses have been normalized to those of **PECH** to show the progressive dilution of the specific responses upon increase of the chain length of the analytes. In spite of that, a satisfactory selectivity gain is retained throughout the alcohol series for **ABii**.

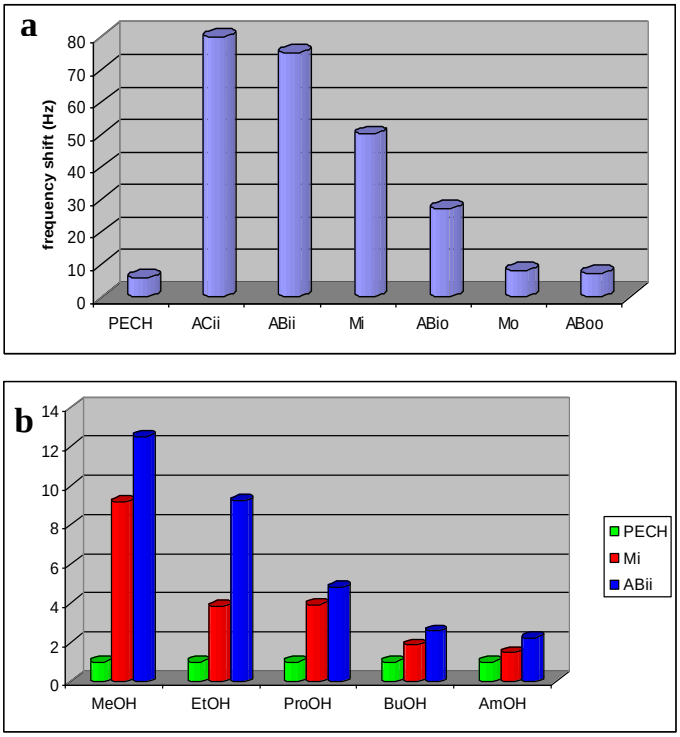

Figure 1.14. (a) Selectivity patterns of cavitands **ACii**, **ABii**, **Mi**, **ABio**, **Mo**, **ABoo** and polymer PECH towards methanol at 1500 ppm. (b) Selectivity patterns of cavitands **ABii**, **Mi** and polymer PECH towards linear C_1-C_5 alcohols (1500 ppm each), normalized to PECH.

1.1.6 SPR SUPRAMOLECULAR SENSORS

The major hurdle in the development of supramolecular mass sensors is the inability to distinguish specific binding events that occur within the cavity from nonspecific dispersion interactions that occur elsewhere in the layer. One of the available options to minimize nonspecific interactions is the reduction of the receptor layer thickness in connection with an appropriate transducer. Thin layers or, even better, monolayers of molecular receptors have been recently employed in connection with SPR transducers.[29] The advantage of SPR over other transduction schemes is its increased sensitivity; SPR can detect vapor interactions with monolayers of molecular receptors. Thin films of

modified γ-cyclodextrins,[30] resorcinarenes and cavitands have been used as receptor layers after spin-coating,[31] self-assembly[32] or Langmuir-Blodgett[33] deposition onto the gold surface of the SPR device. As previously explained, the potential of cavitand receptors in terms of selectivity has not been fully exploited using QCM techniques due to the concomitant presence of dispersion interactions between analyte and alkyl chains, which dilute the specific response. The SPR transduction scheme has shown to combine high sensitivity (part per million or even smaller) with a drastic reduction in dispersion interactions among analytes and sensing layer. This is mainly due to the difference in layer thickness passing from QCM (μm range) to SPR (nm range) techniques. The effectiveness of supramolecular SPR sensing has been recently shown using quinoxaline- (**QxCav**), pyrazine- (**PzCav**) and methylene-bridged (**MeCav**) cavitands (Figure 1.15) as receptors for the detection of aromatic organic vapours.[31]

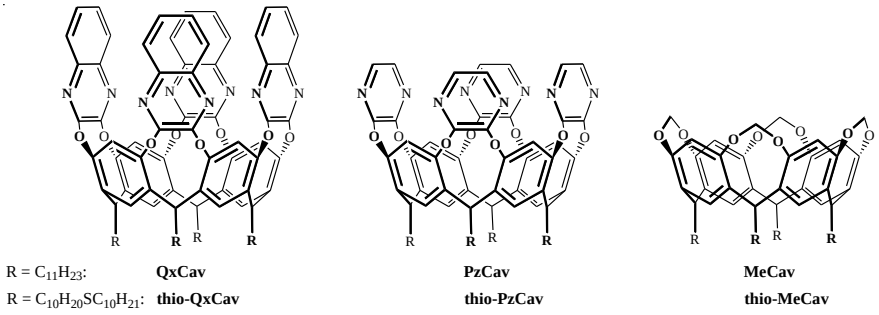

Figure 1.15. Chemical structures of quinoxaline-, pyrazine- and methylene-bridged cavitands.

The cavitand sensing layers were spin coated onto the gold film giving a layer thickness of about 4-6 nm. For comparison, also PIB and PECH were spin coated on the gold film. Seven different analytes were tested: benzene, toluene, acetonitrile, dichloromethane, ethylacetate, propanol and water. Each bar graph of Figure 1.16 illustrates the relative change in plasmon angle shift at equal concentration (110 ppm) of the analyte vapours. Besides aromatic guests, none of the cavitands tested shows significant affinity towards other analytes. The high sensitivity of **QxCav** and, to a minor extent of **PzCav** layers towards benzene and toluene is clearly shown. Comparison with the polymer layers, PIB and PECH, illustrates the importance of having rigid preorganized cavities in the sensing layer for the benzene-toluene uptake. At

the molecular level, this behaviour is consistent with the affinity of **QxCav** for aromatic guests as proved by solid[34] and gas[35] phase complexation studies. The deeper cavity of **QxCav** favours aromatic guests inclusion, offering at the same time size complementarity and multiple CH-π interactions. The same selectivity patterns were not obtained using **QxCav** coated SAW transducers.[36]

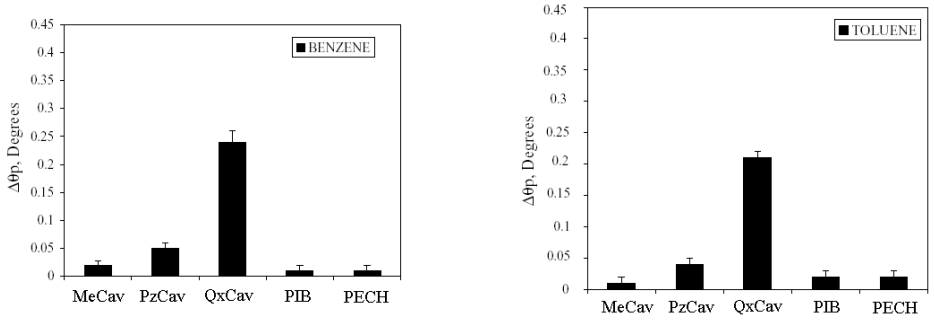

Figure 1.16. Bar graphs showing relative response of **MeCav**, **PzCav**, **QxCav**, PIB and PECH towards 110 ppm of benzene and toluene.

The effect of cavity depth on SPR chemical sensing has been confirmed in a parallel study[32] using SAMs (self-assembled monolayers) of **thio**-**QxCav**, **thio-PzCav** and **thio-MeCav** (see Figure 1.16) as receptor layers. All three cavitands are equipped with four long thioether chains at the lower rim, for the formation of highly ordered SAMs on gold. After exposure of the monolayers to 110 ppm concentrations of benzene and toluene the responses are consistent with the previously reported studies on spin-coated cavitands: the aromatic molecules are selectively complexed by **thio-QxCav** and show less affinity for **thio-PzCav** and **thio-MeCav** owing to their smaller cavity depths. The same **thio-QxCav** monolayer on the gold cover of 10 MHz QCM gave no responses under the same conditions, due to the lower sensitivity of the QCM transduction mechanism.

1.1.7 Differential versus specific binding in sensor arrays

In targeting single analytes in complex vapour mixtures, like food aroma, the strict "lock-and-key" principle does not hold. The reason for this is the absence of truly specific gas sensors, capable of responding to a target analyte alone in a given mixture. The weakness of the sensors cross reactivity has been turned into a strength by using arrays of sensors for analyte pattern recognition.[37] In this way the chemically diverse nonspecific responses of the sensor layers give rise to distinct fingerprint patterns for different odour mixtures. This is a general approach, spanning from inorganic layers, like metal oxide semiconductors (MOX), to optical and polymer sensors. The use of a large number of different sensors coupled with pattern-recognition protocols, has been extremely successful in the identification and assessment of the quality of complex odours, making it possible to develop artificial olfactory systems (electronic noses).
In the field of supramolecular sensing, the concept of differential binding has been introduced to exploit the cross reactivity approach in sensor arrays.[38] Arrays of differential receptors, having different binding characteristics, none of which are necessarily specific or even very selective, have been proposed to mimic the mammalian sense of smell. However, when the identification of a target compound in the presence of many different ones is necessary, specific receptors are still required. Environmental monitoring, chemical warfare and explosive detections are just a few examples. The highly orthogonal responses provided by the insertion of specific receptors into sensor arrays allows excellent analyte discrimination by boosting the pattern-recognition protocol performances.[39]

1.2 Conclusions and Outlook

The use of molecular receptors for gas sensing requires mastering molecular recognition at the gas-solid interface. This is not a trivial task, due to the competing presence of nonspecific dispersion interactions in the solid layer, which very often override the weak specific ones. Several steps must be undertaken to prove, understand and predict complexation phenomena at the gas-solid interface. First, compelling evidence of analyte complexation within

the receptor layer must be obtained via adsorption isotherm measurements. Then, a molecular level understanding of the receptor-analyte interactions in the gas phase and in the solid state has to be acquired, through the combined use of MS and X-ray crystallography. If the dominant interactions in the two phases coincide, the knowledge assumes predicting value for the receptor performances in sensors.

In the case of phosphonate cavitands the following factors turned out to be determining for the selective sensing of alcohols: (i) the simultaneous presence of H-bonding with one of the PO groups and CH-π interactions with the π-basic cavity; (ii) a rigid cavity which provides a permanent free volume for the analyte around the inward facing PO groups, pivotal for effective H-bonding; (iii) a network of energetically equivalent H-bonding options available to the analyte. It is worth noticing that this last factor leads to an entropic stabilization of the alcohol cavitand complex, with relevant influence on the sensor performances.

However, despite all attempts, a fully specific supramolecular sensor, in which nonspecific interactions and competitive binding by undesired analytes have been eliminated, has not been yet obtained. One can legitimately wonder whether such a sensor is possible. Assuming that a truly specific receptor for a given molecule can be designed and prepared, two different strategies can be envisioned to avoid nonspecific interactions. From the receptor side, the challenge is to design a host incorporating a suitable transduction group (i.e. a chromophore), which can be activated exclusively by the molecular recognition event. Alternatively, the collective behaviour of self-organizing materials can be tapped to amplify the molecular recognition phenomena at the macroscopic level. The practicability of such an approach has been recently demonstrated,[40] by triggering an orientational change in a liquid crystal layer upon analyte complexation on the surface. Independently from the strategy used, a better control over molecular recognition at interfaces will lead to a new generation of chemical sensors with significant applicative impact.

1.3 References and Notes

1 L. Pirondini, E. Dalcanale *Chem. Soc. Rev.* **2007**, *36*, 695.

2 J. W. Grate and G. C. Frye, in *Sensors Update*, eds. H. Baltes, W. Göpel and J. Hesse, Wiley-VCH, Weinheim **1996**, *Vol. 2*, 37.

3 J. Janata *Principles of Chemical Sensors*, Plenum Press **1989**, New York, USA.

4 A. Hierlemann, A. J. Ricco, K. Bodenhöfer, W. Gŏpel *Anal. Chem.* **1999**, *71*, 3022.

5 P. Y. Tsoi, J. Yang, Y. Sun, M. Yang *Langmuir* **2000**, *16*, 6590.

6 J. R. Moran, S. Karbach, D. J. Carm *J. Am. Chem. Soc.* **1982**, *104*, 5826.

7 D.J. Cram *Science* **1983**, *219*, 1177.

8 P. Timmerman, W. Verboom, D. N. Reinhoudt *Tetrahedron* **1996***, 52*, 2663.

9 D. J. Cram, S. Karbach, H. E. Kim, Knobbler, E. F. Maverick, J. L Ericsonn, R. C. Helgeson *J. Am. Chem. Soc.* **1998**, 110, 2229**.**

10 J. A. Tucker, C. B. Knobler, K. N. Trueblood, D. J. Cram *J. Am. Chem. Soc.* **1989**, *111*, 3688.

11 J. R. Moran, S. Karbach, D. J. Cram *J. Am. Chem. Soc.* **1982**, *104*, 5826; J. A. Bryant, J. L. Ericson, D. J. Cram *J. Am. Chem. Soc.* **1990**, *112*, 1255; D. J. Cram, H. –J. Choi, J. A. Bryant, C. B. Knobler *J. Am. Chem. Soc.* **1992**, *114*, 7748.

12 E. Dalcanale, P. Soncini, G. Bacchilega, F. Ugozzoli *J. Chem. Soc., Chem. Commun.* **1989**, 500.

13 P. Delangle, J.-P. Dutasta. J.-P. Declercq, B. Tinant *Chem. Eur. J.* **1998**, *4*, 100.

14 R. Pianlli, M. Suman, E. Dalcanale *Eur. J. Org. Chem.* **2004**, *3*, 451.

15 R. W. McGill, M. H. Abraham, J.W. Grate *CHEMTECH* **1994**, *27*, and references therein.

16 J. W. Grate, S. J. Patrash, M. H. Abraham, C. My Du *Anal. Chem.* **1996**, *68*, 913.

17 M. Suman, M. Bacchieri, E. Dalcanale *unpublished results*. Equal amounts of each cavitands (20 KHz) have been coated on the quartzes.

18 F. L. Dickert, U. Geiger, M. Keppler, M. Reif, W.-E. Bulst, U. Knauer, G. Fischerauer *Sens. Actuators B* **1995**, *26*, 199.

19 J. Comyn *Polymer Permeability* **1985**, Elsevier, New York, USA, 29.

20 R. Paolesse, C. Di Natale, S. Nardis, A. Magagnano, A. D'Amico, R. Pinalli, E. Dalcanale *Chem. Eur. J.* **2003**, *9*, 5388.

21 F. L. Dickert, A. Haunschild, V. Kuschow, M. Reif, H. Stathopulos *Anal. Chem.* **1996**, *68*, 1058.

22 K. Bodenhöfer, A. Hierlemann, M. Juza, V. Schurig, W. Göpel *Anal. Chem.* **1997***, 69,* 4017.

23 R. Paolesse, C. Di Natale, A. Macagno, F. Sagone, M. A. Scarselli, P. Chiaradia, V. I. Troitsky, T. S. Berzina, A. D'Amico *Langmuir* **1999***, 15*, 1268.

[24] C. Fietzek, K. Bodenhöfer, P. Haisch, M. Hees, M. Hanack, S. Steinbrecher, F. Zhou, E. Plies, W. Göpel *Sens. Actuators B* **1999**, *57*, 88.
[25] E. M. Armett, E. J. Mitchell *J. Am. Chem. Soc.* **1971**, *93*, 4052.
[26] R. Pinalli, F. F. Nachtigall, F. Ugozzoli, E. Dalcanale *Angew. Chem. Int. Ed.* **1999**, *38*, 2377.
[27] G. A. Jeffrey, W. Saenger *Hydrogen Bonding in Biological Structures* **1991**, Springer-Verlag, Berlin.
[28] For an example of an energetically favourable three-centre H-bond, see: B. Gong, H. Zeng, J. Zhu, L. Yuan, Y. Han, S. Cheng, M. Furukawa, R. D. Parra, A. Y. Kovalevsky, J. L. Mills, E. Skrzypczak-Jankun, S. Martinovic, R. D. Smith, C. Zheng, T. Szyperski, X. C. Zeng, *Proc. Natl. Acad. Sci. U.S.A.* **2002**, *99*, 11583.
[29] A. K. Hassan, A. K. Ray, A. V. Nabok, T. Wilkop *Applied Surface Science* **2001**, *182*, 49.
[30] B. Kieser, C. Fietzek, R. Schmidt, G. Belge, U. Weimar, V. Schurig, G. Gauglitz, *Anal. Chem.* **2002**, *74*, 3005.
[31] E. B. Feresenbet, E. Dalcanale, C. Dulcey, D. K. Shenoy *Sens. Actuators B* **2004**, *97*, 211.
[32] E. B. Feresenbet, M. Busi, F. Ugozzoli, E. Dalcanale, D. K. Shenoy *Sensor Lett.* **2004**, *2*, 186.
[33] A. V. Nabok, A. K. Hassan, A. K. Ray, O. Omar, V. I. Kalchenko *Sens. Actuators B* **1997**, *45*, 115.
[34] P. Soncini, S. Bonsignore, E. Dalcanale, F. Ugozzoli *J. Org. Chem.* **1992**, *57*, 4608.
[35] M. Vincenti, E. Dalcanale, P. Soncini and G. Guglielmetti *J. Am. Chem. Soc.* **1990**, *112*, 445.
[36] J. Greenblatt, N. Kaushansky, Z. Liron, E. Dalcanale *Proceedings-Electrochemical Society* **1997**, *97-19*, 141.
[37] K. J. Albert, N. S. Lewis, C. L. Schauer, G. A. Sotzing, S. E. Stitzel, T. P. Vaid, D. R. Walt *Chem. Rev.* **2000**, *100*, 2595.
[38] J. J. Lavigne, E. V. Anslyn *Angew. Chem. Int. Ed.* **2001**, *40*, 3118.
[39] For a recent, significant example see: N. A. Rakow, A. Sen, M. C. Janzen, J. B. Ponder, K. S. Suslick *Angew. Chem. Int. Ed.* **2005**, *44*, 4528.
[40] R. R. Shah, N. L. Abbott *Science* **2001**, *293*, 1296.

2 A supramolecular approach to sub-ppb aromatic VOCs detection in air[⊗]

2.1 Introduction

Increasing pollution due to vehicular traffic and industrial activities is a major problem nowadays, particularly in large urban or industrial areas. Widespread air quality monitoring is mandatory to ensure healthy living conditions, but available real-time VOCs monitoring systems for in-field environmental monitoring applications are bulky and expensive, being automatic high-end systems derived from laboratory instrumentation.[1] Simple low-cost systems based on solid state gas sensors were recently proposed.[2] Thin-film Metal Oxide Semiconductor (MOX) gas sensors are characterized by high sensitivity and fast response. The structure of a MOX sensor is shown in Figure 2.1.
A layer of material oxide, usually SnO_2, is deposed on a substrate where two metal electrodes are realized. The metal electrodes enable the measurement of the active layer resistance. On the other side of the substrate a metal film (platinum) acts as an heater.

[⊗] Part of the content of this Chapter has been published in *Chem. Commun.* **2007**, 2790-2792.

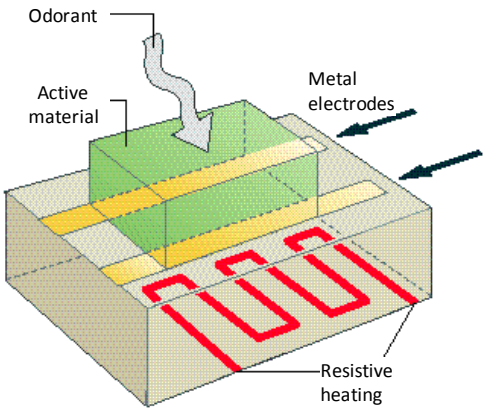

Figure 2.1. Schematic illustration of a MOX sensor

The power dissipated by the heater resistance heats the sensor up to the desired operating temperature usually in the range of 300°C-400°C. This temperature promotes the chemical reactions on the surface of the active layer. The working principle of Metal Oxide sensors is the variation of conductivity in presence of oxidizing and reducing gases. The adsorption and desorption of O^- and O^{2-} changes the electron density at the semiconductor surface. Adsorbed oxygen gives rise to potential barriers at grain boundaries and thus increases the resistance of the sensor surface. On the other hand, reducing gasses decrease the oxygen ion surface concentration and hence the sensor surface resistance. The magnitude of the response depends on the nature and concentration of the volatile molecules, and on the type of metal oxide. Despite their well-established use, some potential applications of MOX are still out of reach due to some unsolved problems, among which the low selectivity, the low steady state stability, and the temperature dependent behavior.

Indeed, the lack of selectivity of MOX gas sensors is one of the major issues in applications where single analytes within complex mixtures must be detected and quantified. Some of the compounds typically found in air samples, such as water vapors, though being harmless to population, are present at high concentrations and can vary rapidly with time, producing significant shifts in the baseline of MOX sensors. Instead, the presence of compounds like benzene, being toxic or even carcinogenic at ppb concentrations, needs to be accurately determined.

Here we report an innovative approach to the sub-ppb level aromatic VOC detection in environmental monitoring. A miniaturized system is proposed, composed of a selective supramolecular concentration unit, a Si-micromachined GC column and a Si-integrated MOX sensor. The issue of achieving at the same time molecular-level selectivity and low-ppb sensitivity for benzene has been solved by disconnecting the recognition element from the detection unit. The recognition event is assigned to a molecular receptor, capable of selectively trapping aromatic vapors at the gas-solid interface.[3] The selective concentration component is interfaced to a miniaturized Si GC column, necessary for the separation of the different aromatic compounds released by the trapping unit, which are then individually channeled to the MOX detector.

For the supramolecular trapping unit we have chosen a quinoxaline-bridged cavitand (QxCav) having a cavity of 8.3 Å deep and 8.0 Å wide, which selectively binds aromatic guests via CH-π interactions with the cavity bottom and walls. In particular the complexation properties of QxCav towards aromatic compounds have been demonstrated both in the solid state[4] and in the gas phase.[5] QxCav is totally insensitive to aliphatic hydrocarbons, water and to polluting gases present in air like CO, SO_x, NO_x.[6]

In 2005 Zampolli and coworkers of the CNR of Bologna developed a miniaturized system to monitor toxic gaseous compounds at ppb level.[7] Their system is based on a micromachined gas chromatographic column to give selectivity to the MOX sensor and they can measure aromatic VOCs as low as 5 ppb. However for outdoor application the monitoring systems must be able to comply with strict legislation, which requires in EU threshold values for benzene below 1 ppb.[8]

2.2 Results and Discussion

In this work we carried out a complete study for the realization of a palm size portable device for the detection of benzene in outdoor air.
We chose to focus our attention only on detection of benzene, the most dangerous of aromatic VOCs. Benzene exposure has serious health effects: breathing high levels of benzene can result in death, while low levels can cause drowsiness, dizziness, rapid heart rate and unconsciousness. The US Department of Health and Human Services (DHHS) classifies benzene as a human carcinogenic. Long-term exposure to high levels of benzene in the air can cause leukemia. Also the other aromatic VOCs are harmful, but we chose to detect only the benzene because in the multidisciplinary science of sensors, simplicity is mandatory. The develop of a simple alarm level device toward a single analyte and use as relative air quality index could be the first step towards commercial success. This could be the first stepping stone for the development of more complex systems which are needed for more demanding application.
Build a sensor requires a diversified set of competence: *chemistry* for the molecular recognition abilities, *physics* to make high sensibility transducers, *engineering* and *informatics* for the assembly of a working prototype (Figure 2.2).

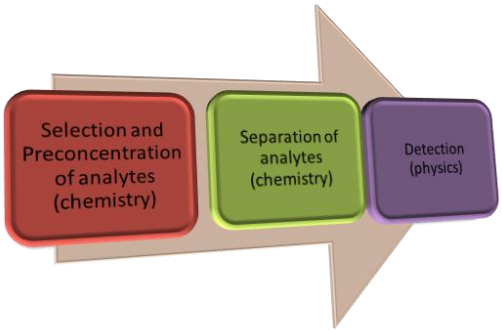

Figure 2.2. Representation of a specific gas sensor.

The first problem was to develop a system to “trap” the benzene from the air and pre-concentrate it to reach the detection limit of the MOX sensor. The idea was to make a sub-ppb limit detector, so the presence of a pre-

concentration unit is fundamental because the MOX systems can detect benzene only above 10 ppb.
The idea is very simple, we thought to create a "trap" with a material able to complex only benzene and small aromatic molecules present in the outdoor air. Then the "trap" is heated and all the analytes are desorbed and funneled to the sensor (Figure 2.3).

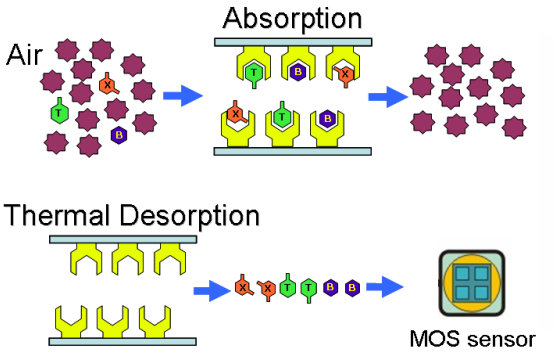

Figure 2.3. Adsorption and desorption phases.

Our work is focused on the synthesis and the development of a material able to complex exclusively aromatic VOCs without interacting with compounds such as water, nitrogen oxides, and aliphatic VOCs. Moreover this "smart" material should release the complexed molecules individually at different temperatures. Thermal and chemical stability is necessary to ensure a reliable device both for laboratory and in-field tests.

2.2.1 Molecular receptor

A versatile class of receptors is represented by resorcin[4]arene cavitands. The nature of bridging groups in this molecules controls the shape and dimension of the cavities, as well as the selectivity in complexation via a combination of shape complementarity and CH-π interactions (Figure 2.4).

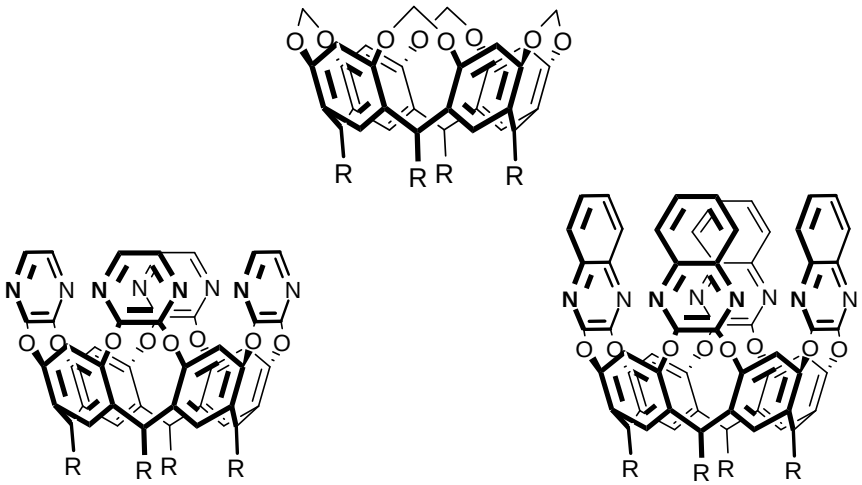

Figure 2.4. Molecular receptors. Pyrazine-bridged cavitand (left), Methylene bridged cavitand (up), Quinoxaline cavitand (right) R=alkyl.

In a previous work[9] the role of the cavitand cavity depth and shape has been studied via theoretical calculation, in particular complexation ability toward small volatile aromatics of the QxCav in comparison to MeCav. The optimized geometries of the QxCav@benzene and QxCav@toluene complexes are in agreement with the molecular geometry of the QxCav@fluorobenzene complex obtained by crystal structure analysis.[4] The complexes are stabilized by weak attractive host-guest interactions involving π electrons of the host, with two C-H_{guest} bonds aligned along the direction of the π orbital of the interacting C_{host} resorcinarene atoms. By contrast, in the case of MeCav complexes the guest is just perching on top of the cavity, with host-guest contacts at the limit of the sum of the Van der Waals radii.
The main idea of our research was to make a material that shows the ability of trapping selectively our target analytes and selectively desorbs them at different temperature. The complexing abilities of QxCav towards benzene and toluene were theatrically investigated by semiempirical molecular orbital calculation using the PM3 model leading to the optimized geometries of the benzene and toluene complex shown in Figure 2.5.

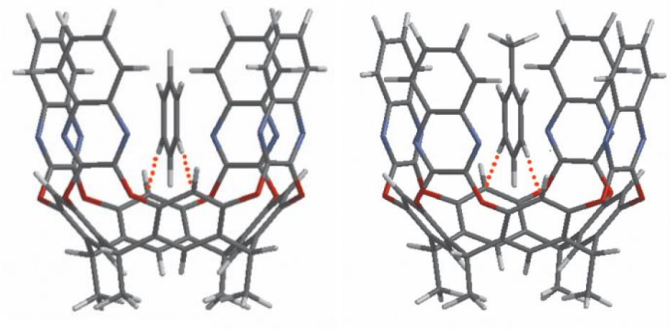

Figure 2.5. Geometry optimized structure of QxCav@benzene and QxCav@toluene (out). In both cases the aliphatic chains of the cavitands have been replaced with methyl groups.

The complexation energies ΔE, calculated as $\Delta E=E_{complex} - [E_{host} + E_{guest}]$, where $E_{complex}$ is the energy of the complex and E_{host} and E_{guest} are the energies of the host and of the guest in the geometry observed in the complex, are summarized in Table 2.1.

Host	Benzene	Toluene-in	Toluene-out
QxCav	-6.85 kJ mol^{-1}	-1.30 kJ mol^{-1}	-6.88 kJ mol^{-1}

Table 2.1. Complexation energies (kJ mol^{-1}), $\Delta E=E_{complex} - [E_{host} + E_{guest}]$ for QxCav and benzene and toluene guests.

In addition the complexation energies of benzene and toluene-out (CH_3-OUT) complexes of QxCav have almost the same value and are both preferred over toluene-in. Experimentally, a slight preference for toluene versus benzene is shown by QxCav both in solution and in the gas phase. The analysis of the Molecular Electrostatic Potential plotted onto the molecular surface of the complexes explains this selectivity. In fact, for benzene and toluene-out, the negative electrostatic potential area on the benzene nucleus is just faced on the complementary positive electrostatic potential area on the quinoxaline nucleus owing to the presence of the quinoxaline rings, whereas when the toluene points the methyl group inside the cavity the complementarity between the electrostatic potential of host and guest is partially destroyed making the interaction less attractive. The large intramolecular cavity of the

cavitand available for complexation can be described as a truncated cone surmounted by a cylinder.[10]

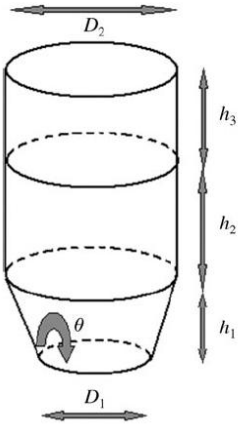

	QxCav	PzCav
D_1 [Å]	5.013	5.173
D_2 [Å]	8.013	8.989
θ[°]	125.5	133.8
θ_1[°]	83.6	83.47
h_1[Å]	2.209	1.734
h_2[Å]	3.420	2.904
h_3[Å]	2.365	-

Figure 2.6. Cavity geometry of Quinoxaline (QxCav) and Pyrazine (PzCav) cavitands.

For our purpose we need a cavitand able to complex benzene, toluene and xylenes and then desorb selectively each analyte at different temperatures. The QxCav is a good host, with its four aromatic walls, with the right size for all the BTEX, on the other hand the PzCav, with its smaller cavity, could show a better discrimination between benzene and the other aromatics VOCs.
We have decided to test two classes of cavitands, the Quinoxaline bridged (QxCav) and the Pyrazine bridged (PzCav).
Our first approach was to explore the influence of the cavity depth on the absorption/desorption test.
The synthesis of pyrazine-bridged cavitand was carried out following the established procedures for the preparation of homo-bridged cavitands.[10]
Resorcin[4]arene was treated with 2,3-dibromopyrazine in the presence of K_2CO_3 to give pyrazine cavitand in good yield. Analogously, when 2,3-dichloroquinoxaline was used as bridging agent quinoxaline cavitand was obtained.

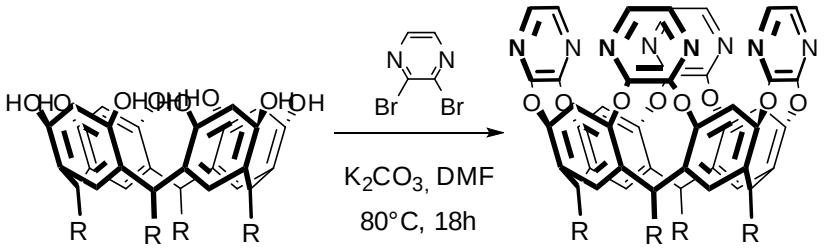

Scheme 2.1. Synthesis of Pyrazine cavitand **2** (R=C_2H_5).

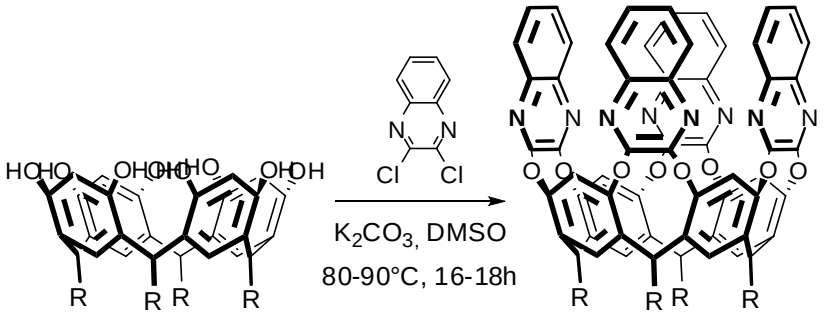

Scheme 2.2. Synthesis of Quinoxaline cavitands (**3**: R=CH_3, **4**: R=C_6H_{13}, **5**: R=$C_{11}H_{23}$).

The pure products were crystallized in powder to be used as filler in a glass column and they were tested in our laboratory apparatus. The crystallization was made by adding a particular solvent to a warm concentrated solution of the cavitand leading the precipitation of the cavitand. Several experiment were carried out to identify the right conditions to obtain a powder with the desired granulometry.

The experimental setup used to test the performances of QxCav as selective concentration unit for aromatic VOCs (Figure 2.7) is composed by a gas distribution system comprising several mass flow controllers connected to certified cylinders provides a calibrated mixture of aromatic VOCs at different concentrations eluted in synthetic air, which is sampled by the cavitand in a "trap" configuration. During sampling the cavitand unit is kept at room temperature. A MOX sensor is mounted in a low-volume chamber and connected to the outlet of the cavitand cartridge.

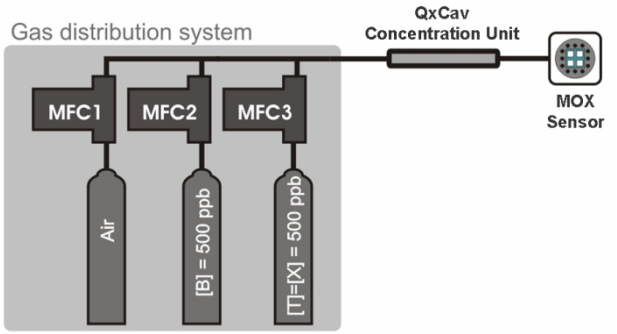

Figure 2.7. Apparatus setup for adsorption/desorption measures.

The absorption efficiency of the cavitand is measured by comparing the sensor response in case of a cartridge filled with QxCav or PzCav with the response in case of an empty cartridge.

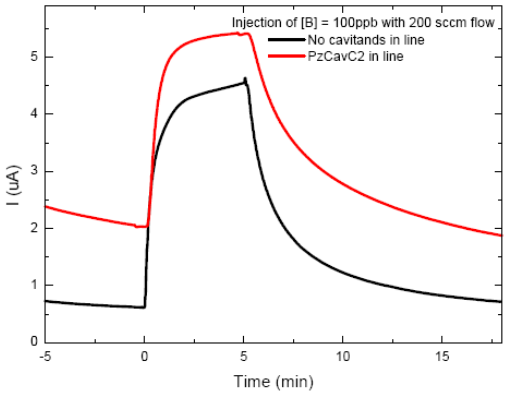

Figure 2.8. Measure of the PzCavC2 (**2**: R=C_2H_5) adsorption efficiency towards 100 ppb of benzene.

Figure 2.8 shows the response of the MOX sensor after the injection of 100 ppb of benzene for 5 minutes in the presence (red line) or in the absence of (black line) the PzCavC2 (**2**). The PzCavC2 filled cartridge does not retain benzene at all.

In case of QxCav as filler of the column we observed a completely different behavior (Figure 2.9).

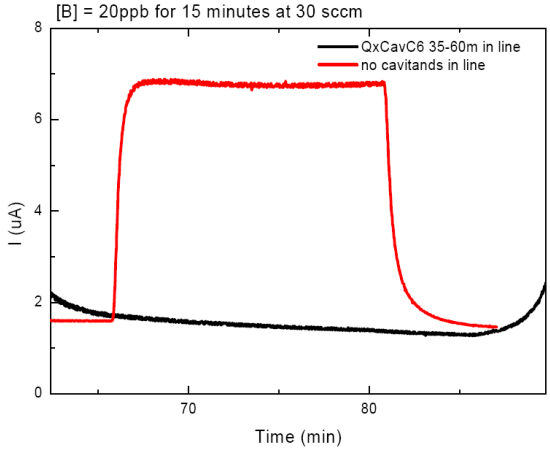

Figure 2.9. Measure of the QxCavC6 (**4**: R=C_6H_{13}) adsorption efficiency towards 20 ppb of benzene.

In the plot the Figure 2.9 typical sensor response during absorption of benzene is shown. The red plot shows the sensor response in case of an empty cartridge, representing the sensor response to the injection of 20 ppb of benzene for 15 minutes. The flat black plot represents the sensor response of QxCavC6 (**4**) under the same conditions. The comparison of these responses clearly shows the high absorption efficiency of the QxCav in comparison to the PzCav. The small pyrazine cavity is not sufficient to complex benzene, so it is inappropriate for our purpose; QxCav instead completely adsorbs benzene.
Furthermore, to estimate the desorption behavior of the filler material (QxCav or PzCav), after a given sampling time (5 or 15 minutes), the cartridges were heated with a linear temperature ramp from room temperature to 80°C in 25 minutes, and the MOX sensor is used as detector of the released volatiles.
In Figure 2.10 (left) we report the response of MOX sensor interfaced with PzCavC2 (2) cartridge after 100 ppb of benzene sampled for 5 min and heated from 20°C to 80°C (black line). If we compare this signal to a desorption after a sampled clean air (red line) we can conclude that no desorption of the analytes has occurred. In Figure 2.10 (right) the black plot shows the sensor response to the compounds released by the QxCavC6 (**4**) after a 20 minutes absorption of 20 ppb of benzene, while the dotted blue plot refers to the release of a mixture of 5 ppb of toluene and 5 ppb of m-xylene, compared to a reference desorption after sampling of humidified air without any VOCs.

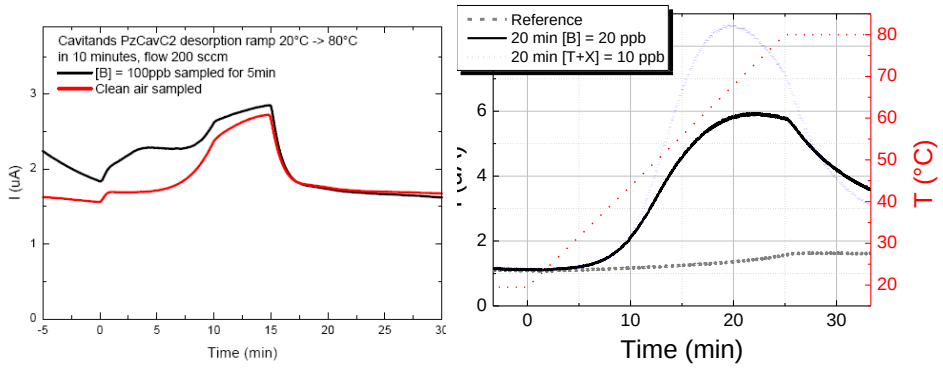

Figure 2.10. Measurement of PzCavC2 (**2**)(left) and QxCavC6 (**4**)(right) desorption kinetics.

Both for the case of benzene and the mixture of toluene and xylenes, there is a maximum peak at around 70°C, which is a temperature low enough to be easily implemented in a miniaturized and portable device. On the other hand, the temperature at which the release occurs is very similar for all of the considered compounds, therefore the selectivity needs to be enhanced for a reliable quantification of each single aromatic compound.

2.2.2 SPECIFIC VS UNSPECIFIC INTERACTION

In a material made of pure cavitand not only the presence of specific interaction sites towards the analyte is important but also their availability. In a compact material the permeability of the analytes in the bulk is very low and the major number of interactions take place on the surface, consequently the most part of the receptors do not participate to the recognition event. A simple method to make the material permeable is to introduce in the molecules long alkyl chains which increase substantially the free volume in the solid. The drawback of the use of alkyl chains is the increase in unspecific interaction with all the apolar organic substances. The problem is to balance this two factors. Four long chains at the lower rim of the cavitand receptor maximize the permeability but they decrease the specificity. On the other hand short chains ensure a more specific interaction but only on the surface. It is obvious that the right length of the chains must be a compromise from this

two extreme conditions. To confirm this theory we synthesize and tested a series of QxCav bearing different alkyl chains at the lower rim.
We decided to test three cavitands having at the upper rim a quinoxaline cavity and at the lower rim a C_1, C_6, and C_{11} alkyl chains (Figure 2.11).

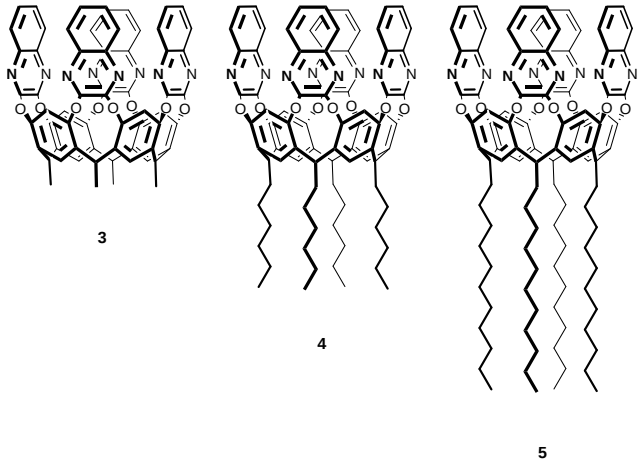

Figure 2.11. Quinoxaline cavitands, **3**: R=CH_3, **4**: R=C_6H_{13}, **5**: R=$C_{11}H_{23}$.

In the case of QxCavC1 (**3**) the absorption efficiency was quite low and a rise of the baseline was observed both in presence of analytes and with sampled air only (Figure 2.12).

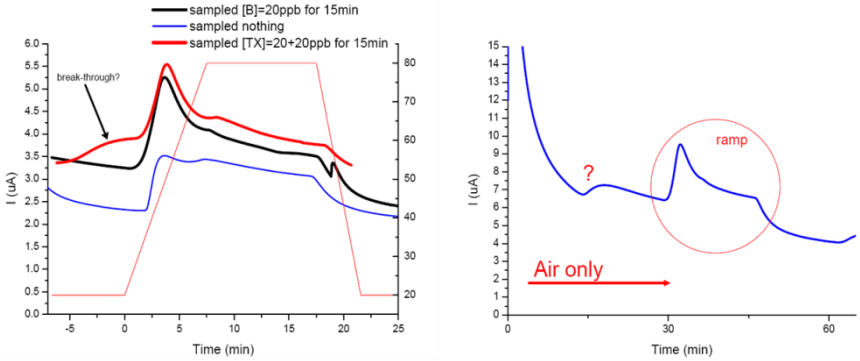

Figure 2.12. Plots of desorption kinetics of QxCavC1 (**3**) after sampling VOCs (left) or only air (right).

Moreover we observed a bigger rise of the baseline after a cleaning cycle at 150°C in air in comparison with a clean cycle in nitrogen. This behavior, initially imputed to a break-through phenomena, is probably due to the relative polarity of the layer that can absorb traces of water present in air used as a carrier gas. A characterization cycle of mixtures of benzene, toluene, and xylenes was anyway performed and reported in Figure 2.13.

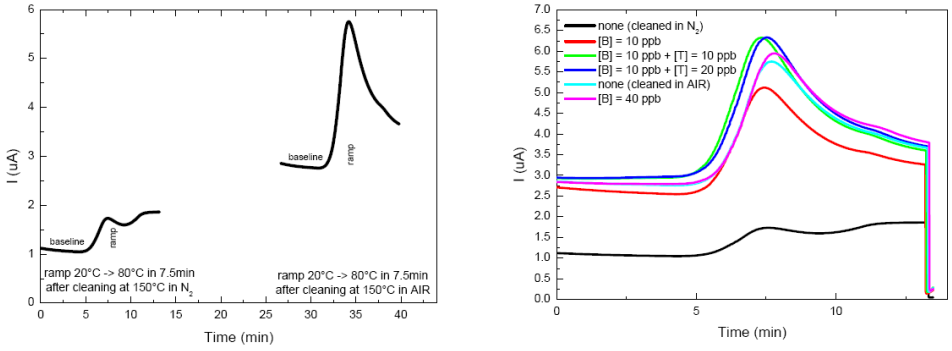

Figure 2.13. Plots of desorption kinetics of QxCav C1 **3** after cleaning with nitrogen or air (left). Sensor responses after sampling VOCs at different concentrations (right).

From the plots reported in Figure 2.13 we observed the high rise of the baseline after a clean in technical air (red and black lines). The low changes in the peaks areas in presence of different concentrations of aromatic are probably due to the low efficiency in the absorption phase. Therefore QxCavC1 (**3**) is unsuitable as sorbent material for our application.

Regarding the cavitand QxCavC11 (**5**) the responses were quite unexpected. From a very apolar layer made by a cavitand with long alkyl chains we would have expected a very efficient absorption of the organic VOCs and no water adsorption. Instead the experiment showed a very low efficiency especially in comparison with the QxCavC6 (**4**) (blue line) Figure 2.14.

In Figure 2.14 are reported the desorption plots after an absorption of 10 ppb of toluene (black line) or 10 ppb of benzene (green line) with a thermal ramp from 21°C to 100°C in 10 minutes together with a reference line (blue line). We observe a very low sensor response due to the scarce absorption efficiency. The higher response toward toluene is only due to the higher catalytic efficiency of the MOX sensor to toluene with respect to benzene.

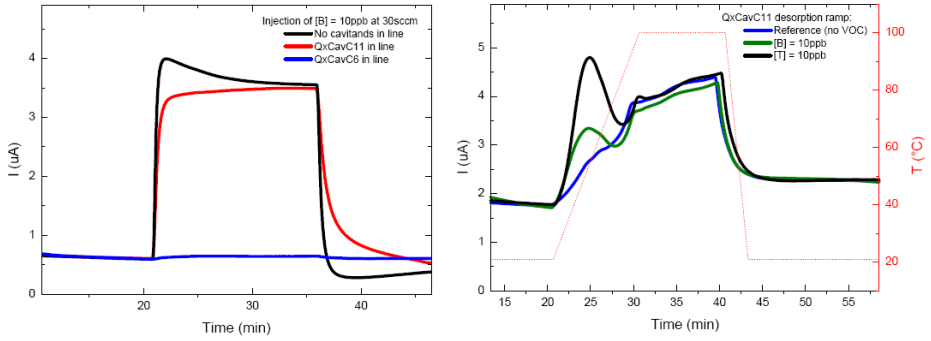

Figure 2.14. Comparison plots between adsorption efficiency of QxCavC11 (**5**) (red line) and QxCavC6 (**4**) (blue line) (left). Plot of desorption kinetics of QxCavC11 (**5**) (right).

This results together with the QxCavC1 (**3**) and QxCavC6 (**4**) ones clearly confirm the initial hypothesis that the right chain length is a average situation between the two extremes. The shorter chains make the layer too impermeable to the analytes and prone to water adsorption. In contrast the longer chain show a low efficiency, probably due to a change in morphology, that compromise its use as sorbent material. In conclusion, the QxCavC6 (**4**) has a very high efficiency in aromatic VOCs adsorption and it is totally insensitive to low chain aliphatic hydrocarbons, water and to pollutants gases present in the air like CO, SO_x, and NO_x.

2.2.3 FLUIDODYNAMIC OF THE TRAP

One of the most important factors that must be considered in the design of a pre-concentrator is the fluidodynamic of the gas. At the beginning of our research we used a "trap" made by a cylindrical Pyrex® tube filled with the pure cavitand. Moreover we observed an overpressure due to the small particles that filling the tube. Small particles ensure high surface area and are easier to make but cause several problems especially for the realization of portable devices that work with small pumps. On the other hand, bigger particles are very difficult to prepare but show low counter pressure.
To evaluate the effect of the size of the particles on the fluidodynamic of the system we prepared different cartridges filled with QxCavC6 (**4**) with different

granulometry. We crystallized the cavitand from acetone and the resulting crystalline solid was passed through different size sieves to obtain a powder having a homogeneous distribution. We chose to test four different distribution of particle size: <60 mesh (>250 µm), 35-60 mesh (500-250 µm), 60-80 mesh (250-177 µm), 80-120 mesh (177-125 µm). In Figure 2.15 we reported the flow rate as a function of the overpressure for each particle size distribution.

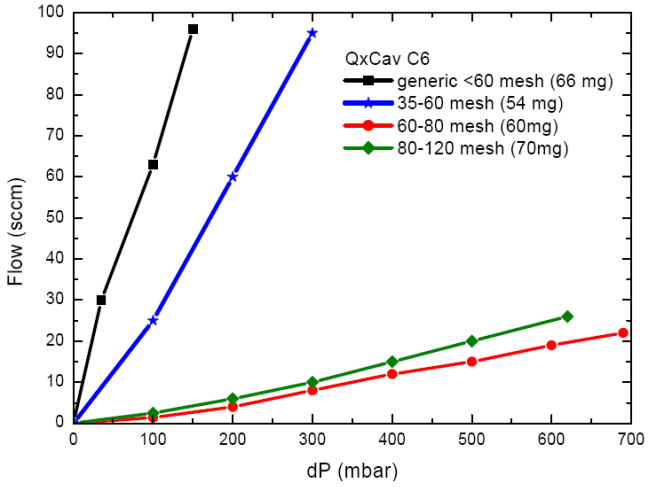

Figure 2.15. Plots of the overpressure with "traps" filled with different granulometry of QxCavC6 (**4**).

While the smaller particles generate high overpressure the larger particles distribution (black and blue lines) produce a very small increase in pressure, which permits to the cartridge to be integrated in a low power portable device. We chose to use as default the 500-250 µm (35-60 mesh) size distribution because has a well define size that ensure more reproducibility.

2.2.4 KINETICS OF ADSORPTION AND DESORPTION

As reported in paragraph 2.2.1, the calculation gives the interaction energy between the QxCav and the guest and accounts for the energy necessary to extract the guest from the frozen host. This approach seems reasonable in view of complexation energies of benzene and toluene-out complexes of QxCav have almost the same value and are both preferred over toluene-in. Experimentally, a slight preference for toluene versus benzene is shown by QxCav both in solution[11] and in gas phase[12]. Moving from this data we thought to use our system also for separate selectively benzene from toluene and xylenes with the only modulation of the temperature of the "trap". The evaluation of kinetics of desorption of benzene and mixture of toluene and xylenes were made with different carrier gas fluxes (30 and 80 sccm). To compare two different analytes in a MOX system, we need to normalize the concentration to the sensor response, that is different for each analyte. We found that 20 ppb of benzene [B] give the same response of 5 ppb toluene and 5 ppb xylenes mixture [TX] as reported in the Figure 2.16.

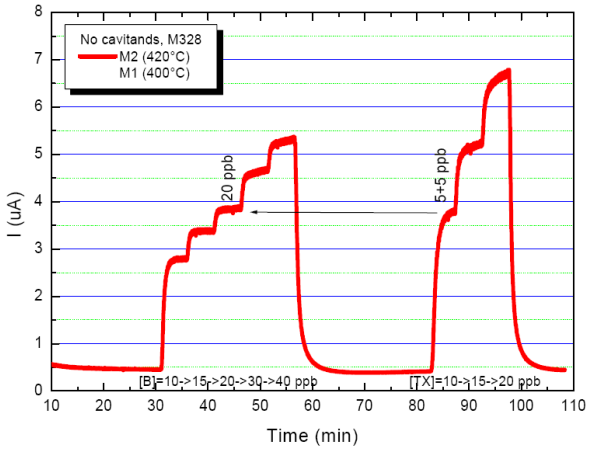

Figure 2.16. MOX sensor responses toward different concentrations of toluene and benzene.

In Figure 2.17 the desorption plots of QxCavC6 (**4**) are shown after a sampling of 20 minutes of benzene or toluene plus xylenes at different flow rates. The thermal ramp is the same, from 20°C to 80°C in ten minutes (dotted red trace).

From these experiment it is clear that the desorption starts at lower temperatures for high flow rate.

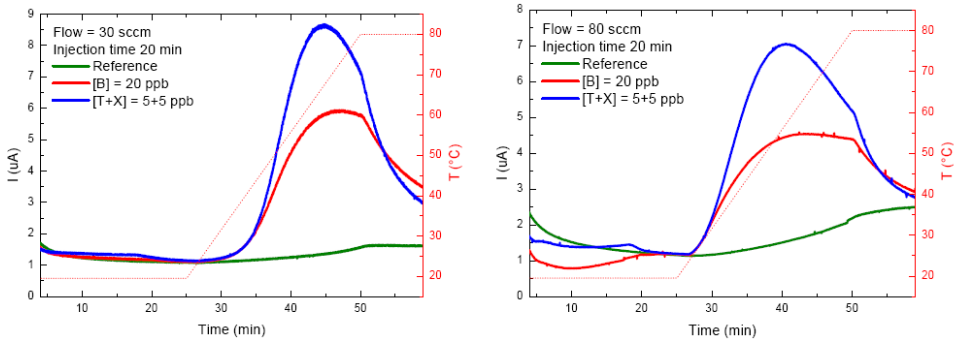

Figure 2.17. Plots of desorption kinetics with different flow rate, 30 sccm (left), and 80 sccm (right).

In both cases, the release has a maximum peak around 60-70°C, which is a temperature low enough to be easily implemented in a miniaturized and portable system. On the other hand, the temperature at which this release occurs is very similar for all compounds, therefore the selectivity needs to be enhanced for a reliable quantification of each single aromatic compound.
This limitation compromises the possibility to detect benzene in the presence of other aromatic VOCs. Therefore, we modified the system with the introduction of a GC separation column (Carbograph + 5% of Carbowax) between the "trap" and the MOX sensor (Figure 2.18).

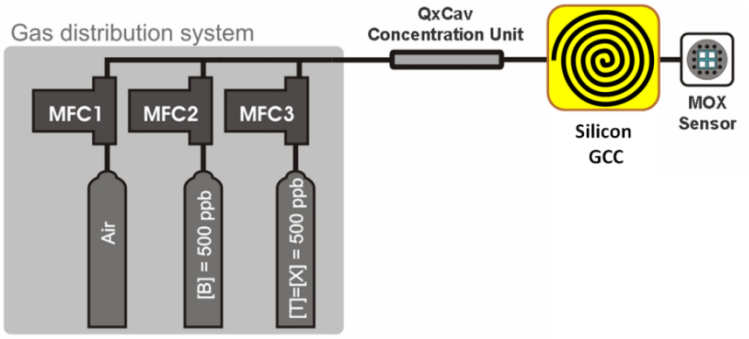

Figure 2.18. Apparatus setup for QxCav tasting with GC separation column.

The presence of a GC system does not underestimate the role of the cavitand-base “trap”. Our “trap” have two fundamental features: it is a concentrator that allow to decrease the limit of detection of MOX sensor up to sub-ppb level and it selectively traps only aromatic VOCs present in air. The system without the “trap” is useless as benzene sensor for outdoor application because it is not enough sensitive and specific.
To use the cavitands as pre-concentration unit before the GC column we need to minimize the desorption time. It must be lower than two minutes because higher desorption times cause broad chromatogram peaks. Unfortunately, two minutes at 100°C are not sufficient to desorb all the adsorbed molecules, so it is preferred perform partially desorption of two minutes followed by clean cycles.
In Figures 2.19 and 2.20 we report the calibration chromatograms and a systematic characterization of the sensor at different concentration of BTX. Unfortunately with our calibrated cylinders and mass flow controllers it is not possible to reach concentrations under 5 ppb so to evaluate the limit of detection of our system we performed short absorption of 5 minutes that are extrapolated to a virtual adsorption of 25 minutes.

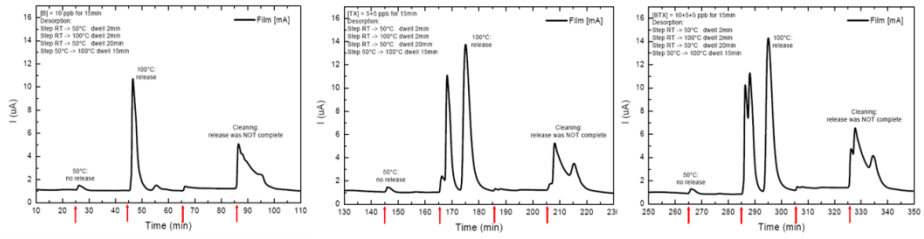

Figure 2.19. Chromatograms after sampling 10 ppb of benzene (left), 5+5 ppb of toluene and xylene (middle), and 10 ppb of benzene mixed with 5+5 ppb of toluene and xylene (right).

The data reported in Figure 2.20 clearly show the possibility to make a integrated system for the evaluation of sub-ppb traces of benzene in outdoor air. In fact despite of a partial superimposition of the peak of benzene with toluene we can well estimate the high of the benzene peak and correlate it to the concentration to calibrate the system.
The next step was the miniaturization of the system.

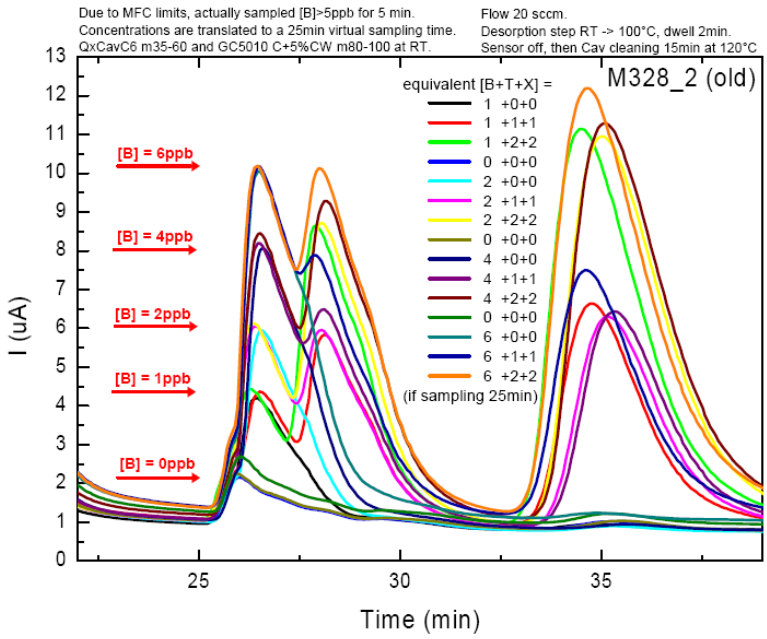

Figure 2.20. Set of fifteen chromatograms relative to QxCav desorption of BTX at different initial concentrations.

2.2.5 MINIATURIZATION OF THE SYSTEM

All the experiments preformed until now were made on a lab scale apparatus and in the last part of the work the measures were performed on a palm size prototype of sensor.
The disassembled prototype system with all the components visible and compared to a 1 euro coin is shown in Figure 2.21.

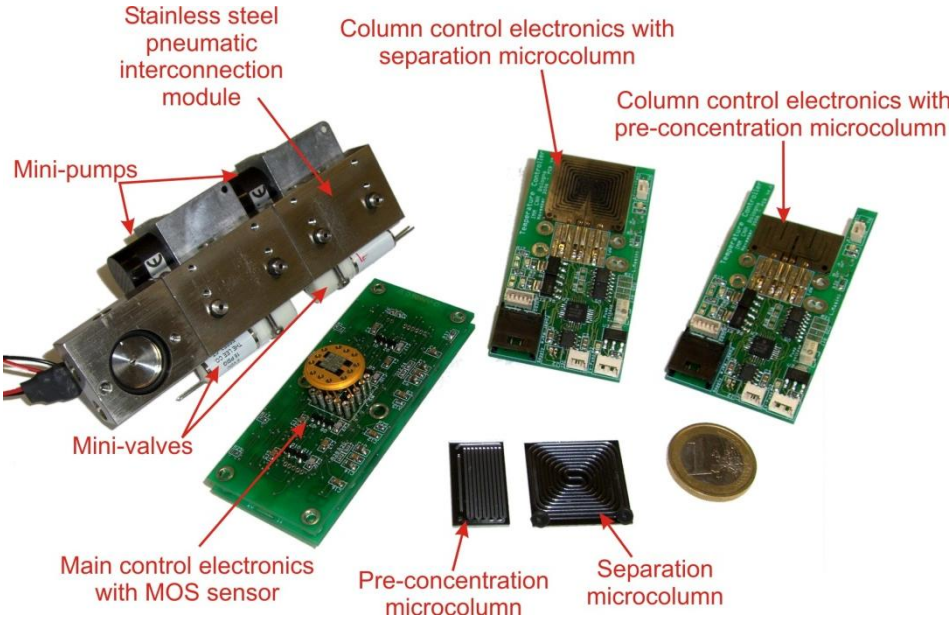

Figure 2.21. Photograph of the disassembled prototype of monitoring system.

The main part of the system are:

- The MOX sensors, the sensing core of the system.
- The pre-concentration unit for molecular recognition and analytes concentration.
- The GC column, for the separation of aromatic VOCs.
- The fluidic system.

The MOX sensor is a Si-micromachined thin film MOX sensor. The sensing layer was deposited by a sputtering process on a Si-microhotplate based SiN_4 membrane and with a thin gold layer as catalyst. The thin film metal oxide gas sensors operate at 400°C, which was found to be the best temperature for aromatic VOCs detection. The sensing layer conductivity was acquired by reading out the sensing layer current under a fixed bias voltage of U = 1.2 V.
The pre-concentration unit was strongly modified in the miniaturization process. The cylindrical Pyrex column of 10 cm of length used in the lab scale and heated with a solenoid shape electrical resistance with a thermocouple was substituted with a more efficient array of columns. The new pre-concentration unit was made in silicon via advanced silicon etching (ASE) technique. It is composed by ten parallel columns. The parallel geometry

enable the best adsorption/desorption efficiency because the path of the analytes is shorter than in a single long column.

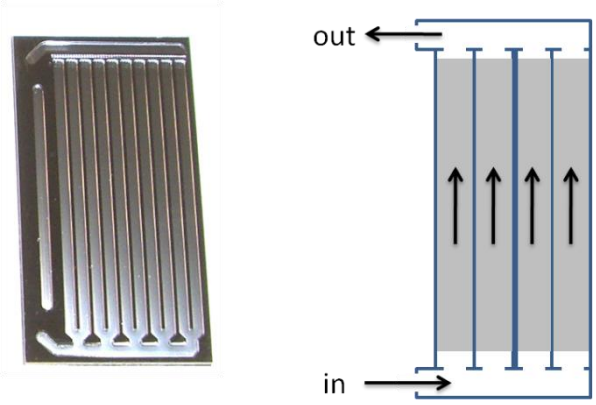

Figure 2.22. Photograph (left) and graphical representation (right) of the pre-concentration unit.

The pre-concentration unit is located on a plate able to heat the columns at the desorption temperature and its thermal control is preformed using a custom electronic interface connected to a PC.

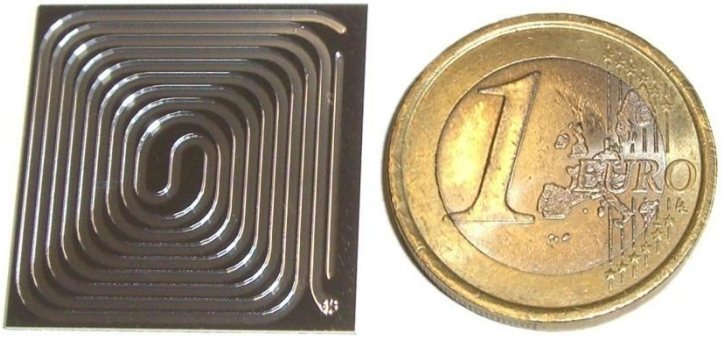

Figure 2.23. Photograph (left) of the GC column unit together with a 1 euro coin.

The GC column used in the prototype is a spiral-shaped channel with cross sectional area of 0.8 mm^2 and length of 50 cm, realized by ASE on a 1 mm thin silicon wafer polished on both size, with etching dept of 850 μm. To control the temperature of the GC column during separation, a platinum heater was fabricated on the bottom of the Si wafer. Finally, a Pyrex wafer with pre-formed drillings for the gas in- and outlet was anodically bonded onto the Si wafer for encapsulation. After encapsulation, the GC columns were filled with a commercial packed gas chromatographic stationary phase.
The GC column and MOX detector, together with the pre-concentration unit, were integrated into a simplified GC system together with some commercial components. The system comprises two pumps (KNF NMP09), a zero grade air generator (activated carbon mesh) and some commercial 3-way microvalves for gas flow control. All of these components were assembled on a stainless steel pneumatic interconnection board, and connected to specifically designed control and read-out electronics, fabricated using small footprint stacked SMD PCBs. The system does not require any external inert gas cylinder, since the carrier gas is generated directly on-board. The whole assembled system is reported in Figure 2.24.

Figure 2.24. Photograph of complete monitoring system. The size is compared with that of a pencil.

2.2.6 PROTOTYPE TESTING

Benzene, toluene, ethylbenzene and m-xylene (BTEX) in a concentration range between 0.1 ppb and 5.0 ppb and eluted in humidified synthetic air were provided by the gas distribution in a constant 500 sccm flow. The sampling pump of the mini-GC was used to sample 200 sccm from this flow for 50 minutes, while the remaining flow was flushed to vent. After 50 minutes of concentration, the QxCav pre-concentration unit was heated to the desorption temperature of 100°C for 2 minutes, and a valve was switched to connect the outlet of the cavitand columns array to the inlet of the GC pump, which drives the released analytes through the GC separation column to the MOX detector. During the chromatogram acquisition, which lasts approximately 15 minutes, the concentration unit column was cooled down and starts the next concentration cycle. In this way the chromatogram acquisition and the concentration can be performed in parallel, therefore the cycle duration was mainly determined by the chromatogram duration or by the concentration time, whichever the longest. Obviously, longer concentration times allow to reach lower detection limits, while in case of higher concentrations shorter measurement cycles can be applied.

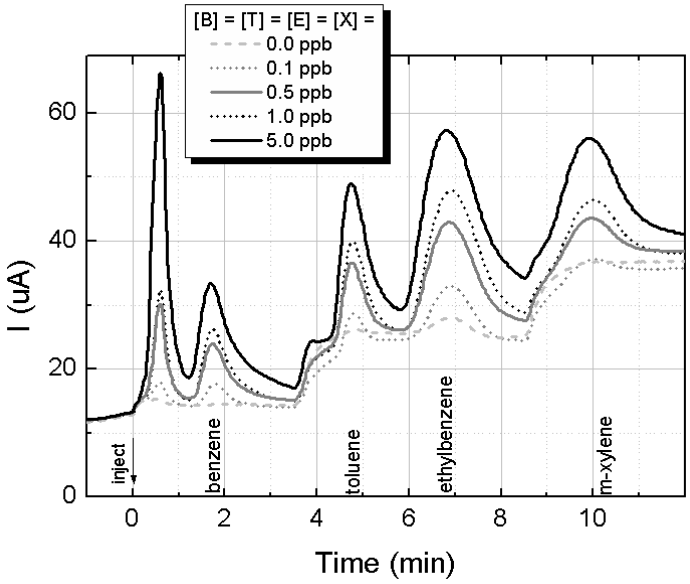

Figure 2.25. Set of five chromatogram relative to QxCav desorption of BTEX at different initial concentrations.

In Figure 2.25 is reported a set of five measurement cycles, with four different analyte concentrations in the range between 0.1 ppb and 5.0 ppb, together with a reference chromatogram relative to humidified air only. The injections were not performed in any increasing or decreasing order, but in a random sequence, to exclude any systematic error due to analyte residues. After a first injection peak at time lower than one minute, the four peaks relative to benzene, toluene, ethylbenzene and m-xylene are released at time = 2, 5, 7 and 10 min respectively. The peaks are well separated, and the baseline drift at time > 4 min is due to the increase of the GC column temperature to allow a faster release of the heavier analytes (programmed temperature ramp). For all of the concentrations, including the lowest 0.1 ppb injection, the peaks were clearly visible and a peak area can be extracted, which can be correlated to the concentration of the single analytes. The correlation between the chromatographic peak areas of eight different chromatograms with the analyte concentrations for benzene, toluene and m-xylene is shown in Figure 2.26.

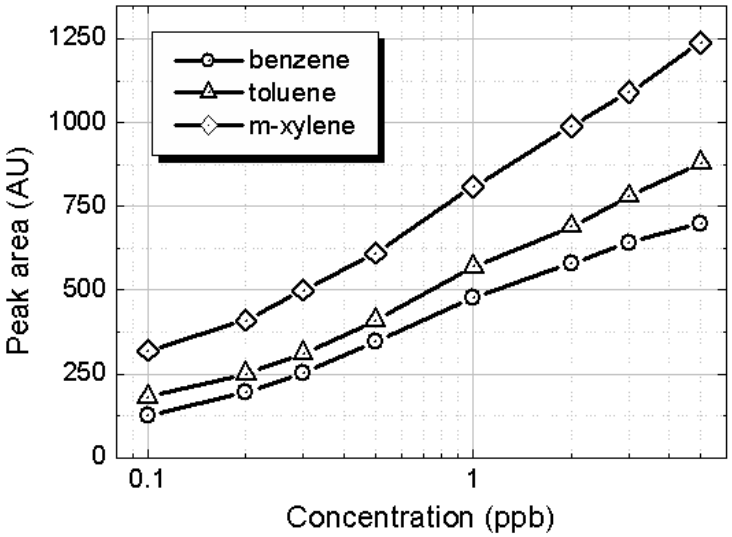

Figure 2.26. Calibration curve: peak area as function of analyte concentration of benzene toluene and m-xylene.

A regular trend of the peak areas as a function of the gas concentrations in a semi-logarithmic scale was found. The nonlinearity of the correlation is due to the non-linearity of the MOX sensors used as detector, which are well known

to saturate at high concentrations. Nevertheless, the regular trend of Figure 2.25 allows a precise calibration of the system. The relation of peak area as a function of gas concentrations was found to be stable and reproducible within two months measurements. Preliminary measurements in real outdoor air were successfully performed, and the system is now being characterized in direct comparison with a commercial GC used for environmental monitoring.

2.2.7 REAL WORLD MEASUREMENTS

After the tests in laboratory, Real-Word tests were performed to evaluate the possibility of a real application as benzene sensor in the environmental monitoring on the streets. Our prototype was put in a A.R.P.A. Control Station in Bologna. The control station use a commercial gas chromatograph (Syntech Spectras GC855) to estimate the concentration of benzene through a validated method. Despite some minor problems such as the high temperature of the station that does non allow a fast cooling of the prototype unit and the presence in the chromatograms of unknown peaks due to residual aliphatic VOCs present in very high concentration in air, a complete parallel set of measurements was performed.

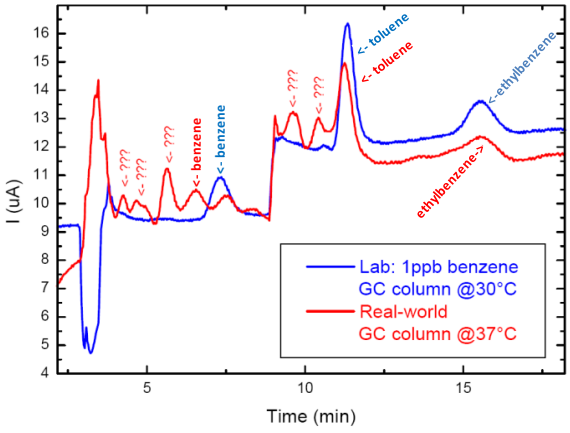

Figure 2.27. Superimposition of Real-World chromatogram (red line) with the laboratory measurement at 1 ppb (blue line).

In the Figure 2.27 is reported a comparison between the Real-Word chromatogram and the laboratory measurements. The real world chromatogram is more complicated due to the presence of unknown peaks and to minimize the errors in the evaluation of benzene we thought to correlate the concentration of benzene to the height of the peaks rather then to the area. The shift between the benzene peak in laboratory and in real world measurements is due to the different temperatures of the GC separation column.
Comparing our results with the measurement of A.R.P.A. system we can conclude that the two system give the same values for the benzene concentration. In fact despite of small different the daily average concentration is very close as shown in Figure 2.28.

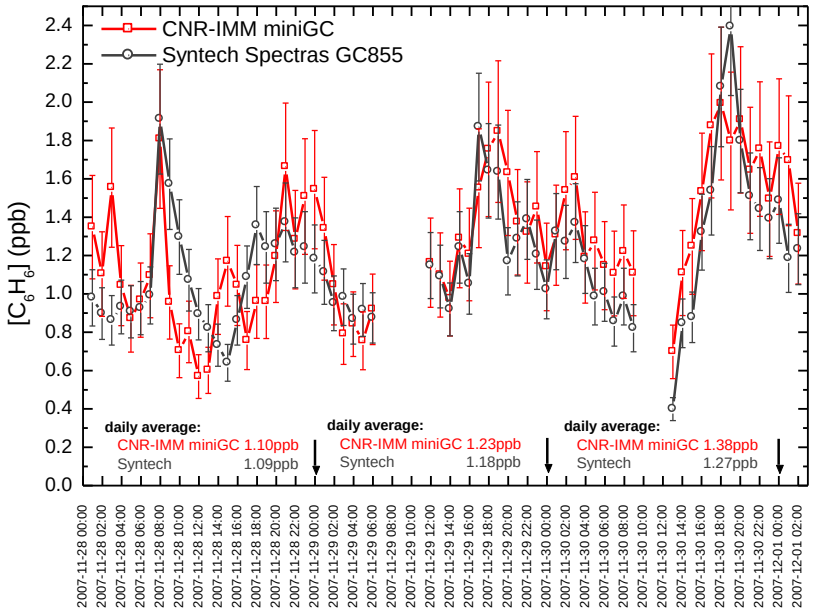

Figure 2.28. Comparison between our prototype (red squares) and ARPA system (black circles) measurements.

The outcome of three month of continuous measurement in the streets of Bologna validated the ability of our analytical system to detect benzene at low ppb level. The positive comparison with the state of the art GC instrument

bodes well for the use of this supramolecular device in the environmental monitoring of benzene.

2.2.8 DEEPER AND MORE RIGID CAVITIES

Despite the very promising results of the quinoxaline bridged cavitand, the possibility to make a material able to concentrate and selectively separate via thermal desorption benzene from the other aromatic VOCs is very appealing.
The main problem of working whit QxCav is that it is conformationally flexible and flutters between C_{4v} and C_{2v} symmetries.[13] The former is preferred at higher temperature and has all four "walls" up. The latter has this wall flipped outward in a kite-like shape and is the dominant conformation below room temperature. In solution the barrier of to interconversion is typically 10-12 kcal/mol. Thanks to this flexibility the QxCav is a good host for all the aromatic VOCs. However this "versatility" is probably the reason why we are unable to selectively desorb the analytes, since the desorption is run at relatively high temperature, where breathing of the cavity can occur also in the solid state.
Within the last ten years, numerous synthetic attempts were made to deeper the cavity, rigidify the structure and functionalize the cavitand surface for further application.
One interesting class of cavitands, called self-folding cavitands, develop by Rudkevich and Rebek in 1997[14] is reported in figure 2.29.

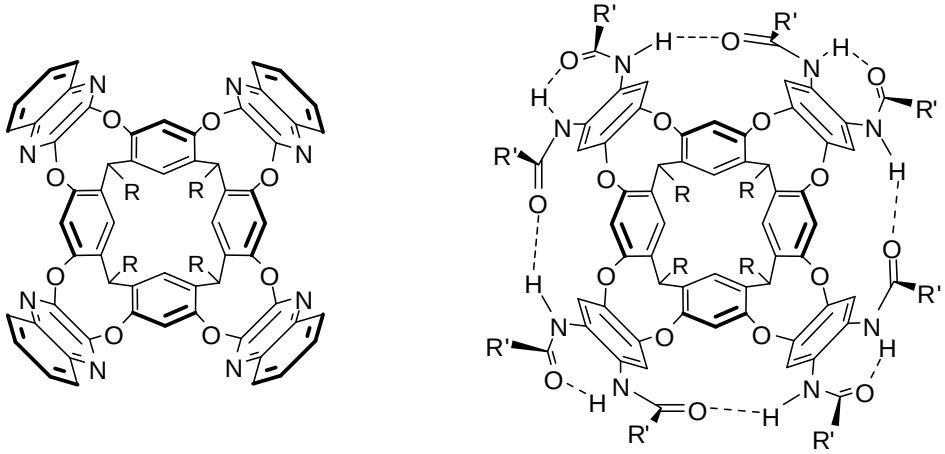

Figure 2.29. Molecular structures of Quinoxaline cavitand (left) and Octa-amido cavitand (right).

In Octa-amido cavitands, the vicinal secondary amines at the upper rim of the molecule form intermolecular, intraanular hydrogen bonds through a seven-membered ring and also bridge-adjacent rings. The result is a self-folded deep vase. The amine groups deepen the cavity to a dimension of ca. 8 x 10 Å. The size and the shape of the cavity resembles very much that of QxCav with the additional feature that the vase form is stabilized by hydrogen bonds.
We reasoned that a more rigid cavity would have allowed a more selective thermal desorption of aromatic VOCs, thus avoiding the need of the miniaturized GC column after the pre-concentration unit.
Most often, the resorcinarene-based cavitands are prepared by coupling resorcinarene with an appropriate bridging module. The yield of these reactions are not uniformly high. In this case, a different synthetic strategy was pursued. First, the resorcinarene was coupled with 1,2-difluoro-4,5-dinitrobenzene followed by a reduction to amine and subsequently acylated with appropriate acyl chlorides under Schotten-Baumann condition.
The 1,2-difluoro-4,5-dinitrobenzene is not commercially available so we performed an aromatic nitration via electrophilic aromatic substitution on 3,4 difluoronitrobenzene.

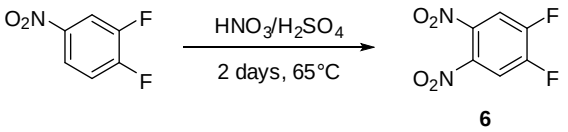

Scheme 2.3. Synthesis of 1,2-difluoro-4,5-dinitrobenzene (**6**).

In the second step the resorcinarene was bridged with 1,2-difluoro-4,5-dinitrobenzene in DMF in the presence of Et_3N at 65°C to give the octanitro cavitand [15].

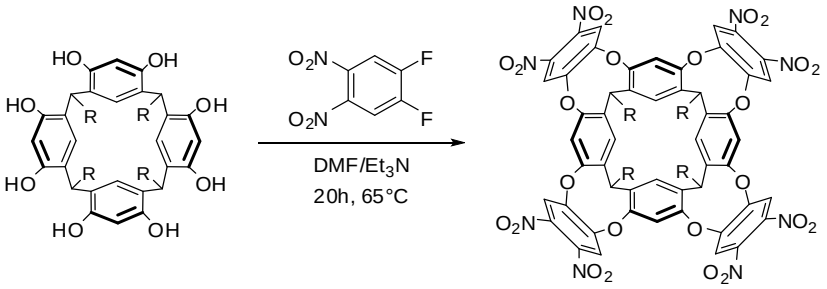

Scheme 2.4. Synthesis of octanitro cavitands (**7**: R=C_2H_5, **8**: R=C_5H_{11}, **9**: R=$C_{11}H_{23}$).

The subsequent reduction can be performed in several ways. In one article[16] H_2 and Raney-Ni are employed, in another article[17] tin chloride in the presence of hydrochloric acid is used. We preferred to use the latter methodology since it is more efficient.

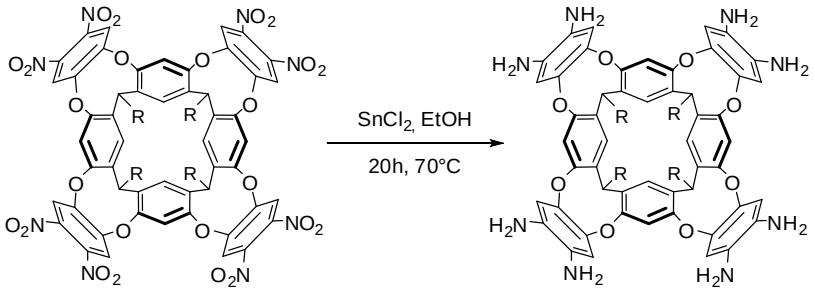

Scheme 2.5. Synthesis of octa-amine cavitands (R=C_2H_5, R=C_5H_{11}, R=$C_{11}H_{23}$).

The Octaamine cavitand obtained was immediately acylated with propionyl chloride in AcOEt/H_2O in presence of K_2CO_3 to afford octaamide cavitands **10**, **11**, and **12**.

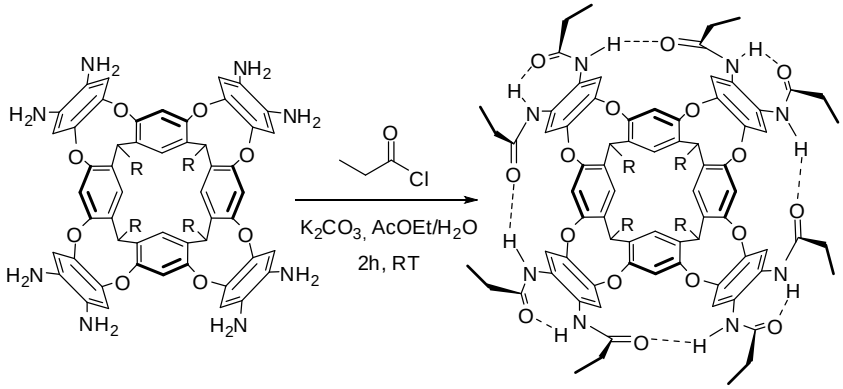

Scheme 2.6. Synthesis of octa-amido cavitands (**10**: R=C_2H_5, **11**: R=C_5H_{11}, **12**: R=$C_{11}H_{23}$).

2.2.9 OaCav measurements

We synthesized three cavitands having different chains at the lower rim with R = C_2H_5 (**10**), C_5H_{11} (**11**), and $C_{11}H_{23}$ (**12**) to test also in this case the effect of the alkyl feet on VOCs adsorption.
The earlier tests were made with the longer chains octa-amido cavitand. In the Figure 2.30 we report the measurements made with a 30 sccm flux.

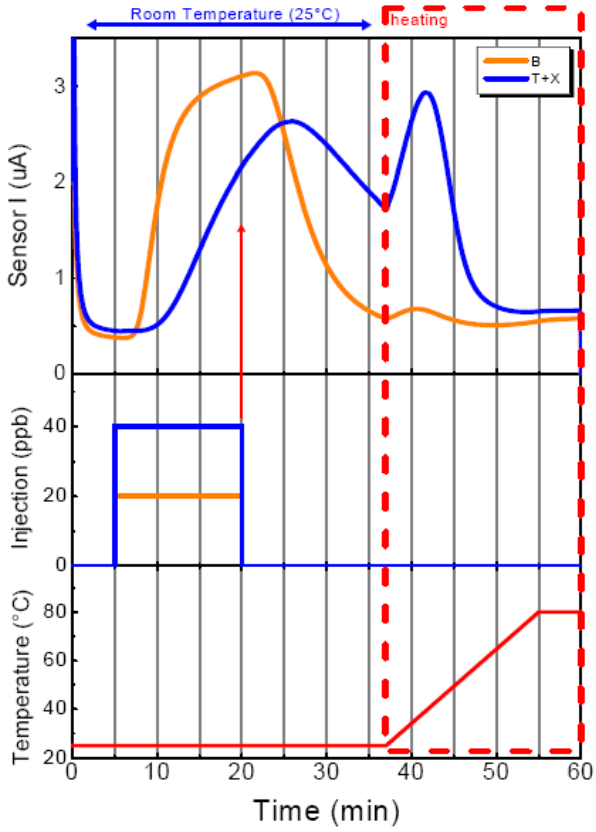

Figure 2.30 Adsorption/desorption plot of OaCavC11(**12**) together a plot of injection concentration and thermal ramp.

The orange line represents the injection of 20 ppb of benzene while the blue line 40 ppb of mixture of toluene and xylenes. The adsorption at 25°C was very low but we can notice a difference between the response of benzene and

other analytes. After 35 minutes at room temperature the trap was heated from room temperature to 80°C and the release of toluene and xylenes was accelerated, while the benzene was already desorbed at room temperature. This results suggest that the cavitand at 25°C may work as a "separator" instead as "pre-concentrator". A different behavior between the kinetics of desorption of benzene and other aromatic VOCs is our target from the start of this study. However the efficiency of adsorption is very low and it is probably due to the presence of long alkyl chains at the lower rim, as reported previously for the corresponding quinoxaline cavitand.
Following the same research path used for QxCav we tested also the OaCavC5 (**11**) cavitand.
The absorption/desorption plot of OaCavC5 (**11**) reported in Figure 2.31 show a very high adsorption efficiency, with only a minimum presence of breakthrough.

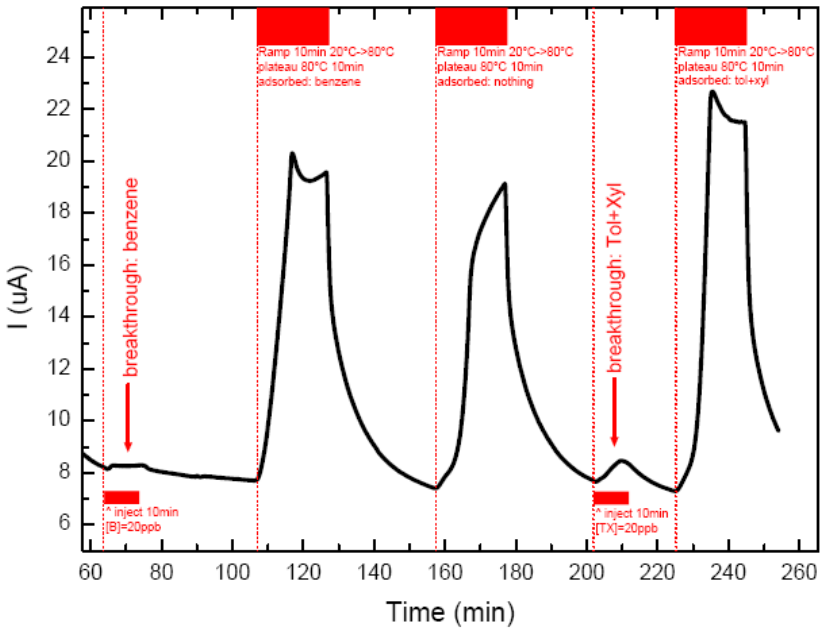

Figure 2.31. Adsorption/desorption plot of OaCavC5 (**11**).

The sensor response in absence of the analytes (second peak in Figure 2.31) is due to the change in temperature of the carrier gas. Also the adsorption

efficiency of toluene and xylene is quite good although it does not reach the 100% of efficiency obtained with QxCav.
This results, together with those obtained by OaCavC11 (**12**) suggest the possibility to desorb selectively the benzene before the other VOCs. If we slowly heat the "trap" from 20°C to 100°C in ten minutes we obtain the sensor responses reported in Figure 2.32:

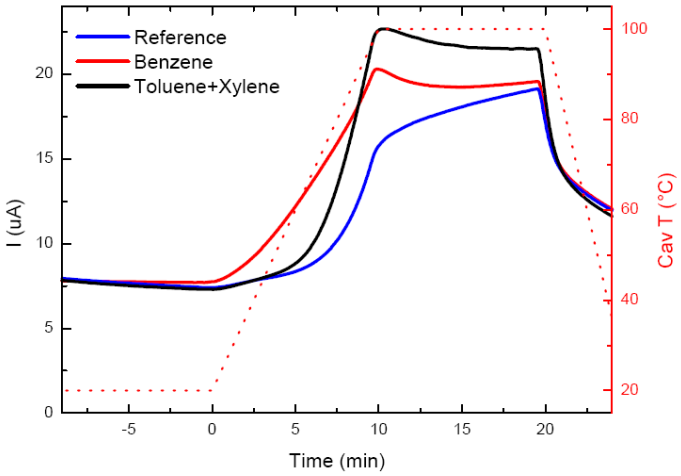

Figure 2.32. Measurement of desorption kinetics of OaCavC5 (**12**).

The plot represents the desorption after sampling 20 ppb of benzene (red) or a mixture of 5 ppb of toluene and 5 ppb of xylenes (black) together with a reference line (blue). From this plot we can observe that the benzene release starts before, at 30°C, and the other analytes start to desorb after 50°C.
We used this experimental evidences to develop a thermal steps ramp to optimize the desorption of the benzene only. The ramp started from the room temperature of 20°C and in 15 seconds was heated at 40°C and then it was keep constant for 15 minutes. Afterwards two steps of 20°C for 15 minutes were applied to reach 80°C, followed by a cleaning cycle at 120°C.
As reported in the Figure 2.33, when the first heating step starts, only benzene is released by the cavitands and the other analytes remain complexed into the cavities.

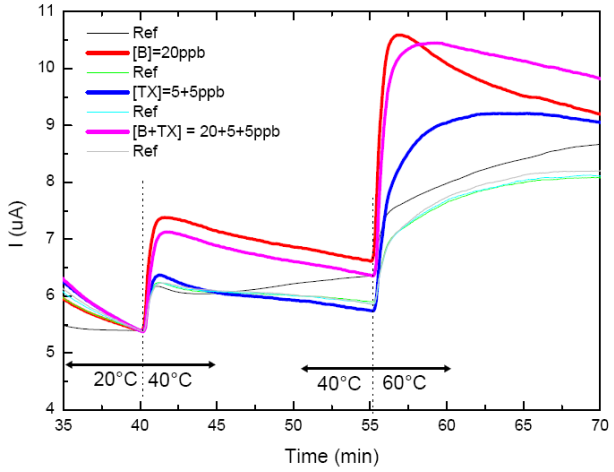

Figure 2.33. Measurement of desorption kinetics of OaCavC5 (**11**) with thermal steps ramp.

Not all the benzene was released in the first step but is the only species released. Better results are obtained with the shorter chains cavitands, in fact the OaCavC2 shows a beautiful peak of desorption, also with a linear heating ramp as report in Figure 2.34:

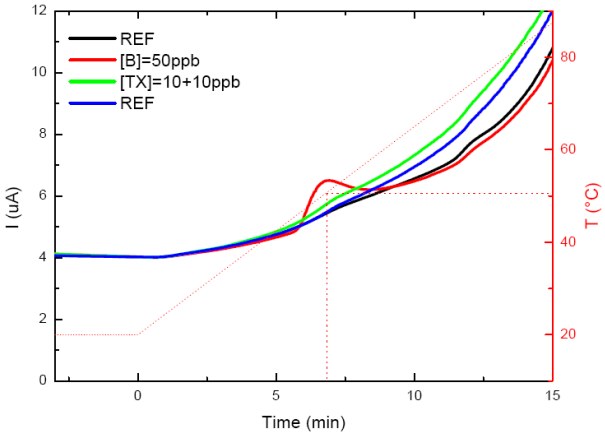

Figure 2.34. Measurement of desorption kinetics of OaCavC2 (**10**).

However despite this good results, this kind of cavity cannot be used in our system for the detection of the benzene in air, due to high baseline values of the sensor. Typically a MOX baseline without cavitand was 0.3 μA, but in the case of a OaCav online the baseline reached values over 60μA. After a cleaning of ten days in nitrogen flux at the temperature of 100°C we reach a baseline value less than 5 μA, sufficient for preliminary measures but not for evaluation of benzene at ppb level. The reason of this behavior was water. The water, that is present in air (also in the air used as carrier gas), was complexed by OaCav in high amount during the cleaning procedures and released in small amount during the measurements. This hypothesis is supported by the fact that the cavity presents an hydrogen bonding network at the upper rim and the water can participate in it. This limitation hampers the use of OaCav to sample benzene in atmospheric air.

2.3 Conclusions

In summary, a palm-sized sensor prototype for the detection of airborne benzene was fabricated, integrating QxCav as selective concentration material, a micromachined gas chromatographic column and a MOX sensor array as detector. QxCav showed excellent performances as concentration material in terms of absorption efficiency, desorption kinetics and reproducibility.
Furthermore, with QxCav being selective as sorbent material, only aromatic VOCs are retained from the sampled gas, greatly reducing the necessary resolution of the GC column. QxCav sampling and desorption are not influenced by relative humidity, making the system suitable for direct environmental sampling of aromatic VOC. All these advantages make the proposed monitoring system capable of complying with the strict EU legislation, which requires threshold values for benzene below 0.7 ppb (≈2 μg m^{-3}) by 2010.
Preliminary tests in the real environment (a detecting position in Bologna) showed promising results. Our system has been tested in parallel with a certified GC-MS giving comparable results (see Figure 2.28). Our device is cheaper, smaller, and more robust than the existing technology. Moreover it does not require inert gas to work and its maintenance is very simple. All these features make this miniaturized system a valuable alternative for environmental monitoring of benzene.

2.4 Acknowledgements

S. Zampolli, I. Elmi, G. C. Cardinali, M. Severi, L. Masini, A. Zani, M. Passini, M. Sanmartin, F. Tamarri, P. Negrini, G. Pizzocchero and S. Guerri of CNR-IMM for the setup of the MOX sensor and the prototype.
E. Menozzi for the help in the synthesis of octa-amido cavitands.

2.5 Experimental section

General method: All commercial reagent were ACS reagent grade and used as received. For the synthesis all solvents were dried over 3 Å and 4 Å molecular sieves. The ^{1}H-NMR spectra were recorded on Bruker Avance 300 (300 MHz) spectrometer and all chemical shifts (δ) were reported in parts per million (ppm) relative to proton resonances resulting from incomplete deuteration of NMR solvents. ESI-MS experiments were performed on a Waters ACQUILITY SQD Detector equipped with a ESCi® multi mode ionization (APCI/ESI).
Column chromatography was performed using silica gel 60 (Merck 70-230 mesh). Resorcinarenes R=CH_3, R=C_2H_5, R=C_5H_{11}, R=C_6H_{13}, and R=$C_{11}H_{23}$ were prepared according to literature procedures[18].

2,3-Dibromopyrazine (1): 2,3-dichloropyrazine (2.0 g, 13,3 mmol) and phosphorous tribromide (12 mL, 1.27 mol) were mixed and stirred at 180°C for 24h. The reaction was monitored via GC-MS until the formation of desired product. The dark solution was poured in cold water and extracted with diethyl ether. The organic layer was evaporated *in vacuum* to give the pure product (2.93 g, 92%).
^{1}H NMR (300 MHz, $CDCl_3$): δ= 8.32 (s, 2H, Ar*H*); **GC-MS**: *m/z* (%): 238 [M, 100].

Pyrazine-bridge Cavitand (R=C_2H_5) (2): A mixture of resorcinarene (R:C_2H_5) (0.504 g, 0.84 mmol), K_2CO_3 (0.927 g, 6.72 mmol) and 2,3-dibromopyrazine (1.00 g, 4.2 mmol) in 15 mL of DMF was stirred in a sealed tube at 80°C for 18h. The reaction was quenched by addiction of HCl_{aq} (10%) and the solid formed was filtered, washed with water, and dried. The crude product was purified by column chromatography on silica gel by using CH_2Cl_2/EtOH (9:1 v/v) as eluant to give compound **2** as a white solid (0.393 g, 52%).
^{1}H NMR (300 MHz, $CDCl_3$): δ= 8.14 (s, 8H, Pz*H*), 7.86 (s, 4H, Ar*H*), 7.71 (s, 4H, Ar*H*), 5.40 (t, 4H, C*H*Ar_2, J=7.8 Hz), 2.43 (m, 8H, C*H*$_2$$CH_3$), 0.96 (t, 12H, C*H*$_3$, J=6.4 Hz); **MS (CI)** *m/z* (%): 905 [M^+, 100].

Quinoxaline-bridge Cavitand (R=CH_3) (3): Resorcinarene (R:CH_3) (1.00 g, 1.83 mmol) and 2,3-Dichloroquinoxaline (1.60 g, 8.03 mmol) were dissolved in 60

mL of dry DMF. K_2CO_3 (3.00 g, 21.7 mmol) was added, and the mixture was stirred at 90°C for 16h. The reaction was quenched by addiction of HCl_{aq} (10%) and the solid formed was filtered, washed with water, and dried. The residue was purified by column chromatography on silica gel by using CH_2Cl_2/EtOH (95:5 v/v) as eluant to give compound **3** as a white solid (0.598 g, 31%).
^{1}H NMR (300 MHz, $CDCl_3$): δ= 7.91 (s, 4H, Ar*H*), 7.82 (m, 8H, AA' part of an AA'BB' system), 7.53 (m, 8H, BB' part of an AA'BB' system), 7.20 (s, 4H, Ar*H*), 5.36 (bq, 4H, C*H*Ar_2), 1.77 (d, 12H, CH_3, J=7.3 Hz); **ESI-MS** *m/z* (%): 1050 [M+H$^+$, 100].

Quinoxaline-bridge Cavitand (R:C_6H_{13}) (4): Resorcinarene (R:C_6H_{13}) (10.00 g, 12.1 mmol) and 2,3-Dichloroquinoxaline (10.6 g, 53.3 mmol) were dissolved in 350 mL of dry DMSO in presence of an excess of K_2CO_3 (16.7 g, 121 mmol). The mixture was heated and stirred for 16h at 80°C. The reaction was quenched by addiction of acidic water (with HCl) and the solid formed was filtered, washed with water, and dried. The crude product was crystallized from ethyl acetate : chloroform (9:1 v/v) to afford the pure product as white solid (14.2 g, 88%).
^{1}H NMR (300 MHz, $CDCl_3$): δ= 8.13 (s, 4H, Ar*H*), 7.77 (m, 8H, AA' part of an AA'BB' system), 7.45 (m, 8H, BB' part of an AA'BB' system), 7.19 (s, 4H, Ar*H*), 5.54 (t, 4H, C*H*Ar_2, J=7.9 Hz), 2.25 (m, 8H, CHCH_2), 1.55-1.31 (m, 32H, CH_2), 0.90 (t, 12H, CH_3); **ESI-MS** *m/z* (%): 1328 [M+H$^+$, 100].

Quinoxaline-bridge Cavitand (R:$C_{11}H_{23}$) (5): 2,3-dichloroquinoxaline (420 mg, 2.11 mmol) and K_2CO_3 (0.500 g, 3.62 mmol) was added to a solution of resorcinarene (R:$C_{11}H_{23}$) (0.40 g, 0.36 mmol) and 30 mL of dry DMF. The mixture was stirred at 80°C for 18h. The reaction was quenched in acidic water by addiction of HCl_{aq} (10%) and the solid formed was filtered, washed with water, and dried. The residue was purified by column chromatography on silica gel starting form Hexane/Ethyl Acetate (9:1 v/v) to Hexane/Ethyl Acetate (8:2 v/v) as eluent and then recrystallized from CH_2Cl_2 whit ethanol to give compound **5** as a white solid (0.355 g, 61%)
^{1}H NMR (300 MHz, $CDCl_3$): δ= 8.15 (s, 4H, Ar*H*), 7.78 (m, 8H, AA' part of an AA'BB' system), 7.45 (m, 8H, BB' part of an AA'BB' system), 7.21 (s, 4H, Ar*H*), 5.57 (t, 4H, C*H*Ar_2, J=7.9 Hz), 2.25 (m, 8H, CHCH_2), 1.28 (m, 72H, CH_2), 0.90 (t, 12H, CH_3); **ESI-MS** *m/z* (%): 1611 [M+H$^+$, 100].

1,2-difluoro-4,5-dinitrobenzene (6). To 87.7 mL of red fuming nitric acid 124,4 mL of sulfuric acid were added dropwise at 0°C in a 2 L flask in 1h30. 3,4 difluoronitrobenzene (50g, 0.31 mol) was slowly added to the solution in 3h at 0°C . The solution was sequentially warm up at 35°C for 1h, at 45°C for 1h at 55°C for 1h and at 65°C for 1h, then 2 days at 65°C. The reaction was cooled down at room temperature and nitrogen was bubbled to remove the excess of HNO_3. The flask was cooled at 0°C and a white precipitate started to form. The water (upper layer) was removed and several amounts of water was added. The mixture was extracted with dichloromethane and the organic phase washed with $NaHCO_3$ 10% and evaporated to give an oil. The pure compound (14.0g, 22%) was obtained by recrystallization from dichloromethane.
^{1}H NMR (300 MHz, $CDCl_3$): δ= 7.85 (t, 2H, J=7.6 Hz); **GC-MS**: *m/z* (%): 204 [M, 100].

Octanitro cavitand (R=C_2H_5) (7). To a solution of resorcinarene R=C_2H_5 (3 g, 5 mmol) and 1,2-difluoro-dinitrobenzene (4.04 g, 20 mmol) in 120 mL of dry DMF NEt_3 (10.55 mL, 80.7 mmol) was added dropwise, in N_2 atmosphere. The mixture was heated at 65°C for 20h. The solvent was removed *in vacuum* and the residue treated with 20 mL of CH_2Cl_2. The precipitate was filtered off and it was suspended in methanol and sonicated for 5 min. After filtration the precipitate was washed with methanol to give 2.57 g of octanitro cavitand as yellow solid. After evaporation of the mother liquor and suspension of the residue in methanol followed by treatment of the collected precipitate with methanol another 2.61 g was obtained (overall yield 82%).
^{1}H NMR (300 MHz, DMSO-d_6): δ= 8.85 (s, 8H, Ar*H*), 8.26 (s, 4H, ArH_d), 7.83 (s, 4H, ArH_u), 5.41 (bm, 4H, C*H*Ar_2), 2.44 (bm, 8H, C$H_2$$CH_3$), 0.92 (t, 12H, CH_2CH_3); **MALDI-TOF** *m/z* (%): 1257 [M+H^+, 80], 1280 [M+Na^+, 100] .

Octanitro cavitand (R=C_5H_{11}) (8). To a solution of resorcinarene R=C_5H_{11} (1.5 g, 1.81 mmol) and 1,2-difluoro-4,5-dinitrobenzene (1.85 g, 9.06 mmol) in 60 mL of DMF dry Et_3N (4.3 mL, 30.8 mmol) was added dropwise under nitrogen atmosphere. The solution was heated at 65°C for 20h, then cooled and diluted with 300 mL of water. The precipitate was filtered off, washed with water and dried. The pure product (760 mg, 28%) was purified by column chromatography on silica gel with CH_2Cl_2/Hexane (8:2 v/v) as eluant.
^{1}H NMR (300 MHz, DMSO-d_6): δ= 8.79 (s, 8H, Ar*H*), 8.46 (s, 4H, ArH_d), 7.79 (s, 4H, ArH_u), 5.50 (bt, 4H, C*H*Ar_2), 2.34 (bm, 8H, CHCH_2), 1.29 (m, 32H, CH_2-CH_2),

0.84 (t, 12H, CH_2CH_3); **MALDI-TOF** *m/z* (%): 1482 [M+H^+, 90], 1504 [M+Na^+, 100].

Octanitro cavitand (R=$C_{11}H_{23}$) (9). To a solution of resorcinarene R=$C_{11}H_{23}$ (2.0 g, 1.81 mmol) and 1,2-difluoro-4,5-dinitrobenzene (1.62 g, 7.90 mmol) in 80 mL of DMF dry Et_3N (4.0 mL, 28.9 mmol) was added dropwise under nitrogen atmosphere. The solution was heated at 65°C for 20h, then cooled and diluted with 400 mL of water. The precipitate was filtered off, washed with water and dried. The pure product (990 mg, 31%) was purified by column chromatography on silica gel with CH_2Cl_2/Hexane (75:25 v/v) as eluent.
^{1}H NMR (300 MHz, CDCl3): δ= 7.63 (s, 8H, Ar*H*), 7.27 (s, 4H, ArH_d), 7.00 (s, 4H, ArH_u), 3.92 (t, 4H, C*H*Ar_2), 2.05 (bm, 8H, CHCH_2), 1.23 (m, 72H, CH_2-CH_2), 0.87 (t, 12H, CH_2CH_3); **MALDI-TOF** *m/z* (%): 1761 [M+H^+, 100].

Octaamide cavitand (R=C_2H_5) (10). To a mixture of octanitro compound **7** (400 mg, 0.32 mmol) in EtOH (50 mL) and HCl_{Conc} (12 mL) $SnCl_2$ $2H_2O$(2.3 g, 10.2 mmol) was added under nitrogen atmosphere and the suspension was stirred for 20h at 70°C. The reaction was cooled and then poured onto 100 mL of water. The pH of the mixture was adjusted to 10 with 2 M aqueous NaOH, then two extraction with CH_2Cl_2 and ethyl acetate were performed and the combined organic layers were dried *in vacuum* without heating to obtain a oil. In a flask the oil was dissolved in 50 mL of ethyl acetate and 10 mL of water containing K_2CO_3 (360 mg, 2.61 mmol) was added. To this vigorously stirred mixture two portion of CH_3CH_2COCl (2x 230 uL, 2.60 mmol) were added by syringe at 0 and 30 min at room temperature and the reaction was stirred for other 1h. The crude product was obtained by extraction with ethyl acetate and then it was purified by column chromatography on silica gel using Ethyl Acetate /Hexane (8:2 v/v) as eluant and recrystallized from CH_2Cl_2 and Hexane to give the pure product as yellow solid (203 mg, 43%).
^{1}H NMR (300 MHz, Acetone-d_6): δ= 9.45 (s, 8H, N*H*), 7.86 (s, 4H, ArH_d), 7,69 (s, 8H, Ar*H*), 7.48 (s, 4H, ArH_u), 5.63 (t, 4H, C*H*Ar_2), 2.82-2.39 (m, 24H, CH_2CH_3 + COCH_2), 1.16 (t, 24H, $COCH_2CH_3$), 0.96 (t, 12H, $CH_2CH_2CH_3$); **MALDI-TOF** *m/z* (%): 1487 [M+Na^+, 20], 1503 [M+K^+, 100].

Octaamide cavitand (R_2=C_5H_{11}) (11). To a suspension of octanitro compound **8** (115 mg, 0.08 mmol) in EtOH (40 mL) and HCl_{Conc} (8 mL) $SnCl_2$ $2H_2O$ (526 mg, 2.33 mmol) was added under nitrogen atmosphere and the mixture was stirred

for 20h at 70°C, then cooled and then poured onto 30 mL of water containing K_2CO_3 (11.0 g, 80 mmol). In a flask the pH of the mixture was adjusted to 8-9 then 30 mL of ethyl acetate and the mixture was vigorously stirred. Two portions of CH_3CH_2COCl (2x 300 uL, 3.40 mmol) were added by syringe at 0 and 30 min at room temperature and the reaction was stirred for another 1h. The crude product was obtained by extraction with ethyl acetate and then with CH_2Cl_2 and it was purified by column chromatography on silica gel using CH_2Cl_2/MeOH (995:5 v/v) as eluant and recrystallized form CH_2Cl_2 and Diethyl Ether to give the pure product as yellow solid (35 mg, 27%).
^{1}H NMR (300 MHz, $CDCl_3$): δ= 9.88 (bs, 8H, N*H*), 9.12 (bs, 4H, Ar*H*), 7,75 (s, 8H, ArH_d), 7.29 (s, 4H, ArH_u), 5.76 (t, 4H, C*H*Ar$_2$), 2.72-2.16 (m, 24H, CH_2CH$_3$ + COCH_2), 1.24 (t, 24H, $COCH_2CH_3$), 0.90 (t, 12H, $CH_2CH_2CH_3$); **MALDI-TOF** *m/z* (%): 1713 [M+Na$^+$, 100], 868 [M+2Na$^+$, 70].

Octaamide cavitand (R=$C_{11}H_{23}$) (12). A mixture of octanitro compound **9** (200 mg, 0.11 mmol) and $SnCl_2$ $2H_2O$(800 mg, 3.6 mmol) in 40 mL of EtOH and concentrated HCl (15 mL) was stirred for 18 h at 70°C under nitrogen atmosphere, cooled, and then poured onto 50 mL of water. The pH was adjusted to 9 with 2 M aqueous NaOH and 60 mL of ethyl acetate were added. The two layers mixture and K_2CO_3 (1.1 g, 0.80 mmol) was vigorously stirred and two portion of CH_3CH_2COCl (300 uL, mmol) was added by syringe at 0 and 30 min at room temperature and the reaction mixture was stirred for other 2 h. The organic layer was separated, and the aqueous layer was extracted with CH_2Cl_2. The combined organic layers were washed with water and then evaporated. Pure amide was obtained as colorless solid by column chromatography on silica gel using CH_2Cl_2/MeOH (995:5 v/v) as eluant to give compound **12** (94 mg, 42%).
^{1}H NMR (300 MHz, Acetone-d_6): δ= 9.42 (s, 8H, N*H*), 7.90 (s, 4H, ArH_d), 7,71 (s, 8H, Ar*H*), 7.49 (s, 4H, ArH_u), 5.83 (t, 4H, C*H*Ar$_2$), 2.52-2.39 (m, 24H, CH_2CH$_3$ + COCH_2), 1.78-1.16 (m, 72H, CH_2-CH_2), 1.12 (t, 24H, $COCH_2CH_3$), 0.89 (t, 12H, $CH_2CH_2CH_3$); **MALDI-TOF** *m/z* (%): 1992 [M+Na$^+$, 20], 2008 [M+K$^+$, 100].

2.6 References and Notes

[1] E. H. Daughtrey, Jr. K. D. Oliver, J. R. Adams, K. G. Kronmiller, W. A. Lonneman, W. A. McClenny *J. Environ. Monit.* **2001**, *3*, 166.
[2] W. Bourgeois, A. –C. Romain, J. Nicolas, M. Stuetz *J. Environ. Monit.* **2003**, *5*, 852.
[3] P. Nelli, E. Dalcanale, G. Faglia, G. Sberveglieri, P. Soncini *Sens. Actuators B* **1993**, *14*, 302; F. L. Dickert, U. P. A. Bäumler, H. Stathopulos *Anal. Chem* **1997**, *69*, 1000.
[4] P. Soncini, S. Bonsignore, E. Dalcanale, F. Ugozzoli *J. Org. Chem.* **1992**, *57*, 4608.
[5] M. Vincenti, E. Dalcanale, P. Soncini, G. Guglielmetti *J. Am. Chem. Soc.* **1990**, *112*, 445; M. Vincenti, E. Dalcanale *J. Chem. Soc. Perkin Trans. 2* **1995**, 1069.
[6] For NOx sorption with calixarenes see: D. M. Rudkevich, Y. Kang, A. V. Leonitiev, V. G. Organo, G. V. Zyryanov *Supramol. Chem.* **2005**, *17*, 93; P. K. Thallapally, B. P. McGrail, J. L. Atwood *Chem. Commun.* **2007**, 1521.
[7] S. Zampolli, I. Elmi, J. Stürmann, S. Nicoletti, L. Dori, G.C. Cardinali *Sensor and Actuators B* **2005**, *105*, 400.
[8] Directive 2000/69/EC *Off. J. Eur. Communities* 13.12.**2000**, *L313/12*.
[9] F. Bianchi, R. Pinalli, F. Ugozzoli, S. Spera, M. Careri, E. Dalcanale *New. J. Chem.* **2003**, *27*, 502.
[10] P. Roncucci, L. Pirondini, G. Paderni, C. Massera, E. Dalcanale, V. A. Azov, F. Diederich *Chem. Eur. J.* **2006**, *12*, 4775.
[11] E. Dalcanale, P. Soncini, G. Bacchilega, F. Ugozzoli *J. Chem. Soc. Chem Commun* **1989**, 500.
[12] M. Vincenti, E. Pelizzetti, E. Dalcanale, P. Soncini *Pure Appl, Chem.* **1993**, *65*, 1507.
[13] J. R. Moran, J. L. Ericson, E. Dalcanale, J. A. Bryant, C. B. Knobler, D. J. Cram *J. Am. Chem. Soc.* **1991**, *113*, 5707.
[14] D. M. Rudkevich, G. Hilmersson, J. Rebek *J. Am. Chem.* **1997**, *119*, 9911.
[15] D. M. Rudkevich, G. Hilmersson, J. Rebek *J. Am. Chem. Soc.* **1998**, *120*, 12216.
[16] A. Shivanyuk, K. Rissanen, S. K. Körner, D. M. Rudkevich, J. Rebek *Helv. Chim. Acta* **2000**, *83*, 1778.
[17] C. H. Haas, S. M. Biros, J. Rebek *Chem. Commun* **2005**, 6044.
[18] L. M. Tunstad, J. A. Tucker, E. Dalcanale, J. Weiser, J. A. Bryant, J. C. Sherman, R. C. Helgeson, C. B. Knobler, D. J. Cram *J. Org. Chem.* **1989**, *54*, 1305-1312; E. E. Dueno, K. S. Bisht *Tetrahedron* **2004**, *60*, 10859.

3 Cavitand based Sol-Gel coatings for solid phase microextraction[⊗]

3.1 Introduction

Comprising over 70% of Earth's surface water is undoubtedly the most precious natural resource that exists on our planet. Water pollution, thus including the contamination of lakes, rivers, oceans, and groundwater can be caused by human activities. According to the American College Dictionary[1], pollution means: "to make foul or unclean, dirty", so water pollution occurs when different contaminants are present in water. Contaminants may include organic and inorganic substances. More precisely in this work we focused the attention on the detection of organic pollutants such as volatile organic compounds VOCs (i.e. industrial solvents), petroleum hydrocarbons (including fuels), and pesticides (i.e. insecticides and herbicides, a huge range of organohalides chemicals). The widespread need for fast, reliable, highly sensitive and selective analytical methodologies for measuring VOCs in the environment poses a fascinating challenge to the chemical community.

[⊗] The work reported in this Chapter has been carried out in collaboration with Federica Bianchi and Monica Mattarozzi of "Dipartimento di Chimica Generale ed Inorganica, Chimica Analitica, Chimica Fisica" of Parma University.

Most VOCs are water pollutants and a number of them are recognized as substances with a high toxicological priority by international organizations.[2] In particular, the detection of airborne aromatic hydrocarbons like benzene, toluene, ethylbenzene and xylene isomers (BTEX) constitutes a long standing problem, due to the need to measure with high precision extremely low analyte concentrations in the presence of overwhelming amounts of other aliphatic and aromatic hydrocarbons.

Most of the approaches implemented so far to solve the problem rely either on spectroscopic methods (LIDAR, etc.)[3] or on gas chromatography/mass spectrometry (GC/MS)[4]. This second approach requires the extraction and preconcentration of the analyte from the sample.

Solid phase microextraction (SPME), purge-and-trap, dynamic headspace are well know solvent-free techniques used for the sampling of volatile compounds from food[5] and environment[6].

SPME was introduced in the early 1990 as a new sampling and sample preparation method.[7] Since its conception, SPME has been widely applied to the sampling and analysis of environmental, food, aroma, forensic, and pharmaceutical matrices.[8] Thousands of articles about SPME have been published over time. Extraction is based on the use of a small silica fiber coated with a proper stationary phase (Figure 3.1).

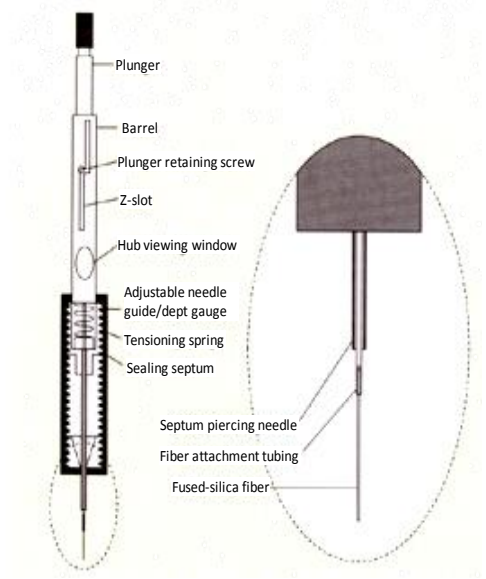

Figure 3.1. Detailed description of a SPME sampling device.

Two different extraction modes can be applied: 1) the headspace sampling (for the most volatile compounds) in which the fiber is exposed into the headspace over the sample and 2) the immersion mode (for the extraction of non volatile compounds from liquid samples) in which the fiber is directly immersed into the liquid matrix.
The solid phase microextraction process is shown in Figures 3.2-3.3. A 1 cm length of fused silica fiber, coated with a polymer, is bonded to a stainless steel plunger and installed in a holder that looks like a modified microliter syringe. The plunger moves the fused silica fiber in and out of a hollow needle. To use the unit, the analyst draws the fiber into the needle, passes the needle through the septum that seals the sample vial, and depresses the plunger, exposing the fiber directly to the sample or to the headspace above the sample.
Organic analytes are adsorbed onto the coating of the fiber. After sampling, the fiber is drawn into the needle, and the needle is withdrawn from the sample vial. Finally, the needle is introduced into the gas chromatograph injector, where the adsorbed analytes are thermally desorbed and delivered to the GC column, or into the SPME/HPLC interface (Figure 3.3).[9]

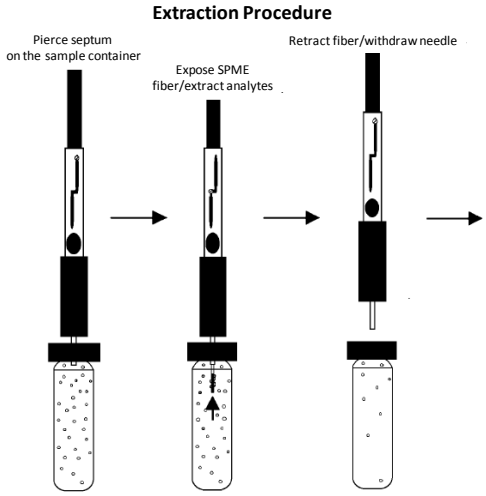

Figure 3.2 Extraction procedure with a SPME device.

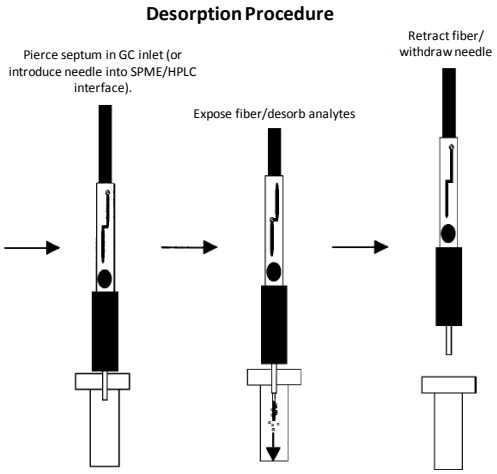

Figure 3.3 Desorption procedure with a SPME device.

In SPME, equilibria are established among the concentrations of an analyte in the sample or in the headspace above the sample, and in the polymer coating of the fused silica fiber. The amount of analyte adsorbed by the fiber depends on the thickness of the polymer coating, on its porosity, and on the partition coefficient of the analyte. The partition coefficient generally increases with the increasing of the molecular weight and boiling point of the analyte. Selectivity can be altered by changing both the type of polymer coating on the fiber and the coating thickness. In general, volatile compounds require a thick coating, whereas a thin coating is most effective for adsorbing/desorbing semivolatile analytes.

For polymeric SPME coatings, the amount of analyte adsorbed by the coating at equilibrium is directly related to the concentration of the analyte in the sample:

$$n = \frac{K_{fs} V_f C_0 V_s}{K_{fs} V_f + V_s}$$

where n = mass of analyte adsorbed by coating
C_0 = initial concentration of analyte in sample
K_{fs} = partition coefficient for analyte between coating and sample matrix
V_f = volume of coating
V_s = volume of sample

The equation shows that the relationship between the initial concentration of the analyte in the sample and the amount of analyte adsorbed on the coating is linear.[10] Through proper calibration, SPME can be used to quantitatively determine the concentrations of analytes in a sample.
The equation also shows that if V_s is very large ($V_s >> K_{fs}V_f$), the amount of analyte extracted by the fiber coating is not related to sample volume. This makes SPME ideally suited for *in situ* sampling and analysis. Thus significantly reducing analysis time by combining sampling, extraction, and concentration into a single process.
The analytes are adsorbed onto the stationary phase of the fiber and then thermally desorbed in the injector of the gas chromatograph. Although the advantages of SPME are related to the fact it is a solvent free. The most disadvantages are due to the limited range of available stationary phases only roughly covering the scale of polarity as well as to the absence of coatings with molecular recognition properties. In fact the commercially available coatings are based on the use of polydimethylsiloxane (PDMS), divinylbenzene (DB), polyacrylate (PA), Carboxen (CAR, a carbon molecular sieve), and Carbowax (CW, polyethylen glycol). Multi-bed fibers are also available in order to extend the field of possible applications.
The most common approach to overcome the above mentioned limitations is the tailor-made preparation of fiber coatings via sol-gel technology, which provides efficient incorporation of organic components into inorganic polymeric structures by operating under mild thermal conditions.[11] In general, the sol-gel process, involves the evolution of inorganic networks through the formation of a colloidal suspension (SOL) and gelation of the sol to form a network in a continuous liquid phase (GEL).[12] Through this process, homogeneous inorganic oxide materials with desirable proprieties of hardness, chemical and thermal resistance, polarity and porosity can be produced at room temperature. The precursors for synthesizing these colloids consist of a metal or metalloid element surrounded by various reactive ligands. Metal alkoxydes, such as the alkoxysilanes tetrametoxysilane (TMOS) or tetraethoxysilane (TEOS) are most popular because they react readily with water. To describe the sol-gel process at the level of functional groups, three consecutive reactions, as shown in Scheme 3.1, are generally used: hydrolysis (R1), water condensation (R2), and alcohol condensation (R3). As shown in reaction R1 alkoxyde groups are replaced with hydroxyl ones through the addiction of water. Subsequent condensation reactions (R2 and R3) involving the silanol groups produce siloxane bonds plus by-products i.e. water or alcohol.

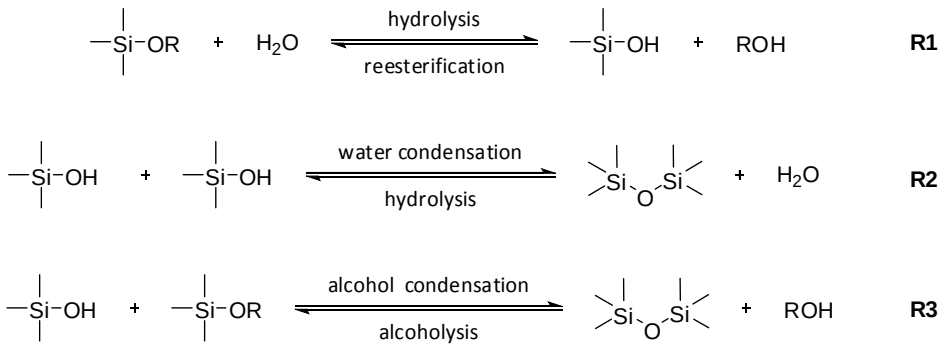

Scheme 3.1. Basic steps in sol-gel coating technology.

As the number of siloxane bonds increases, the individual molecules are bridged and jointly aggregate in the sol, which is a colloidal suspension (solid particles with a diameter of few hundred of nanometers in a liquid phase). When the sol particles aggregate, or cross-link into a network, a macromolecular gel is formed. Upon drying, trapped volatiles are driven off. Thin films can be produced on a piece of substrate by dip-coating, which is the most popular strategy for SPME fiber production. The use of the sol-gel technique has allowed the development of innovative coatings used for determination of BTEX[13], organophosphorous pesticides[14], aromatic amines[15], and phenolic compounds[16]. Different calix[4]arene compounds have been also applied to the determination of chloro-containig pesticides[17], chlorophenols[18], phenolic compounds[19], and polycyclic aromatic hydrocarbons (PAHs)[20]. However, the characteristics and proprieties of a particular sol-gel coating are strongly related to a great number of factors, such as, H_2O/Si molar ratio, pH, nature and concentration of the catalyst, temperature and time of reaction, aging temperature and time of drying during the synthesis of the coating.
The purpose of this work is to prepare innovative SPME fiber coatings via sol-gel technology including synthetic molecular receptors to impart selectivity to the resulting SPME fiber.

3.2 Result and discussion

3.2.1 MOLECULAR RECEPTOR

For this work we have chosen two different cavitands having methylene (MeCav) and quinoxaline (QxCav) bridges (Figure 3.4). The MeCav was synthesized to be used as model compound in the sol-gel experiments whereas the QxCav was chosen as molecular receptor for its deep cavity able to completely engulf aromatic guests, providing weak CH-π interaction with the cavity wall. QxCav complexation toward aromatic compounds have been demonstrated both in solution[21] and in the gas phase[22].

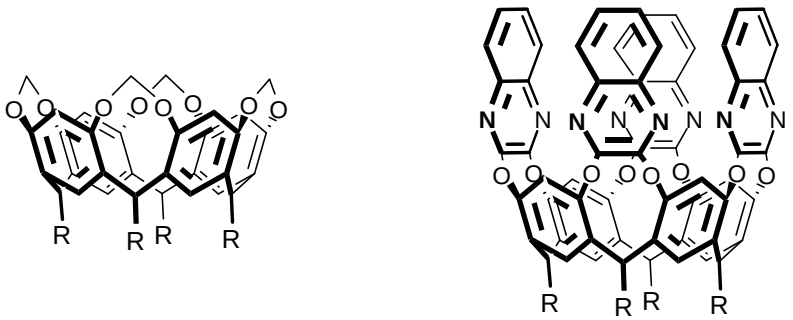

Figure 3.4. Chemical structures of methylene (MeCav) and quinoxaline (QxCav) bridged cavitands.

To be used as coating for silica fiber via sol-gel process the cavitands requires the introduction of a suitable substituent at the lower rim. Among the available sol-gel precursors, triethoxysilane was chosen as a consequence both of the mild polymerization conditions and of its regioselective introduction on the double bond of the alkyl chain (R) of the cavitand via hydrosilylation. More precisely the building block used for this purpose was a cavitand , having at the lower rim four chains with terminal double bonds. The synthetic protocol used required two steps: the functionalization of the upper rim with the appropriate bridging group, followed by the silylation at the lower rim. The fourfold bridging reactions were carried out following published procedures using bromochloromethane [23] , and 2-3-dichlorquinoxaline [24] respectively. The

hydrosilylation reaction was tested in a previous work[25] using two different catalysts: (H_2PtCl_6) and [$RhCl(PPh_3)_3$]. The first one led exclusively to the double bonds isomerization into internal olefins, while Wilkinson's catalyst favored the formation of mono and di-silylated derivatives. It has to be consider that the first aim of this study was based to the development of a synthetic procedure able to functionalization of the lower rim with the highest number of silylated groups (Figure 3.5).

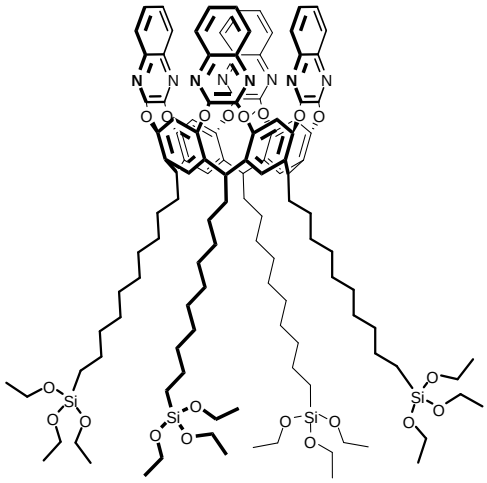

Figure 3.5. Target molecule with four silylated groups at the lower rim.

In fact by using the Wilkinson's catalyst it is possible to obtain only 7% of di-silylated and 45% of mono-silylated products. In order to improve the reaction different procedures were optimized i.e. the choice of catalyst and the solvent. Among the several catalysts available in literature[26] a catalyst based on Pt(0), named Karstedt's catalyst, reduces the occurrence of internal isomerization of the terminal olefin to less than 20%, which is the best result in this type of reaction (Scheme 3.2).
The hydrosilylation with the Karstedt's catalyst is usually carried out using toluene as reaction solvent but unfortunately this solvent could not be used for this study owning to its inclusion into the quinoxaline cavity.

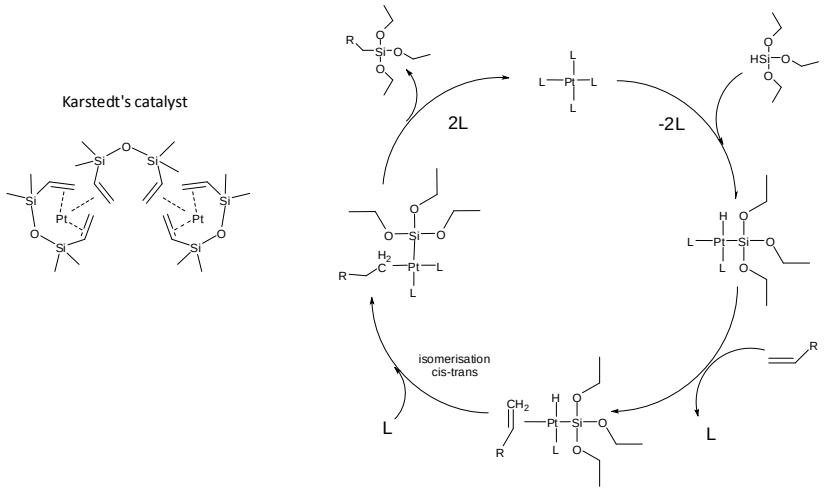

Scheme 3.2. Mechanism of hydrosilylation with Karstedt's catalyst

The selection of a new solvent for the quinoxaline cavitand **1** functionalization was required: the new solvent should dissolve all the reagents but it should have also a boiling point higher than 70°C to ensure the correct heating of the reaction at atmospheric pressure. We chose to use the cyclohexane since unlike aromatic solvents it is not complexed by the cavity and can be easily removed under reduced pressure (Scheme 3.3).

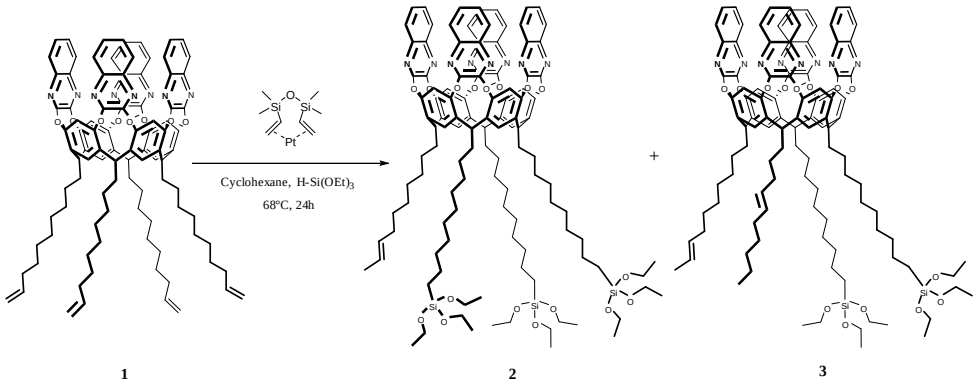

Scheme 3.3. Hydrosilylation of QxCav.

ESI-MS spectra showed the presence of both di- and tri-functionalized products (**3** and **2**). Whereas the integration of peaks of the siloxane moiety in ^{1}H-NMR spectra demonstrated that the tri-silylated **2** is the predominant product (Figure 3.6). Further purification to reach a better purity of cavitand **2** is useless because traces of di-functionalized and tetrafunctionalized by-products can take part to the formation of the network.

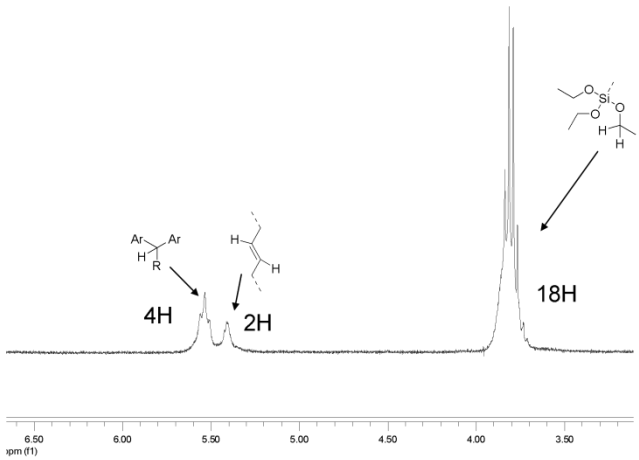

Figure 3.6. Expansion (6.50-3.00 ppm) of a 1H-NMR of **2** and **3** mixture in $CDCl_3$.

The problem of toluene as reaction solvent is not present in the case of the methylene-bridged cavitand **4** (scheme 3.4) because it has been demonstrated that the MeCav is unable to complex this small aromatic compound due to its small cavity dimension.

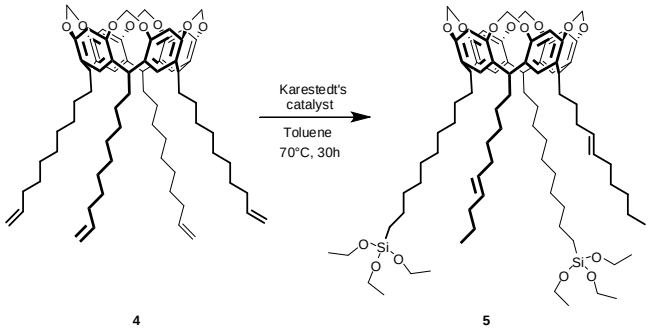

Scheme 3.4. Hydrosilylation of MeCav.

3.2.2 THE SOL-GEL

Sol-gel were used as a powerful and versatile technique for the development of new materials. In this study this procedure was used for the immobilization of the coating on the fiber support consisting in a silica rod of about 100 µm of diameter (Figure 3.7).

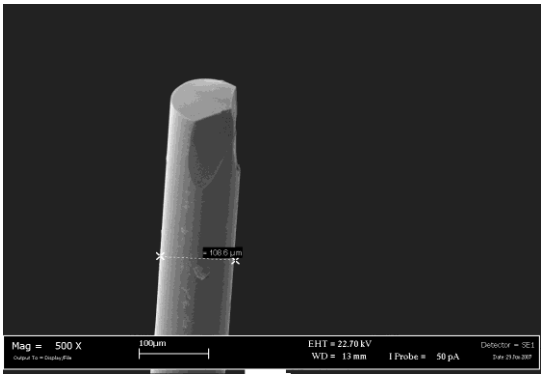

Figure 3.7. SEM image of a bare fiber (MAG 500X).

Prior to the use, the silica surface has to be cleaned and activated. Normally it is activated by immersion in NaOH solution[27] but the activation with HF 40% (v/v) was found to be more effective probably as a consequence of the etching on the silica surface. In fact by operating under these condition the Si-OH bonds can be easily exposed onto the surface, thus improving the adherence of the coating.

3.2.2.1 QXCAV SOL GEL WITH PLASTICIZER

The first approach to the sol-gel material preparation followed a protocol used by Zeng and coworker[15-20]. The original trick reported in their work is to use two silicon polymers as plasticizers (Hydroxy-terminated silicone oil and poly(methylhydrosiloxane)) in connection to tetraethoxysilane, a well known

precursor for inorganic networks. The presence of plasticizers contribute to relax the network otherwise rigid as reported in Figure 3.8.

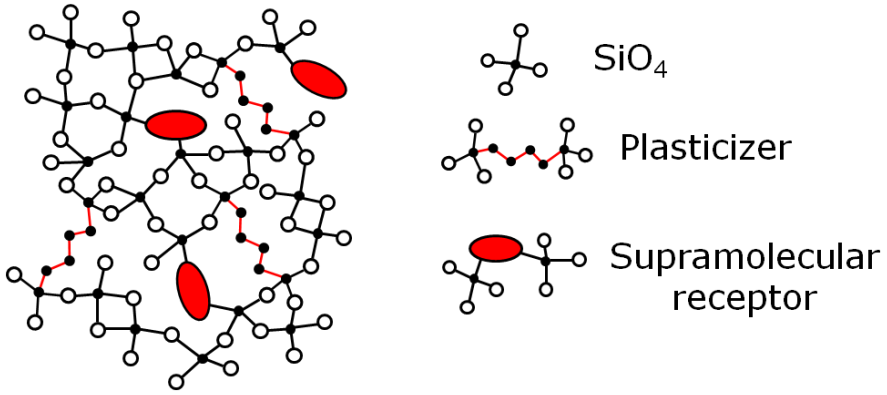

Figure 3.8. Graphic representation of a silica network with a plasticizer.

High network rigidity induces cracks or low adhesion to the substrate especially in the case of thin films.
In the formulation of our gel the first aspect to be considered was the choice of the solvent, because the synthesized cavitand is insoluble in the polar solvents normally used in the sol-gel process. We chose to use CH_2Cl_2 because it dissolves very well the cavitand and it has a low boiling point that allow a rapid drying. Unfortunately it is not miscible with one of the reagents, water, but, if mixed vigorously, it works very well. The second aspect was the ratio between plasticizer, matrix precursor, and the cavitand. The only way to obtain the right ratio is preparing many gels with different precursors ratio then analyzing the morphology of the gels after aging by SEM microscopy, until a good adherence and coverage of the substrate are obtained. Several experiments were carried out to maximize the cavitand concentration in the coating, while maintaining a reasonable gelation time to allow the dip-coating of the fiber. In fact the cavitand, being mainly tri-silylated, acts like a cross-linking agent and at high concentration level the gelation time was too short for the coating. The last aspect of the formulation was the choice of catalyst. There are three possible catalyst classes: basic and acid catalysts, and fluoride ions. We chose the acid catalysis since it allows a reduced cross-linking of the polymeric chains[28] (Figure 3.9). Trifluoroacetic acid (TFA) was selected for our case since it is a strong acid soluble in organic solvents.

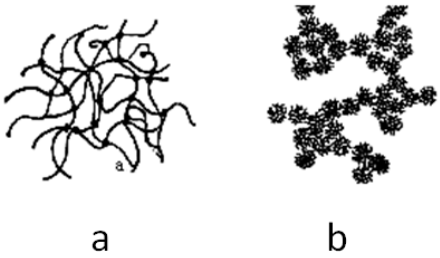

Figure 3.9. Structures of gel obtaining by: A)acid catalysis B)basic catalysis.

There are also other parameters to be considered in a sol-gel process such as the reaction and aging times as well as the temperature: all this parameters are able to influence the gelation time.
Several experiments were performed to reach the correct combination of all parameters to obtain the coated fiber.
In the following schemes we report a graphical representation of the steps involved in a sol gel process (schemes 3.5, 3.6, 3.7, 3.8).
In the first step we have the hydrolysis of the ethoxysilane groups of cavitand **2** and TEOS catalyzed by trifluoroacetic acid.

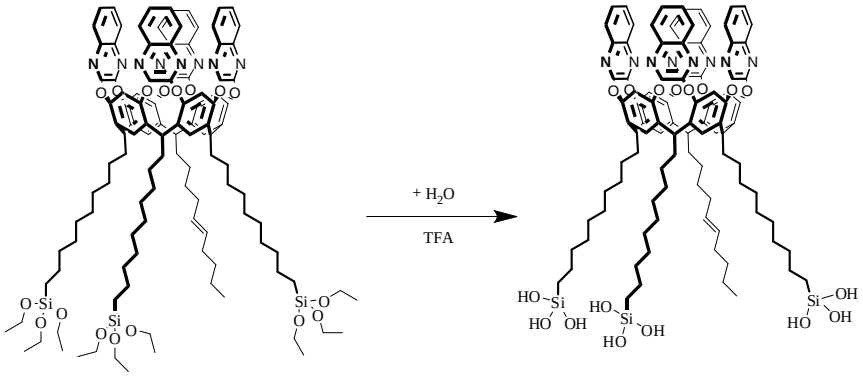

2

Scheme 3.5. Hydrolysis of cavitand **2**.

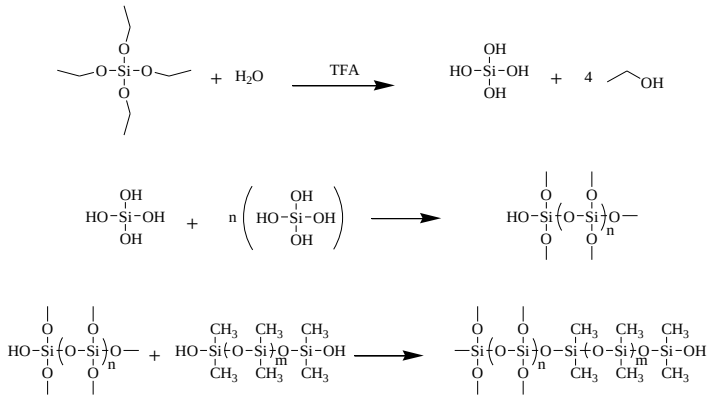

Scheme 3.6. Hydrolysis of sol precursor.

After the hydrolysis, the network starts to grow via a condensation reaction that involves also the plasticizer as generically shown in Scheme 3.7.

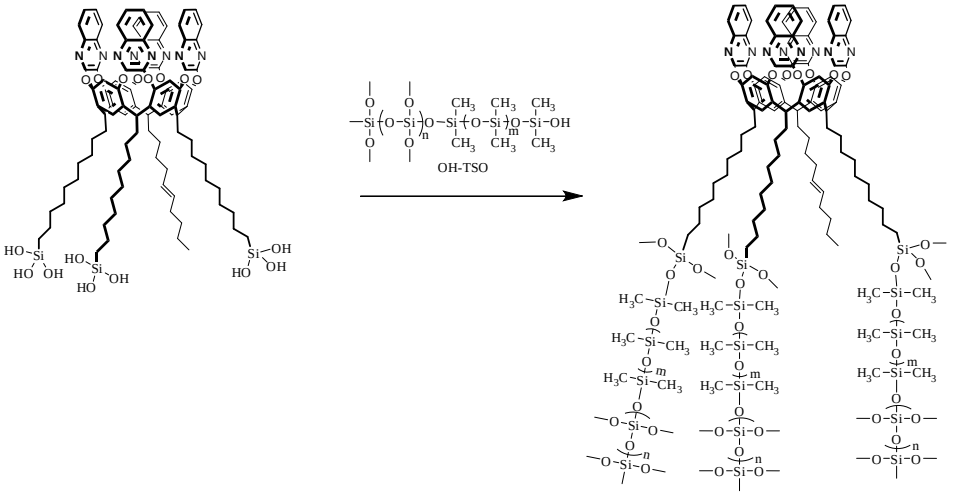

Scheme 3.7. Sol-Gel process of the cavitand receptor

When the sol reaches the adequate viscosity (before the gelation time) we can functionalize the fiber with a thin film *via* dip-coating.

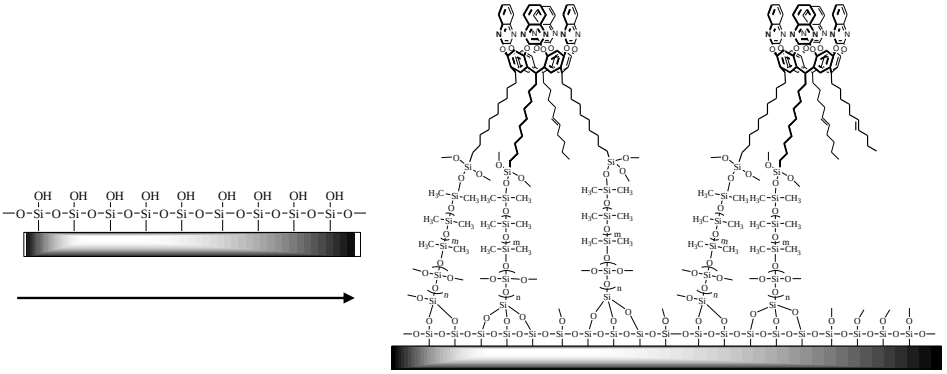

Scheme 3.8. Fiber coating.

The dip-coating technique can be described as a process where the substrate to be coated is immersed in a liquid and then withdrawn with a well defined withdrawal speed under controlled temperature and atmosphere conditions. The coating thickness is mainly defined by the withdrawal speed, by the solid content and the viscosity of the liquid. If the withdrawal speed is chosen such that the sheer rates kept the system in the Newtonian regime, the coating thickness can be calculated by the Landau-Levich equation:

$$\boldsymbol{h = 0.94 \frac{(\eta \cdot \nu)^{2/3}}{\gamma_{LV}^{1/6} \cdot (\rho \cdot g)^{1/2}}}$$

h = coating thickness; η = viscosity; ν = withdrawal speed; γ = liquid-vapor surface tension; ρ = density; g = gravity.

Unfortunately in our case same of the parameters are unknown so we carried out experiments under different conditions, by performing successive coatings (about 10) on the same substrate to increase the thickness of the layer, that was evaluate from SEM analysis.
One of the critical parameter is the viscosity of the mixture since it is not constant and increases over time. Therefore it was important to keep constant all the other experimental parameters such as temperature and shape of the reaction container in order to correlate the viscosity only with time. A low viscosity in fact causes very thin thickness, by contrast a too high viscosity

causes the formation of macroscopic lumps on the fiber, jeopardizing its utilization.
Once all the parameters were optimized the dip-coating both of several silica rods and three fibers assembled was made. The coatings were made on the same batch and in different batches to test the fiber-to-fiber and batch-to-batch reproducibility. The silica rods were used for SEM analysis (the sample preparation for SEM, i.e. metallation, make this analysis destructive).
The SEM images (Figure 3.10) give the impression of a dense, non-porous structure of the coatings. However the SEM technique does not possess enough resolution to show clearly both micro- and mesopores, since they fall in the 20-500 Å range. The images show the homogeneous distribution of the coating on the fibers. The thickness was evaluated by comparison with a naked fiber image. We estimate an average thickness of 10±2 µm.

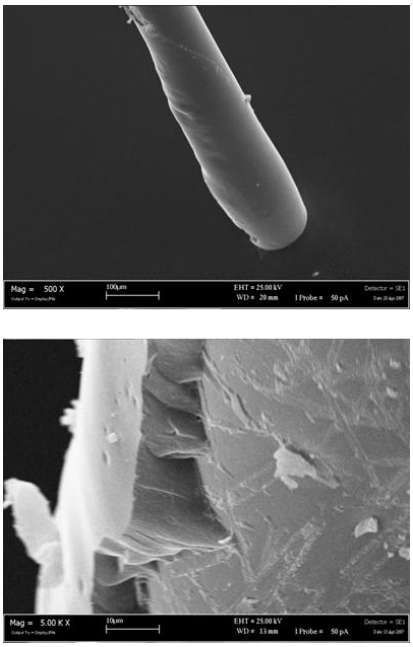

Figure 3.10. SEM images of coated fiber with plasticizer (Sol-Gel procedure 1) at MAG x500 (up) and x5000 (down).

The good results obtained from this material with the use of a plasticizer have to pay a tribute from the point of view of molecular recognition. The cavitand

in fact was present in the fiber coating only in a quantity of 10-15% (w/w), mixed in a network formed by silica and silicon oil. This last compound make the coating similar to the commercial available PDMS coated fibers (unspecific) and make our coating less specific toward our target analytes (Figure 3.11). Consequently the molecular recognition abilities of the cavitand were averaged by the "unspecific" part of the matrix.

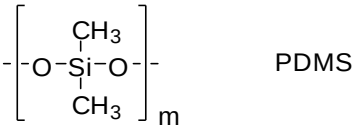

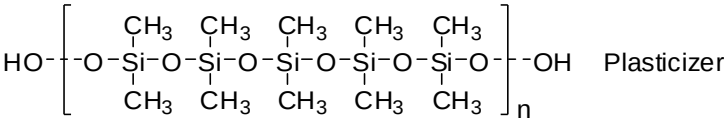

Figure 3.11. Chemical structure of PDMS and OH-TSO (plasticizer).

3.2.2.2 QXCAV SOL-GEL

Therefore the challenge became to make a material with high concentration of specific molecular receptors in a "neutral" matrix. We need to minimize the unspecific moieties of the matrix such as Si-CH_3 then developing a network made only by silica and cavitands. Therefore the only precursors useful for this purpose are TEOS and the cavitand. The main problem of this approach is to find the right reaction conditions to avoid the cracking of the network. The absence of a plasticizer in a rigid network such silica make the network improper to host big molecules such as Quinoxaline bridged cavitands, so the idea was to use the flexibility of the lower chains of the cavitand as plasticizer to relax the network strain.

In a previous work[29] a SPME fiber was coated with a material made via sol-gel process using diethoxydiphenylsiloxane and TEOS (1:1 molar ratio) as precursor, water , acid (catalyst) and ethanol as solvent. The coating showed a good thermal and pH stability proving its capabilities for the sampling of aromatic polycyclic hydrocarbons. For our system it was impossible to follow the same procedure because the cavitand is insoluble in ethanol. We need to

choose an alternative solvent able to dissolve all the reagents. Normally, to dissolve polar alkoxide, such as SiO_4^- , polar solvent like ethanol or formamide are used, that do not dissolve apolar compounds like cavitands. In preliminary experiments we chose to use acetone as solvent since it is able to solve all the reagents (water included). The bulk material obtained with this solvent is not very compact but it has a very good thermal stability as proved by thermogravimetric analysis. The TGA curve do not show a relevant thermal event and the loss of 9.4 % of weight was attributed to the release of water and other low molecular mass reaction products sorbed and entrapped inside the pore structure of the polymer not released from the gel during its drying in a conventional oven.
As regards the fiber coating, the SEM images show a highly porosity and sponge-like aspect but, unfortunately, it seems not well distributed and grafted on the silica core of the fiber (Figure 3.12).

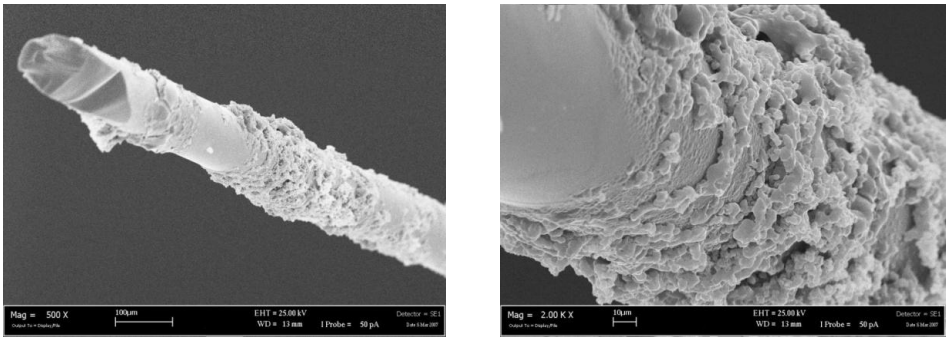

Figure 3.12. SEM images of coated fiber using acetone as solvent (Sol-Gel procedure 2), at MAG x500 (up) and x2000 (down).

We thought that this behavior was due to the solvent so we decided to change it and use CH_2Cl_2. The inconvenient of this solvent was the immiscibility with water, that is one of the most important reagents in the reaction. A phase segregation, in fact, means the impossibility of control the stoichiometric ratio. By using a stoichiometric amount of QxCav in a vigorously stirred reactor, we obtain, a dusted bulk solid. Its macroscopic aspect is reflected also at the microscopic level in the SEM images (Figure 3.13).

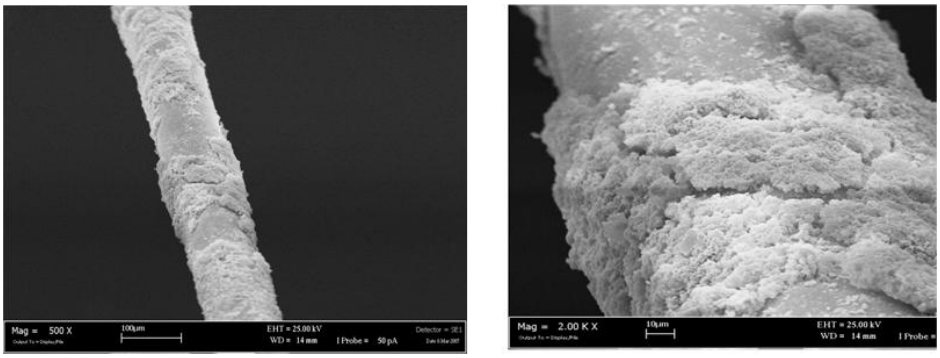

Figure 3.13. SEM images of coated fiber using CH_2Cl_2 and a stoichiometric amount of water (Sol-Gel procedure 3), at x500 (left) and x2000 (right) magnification.

We also tried a protocol with an excess of water, to ensure the complete hydrolysis of siloxane. Before the dipping procedure the aqueous layer was removed and the dipping was made in the organic layer. In this case the SEM images showed an high porous, sponge-like material uniformly distributed on the whole surface of the fiber (Figure 3.14).

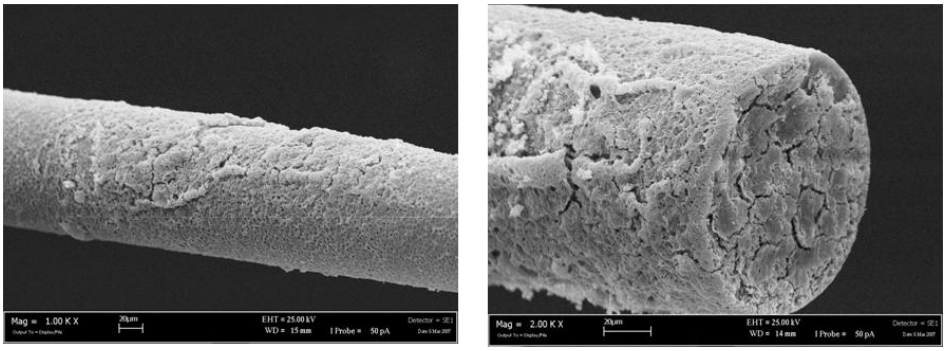

Figure 3.14. SEM images of coated fiber using CH_2Cl_2 and a excess of water (Sol-Gel procedure 4), at x1000 (left) and x2000 (right) magnification.

However detailed images showed that the tweezers, used to handle the fiber, damaged the coating thus suggesting that the coating is not chemically bonded

to the silica core of the fiber (Figure 3.15). The network must be chemically grafted to the fiber, since the lack of chemical covalent bonds between coating and the silica core may cause a disaggregation of the coating, both in the case of direct sampling, where the fiber is dipped in liquid sample and in the GC injector, where it is experiences to a high thermal stress.

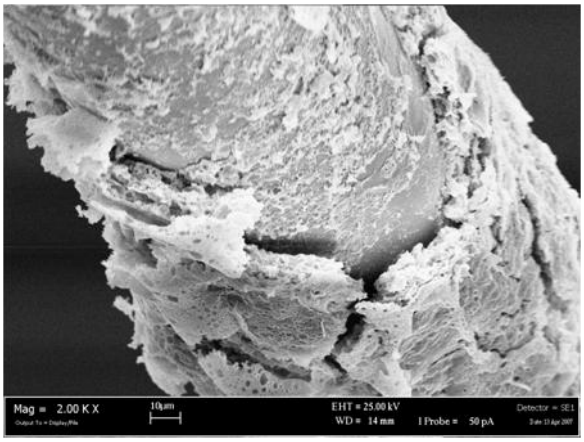

Figure 3.15. SEM image of coated fiber using CH_2Cl_2 and an excess of water (Sol-Gel procedure 4), at MAG X2000.

We maintained that the choice of the CH_2Cl_2 as solvent was correct, so the problem was related to the optimization of the reaction conditions in particular the reaction time and the ratio between the reagents.
The difficult with this optimization was related to the high number of the experiments to be performed with an high consumption of QxCav, thus requiring a strong synthetic effort.
Therefore we decided to use model cavitand **5** easier to synthesize. The variables of each experiment were: the reaction time, the quantity of the solvent, and the ratio between cavitand, TEOS, acid, and water. After several experiments we obtained a good coating with a reasonable gelation time and a good distribution on the fiber as show in the SEM images (Figure 3.16). The critical parameter turned out to be the reaction time upon solvent removal. The best procedure is reported in the experimental section as Sol-gel 5.

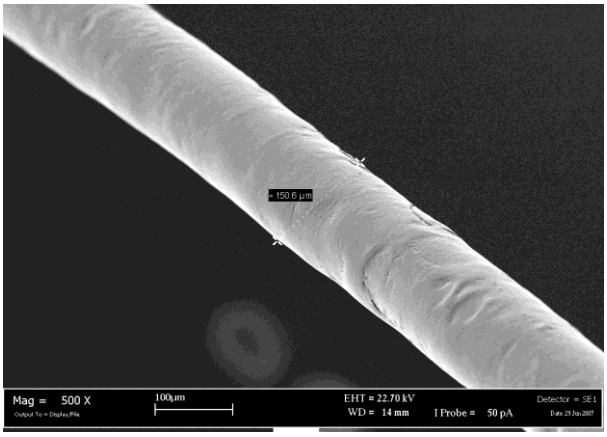

Figure 3.16. SEM images of coated fiber with cavitand **5** (Sol-Gel procedure 5), at x500 magnification.

In analogy to the original coating with plasticizers we observed a non-porous surface, uniformly distributed and without cracks. However the resulting thickness is twice as before (21 ± 2 µm) using about 70% (w/w) of model cavitand in the silica network.

This protocol was adapted to the quinoxaline bridged cavitand, slightly modifying the reaction conditions considering the different weight and grade of functionalization of the model in comparison with the real receptor. In particular, small changes in the ratio of the catalyst (TFA) can change the gelation time also of several minutes (see Sol-Gel 6).

In the Figure 3.17 we report the SEM images of the fiber coated with the quinoxaline based sol gel. From the pictures we can measures the thickness of the coating that is 56 ± 4 µm, a two-fold increase with respect to the methylene bridged cavitand and five times higher than that of the coating with plasticizer.

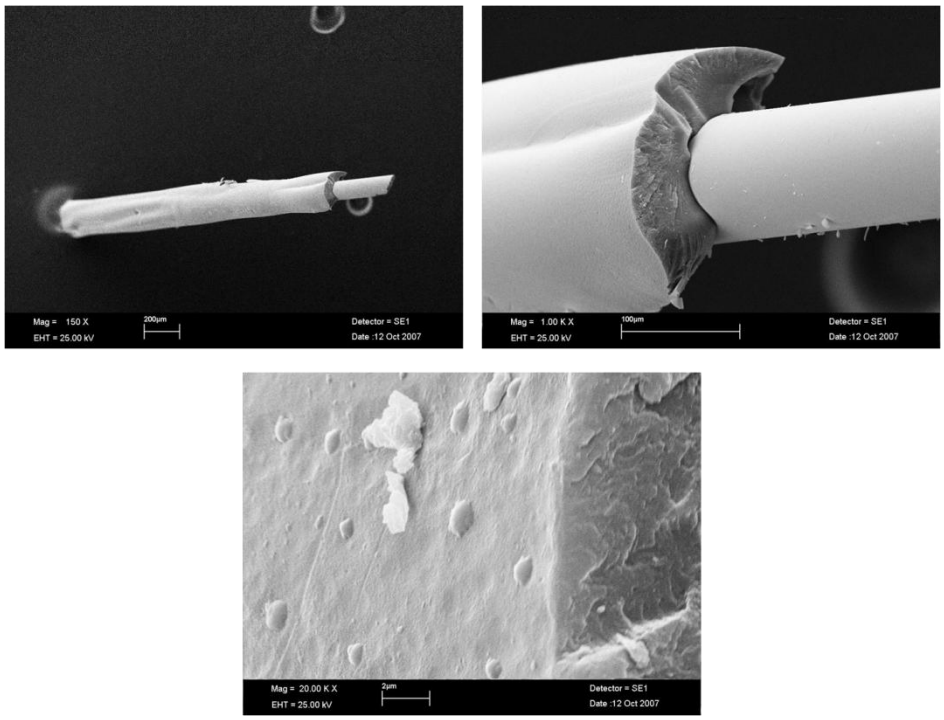

Figure 3.17. SEM images of a coated fiber (Sol-Gel procedure 6), at MAG X150 (left), X1000 (right), X20000 (down).

The resulting material was characterized by solid state NMR (SSNMR). The ^{29}Si spectrum in cross polarization conditions of the dried gel has been recorded (Figure 3.18). The overall signal is constituted by three partially superimposed peaks: Q^2 (≈-92 ppm), assigned to silicon atoms bonded to two hydroxyl groups, Q^3 (≈-101 ppm), assigned to silicon atoms with one hydroxyl group, and Q^4 (≈-111 ppm), assigned to silicon atoms without hydroxyl groups. The intensity ratio of these three components does not reflect the real concentration of the corresponding species in the sample, because in the cross-polarization pulse sequence the intensity of each signal is enhanced in a measure proportional to the number and the proximity of surrounding protons. Beside the signal, in the region between -70 and -55 ppm, two other signal of low intensity appear (T^2 and T^3), belonging to silicon atoms bonded to the organic receptor. The low intensity of these peaks is due to the scarce sensitivity of ^{29}Si solid state NMR, that could not be enhanced either with longer accumulation times or larger quantities of sample. The presence of

grafted cavitands has been independently confirmed *via* ^{13}C SSNMR spectrum performed on the same sample. The ^{13}C-SSNMR spectrum clearly show the presence of the quinoxaline cavitand, exhibiting aromatic and aliphatic carbons belonging to its structure.

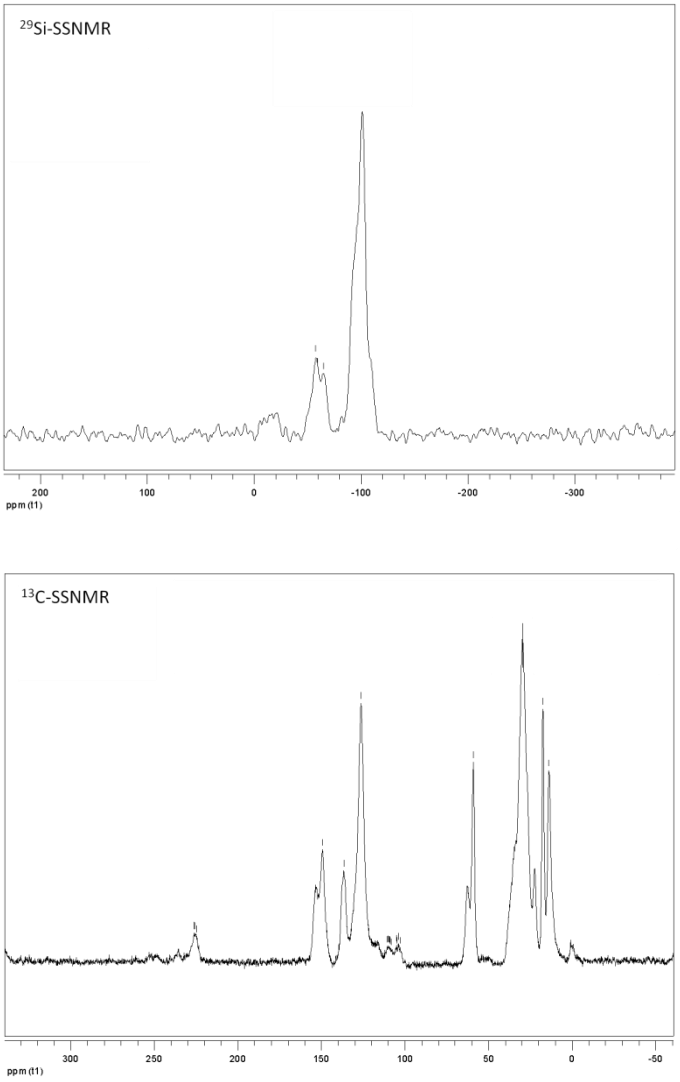

Figure 3.18. ^{29}Si (up) and ^{13}C (down) CP-MAS SSNMR.

3.2.3 FIBER CHARACTERIZATION

Fiber conditioning and bleeding

All the fibers, obtained by dipping the silica rods both in the same Sol and in different Sols were conditioned at 300 °C, the maximum temperature allowed, deduced from TGA analysis, for two hours. Subsequently they were desorbed in the GC-injector for 2 minutes at 100°C and 270°C to evaluate the bleeding. In all the case the fibers did not shown a significant bleeding, thus evidencing a good adherence and stability of the coating on the fiber.

pH resistance

pH resistance of the coated fibers was also proved by using the developed coatings for the sampling of aqueous solution at different pH.

pH is a fundamental parameter to be considered not only for the stability of the silica network but also for its influence on the molecular receptor. In fact the quinoxaline cavitand works as a receptor only in its "vase" conformation, whereas in the flat kite conformation it is unable to complex guests owing to the absence of a deep cavity. In this case pH is one of the factor that influences cavitand switching[30] (Figure 3.19).

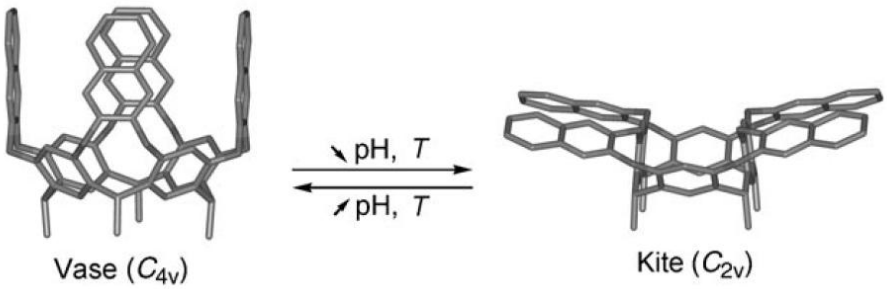

Figure 3.19. Switching behavior of a Quinoxaline cavitand.

The protonation of the nitrogen atoms of the quinoxalines causes the opening of the cavity in the kite position due to the coulombian repulsion strength. pH resistance was evaluated by sampling an aqueous solution of chlorobenzene at 100 ng/L at pH=2, pH=7, and pH=10. Anova did not show significant differences ($p>0.05$) among the main responses obtained for each pH value, thus assessing the capabilities of the developed coatings for the sampling of solution under different pH conditions.

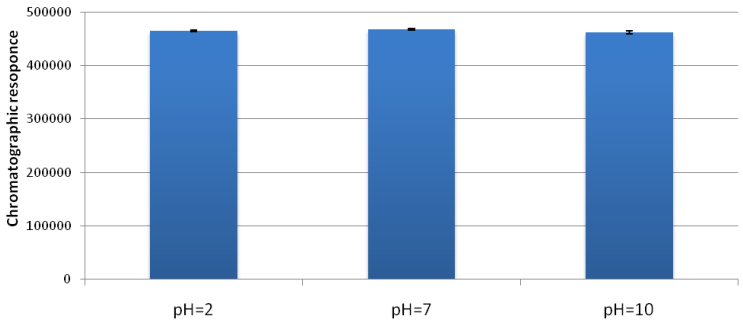

Figure 3.20. Extraction ability of chlorobenzene with the coated fiber in acid, neutral and basic ambient.

Evaluation of fiber-to-fiber and batch-to-batch repeatability

The performance of the developed fibers was also evaluated in term of fiber-to-fiber (by dipping different fibers in the same Sol) and batch-to-batch (by dipping different fibers in different Sol) repeatability: by operating under these condition 3 fibers were prepared and used both for headspace and for immersion analyses. A mixture of benzene and *p*-xylene (each 100 ng/L) was analyzed in the case of headspace analysis, whereas 1,2,3-trichlorobenzene (50 ng/L) was the investigated analyte in the case of immersion analysis. Five replicated measurements for each fiber were always performed. For both the sampling modes the respective deuterated internal standards were used. The same experiments were carried out by using commercial fibers i.e. CAR-PDMS 75 µm. The obtained result are shown in Tables 3.1 and 3.2.

	QxCav fiber (CV%)		Carboxen-PDMS 75 µm (CV%)	
	Benzene	p-xylene	Benzene	p-xylene
Fiber-to-fiber				
same fiber, same day	2.1	2.4	8.5	8.7
same fiber, three different days	5.8	5.1	8.9	9.1
different fibers, same day	3.5	4.2	8.4	8.8
Batch-to-batch				
different fibers, same day	3.8	5.4	-	-

Table 3.1. Headspace sampling of benzene and p-xylene: repetibility intra and inter batch (CV%=RSD%, RSD=Relative Standard Deviation).

	QxCav fiber (CV%)	Carboxen-PDMS 75 µm (CV%)
Fiber-to-fiber	1,2,4-trichlorobenzene	
same fiber, same day	2.4	8.0
same fiber, two different days	2.7	8.5

Table 3.2. Immersion sampling of 1,2,4-trichlorobenzene: repetibility intra batch (CV%=RSD%, RSD=Relative Standard Deviation).

As shown in the tables, by using the QxCav coating CV% lower than 6% were always obtained for both the sampling techniques, also when sampling was performed in different days. The obtained results were better than those achieved using the commercial coatings, thus allowing to assess the feasibility of our proposed coating procedure in the development of highly chemically and thermally stable fibers to be used for the environmental analyses.

3.2.4 Study of the extraction capabilities of fibers with plasticizer

Considering the high repeatability of the quinoxaline cavitand based coating we decided to test the sampling performance of the developed fibers toward sampling of BTEX, with the aim to evaluate the possibility of selective

desorption of benzene in presence of other aromatic and aliphatic hydrocarbons.
This experiments were carried out to evaluate the possibility of using these fibers as passive devices for environmental analyses.
As a general comment, it can be stated that commercial coatings showed an higher "affinity" towards the sampling of aliphatic analytes, with respect to the QxCav coating obtained using the plasticizer (Figure 3.21).

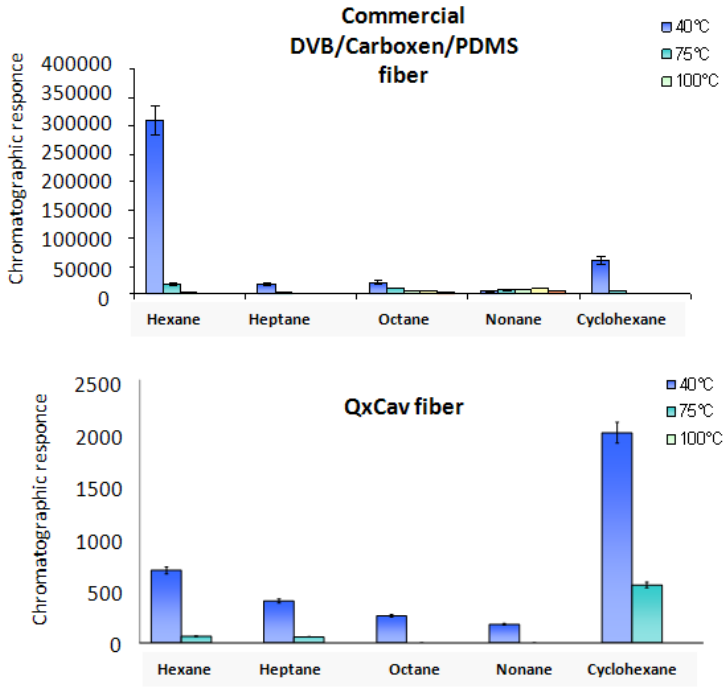

Figure 3.21. Headspace sampling with DVB/CAR/PDMS (up) and QxCav fiber (down) of aliphatic hydrocarbons (aqueous solution: hexane 100 ng/L, other analytes 50 ng/L).

As shown in the Figure 3.21 the quinoxaline cavitand coating fiber showed a different behavior with respect to DVB/Carboxen/PDMS fiber. In particular its ability to retain cyclohexane is enhanced, but it releases all aliphatic hydrocarbons below 75°C, indicating that they are mainly physisorbed in the matrix and not complexed by the cavity.

As far the sampling of BTEX, it was observed that by performing subsequent desorption (increasing the temperature from 40°C to 270°C) the selective detection of benzene was strongly interfered by aliphatic compounds only in the case of commercial coatings.
A different behavior was observed in the case of the QxCav coating. The poor retention of the aliphatic hydrocarbons in the QxCav coating is probably due to unspecific interactions with the siloxane matrix, especially with the Si-CH_3 groups and the alkyl chains at the lower rim of the cavitand.
It has also to be noticed that among the utilized aliphatic hydrocarbons, cyclohexane was the most retained compound, probably as a consequence of its dimensions with respect to linear hydrocarbons.
However the less responses values do not compromise the limit of determination (LOD) that is lower than law limits.

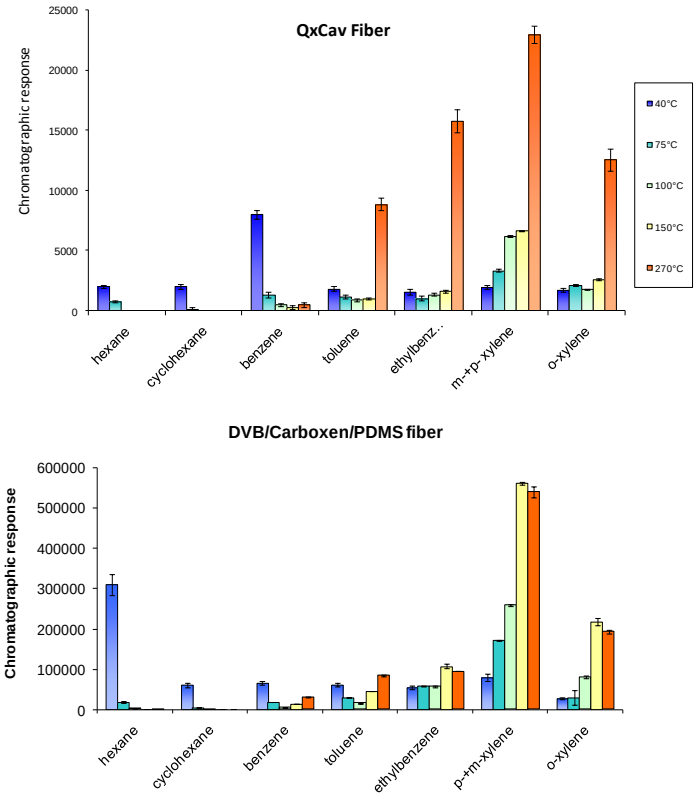

Figure 3.22. Desorption study of aromatic VOCs (aqueous solution: hexane 100 ng/L, other analytes 50 ng/L) with QxCav coated fiber (up) and DVB/CAR/PDMS fiber (down).

It has also to be noticed that the GC responses obtained with the QxCav fiber were lower than those achieved using the DVB-CAR-PDMS (Figure 3.22). This behavior could be explained tacking into account both the greater length of the commercial fiber (2 cm vs 1 cm) and the higher thickness of the coating.
In order to evaluate the role of the coating thickness as well as the effect of the plasticizer added to the silica matrix additional experiment were carried out using PDMS 7 µm fiber.

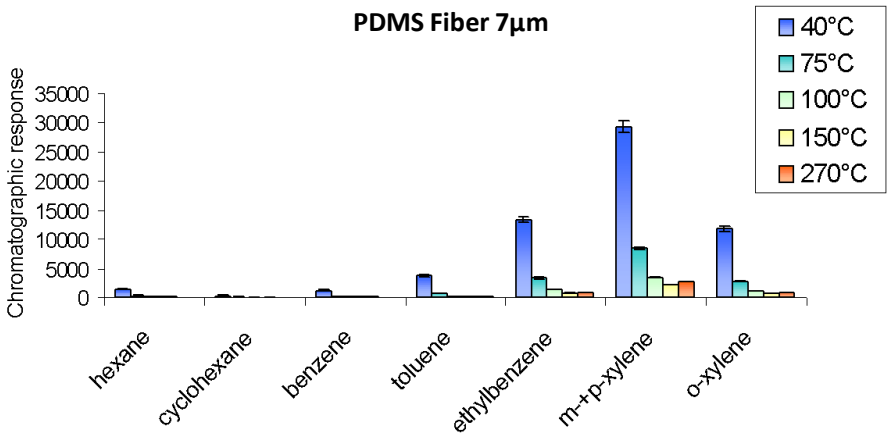

Figure 3.23. Desorption study of aromatic VOCs (aqueous solution: hexane 100 ng/L, other analytes 50 ng/L) with PDMS fiber 7µm.

As shown in Figure 3.23 the GC responses obtained using the PDMS 7 µm fiber and the QxCav coating of the Figure 3.22 were not significantly different, thus meaning that similar coating thickness can produce similar results. However it has to be observed the lack of selectivity of the PDMS coating: in fact all the investigated analytes are desorbed simultaneously at low temperatures.

3.2.5 PERFORMANCES OF FIBERS WITHOUT PLASTICIZER

The performances of the fibers coated with the QxCav gel without plasticizer were tested in order to evaluate the potential selectivity of due to the lack of unspecific interaction of the matrix with analytes. As reported in Figure 3.24, the extraction performances of the fibers were two-fold higher than those obtained using the fiber with the plasticizer. This behavior is mainly due to the higher thickness of the coating not containing the plasticizer but also to the presence in the coating of a greater amount of cavitand.

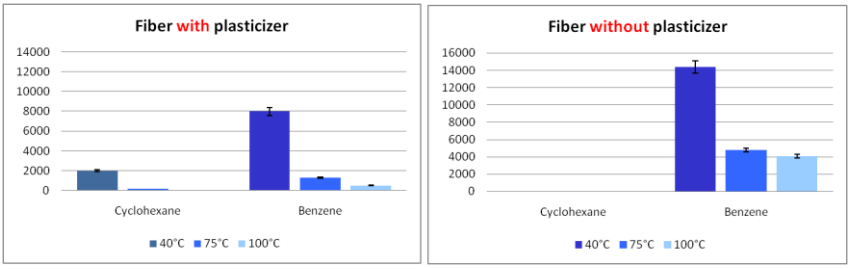

Figure 3.24. Comparison between chromatographic responses.

By comparing the performances of the two coatings, a very interesting results was obtained using the fiber without plasticizer since aliphatic hydrocarbons were not retained. In addition it was possible to selectively desorb benzene at the temperature of 40°C. At this temperature all the other aromatic compounds were retained into the quinoxaline cavity and required higher temperatures to be desorbed.
The separation performances towards aromatic hydrocarbons of QxCav in this setting are better than those as pure solid. In the Chapter 2, QxCav desorbed benzene and toluene together at 70°C, while here benzene are desorbed almost pure already at 40°C. The reason for this different behavior can be attributed to the different instrumental set-up and to the higher precision of the last analytical setting.

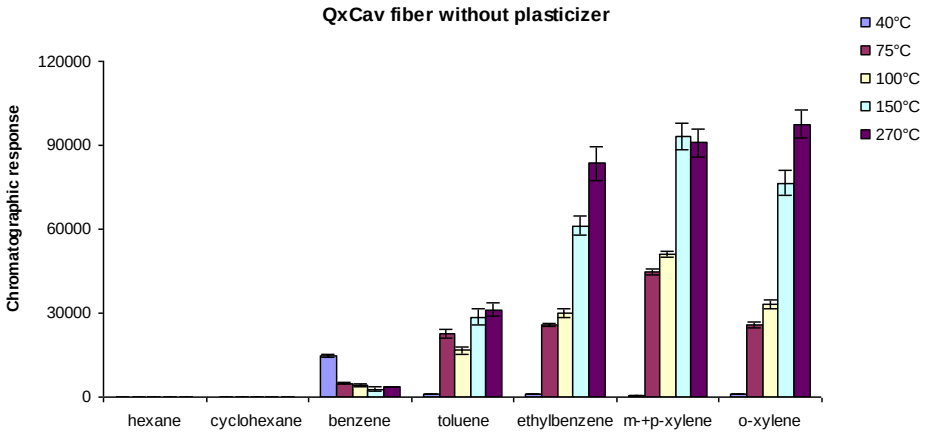

Figure 3.25. Desorption study of aromatic VOCs (aqueous solution: hexane 100 ng/L, other analytes 50 ng/L) with QxCav coated fiber.

3.2.6 Extraction capabilities towards other aromatic compounds

The complexation capabilities of QxCav are not limited to BTEX but can be extended also toward other aromatic compounds such as chlorinated benzenes. These compounds are well known toxic compound of environmental concern. Owning to their toxicity very low detection limits have been set by recent regulations. The sampling of these analytes can be performed both by analyzing the headspace over the sample and by immersion thus exploiting the hydrophobicity of the aromatic compounds which prefer the liphophilic cavity of the cavitand with respect to water solvation. In order to assess the selectivity of the QxCav coating the fiber was used to sample the headspace of a solution containing benzene, toluene, chlorobenzene, 2-chlorotoluene, 1,2-dichlorobenzene, 1,2,4-trichlorobenzene, 2-chloroaniline, and anisole. The results, reported in Figure 3.26, show an higher affinity towards chlorinated aromatic hydrocarbons. This behavior can be explained taking into account both the affinity of the quinoxaline cavity towards the chlorinated compounds and also to the different partition coefficients of the analytes.[31] This last effect is show by the low adsorption of 2-chloroaniline due to the amino groups polarity.

In general the presence of elecronwithdrawing substituent on the aromatic guests tends to enhance complexation by QxCav since they strengthen CH-π interactions with the cavity.

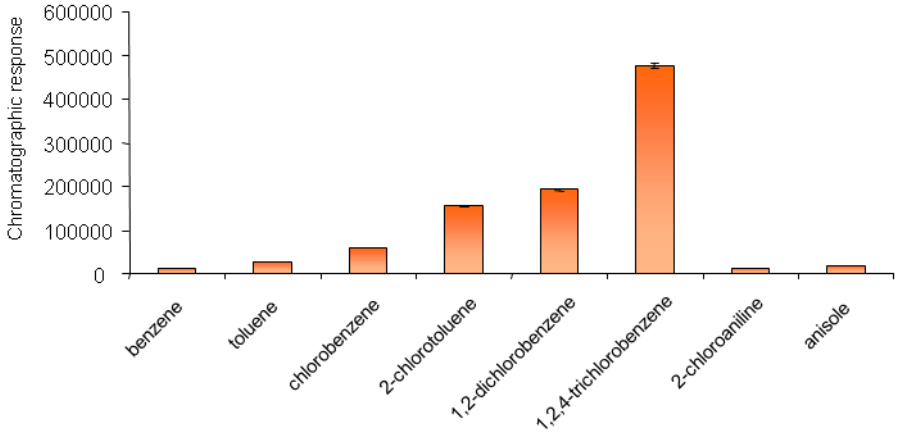

Figure 3.26. Desorption study of aromatic compounds (aqueous solution: analytes 5 ng/L) with QxCav coated fiber.

On the basis of the results reported, the QxCav fiber could be proposed as valid SPME device for the passive sampling of these compounds in occupational environments.

3.3 Conclusions

A novel gel-coating based on quinoxaline cavitands as supramolecular receptor was developed and proposed as a valid alternative for the SPME determination of aromatic hydrocarbons at ultratrace levels. Compared to commercially available fibers, the main feature was the excellent selectivity towards the investigated analytes, thus allowing the selective desorption of benzene also in presence of interfering compounds like aliphatic hydrocarbons. A very good fiber-to-fiber and batch-to-batch repeatability were also obtained with RSD% < 6%. Finally, it can be stated that proposed sol-gel procedure can be really advantageous in terms of fiber lifetime.

3.4 Experimental section

General method: All commercial reagent were ACS reagent grade and used as received. For the synthesis all solvents were dried over 3 Å and 4 Å molecular sieves. The ^{1}H-NMR spectra were recorded on Bruker Avance 300 (300 MHz) spectrometer and all chemical shifts (δ) were reported in parts per million (ppm) relative to proton resonances resulting from incomplete deuteration of NMR solvents. The ^{29}Si and ^{13}C SSNMR spectra were recorded on a Bruker Avance 400 WB 2-channel solid state spectrometer. ESI-MS experiments were performed on a Waters ACQUILITY SQD Detector equipped with a ESCi® multi mode ionization (APCI/ESI). The morphology characterizations were made by scanning electron microscopy on a Leica 430i microscope with EDX OXFORD ISIS (Cambridge, UK).Column chromatography was performed using silica gel 60 (Merck 70-230 mesh). Flash chromatography was performed using Versaflash™ System (Supelco). Resorcinarene R=$C_{10}H_{19}$ was prepared according to literature procedure.[32]

Cavitand 1: To a solution of resorcinarene (R: $C_{10}H_{18}$) (2.00 g, 1.92 mmol) in dry DMF, under nitrogen atmosphere, K_2CO_3 (1.60 g, 8.04 mmol) and 2-3-dichloroquinoxaline (2.12 g, 15.36 mmol) were added. The suspension was heated at 60°C and stirred for 18h. The reaction was quenched in water, vigorously stirred and the pH was neutralized by aqueous HCl till the formation of a precipitate. The suspension was filtered and solid washed with water. The crude product was purified by column VersaFlash™ chromatography on silica gel by using CH_2Cl_2/Hexane (9:1 v/v) as eluant to give cavitand **1** (0.68 g, 23 %). **^{1}H NMR** (300 MHz, $CDCl_3$): δ= 8.16 (s, 4H, Ar*H*), 7.78 (m, 8H, AA' part of an AA'BB' system), 7.47 (m, 8H, BB' part of an AA'BB' system), 7.21 (s, 4H, Ar*H*), 5.83 (m, 4H, C*H*=CH_2) 5.57 (t, 4H, C*H*Ar_2, J=7.7 Hz), 4.98 (m, 8H, CH=C*H*$_2$), 2.27 (m, 8H, Ar_2CHC*H*$_2$), 1.34 (m, 48H, CH_2); **ESI-MS** *m/z* (%): 1547 [M+H$^+$, 100].

Cavitands 2 and 3: To a solution of cavitand **1** (680 mg, 0.440 mmol) in dry cyclohexane, under argon, triethoxysilane (0.487 mL, 2.64 mmol) and platinum(0)-1,3-divinyl-1,1,3,3-tetramethyldisiloxane complex (Karstedt's catalyst, 0.088 mL, 0.1M in poly(dimethylsiloxane)vinyl terminated) were added. The solution was stirred at 68°C for 24h. The solvent was removed

under vacuum and the crude product was purified by column chromatography on silica gel by using Hexane/Ethanol (9:1 v/v) as eluant to give a mixture of compound di-functionalized **3** and tri-functionalized **2** as a yellow solid (480 mg, about 54%).
^{1}H NMR (300MHz, $CDCl_3$): δ= 8.12 (s, 4H, Ar*H*), 7.77 (m, 8H, AA' part of an AA'BB' system), 7.45 (m, 8H, BB' part of an AA'BB' system), 7.18 (s, 4H, Ar*H*), 5.53 (t, 4H, ArC*H*, J=7.7 Hz), 5.41 (bm, 2H, C*H*=CH_2), 3.80 (m, 18H, Si-O-CH_2), 2.24 (m, 8H, -CH_2CHAr_2), 1.99 (m, 8H), 1.40 (m, 52H, CH_2), 1.22 (t, 27H, Si-O-CH_2CH_3 + 3H, CH_3); **ESI-MS** *m/z* (%): **(3)** 1875 [M+H^+, 85], 1898 [M+Na^+, 50], **(2)** 2040 [M+H^+, 50], 2062 [M+Na^+, 30].

Cavitand 4: Cs_2CO_3 **(**9.0 g, 27.67mmol) and CH_2BrCl (8.6 mL, 132 mmol) were added, under nitrogen, to a solution of resorcinarene (R: $C_{10}H_{18}$) (3.0 g, 2.88 mmol) in 70 mL of dry DMSO. The purple mixture was stirred in a sealed tube at 88°C for 3 hours. The reaction was quenched by addition 10 % $HCl_{(aq)}$ solution and the resulting mixture was extracted with CH_2Cl_2. The organic layer was washed with water (3 x 15 mL) and evaporated. The crude product was purified by column VersaFlash™ chromatography on silica gel by using CH_2Cl_2 as eluant to give cavitand **1** as yellow solid (2.50 g, 80 %).
^{1}H NMR (300 MHz, $CDCl_3$): δ= 7.11(s, 4H, ArH_d), 6.48 (s, 4H, ArH_u), 5.80 (m, 4H, C*H*=CH_2), 5.74 (d, 4H, CH_{out}), 4.95 (m, 8H, CH=CH_2), 4.72 (t, 4H, ArC*H*, J=7.7 Hz), 4.43 (d, 4H, CH_{in}), 2.24 (m, 8H, -CH_2CH=CH_2), 2.04 (m, 8H, -CH_2CHAr_2), 1.30 (m, 48H, -CH_2-); **ESI-MS** *m/z* (%): 1113 [M+Na^+, 100].

Cavitand 5: To a solution of cavitand **4** (1.69 g, 1.55 mmol) in dry toluene, under argon, triethoxysilane (1.72 mL, 9.31 mmol) and platinum(0)-1,3-divinyl-1,1,3,3-tetramethyldisiloxane complex (Karstedt's catalyst, 0.310 mL, 0.1M in poly(dimethylsiloxane)vinyl terminated) were added. The solution was stirred at 70°C for 30h. The solvent was removed under vacuum and the crude product was purified by column chromatography on silica gel by using Hexane/Ethanol (93:7 v/v) as eluant to give compound **5** as a white oil (1.07 g, 48%).
^{1}H NMR (300 MHz, $CDCl_3$): δ= 7.10 (s, 4H, ArH_d), 6.48 (s, 4H, ArH_u), 5.74 (d, 4H, CH_{out}), 5.40 (bm, 4H, C*H*=CH_2), 4.71 (t, 4H, ArC*H*, J=7.7 Hz), 4.43 (d, 4H, CH_{in}), 3.81 (m, 12H, Si-O-CH_2), 2.20 (m, 8H, -CH_2CHAr_2), 1.97 (m, 8H), 1.34 (m, 52H, CH_2), 1.24 (t, 18H, Si-O-CH_2CH_3 + 6H, CH_3); **ESI-MS** *m/z* (%): 1442 [M+Na^+, 100].

Sol-gel 1: In a PCR tube TEOS (100 µL, 0.448 mmol), 85 µL of polymethylsiloxane hydroxy-termined (OH-TSO), 10 µL of polymethilhydroxysiloxane (PMHS), and 19 µL of TFA (containing 5% of water) were added to the mixture of cavitands **2** and **3** (21 mg, 0.010 mmol) in 200 µL of CH_2Cl_2,. The sealed PCR tube was stirred for 3 minutes with vortex then centrifugated at 12000 rpm for 5 minutes. The resulting clear solution was used for the dip coating.

Sol-gel 2: In a small round-bottom flask the mixture of cavitands **2** and **3** (25 mg, 0.012 mmol) in 2 mL of acetone was mixed with TEOS (216 µL, 0.971 mmol), water (143 µL, 7.98 mmol), and TFA (296 µL, 3.99 mmol). The reaction was stirred in a sealed reactor for 4h at room temperature and the obtained solution used for the dip coating.

Sol-gel 3: In a small round-bottom flask the mixture of cavitands **2** and **3** (25 mg, 0.012 mmol) in 2 mL of CH_2Cl_2 was mixed with TEOS (216 µL, 0.971 mmol), water (143 µL, 7.98 mmol), and TFA (296 µL, 3.99 mmol). The reaction was stirred in a sealed reactor for 4h at room temperature and the obtained solution used for the dip coating.

Sol-gel 4: In a small round-bottom flask the mixture of cavitands **2** and **3** (25 mg, 0.012 mmol) in 2 mL of CH_2Cl_2 was mixed with TEOS (216 µL, 0.971 mmol), water (2 mL, 111.1 mmol), and TFA (296 µL, 3.99 mmol). The reaction was stirred for 4h at room temperature and the organic solution used for the dip coating.

Sol-gel 5: In a PCR tube TEOS (75 µL, 0.336 mmol), 5 µL of water, and 5 µL of TFA were added to the cavitand **5** (50 mg, 0.035 mmol) in 250 µL of CH_2Cl_2. The sealed PCR tube was stirred for 3 minutes with vortex, then centrifugated at 12000 rpm for 5 minutes. The resulting clear solution was used for the dip coating.

Sol-gel 6: In a PCR tube TEOS (75 µL, 0.336 mmol), 5 µL of water, and 5 µL of TFA were added to the mixture of cavitands **2** and **3** (70 mg, 0.034 mmol) in 250 µL of CH_2Cl_2. The sealed PCR tube was stirred for 3 minutes with vortex,

then centrifugated at 12000 rpm for 5 minutes. The resulting clear solution was used for the dip coating. (Best procedure)

Fiber activation: All the silica fibers (Supelco) were activated by immersion in HF 40% (v/v) followed by washing in distilled water for 10 times. After the activation the test fiber was cut in 2 cm pieces with a blade and they were handled very carefully with tweezers because they can easily break and be propelled.

Fiber dip-coating: The fibers were vertically immersed (1 cm) inside a PCR tube containing the sol for 10 seconds and then dried with hot air. The procedures was repeated performed several times (3-10 times) in order to increase the coating thickness. Several fibers were coated with the same sol solution.
The morphology characterization was carried out by scanning electron microscopy (SEM) with a Leica 430i microscope with EDX OXFORD ISIS (Cambridge, UK) with an acceleration voltage of 25kV.

Fiber conditioning: The fibers were conditioned in the injector of gas chromatograph at different temperatures: from 50°C to 300°C for about 2 hours.

Fiber bleeding: The bleeding was tested by expositing the fiber in the GC injector for 2 minutes at 250°C. For each fibers stock 3 replicated measurements were performed.

Sample preparation: Solutions of hexane, heptane, octane, cyclohexane, benzene, benzene-d_6, toluene, ethylbenzene, *o*-xylene, *m*-xylene, *p*-xylene, *p*-xylene-d_{10} at the concentration of 100 mg/L were obtained from pure compounds in 10 mL volumetric flasks using pentane as solvent. For the dilutions were used working solutions with a concentration of 10 µg/L.
The stock solution of 1,2,4-trichlorobenzene and chlorobenzene with a concentration of 100 mg/L were made from pure compounds in 10 mL volumetric flasks using ethanol as solvent. Working solutions at the concentration of 10 µg/L were obtained by dilution from the stock solutions.
All the solutions were stored at 4°C.

The samples were prepared at the concentration of 100 ng/L or 50 ng/L in distilled water (10mL).

SPME Sampling

Headspace Sampling: The fiber was exposed in the headspace of a 30 mL vial containing 10 mL of stirred aqueous solution for 30 minutes at 50°C.

Direct sampling: The fiber was dipped in a 15 mL vial containing 10 mL of stirred aqueous solution for 30 minutes at 30°C.

The vials were sealed with closed-top seals with SPME stopper (Supelco). The fiber was desorbed for 2 minutes in the GC injector.

Commercial available fibers: for a comparison of the results the analyses were carried out also by using commercial available fibers:

75 µm Carboxen™-PDMS (Supelco)

2cm-50/30 µm DVB/Carboxen™/PDMS (Supelco)

GC-MS analysis

Gas-chromatograph HP 6890 Series Plus, Agilent Technologies (Milano, Italy)

Column:	Factor Four-5MS (l = 30 m, i.d. = 0.25 mm, d.f. = 0.25 µm) Varian (Torino, Italy)
Carrier gas:	helium
Carrier gas flux:	1 mL/min
Injector Temp PVT:	260°C
Injection mode:	splitless (ratio 10)
Temperature ramp:	[Solution (benzene, *p*-xylene, benzene-d_6) Solution (benzene, *p*-xylene, *p*-xylene-d_{10}) Solution (hexane, heptane, octane) Solution (hexane, heptane, octane, nonane, cyclohexane, benzene, toluene, ethylbenzene, *o*-xylene, *m*-xylene, *p*-xylene, *p*-xylene-d_{10})] 40°C for 5 min, 10°C/min from 40°C to 300°C

Mass Spectrometer MSD 5973, Agilent Technologies.

Source Temperature:	150°C
Transfer Line temperature:	280°C
Electromultiplier voltage:	1700 V
Ionization:	E.I. (70 eV)
Acquisition Mode:	Full scan (35-350 amu)

	SIM
Ions monitored in SIM:	Solution (benzene, *p*-xylene, benzene-d_6) *m/z*: 77; 78; 82; 84 from 0 to 5 min *m/z*: 91; 98 from 5 to 10 min Solution (benzene, *p*-xylene, *p*-xylene-d_{10}) *m/z*: 77; 78 from 0 to 5 min m/z: 91; 98; 106; 116 from 5 to 10 min Solution (hexane, heptane, octane) *m/z*: 43; 72 from 0 to 2.60 min *m/z*: 57; 86 from 2.60 to 3.5 min *m/z*: 43; 100 from 3.5 to 5 min *m/z*: 43; 114 from 5 to 8 min Solution (hexane, heptane, octane, nonane, cyclohexane, benzene, toluene, ethylbenzene, *o*-xylene, *m*-xylene, *p*-xylene, *p*-xylene-d_{10}) *m/z*: 43; 72 from 0 to 2.60 min *m/z*: 57; 86 from 2.60 to 3.35 min *m/z*: 56; 78; 84 from 3.35 to 4 min *m/z*: 43; 100 from 4 to 5 min *m/z*: 91; 92 from 5 to 6.5 min *m/z*: 43; 114 from 6.5 to 8 min *m/z*: 43; 91; 98; 99; 106; 116 from 8 to 11 min

3.5 References and notes

[1] *Oxford American College Dictionary*, Oxford University Press.

[2] GESAMP (IMO/FAO/Unesco/WMO/IAEA/UN/UNEP Joint Group of experts on the Scientific Aspects of Marine Pollution),*Review of potentially harmful substances, Choosing priority organochlorines for marine hazard assessment, Food and Agricultural Organization*, Rome, Italy, **1990**, p. 10.

[3] M. W. Sigrist *Air monitoring by Spectroscopic Techniques*, Wiley, **1994**.

[4] J. Dewulf, H. Van Langenhove *Atmos Environ* **1997**, *31*, 3291.

[5] F. Bianchi, M. Careri, C. Corradini, M. Musci, A. Mamgia *CAC* **2005**, *1*,129; F. Bianchi, M. Careri, A. Mangia, M. Musci *J. Chromatogr. A* **2006**, *1102*, 268; F. Bianchi, C. Cantoni, M. Careri, L. Chiesa, M. Musci, A. Pinna *Talanta* **2007**, *72*, 1552.

[6] F. Bianchi, M. Careri, E. Marengo, M. Musci *J. Chromatogr. A* **2002**, *975*, 113; F. Bianchi, M. Careri, C. Mucchino, M. Musci *Chromatographia* **2002**, *55*, 595; B. Antolini, F. Bianchi, M. Bottazzi, M. Careri, M. Musci *Chromatographia* **2004**, *60*,232.

[7] C. L. Arthur, J. Pawliszyn *Anal. Chem* **1990**, *62*, 2145.

[8] J. Pawliszyn *Applications of solid phase microextraction*, RCS, **1999**.

[9] *Bulletin 923* **1998**, SUPELCO.

[10] Z. Zhang, M. J. Yang, J. Pawliszyn *Anal. Chem.* **1994**, *66*, 844.

[11] S. L. Chong, D. Wang, J. D. Hayes, B. W. Wilhite, A. Malik *Anal. Chem.* **1997**, *69*, 3889.

[12] R. Zusman, I. Zusman *J. Biochem. Biophys. Methods* **2001**, *49*, 175.

[13] D. Wang, J. Xing, J. Peng, C. Wu *J. Chromatogr. A* **2003**, *1005*, 1; L. Yun *Anal. Chem. Acta.* **2004**, *63*, 486.

[14] J. Yu, C. Wu, J. Xiang *J. Chomatogr A* **2004**, *1036*,101.

[15] Z. Zeng, W. Qiu, M. Yang, X. Wei, Z. Huang, F. *Li J. Chromatogr. A* **2001**, *51*, 934.

[16] Z. Zeng, W. Qiu, Z. Huang *Anal. Chem.* **2001**, *73*, 2429.

[17] C. Dong, Z. Zeng, X. Li *Talanta* **2005**, *66*, 721.

[18] X. Li, Z. Zeng, J. Zhou *Anal Chem Acta* **2004**, *47*, 509.

[19] F. Zhou, X.Li, Z. O. Zeng *Anal Chem. Acta* **2005**, *63*, 538.

[20] X. Li, Z. Zeng, S. Gao, H. Li *J. Chromatogr A* **2004**, *1023*, 15.

[21] P. Soncini, S. Bonsignore, E. Dalcanale, F. Ugozzoli *J. Org. Chem* **1992**, *57*, 4608.

[22] M. Vincenti, E. Dalcanale *J. Chem. Soc. Perkin Trans. 2* **1995**, 1096.

[23] E. U. Thoden van Valzen, J. F. J. Engbersen, D. N. Reinhoudt *J. Am. Chem. Soc.* **1994**, *116*, 3597.

[24] J. R. Moran, J. L. Ericson, E. Dalcanale, J. A. Bryant, C. B. Knobler, D. J. Cram *J. Am. Chem. Soc.* **1991**, *113*, 5707.
[25] F. Bianchi, R. Pinalli, F. Ugozzoli, S. Spera, M. Careri, E. Dalcanale *New. J. Chem* **2003**, *27*, 502.
[26] P.W. van Leewen *Homogeneous Catalysis: Understanding The Art* **2004**, Kluwer.
[27] M. Azenha, C. Malheiro, A. F. Silva *J. Chromatogr. A.* **2005**, *1069*, 163-172.
[28] C. J. Brinker, G. W. Scherer *Sol-Gel Science* **1990**, Acad. Press. San Diego.
[29] F. Bianchi, F. Bisceglie, M. Careri, S. Di Berardino, A. Mangia, M. Musci *J. Chromatogr. A* **2008**, in press.
[30] P. Roncucci, L. Pirondini, G. Paderni, C. Massera, E. Dalcanale, V. A. Azov, F. Diederich *Chem. Eur. J.* **2006**, *12*, 4775.
[31] A. Leo, C. Hansch, D. Elkind *Chem. Rev.* **1971**, *71*, 525.
[32] U. E. T. van Velzen, J. F. J. Engbergsen, D. N. Reinhoudt *Synthesis* **1995**, 989.

Supramolecular fluorescent sensors 4

4.1 Introduction

Sensing typically refers to the continuous monitoring of the activity of chemical species, called the analytes, in a given matrix. Even if a sensor may have macroscopic or microscopic dimension, in both cases the sensing process relies on an interaction occurring at the molecular level. The binding of an analyte to a molecular fragment called receptor, is defined by biologist and chemists as “recognition”. This process has to be fast, reversible and characterized by a moderate energy gain.
However, sensing is not simply recognition, but it requires that the recognition event is signaled by a detectable change of a propriety of the system.
Among the different chemical sensors, fluorescent based ones present many advantages: fluorescence measurements are usually very sensitive (even single molecule detection is possible, although only under special condition), of low cost, easily performed, and versatile. The versatility of fluorescence-based sensors originates also from the wide number of parameters that can be tuned in order to optimize the convenient signal. Even very complex analytical problems can be indeed overcome by controlling the excitation and emission wavelengths, the time window of signal collection, and the polarization of the excitation beam or the emitted light. In most cases luminescence intensity

changes represent the most directly detectable response to target recognition; more recently, however, other proprieties such as exited state lifetime and fluorescent anisotropy have also been chosen as diagnostic parameters, since they are less affected by the environmental and experimental conditions.[1]
During the last decade a large number of luminescent sensors have been developed for a variety of applications, such as cell biology investigation, medical diagnosis, environmental analysis, and food quality control.[2]
In this Chapter we describe the design and synthesis of a new class of molecular receptors based on luminescent proprieties. In the Chapter 1 we have described a class of phosphonated cavitand that may be used as sensors for short chain alcohol. The main problem with the use of this kind of molecule in mass transducer such as QCM is the presence of unspecific interaction of some analytes with the organic layer of the sensor that generate a signal not directly correlate to the specific host-guest interaction.
The aim of this project is the design of new class of phosphonated cavitands able to change their luminescent properties after the complexation with a specific analyte and totally insensible to the unspecific interaction. The method based on fluorescent sensors offers many advantages[3] in terms of sensitivity, selectivity, response time, and local observation. Moreover, remote sensing is possible by using optical fiber with a molecular sensor immobilized at the tip.[4]

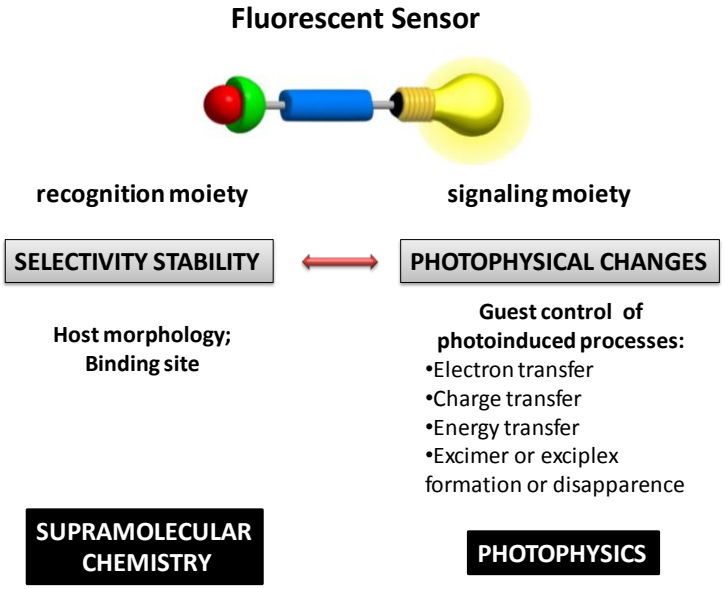

Figure 4.1. Main aspect of fluorescent molecular sensor.

A “Supramolecular Fluorescent Sensor” consists of a fluorophore linked to a binding site able to make supramolecular interaction with a target analyte (Figure 4.1.). In the design of fluorescent sensors, attention should be paid to both the recognition and the transduction schemes. The “signaling moiety” acts as a signal transducer, and it converts the recognition event into an optical signal expressed as the changes in a photophysical state of the fluorophore. These changes are due to the perturbation of photoinduced process such electron transfer, charge transfer, energy transfer, excimer or exciplex formation or disappearance. These aspect are relevant to the field of *photophysics*.

The “recognition moiety” is responsible for selectivity and efficiency of binding which depend on the host characteristic. These aspects are relevant to the field of *supramolecular chemistry*.[5]

There are two principal types of photoinduced process that may be used in a fluorescent sensor: the photoinduced electron transfer (PET) and the photoinduced charge transfer (PCT).

In a PET sensor, upon excitation of the fluorophore, one of its electron in the highest occupied molecular orbital (HOMO) is promoted to the lowest unoccupied molecular orbital (LUMO). This promotion enables photoinduced electron transfer from the HOMO of the donor to that of the fluorophore and causes fluorescent quenching of the latter. Upon analyte binding the relevant HOMO of the donor becomes lower in energy than that of the fluorophore. Consequently PET is not possible anymore and fluorescent quenching is suppressed, in other words, fluorescent intensity is enhanced upon analyte binding (Figure 4.2).

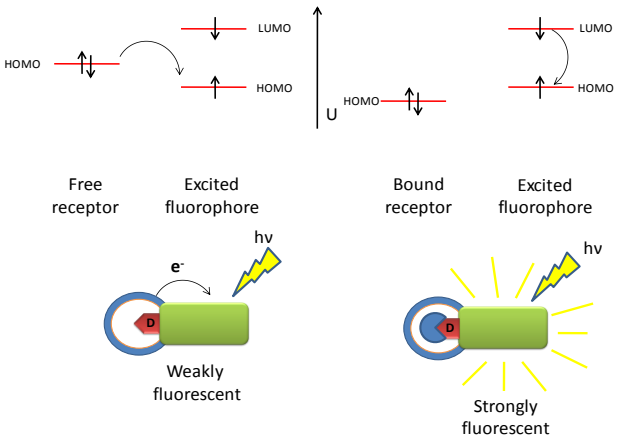

Figure 4.2. Principle of fluorescent PET sensors

Instead, in a PCT sensor, when a fluorophore contains a electron-donating group such as an amino group conjugated to an electron-withdrawing group, it undergoes intramolecular charge transfer from the donor to the acceptor upon excitation light. The target analyte interacting with the acceptor moiety will change the photophysical proprieties of the fluorophore because the host-guest complexation affects the efficiency of intramolecular charge transfer. When an analyte interact with the acceptor group of the fluorophore enhances the electron-withdrawing character of this group; the absorption spectrum is thus red-shifted and the molar absorption coefficient is increased. The photophysical changes upon complexation can also be described in terms of charge dipole interaction.[6] When the dipole moment in the exited state is smaller than in the ground state, the exited state is more stabilized by the complexation with an analyte than the ground state, and this leads to a red shift of the adsorption and emission spectra (Figure 4.3.).

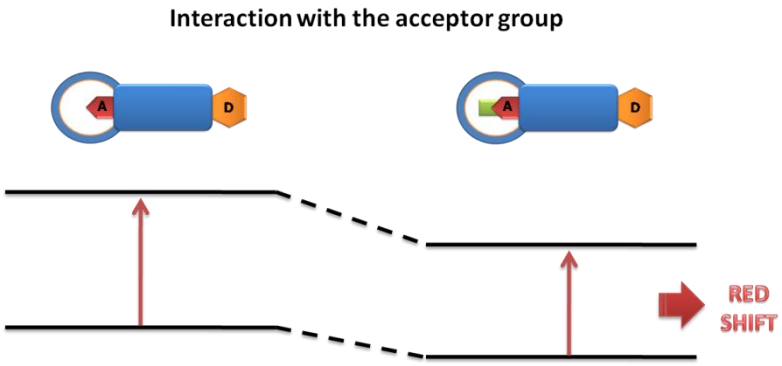

Figure 4.3. Spectral displacement of PCT sensors resulting from interaction of analyte with a electron-withdrawing group.

In an unpublished previous work we synthesized a new fluorescent cavitand with the purpose to create a gas-solid interface sensor for short chain alcohols. This cavitand was functionalized at the upper rim with three methylene bridges. The fourth bridge consists on a phosphonated group linked through a oxygen atom to a cumarine moiety. The cumarine was chosen as fluorescent group for its capacity to give electron transfer. Both in and out isomer were isolated (Figure 4.4.).

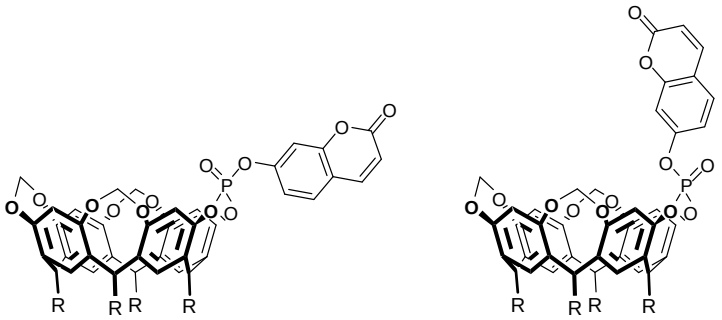

Figure 4.4. Cumarine Cavitands (R=C_6H_{13}), Isomer “in” and “out”.

The main idea of this work was that any binding event on the P=O group can change the HOMO energy of the bridging oxygen to give an increase of the intensity of fluorescence both in solution and at gas-solid interface. The out isomer was used as reference. The titrations made in solution with short chain alcohols such as ethanol, propanol, and butanol showed a increase of emission signal, as show in Figure 4.5 both isomers responded to ethanol, that is a typical behavior of a fluorescence PET sensor.

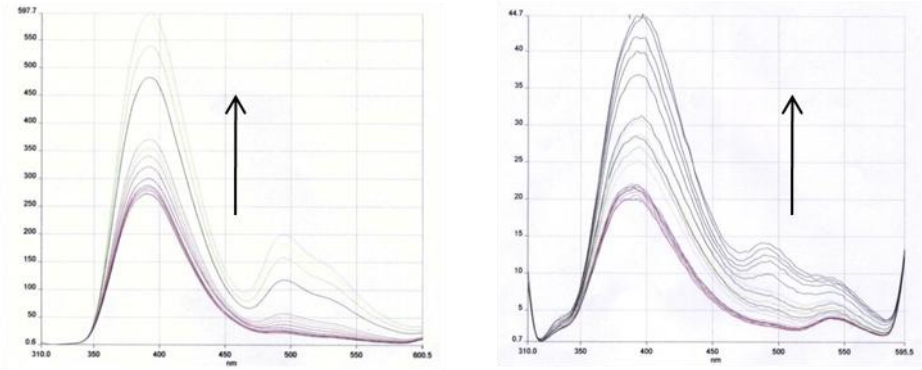

Figure 4.5. Fluorescence titration in $CHCl_3$ with ethanol of cumarine cavitand “in” (left) and “out” (right).

On the other hand the first experiment made at the gas-solid interface did not show any significant change of the emission of the cumarine moiety. After an exposition of the sensing layer to a concentration of 600 ppm there was not a significant difference in the responses. This behavior can be explain with the relative distance between the fluorescent group and the binding site. Moreover the presence of an atom of oxygen as linker between the P=O and the cumarine did not help the PET process.

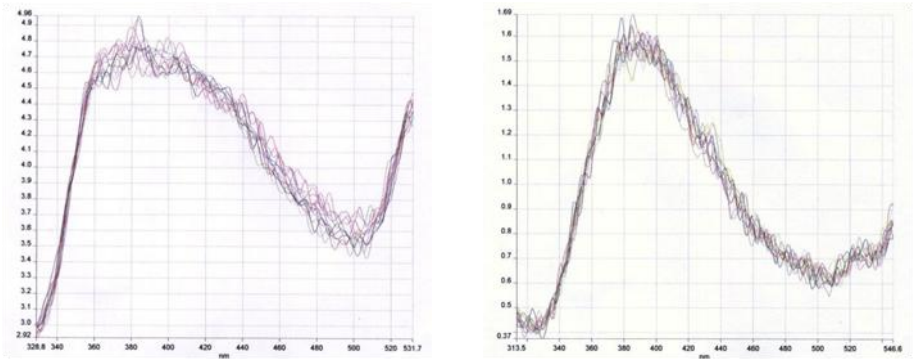

Figure 4.6. Gas-Solid Luminescent titration with Ethanol of cumarine cavitand “in” (left) and “out” (right).

The results of this first attempt prompted as to completely change the approach, both in terms of cavitand receptors and of transduction mode.
We designed, synthesized, and tested a new class of fluorescent receptors directly linked to the P=O binding group based on a fluorescent PCT moiety with the aim of create a fluorescent chemical sensor for short chain alcohols. The use of luminescence should overcome the problems of lack of specificity of the QCM transducers.

4.2 Results and discussion

4.2.1 The fluorescent receptor

To make a fluorophore we need a molecule able to "sense" the perturbation of charge distribution of the acceptor group (a P=O moiety) lead a photoinduced charge transfer with a donor group (Figure 4.7).

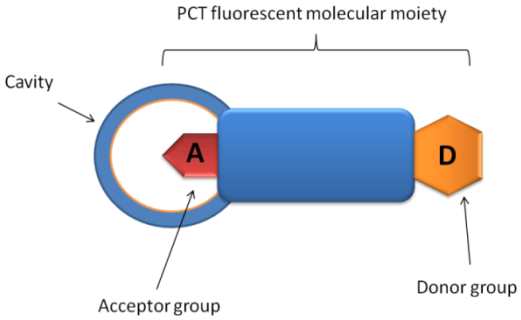

Figure 4.7. Representation of a cavitand based fluorescent PCT sensor

For the design of this kind of receptor we chose a conjugated rigid fluorescent scaffold such as naphthalene, directly linked via phosphorous-carbon bond to the P=O binding group (the electron-withdrawing group). An tertiary amine substituent (the electron-donating) provide the electrons to make a charge transfer system. A prototype of the desired system is compound **5** of Figure 4.8.

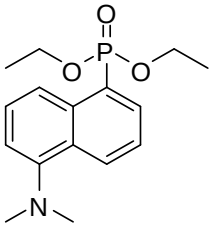

5

Figure 4.8. Target fluorescent moiety **5**.

The structure is very similar to the commercial available dansyl chloride, a fluorimetric detection reagent emitted by UV light, which is used as a fluorescent label in immunofluorescence methods and in peptide derivates. An example of photoinduced charge transfer (PCT) sensors based on calixarenes are given in Figure 4.9. The molecule bears two dansyl groups linked to a calix[4]arene receptor selective towards Li^+ in solution. In the protonated form complexation with Li^+ induces a red shift of the emission spectra as a result of cation-induced proton ejection leading to a phenolate-cation pair.[7]

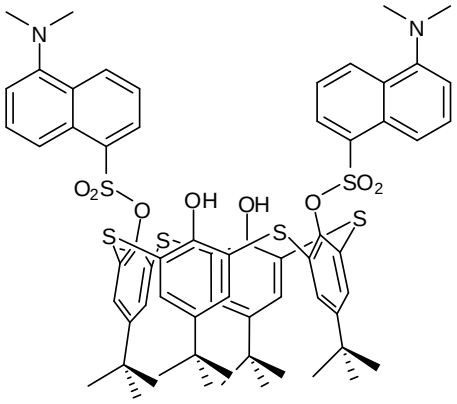

Figure 4.9. Calixarene based PCT sensor

4.2.2 Synthesis of the fluorescent bridging group 7

In order to make a supramolecular PCT sensor based on a cavitand scaffold we need to synthesize a reactive fluorescent group suitable as a bridging agent for a resorcinarene. We need two phosphorous-chloride bonds reactive enough to be use as bridging group so the desired synthon is compound **7** (Figure 4.10.).

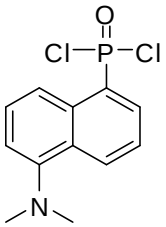

7

Figure 4.10. Fluorescent bridging group **7**.

To synthesize **7** we started following a related procedure present in literature[8]. The construction of the fluorophore involve a multistep process starting from the commercially available 1,5-dinitronaphtalene (Scheme 4.1).

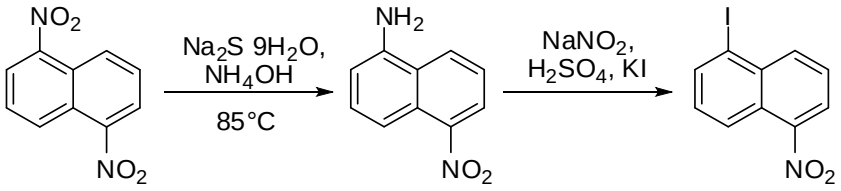

1 **2**

Scheme 4.1. Synthesis of 5-nitronaphtalen-1-amine (**1**) and 1-iodo-5-nitronaphtalene (**2**).

Mono reduction of 1,5-dinitronaphtalene with sodium sulfide in aqueous ammonium solution afforded **1** in good yield (77%). In the following step the amino group of **1** was transformed into iodo derivate via diazonium salt reaction with potassium iodide. Then the residual nitro group was reduced with $SnCl_2$ giving **3** as a brown oil in good yield (78%). Treatment of **3** with aqueous formaldehyde and sodium cyanoborohydride in glacial acetic acid gave the corresponding dimethylamine **4** (yield 67%). The yield of the fourth step was not quantitative as reported in literature[8] due to the formation of partials alkylated products.

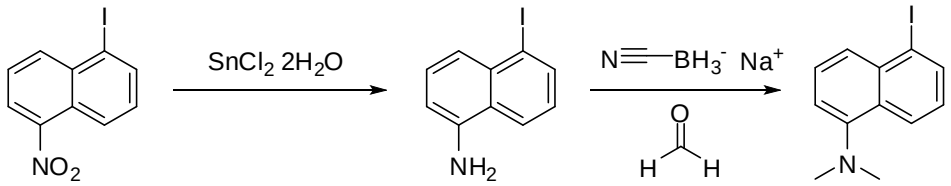

2 **3** **4**

Scheme 4.2. Synthesis of 5-iodonaphtalene-1-amine **3** and 5-iodo-N,N-dimethylnaphtalene-1-amine **4**.

Replacement of the iodide with a phosphonate was done using $NiCl_2$ as catalyst and $P(OEt)_3$ as solvent to give the phosphonate diethyl ester which was then hydrolyzed to phosphonic acid **6** with HCl concentrated 12M (Scheme 4.3.).

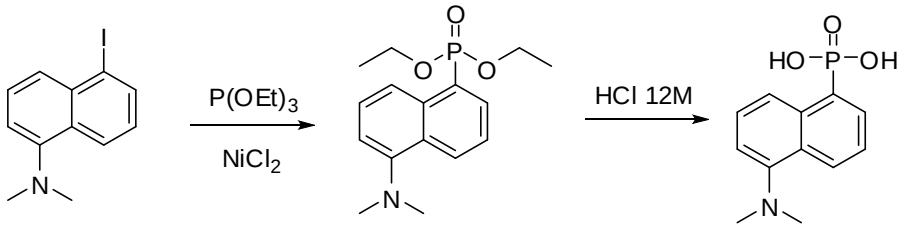

4 **5** **6**

Scheme 4.3. Synthesis of phosphonate ester and phosphonic acid derivatives.

The last step was the formation of phosphorus dichloride **7**. Several attempts were carried out using $SOCl_2$ as chlorinating agent under different conditions with no results. PCl_5 in $POCl_3$ as solvent turned out to be the reagent of choice (Scheme 4.4). Due to its reactivity the phosphonate dichloride **7** was not isolated and used it directly as bridging reagent for the resorcinarene. The major problem was the removal of the solvent $POCl_3$ from the crude of reaction because also $POCl_3$ can react as bridging group with the resorcinarene. For this reason the compound **7** must be dried for several hours under *vacuum*.

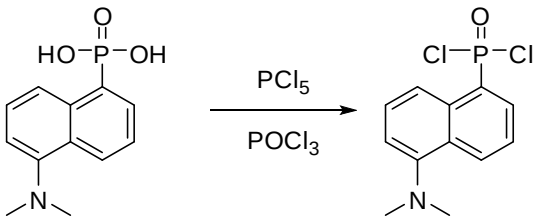

6 **7**

Scheme 4.4. Synthesis of the phosphonate chloride bridging group.

4.2.3 Synthesis of fluorescent cavitand 8

The procedure to synthesize a tri-methylene bridged resorcinarene followed the same protocol of the tetrabridged cavitand controlling the stoichiometric of the bridging agent. The most used bridging reagent[9] for tetramethylene bridged cavitands is CH_2ClBr but for a partially bridged resorcinarene we preferred to use the most reactive CH_2Br_2 because it has a higher boiling point and it allows a best control of its stoichiometric ratio (Scheme 4.5).

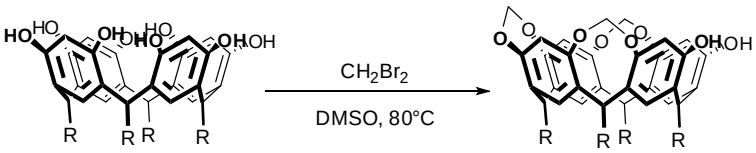

13

Scheme 4.5. Synthesis of partially bridge methylene cavitand ($R=C_2H_5$).

However the yield of this reaction is very low (13%) due to the presence of the tetrabridged cavitand as byproduct also working in defect of CH_2Br_2. This behavior is due to the high reactivity of the tribridged derivative under the reaction conditions.

The last step of the synthetic path was the bridging with the fluorescent moiety using the phosphonate chloride derivative as reagent (Scheme 4.6).

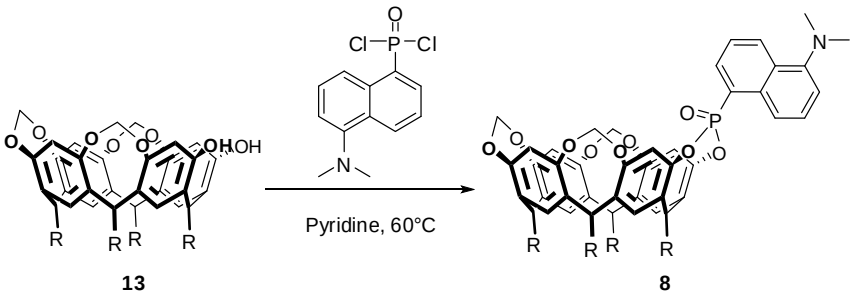

Scheme 4.6. Synthesis of the fluorescent receptor (R=C_2H_5).

Normally in this kind of reaction both isomers are formed, one with the P=O pointing into the cavity (PO_{in}) and the other pointing outside (PO_{out}). However in our case only the "in" isomer **8** was isolated as confirmed by ^{1}H-NMR (1D and 2D). The NMR proton chemical shifts are very similar to the protons of **5** where the absence of a shielding effect of the cavity proves that the naphthalene moiety points outside the cavity.

4.2.4 SOLUTION TESTING OF 8

Before performing the study at the gas-solid interface we decided to carry out a preliminary study in solution to understand the behavior of cavitand **8**. The titration was made in $CHCl_3$ Chromasolv® by adding absolute ethanol and UV-Vis and Fluorescence spectra were recorded.

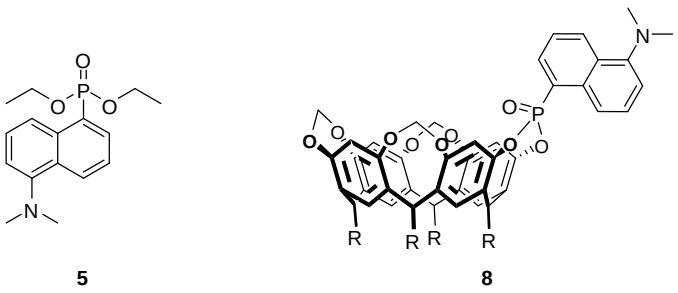

Figure 4.11. Molecules tested with solution titrations. The model compound **5** (left) and the cavitand receptor **8** (R=C_2H_5) (right).

We chose to test two molecules, the first is the model compound **5** and the second is our receptor **8** (Figure 4.11).
First of all we report the plot of the trend of the absorbance spectra at 340 nm and the trend of emission with an excitation light at 340 nm of the model compound **5** (Figure 4.12). It is very important to test a model compound without a cavitand scaffold to clearly identify its contribution in the recognition event.

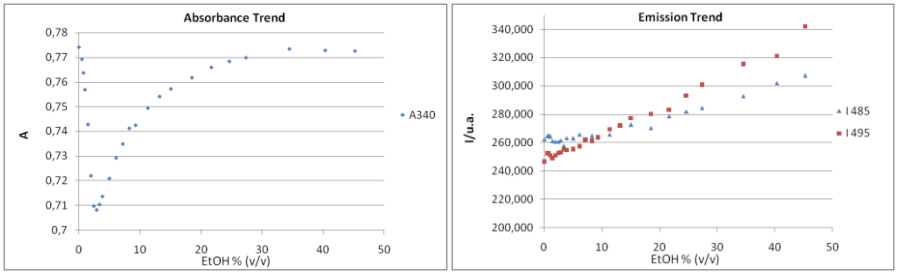

Figure 4.12. Plots of the trends of absorbance and emission spectra of the model compound **5**.

The absorbance trend at 340 nm is quite strange and present a "V" shaped form that indicates that the same absorption is present at two different concentrations of ethanol. However the emission trend (plot at 485 and 495 nm) is almost linear and it does not seem to reach a plateau. This is a strange behavior considering the amount of ethanol used in the titration.
For cavitand **8** we did the same titration and we found the same unexpected trend both in absorbance and emission trend (Figure 4.14).

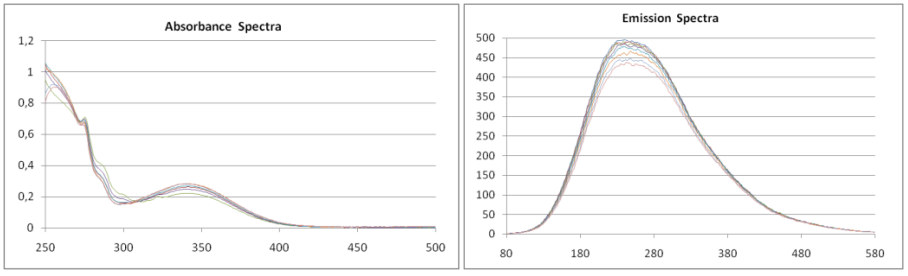

Figure 4.13. Absorbance and Fluorescence titration of the cavitand **8**.

Moreover in the emission spectra a red shift of the plots was expected, but only a change in intensity of emission was found. The maximum of the plots remained almost the same.

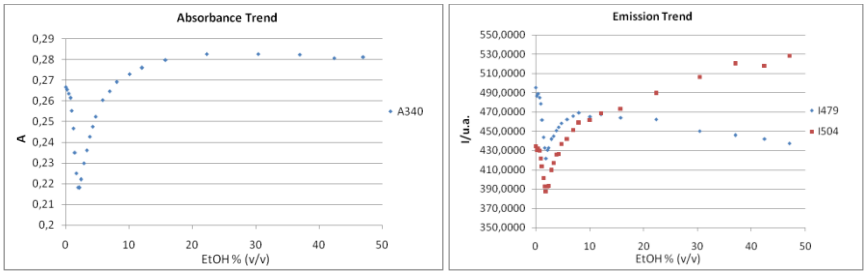

Figure 4.14. Plots of the trends of absorbance and emission spectra of the cavitand **8**.

Solution measurement are very important to understand the behavior of the receptors. Despite in the solution measurements the most important factor influencing the emission is the solvation and not the recognition event, with this results the use of this molecule as a sensor using its PCT characteristic is not possible.
We have not an explanation for this behavior but probably the hydrogen bond is not sufficient to change the chromophore emission system or there are some other interactions that mask its effect.

4.2.5 DESIGN OF A NEW FLORESCENT RECEPTOR

Since the first receptor made did not work as a luminescent sensors for alcohols we had to restart from molecular design to overcome the problem. The cavitand moiety did not seem to be the responsible of the malfunctioning of the receptor because also the model compound without the cavitand scaffold had unusual behavior in absorption spectra . As for chromophore **8** we need to have a hydrogen bond acceptor, and we cannot change this part of the molecule because the P=O group is the best choice as demonstrated in previous works with cavitands. [10] We need also a rigid conjugated scaffold and we decided to use again the naphthalene group because dimension is compatible with our cavitand system and its chemistry is familiar.

Another known fluorescent probe used in biochemistry is 8,1-ANS.[11] The corresponding phosphonate bridging derivative for our purposes is compound **12** (Figure 4.15).

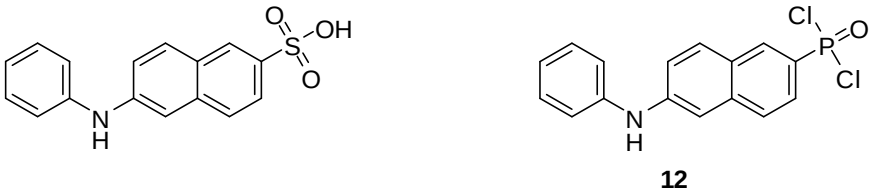

Figure 4.15. Fluorescent moieties. 8,1-ANS (left) and our fluorescent chromophore **12**.

The multistep synthesis of **12** starts from the bromo substituted naphthalene as show in the Scheme 4.7.

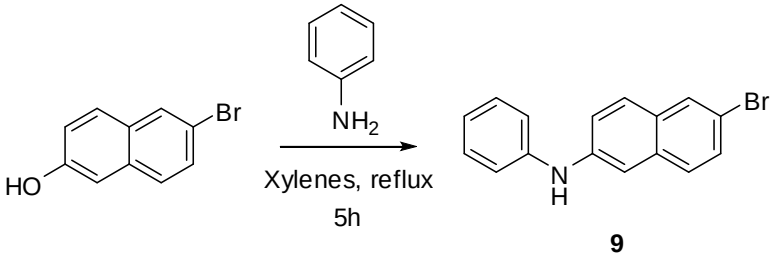

Scheme 4.7. Synthesis of 6-bromo-N-phenyl-2-naphthylamine (**9**).

Afterwards following the same protocol used for the molecule **5** we introduced in the molecule the P=O functionality.

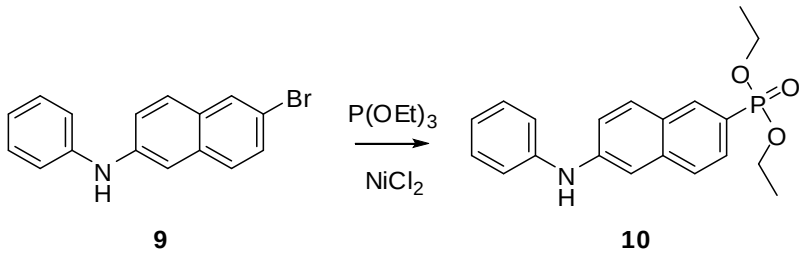

Scheme 4.8. Synthesis of the phosphonate ester naphthalene.

This reaction works well both on bromine and iodine substrates to give the desired product in 43% yield. Hydrolysis of the phosphonate ester with $(CH_3)_3SiBr$ and subsequently with methanol give the corresponding phosphonic acid in quantitative yield (Scheme 4.9).

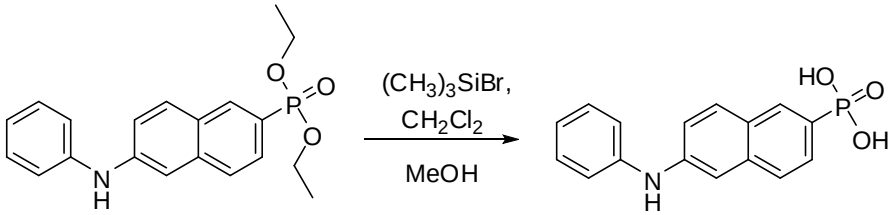

10 **11**

Scheme 4.9. Hydrolysis of ester to phosphonic acid.

The last step was the formation of the phosphonate dichloride. Following the same procedure used to synthesize the molecule **7**, the phosphonate dichloride was formed. Also in this case it was not isolated and used directly as bridging reagent for resorcinarene **13**.

The reaction was run in pyridine under mild conditions and it gave both **14-in** and **15-out** isomers (Scheme 4.10).The identification of the two isomers was achieved with a combination of NMR techniques (1D ^{1}H-NMR, 2D COSY ^{1}H-^{1}H NMR, ^{31}P-NMR). The ^{31}P-NMR spectra in acetone-d_6 shows a significant upfield shift of the peak belonging to **15-out** which is the result of the shielding effects exerted by the aromatic rings of the resorcinarene moiety on the naphtalenic group orientated inside the cavity, as described also by Dutasta and coworkers (Figure 4.16).[12]

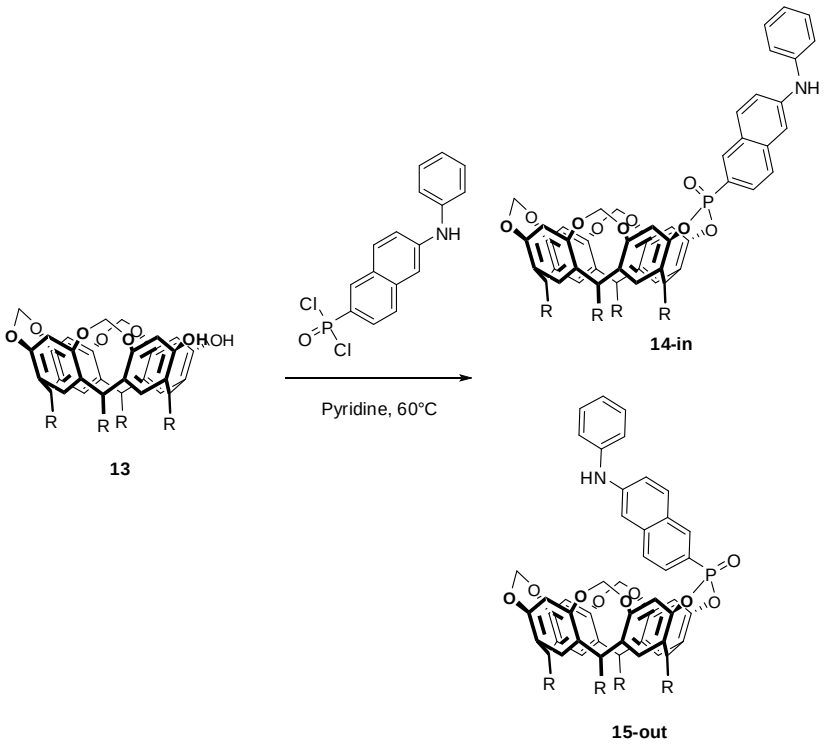

Scheme 4.10. Synthesis of the fluorescent cavitand receptors (R=C_2H_5). Isomer **14-in** and isomer **15-out**.

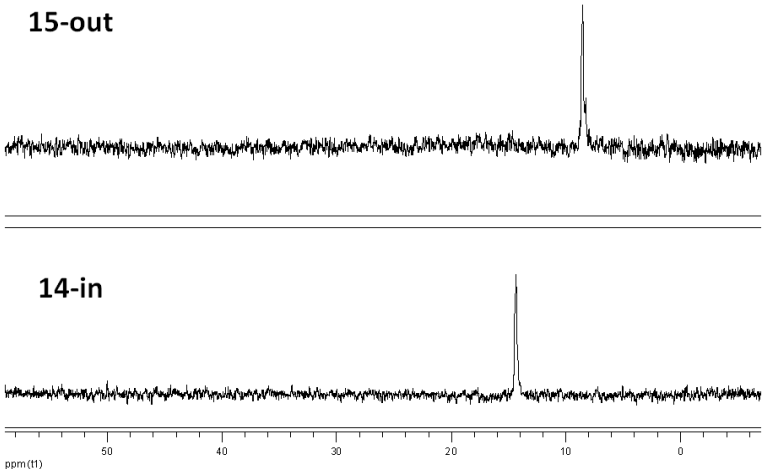

Figure 4.16. ^{31}P-NMR in acetone-d_6. Isomers **15-out** (up) and **14-in** (down).

The same shielding effect was responsible of the upfield shifting of hydrogens of naphthalene moiety in the ^{1}H-NMR spectra (Figure 4.17).

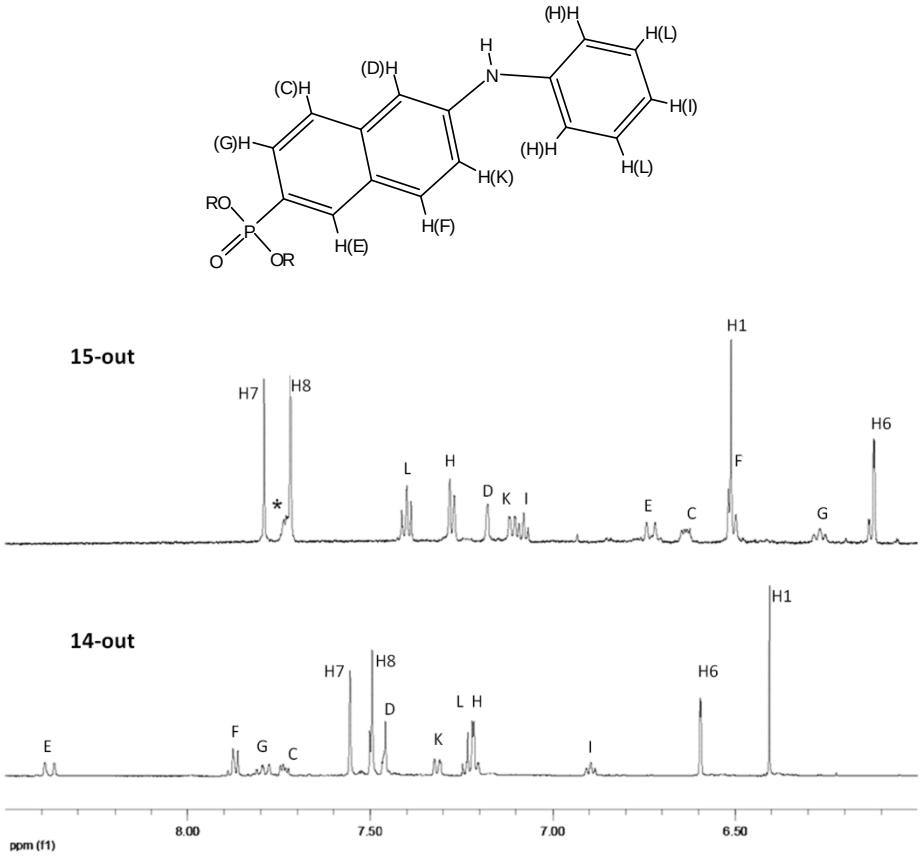

Figure 4.17. ^{1}H-NMR in Acetone-d_6. Isomer "out" **15-out** (up) and Isomer "in" **14-in** (down).

4.2.6 Solution meaurements of 14-in

In order to estimate the ability of our cavitands **14-in** and **15-out** to recognize short chain alcohols we performed fluorimetric titrations with ethanol. Moreover, we compared the results of this titration with that of the model fluorophore **10** to estimate the cavity effect. All the measurements were performed in two different solvents, chloroform and acetonitrile, in order to understand the effect of the polarity of the media.
The variation observed in the absorption spectra from the start (0% of Ethanol) to the end (50% of Ethanol) of titration can be attributed, for all three molecules, to the change of solvation of the ground state. Higher variation was found in chloroform in comparison to the more polar acetonitrile).
The emission spectra, follow the theoretical predictions with a shift to higher wavelength of the maximum peak (Red Shift).

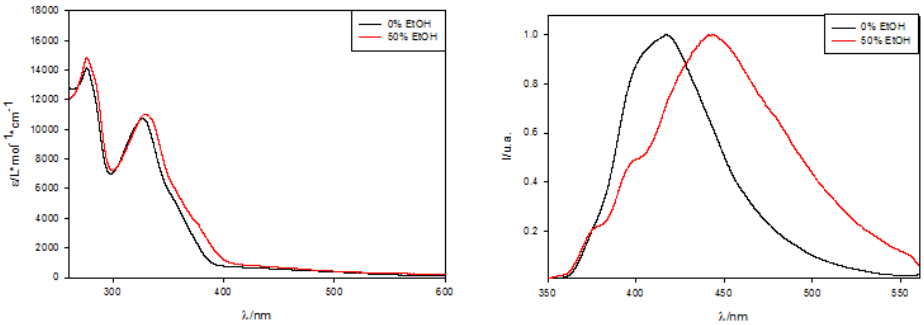

Figure 4.18. Absorption (left) and emission (right) spectra of the isomer **14-in** compound in $CHCl_3$. With 0% (black line) and 50% (red line) of abs. ethanol.

This behavior can be explained by the two factors that perturb our fluorophores. The first factor is the formation of an hydrogen bond between the P=O and the ethanol, and the second is the solvation of the fluorescent moiety by the ethanol. Obviously in solution, with high concentration of analyte, the second factor overpowers the first but at gas-solid interface the former will be the only present.
In the plots show in Figure 4.19 we report an analysis of the titration followed via fluorescence spectra. There is reported the intensity of emission light at a fixed wavelength versus the amount of ethanol during the titration.

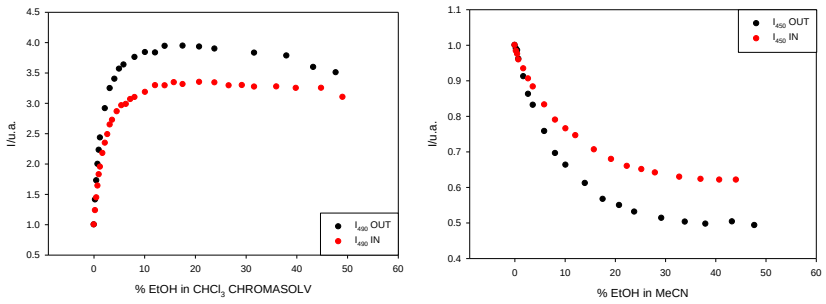

Figure 4.19. Comparison of trend of emission spectra in $CHCl_3$ (left) and MeCN (right). Isomer "out" (red dots) and Isomer "in" (black dots).

By comparing the plots of Figure 4.19 with the previous one relative to the fluorophore **8** we observe, in this case, the absence of a "V" curve that is correlated to a regular red shift of the emission spectra. With this trend we can correlate the adsorption to a single concentration of ethanol and we can build a sensor to detect this analyte.
We also measured of the Exited-State Lifetime and the Quantum Yield of the **14-in**, **15-out**, and **10** in $CHCl_3$.

Excited-State Lifetime			
Solvent	Compound		
	10	**14-in**	**15-out**
$CHCl_3$	2 ns	3.2 ns	3.1 ns
$CHCl_3$+ EtOH	6.2 ns	2.1 - 6.4 ns	2.6 – 6 ns
Ratio		1:8	1:1.25

Quantum Yield	
Compound	
10	1
14-in	1
15-out	0.5

Table 4.1. Tables of Exited-State Lifetime and Quantum Yield of Model compound and the two isomers **14-in** and **15-out** (Normalized to **14-in**) .

The results show that the cavitand **14-in** and the model **10** gave off the same quantity of light if excited with the same number of photons, whereas the cavitand **15-out** emitted half number of photons in comparison to the other two molecules.

We normalized the emission values recorded in the titration in chloroform and compared the emissions at 490 nm (Figure 4.20).

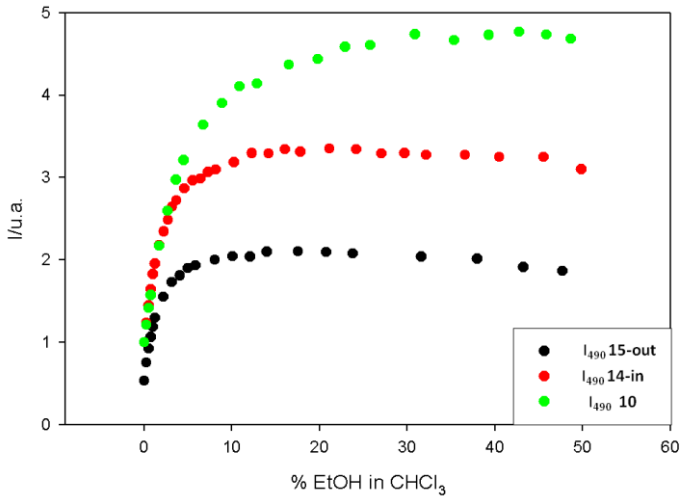

Figure 4.20. Comparison of emission trend plots normalized for quantum yield. **15-out** (black dots), **14-in** (red dots), and the model compound **10** (green dot).

First of all the slope of the plot before reaching the plateau are the same for the isomer **14-in** and **15-out** but it is different for the model **10**. Probably in solution there are no differences due to the orientation of the P=O because the ethanol can interact also with the out isomer so the role of the cavity is relevant only in the solid state. Moreover the amount of ethanol is huge in comparison to the quantity of the host molecules (10^{-4} M). For the model compound **10** the slope is quite lower but the absolute emission intensity reached is higher. The differences between slopes give information about "complexation constant" in other word how much the host-guest system is far from the ground state, so the model can detect the ethanol in a less efficient way but its excited state is more different from its ground state in comparison to the other two molecules. This observation is also confirmed by the analysis of single-photon lifetime in two different situations: the first in the case of the presence of the only $CHCl_3$ (free host) and the second in presence of 50% of ethanol (host totally complexed). In the first case the decay of the excited state is monoexponetial, which means that there is only a single emitting exited compound, about 3 ns for the cavitands and 2 ns for the model compound. The situation is more complicated in the second case, in the presence of the guest.

The model compound has still a single lifetime of 6 ns, longer with respect to the free host due to the solvation of the ethanol that stabilize the PCT excited state. In the case of the two cavitands the decays of emission do not fit with a single lifetime. Rationalizing the data we can fit the decays with two lifetimes referable to two types of the emitting excited state. The first lifetime is about 2 ns and the second is about 6 ns similar to the lifetime of the model compound. The proportion of the two types of the excited state can be obtain by the fitting equations. In the case of cavitand **14-in** the ratio it is about 1 to 8 in favor of the state similar to the model compound but in the cavitand **15-out** case the ratio is 1 to 1.25. If we consider a longer lifetime of the model as a consequence of its completely solvation by ethanol, in the case of the isomer "in" compound we have a solvation of about 88% versus 55% of the isomer "out", that agrees with the different conformation of the two molecules.

4.2.7 GAS-SOLID INTERFACE APPARATUS

Film deposition

To be used as gas sensors the cavitands must be deposited on a suitable surface. In this paragraph we describe how we prepared the sensing layer.

For our purpose the principal characteristic of the sensing material is the transparency so we used a glass substrate. The cavitands were diluted in a polymeric matrix.

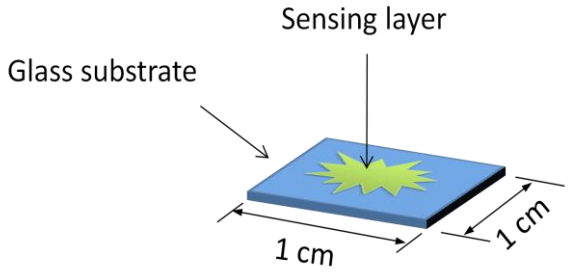

Figure 4.21. Representation of the sensing layer on the glass substrate.

A common polymer used to make transparent thin film is the Polyvinyl Chloride (PVC). PVC has a T_g of 80°C, so to make a transparent thin film in PVC we need to mix it with a plasticizer to reduce its T_g and make it permeable to

the analytes. A frequent class of colorless plasticizer used also in medical devices is dioctyl sebacate (Figure 4.22).

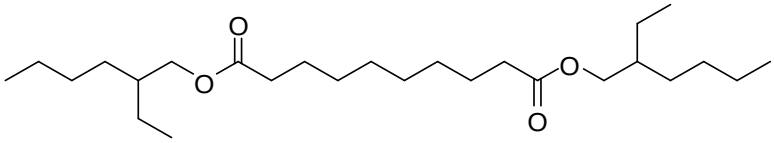

Figure 4.22. Dioctyl sebacate

The material obtained from the mixing of PVC, dioctyl sebacate and fluorophore is colorless, flexible and it adheres very well to the glass substrate, in addition it is permeable to the gas and the analytes. The active molecule (the fluorescent receptor) in the matrix is present only in a small amount (0.1%-0.2% w/w), higher concentration cause a saturation of the signal of the fluorimeter due to a too high intensity of light emitted.
We made the deposition via spin coating of the matrix dissolved in THF. We chose this deposition technique for its characteristics of reproducibility and user-friendliness. With this technique we spotted several substrates containing **14-in**, **15-out** and model compound **10**.

Instrument set-up

To test the gas sensor we need to put in contact the sensing layer with the analytes and at the same time to excite the fluorophore and acquiring the light emitted. We used a hand-made prototype of a sealed chamber mounted on a platform able to be inserted in a Perkin-Elmer LS 55 Luminescence Spectrometer (Figure 4.23). The glass substrate is put in the window and it leans on a gasket to ensure the gastight of the chamber. The face of the substrate with the sensing layer is in the chamber and the exciting light can reach the fluorophore through the glass substrate.

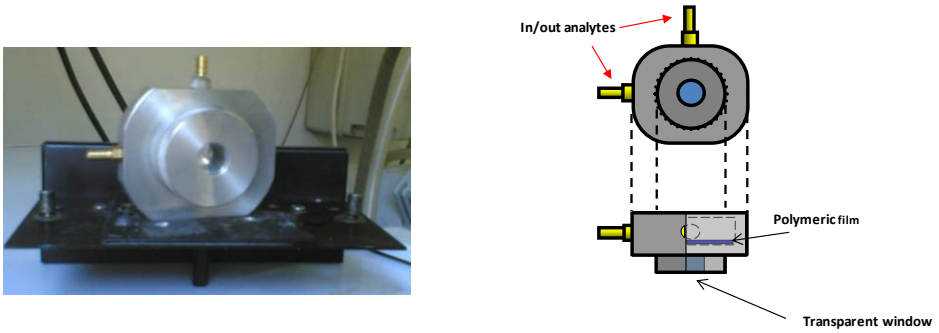

Figure 4.23. Sampling chamber. Picture (left) and graphic representation (right).

The geometry of the system is optimized for the detection of luminescence from a solid sample with 40° of inclination.

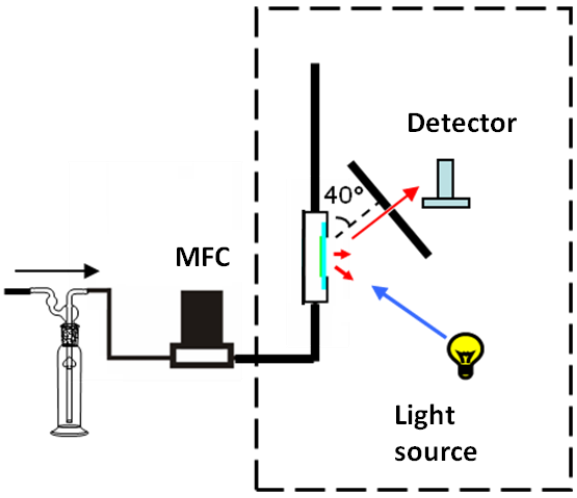

Figure 4.24. Representation of the instrument setup.

4.2.8 Sensor measurements

The first set of measurements was done fluxing a high concentration of analyte diluted in nitrogen (about 10000 ppm). The aim of the fist experiment was to test the main characteristic of a sensor: the sensibility and the reproducibility. Three molecules were tested: cavitands **14-in** and **15-out** and the model compound **10**. The emission spectra of the free hosts in the polymeric matrix show the same trend of the corresponding spectra in solution.

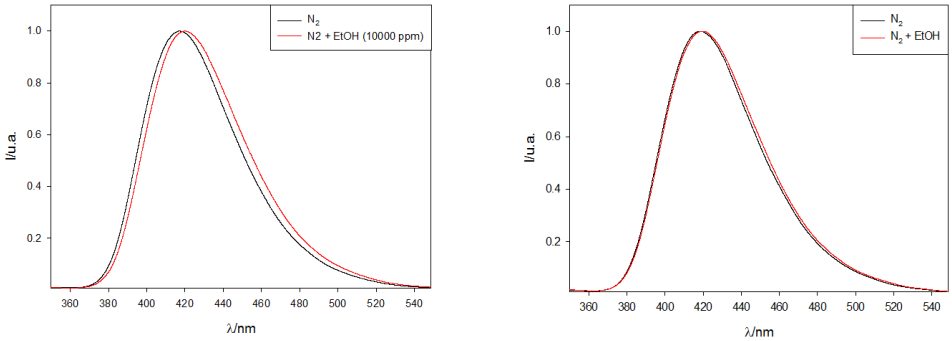

Figure 4.25. Normalized solid state emission spectra of **14-in** (left) and **15-out** (right). Red line with pure nitrogen and black line with 10000ppm of abs. ethanol.

As show in Figure 4.25 there is a red shift of the maximum peak, but in comparison with the spectra in solution the shift is smaller due to the lack of the solvation contribute present in solution. The red shift is only attributable to the perturbation of the fluorophore due to the hydrogen bonding with the analyte (ethanol). If we compare the isomer **14-in** spectra whit the **15-out** spectra the shift is almost absent in the **15-out** case while it is bigger in solution. As a matter of fact we saw in solution the same shift for the two isomers, but in the solid state the cavity plays a fundamental role in the recognition event. In the **14-in** isomer the presence of a rigid, preorganized cavity embracing the P=O group eliminates the need of generating a void in the lattice for the incoming analyte, on the contrary in the **15-out** one this volume is occupied by the fluorophore and the binding site, the P=O, point outside in the PVC matrix.

In “sensor science” is fundamental to have a reference molecule structurally similar to the main sensor molecule but insensible to the analyte. It is important to better understand the mechanism of the recognition event and

to report all the measure to this “zero” signal molecule. In our case cavitands bearings the same fluorescent moiety but having different orientation of the hydrogen bonding acceptor with respect to the cavity make one a good sensor and the other a bad one.
To be use as a sensors in a dynamic setting we have to record a signal versus time, so we need to measure a single parameter varying in the time. We cannot measure the maximum shift because to record all the plot, we need to scanning all the wavelengths form 540 nm to 340 nm. So we decided to measure only the variation of emission intensity at one wavelength with the “time drive” function of the Luminescence Spectrometer.
In Figure 4.26 there is an example of the plot recorded in “time drive” mode. The black plot represent the emission light intensity at 460 nm of **14-in** excited at a wavelength of 333 nm. We can see the reversibility and the quickness of the response in comparison with the red line (**15-out**) almost insensible to the analyte.
Several coatings have been tested showing the complete reproducibility of the deposition.

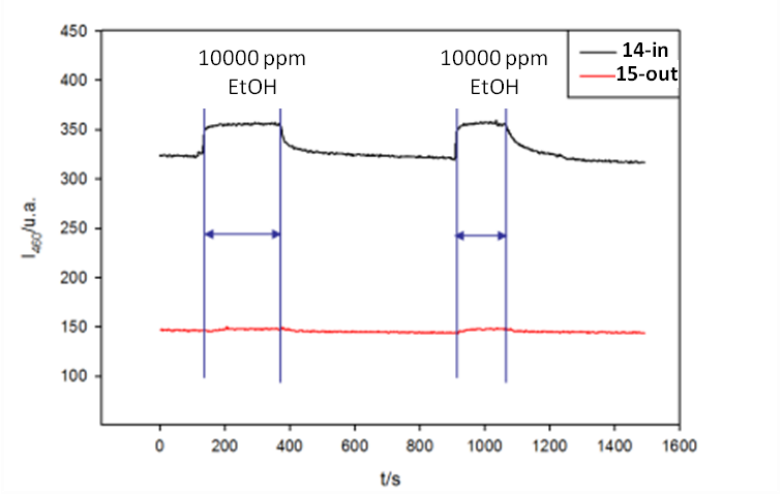

Figure 4.26. Sensor measurements: Time drive at 460 nm of **14-in** (black line) and **15-out**.

Working with saturated gas is not easy and there are a lot of error sources. To make more precise measurements and to test our sensor with several alcohols at the same concentration we need to use calibrated cylinders e a system of gas distribution with two or three mass flow controllers to minimize the errors.

Unfortunately the certified calibrated cylinder commercially available are only in the range of 100-500 ppm. At this low concentration of analytes, with our instrumental setup, the ratio signal/noise is not very good but the results are sufficient accurate to make a preference scale of the sensor (Figure 4.27). This problem is principal imputable to the software of the Perkin Elmer fluorimeter (FL WINLAB 4.00.02) that does not allow to redefine the arbitrary units of the emission that have a maximum value of 1000; above this limit the plot is not recorded.
The responses toward methanol, ethanol and propanol at respectively 516, 500, and 501 ppm as reported in Figure 4.28. The observed trend is methanol>ethanol>propanol. The same trend is observed at 100 ppm where the response on n-pentanol is within the experimental error, as expected (see later).

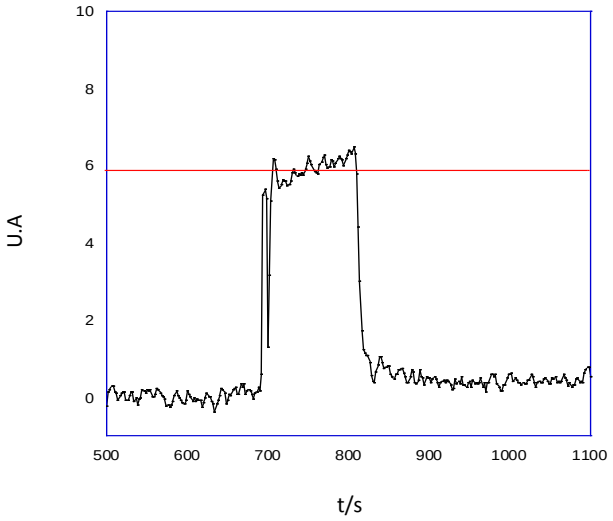

Figure 4.27. Response of the sensor (isomer **14-in**) to a concentration of 500 ppm of methanol (base line normalized).

A statistical treatment of the data for the isomer **14-in** is reported in the histogram in figures 4.28 and 4.29.
The **15-out** and the model compound **10** coatings show a signal within the instrumental noise for all analytes. This behavior, in contrast with the solution measurements, confirms the importance of a free cavity in a solid lattice able to host the analyte.

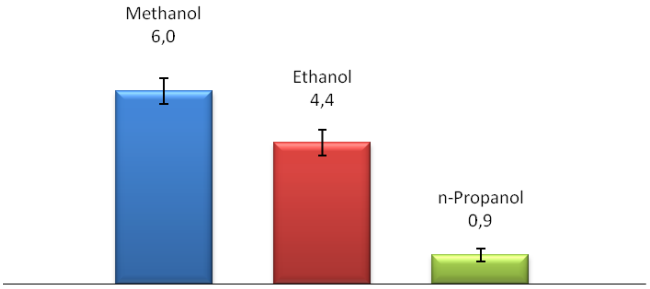

Figure 4.28. Histogram of sensor responses versus 500 ppm of methanol, ethanol and n-propanol.

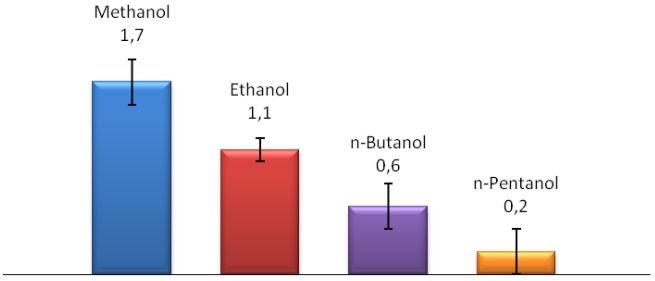

Figure 4.29. Histogram of sensor responses versus 100 ppm of methanol, ethanol, n-butanol, and n-pentanol .

To better understand the recorded data we can compare them with a previous study[10] about the detection of alcohols with cavitand made with QCM transducers, with a molecule very similar to our host (Figure 4.30).
The figure summarized the responses (-Δ*f*/Hz) of the monophosphonated cavitand and PECH (polyepichlorohydrin a reference polymer) to linear C_1-C_5 alcohols. The trend of QCM measurements is the opposite of our results with the luminescent approach. In the QCM measurements general enhancement of the responses of the cavitand is associated with increasing number of carbon atom of the alkyl chain of the alcohols.

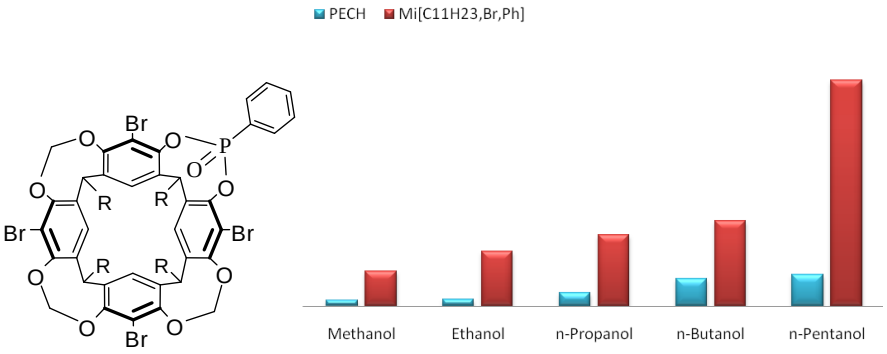

Figure 4.30. Histogram of QCM responses of monophosphonated cavitand (red) and PECH (light blue) to 3000 ppm alcohols (C_1-C_5).

This behavior is due to a greater number of purely dispersive interactions, which are directly related to chain length, and not to any strengthening of the specific CH-π and hydrogen bonding interactions, which should be comparable for all alcohols of the series. The reason is that the QCM transducers are absolutely unspecific, since they do not make any difference whether the interaction takes place in the molecular recognition site or elsewhere in the layer. In our system only specific interactions between the analyte and the receptor induce a variation of luminescence, therefore excluding unspecific interactions.

As a matter of fact by normalize the responses to those of PECH, that is totally unspecific, we obtain a trend similar to the behavior of our fluorescent sensors **14-in** (Figure 4.31).

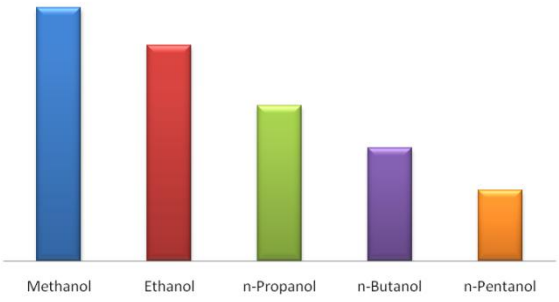

Figure 4.31. Histogram of QCM responses of QCM coated with Mi[$C_{11}H_{23}$,Br,Ph] to 3000 ppm alcohols normalized to those of PECH.

Crystal structure determinations showed that the source of selectivity in this type of cavitands is linked to the presence of two synergistic interaction namely CH-π interactions between the methyl group of each alcohol chain and the H-bond between the P=O and the alcoholic OH. This synergy is possible only for C_1-C_4 alcohols and not for C_5 alcohol. Therefore the responses of **14-in** to n-pentanol should be zero, as experimentally prove in Figure 4.20. The next step is to prepare a cavitand receptor even more specific, capable of binding only methanol and ethanol.
This can be achieved via a rational design of the cavity reducing the space available for the alcohol chain inclusion.
The cavity of **14-in** has a relative large space allowing the positioning of several different guests.

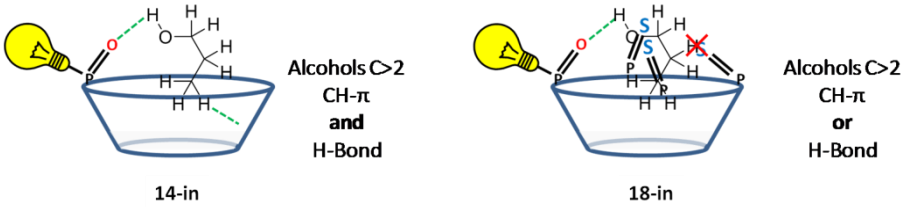

Figure 4.32. Graphical explanation of shape selectivity.

Introducing other P=O groups would reduced the fluorophore perturbation since the H-bonding would have been distributed among four P=O. Instead the introduction of three P=S bridging groups, without fluorophore attached, will confine the H-bonding on the remaining P=O, since the P=S is by far less efficient on H-bonding. The bulkiness of the three P=S will reduce and shape the cavity size with respect to **14-in** as show in Figure 4.32.
As reported in the molecular modeling of two cavitands (Figure 4.33), one with four P=O group and one with three P=S and one P=O groups, the possibility of make hydrogen bond together with CH-π interactions is possible only for short chain alcohols like methanol and ethanol. A longer chain alcohol does not fit in the cavity and can only make CH-π or hydrogen bond interaction but not both in the same time.

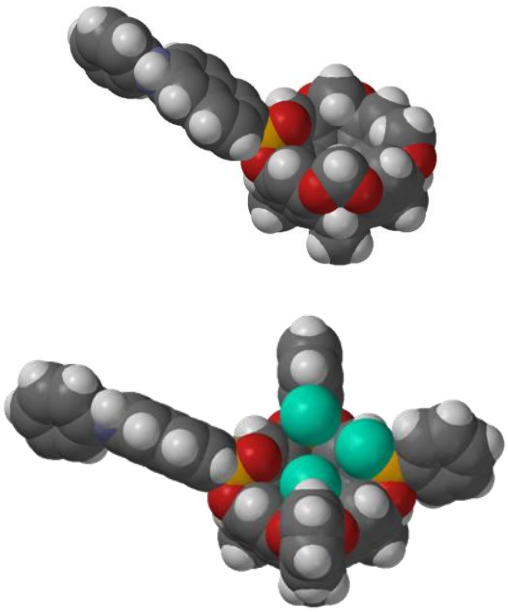

Figure 4.33. Energy minimized molecular modeling of **14-in** (up) and **18-in** (down).

4.2.9 Synthesis of cavitand 18-in

By analyzing retrosynthetically the possible routes to cavitand **18-in**, the simplest approach require the introduction of the P=O bridge with the fluorophore as the last step, as in the case of **14-in**.
As described in Chapter 6 the better way to make a partially bridged cavitand with three P=S is not the direct synthesis but the selective excision of one of the P=S bridges of a tetrabridged cavitand.
The first step is the therefore the formation of TSiiii [C_2H_5, H, Ph] **16** as reported in Scheme 4.11.

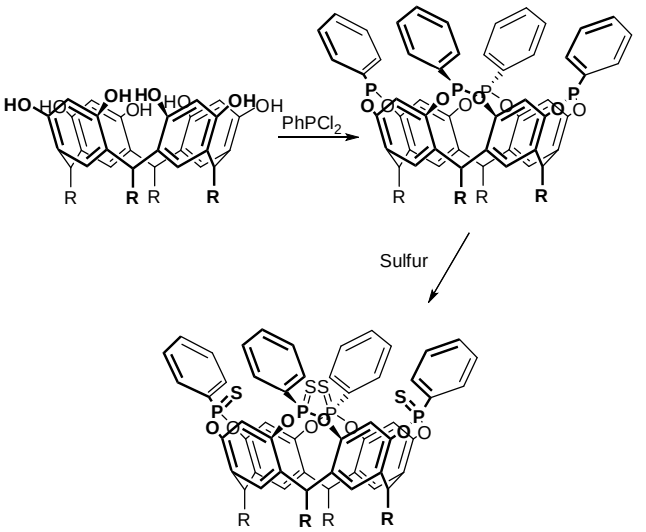

Scheme 4.11. Synthesis of the TSiiii [C_2H_5, H, Ph] **16** tetrathiophosphonate cavitand R=C_2H_5.

The starting cavitand **16** (Scheme 4.11) was prepared in good yields according to the protocols reported in the literature[13] starting from the ethyl-footed resorcinarene. Briefly, 4.05 equivalents of dichlorophenylphosphine were added to the resorcinarene solution under basic conditions to give a tetraphosphonito cavitand. The intermediate was treated with sulphur to obtain the desired tetraphosphonated cavitand **16**. This synthetic procedure allows the formation of the [iiii] stereoisomer with the four P=S oriented towards the molecular cavity as only product.
In the second step the excision of one bridge was made using a stoichiometric amount of catechol in the presence of K_2CO_3 as base (Scheme 4.12).

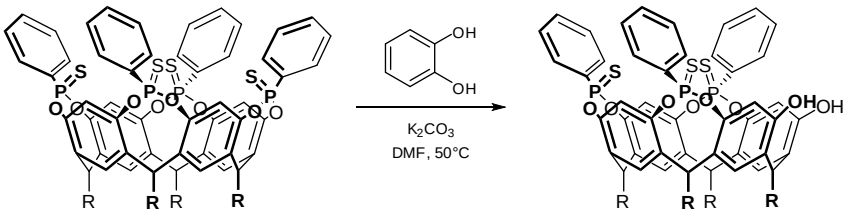

16 **17**

Scheme 4.12. Synthesis of cavitand **17** (R=C_2H_5).

In the last step the P=O bridging was made under mild conditions using the phosphonate chloride **12**. As reported for the synthesis of **14-in** and **15-out**, also in this case we obtained both in and out stereoisomers.

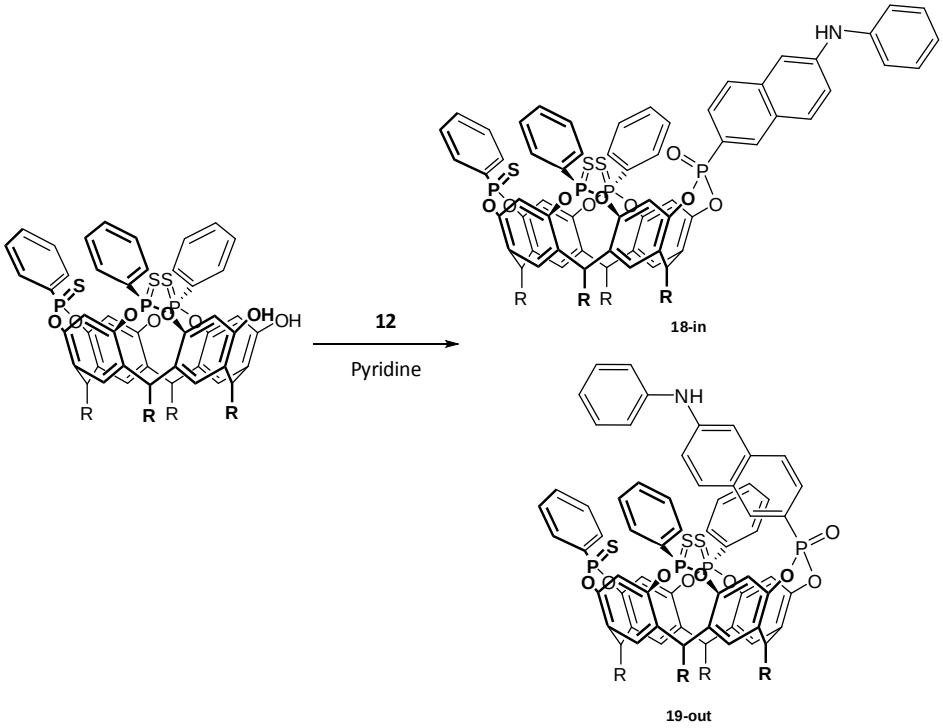

Scheme 4.13. Synthesis of cavitand **18-in** and **19-out** (R=C_2H_5).

4.2.10 SOLUTION MEASUREMENT OF 18-IN

The cavitand receptor **18-in** was tested in solution together with its isomer **19-out** in order to verify the absorption and emission behavior in titration with alcohols.
As reported in the plots in Figure 4.34, after ethanol titration, no significant changes of absorption spectra both for **18-in** and **19-out** were observed.

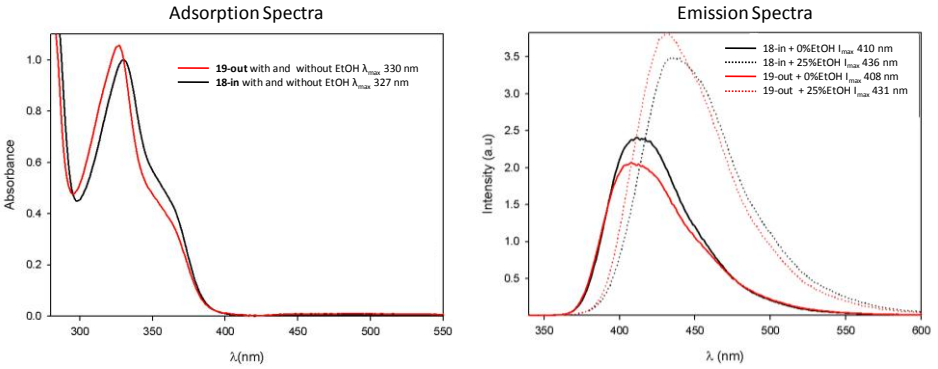

Figure 4.34. Absorption and Emission spectra of **18-in** and **19-out** in chloroform before and after the titration with ethanol.

Instead, in the case of the emission spectra, we observed a significant enhancement in intensity and batochromic shift of the maximum of emission in both cases. The excited-state lifetime and the quantum yields were calculated and reported in Table 4.2.

Excited-State Lifetime		
Solvent	Compound	
	18-in	**19-out**
$CHCl_3$	1.3 ns	5.25 ns
$CHCl_3$+ 20 %EtOH	1.27 ns	5.21 ns

Quantum Yield	
Compound	
18-in	1
19-out	0.8

Table 4.2. Tables of Exited-State Lifetime and Quantum Yield of the two isomers **18-in** and **19-out** (Normalized to **18-in**).

The higher quantum yield of **19-out** with respect to **15-out** is an indication that the fluorophore is more solvated, therefore less included in the cavity of **19-out**. This is a clear effect of the presence of larger P=S bridges on the cavity availability as shown also by NMR.
We carried out four titration in $CHCl_3$ to evaluate the selectivity of our sensor. In Figure 4.35 the titration of **18-in**@ethanol, **18-in**@propanol, **18-in**@1-butanol, and **19-out**@ethanol are reported. All plots showed a common increase trend in the first part and a plateau region at high concentrations of the analyte, but for the **18-in**@ethanol the increase curve was steeper, proving a superior response to ethanol.

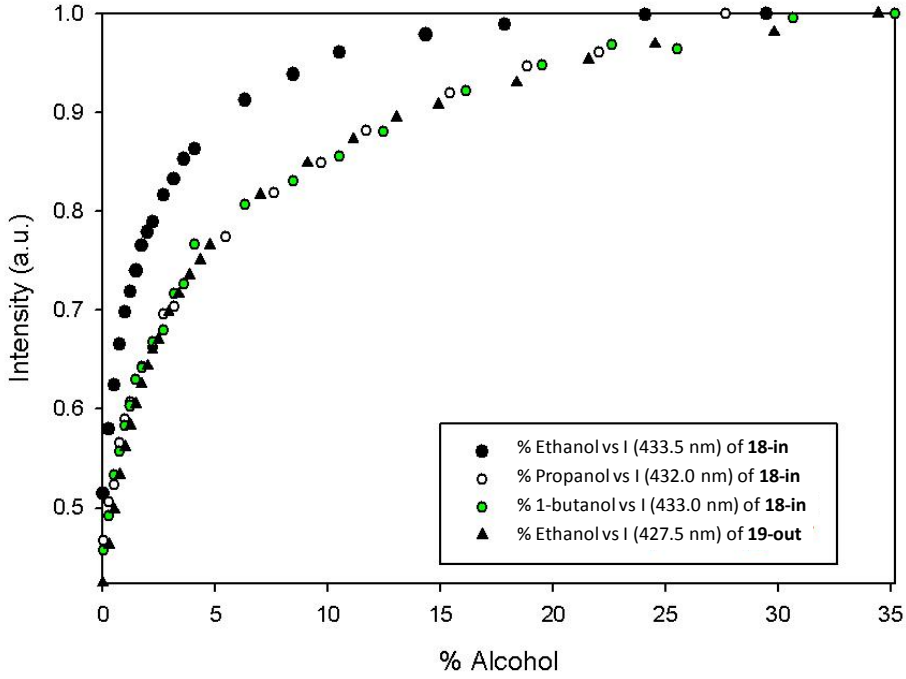

Figure 4.35. Comparison of trend of emission spectra in $CHCl_3$ of **18-in**@ethanol, **18-in**@propanol, **18-in**@1-butanol, **19-out**@ethanol.

The remarkable difference of the behavior of **18-in** towards ethanol is supported by the response of **19-out** to the same analyte. The curve of the latter overlap nicely with all the others. Since **19-out** does not bind ethanol, we attribute the responses of **18-in** to propanol and butanol to solvation effect as for **19-out**. Consequently the enhanced response of **18-in** to ethanol can be

attributed to cavity inclusion. Therefore the cavity reduction due to the presence of three inward facing P=S bridges further increases selectivity with respect to the case of the methylene bridged **14-in**. Gas-phase experiments are needed to verify the sensing behavior of **18-in**.

4.4 Conclusions

In this Chapter we reported an innovative approach to alcohols sensing. The QCM transducers have been replaced by a fluorescence transduction mode. This has required selection of the appropriate fluorophore to be inserted on the cavitand in the correct position. The correct solution turned out to be cavitand **14-in** bearing a 8,1-ANS derivative directly on the H-bonding P=O. This cavitand respond selectively to C_1-C_4 linear alcohols at the gas-solid interface, in a decreasing intensity moving from C_1 to C_4. This result is perfectly in line with the solid state prediction of cavitand complexation behavior towards alcohols.[14] A further improvement in selectivity has been achieved by reducing the cavity opening at the upper rim, by substituting the three methylene bridges with three P=S ones. The corresponding cavitand **18-in** is responding in solution only to methanol and ethanol. In both receptors, the remarkable difference in behavior of *in* and *out* isomers clearly proves the importance of the cavity for selective inclusion. The *out* isomers are useful as blank reference in sensors array to avoid false alarms.

4.5 Acknowledgments

Special tanks to Francesca Panciroli and Laura Pirondini of University of Parma and Luca Prodi, Marco Montalti, Gionata Battistini and Sara Bonacchi of University of Bologna.

4.6 Experimental section

General method: All commercial reagent were ACS reagent grade and used as received. For the synthesis all solvents were dried over 3 Å and 4 Å molecular sieves. The ^{1}H-NMR spectra were recorded on Bruker Avance 300 (300 MHz) and Varian INOVA 600 (600 MHz) spectrometers and all chemical shifts (δ) were reported in parts per million (ppm) relative to proton resonances resulting from incomplete deuteration of NMR solvents. The ^{31}P-NMR was recorded on Bruker AMX-400 (162 MHz) and all chemical shifts were reported to external 85% H_3PO_3 at 0 ppm. ESI-MS experiments were performed on a Waters ACQUILITY SQD Detector equipped with a ESCi® multi mode ionization (APCI/ESI). Absorption spectra in solution were recorded on Perkin-Elmer Lambda 40 spectrophotometer. The Fluorescent spectra (450W Xe Lamp), in solution and in the solid state, were recorded on a Perkin-Elmer LS55 equipped with a R928P photomultiplier detector.

5-Nitronaphthalen-1-amine (1): To a suspension of 1,5-dinitronaphtalene (10 g, 45.8 mmol) in 250 mL of water, a solution of ammonium chloride (17.4 g, 325 mmol) in concentrated aqueous ammonia 28% was added. The mixture was stirred and warmed at 85°C, and Na_2S-$9H_2O$ (36.32 g, 151 mmol) was added in three portions each 10 minutes. The mixture was heated at 85°C for 4h and then filtered through a heated Büchner funnel. The solid was extracted twice with dichloromethane and water and the organic layer was dried to give the pure product (6.65g, 77%).

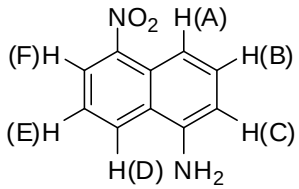

^{1}H NMR (300 MHz, $CDCl_3$): δ= 8.12 (d+d, 2H, H_A + H_D), 7.88 (d, 1H, H_F, J=8.7 Hz), 7.51 (t+t, 2H, H_B + H_E), 6.89 (d, 1H, H_C, J=7.5 Hz), 4.25 (bs, 2H, NH_2); **ESI-MS** *m/z* (%): 143 [M-NO_2+H^+, 60].

1-Iodo-5-nitronaphtalene (2): To a solution of sodium nitrite (805 mg, 11.7 mmol) in 8 mL of concentrated sulfuric acid at 0°C a solution of 5-nitronaphthalen-1-amine **1** (2.0 g, 10.6 mmol) in 15 mL of glacial acetic acid was added dropwise and stirred for 30 minutes. Then, the mixture was poured into ice (14 g), additioned with urea (0.14 g), potassium iodide (29 g, 0.2 mol), and water (29 mL) and stirred for 18h at room temperature. The solid was filtered, dried and extracted with water and CH_2Cl_2 and the organic layer was dried to give the pure product (2.24g, 70%).

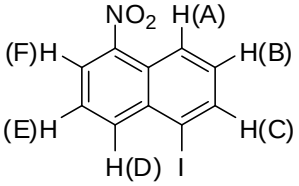

^{1}H NMR (300 MHz, $CDCl_3$): δ= 8.48 (d+d, 2H, H_A + H_D), 8.23 (d+d, 2H, H_F + H_C), 7.64 (t, 1H, H_B, J=7.7 Hz), 7.39 (t, 1H, H_E, J=8.0 Hz); **GC-MS** *m/z* (%): 299 [M^+, 100].

5-Iodonaphtalen-1 amine (3): To a solution of 1-Iodo-5-nitronaphtalene **2** (1.2 g, 4.01 mmol) in 30 mL of freshly distilled ethyl acetate $SnCl_2$-$2H_2O$ (4.53 g, 20.1 mmol) was added under argon atmosphere. The mixture was stirred for 16h at 80°C and then poured onto ice (160 g). The pH of the mixture was made basic (pH about 10) by addition of aqueous sodium hydroxide and finally extracted with CH_2Cl_2. The organic layer was dried to give the pure product as a brown oil (0.841g, 78%).

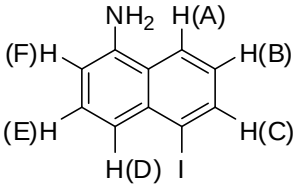

^{1}H NMR (300 MHz, $CDCl_3$): δ= 8.08-7.92 (d+d, 2H, H_A + H_D), 7.83-7.60 (d+d, 2H, H_F + H_C), 7.15 (t, 1H, H_B, J= 7.7 Hz), 6.90 (t, 1H, H_E, J=8.1 Hz), 4.20 (bs, 2H, NH_2); **GC-MS** *m/z* (%):269 [M^+, 100], 142[M^+-I, 20].

5-Iodo-N,N-dimethylnaphthalen-1-amine (4): To a solution of compound 5-Iodonaphtalene-1-amine **3** (841 mg, 3.13 mmol) and aqueous formaldehyde 37% (800 mL) in 160 mL of acetonitrile, sodium cyanoborohydride (196 mg, 3.12 mmol) was slowly added, under argon atmosphere. The mixture was stirred at room temperature, and 0.67 mL of glacial acetic acid was added dropwise in 1h. The mixture was stirred for 4h and then poured into basic water (pH 9-10 with KOH) and extracted twice with CH_2Cl_2. The organic layer was dried and purified by column chromatography on silica gel by using Hexane/CH_2Cl_2 (6:4 v/v) as eluent to give compound **4** as a dark brown solid (622 mg, 67%).

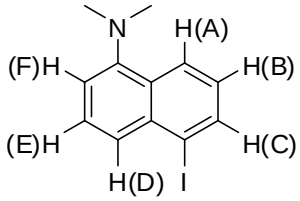

^{1}H NMR (300 MHz, $CDCl_3$): δ= 8.27 (d, 1H, H_A, J=8.5 Hz), 8.06 (d, 1H, H_D, J= 7.2 Hz), 7.78 (d, 1H, H_C, J=8.5 Hz), 7.50 (t, 1H, H_E,J=7.8 Hz), 7.25-6.98 (m, 2H, H_B + H_F), 2.87 (s, 6H, CH_3); **GC-MS** *m/z* (%):297 [M^+, 100], 170[M^+-I, 80].

diethyl 5-(dimethylamino)naphthalen-1-phosphonate (5): To a solution of **4** (900 mg, 3.03 mmol) in 4 mL of triethyl phosphate a catalytic amount of $NiCl_2$ (40 mg, 0.31 mmol) was added, under argon, in a sealed tube and the solution was stirred for 20h at 180°C. The solution was poured into water and extracted twice with CH_2Cl_2. The organic layer was dried under high *vacuum* and the crude product was purified by preparative TLC on silica gel by using Ethyl acetate/CH_2Cl_2 (3:7 v/v) as eluent to give the pure compound (414 mg, 45%).

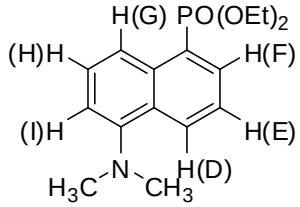

^{1}H NMR (300 MHz, $CDCl_3$): δ= 8.49 (d, 1H, H_D, J=8.4 Hz), 8.26-8.16 (m, 2H, H_E + H_F), 7.50 (m, 2H, H_G + H_H), 7.14 (d, 1H, H_I, J=7.3 Hz), 4.26-4.00 (m, 4H,

OCH_2CH_3), 2.87 (s, 6H, NCH_3), 1.30 (t, 6H, OCH_2CH_3, J=7.0 Hz); **GC-MS** *m/z* (%):307 [M^+, 80], 170 [M^+-$PO(OEt)_3$, 100].

5-(dimethylamino)naphthalen-1-phosphonic acid (6): A solution of **5** (114 mg, 0.37 mmol) in 5 mL of HCl_{conc} was stirred for 18h at 90°C. The yellow solution was dried under *vacuum* to give the pure product as white powder (90 mg, 97%).

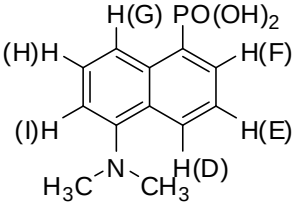

^{1}H NMR (300 MHz, CD_3OD): δ= 8.85 (d, 1H, H_G, J=8.6 Hz), 8.63 (d, 1H, H_I, J=8.6 Hz), 8.30 (dd, 1H, H_F), 8.12 (d, 1H, H_D, J=7.6 Hz), 7.86-7.78 (m, 2H, H_E + H_H), 3.53 (s, 6H, NCH_3); **ESI-MS** *m/z* (%): 274 [M+Na^+, 100].

5-(dimethylamino)naphthalen-1-phosphonic dichloride (7): To a solution of **6** (285 mg, 0.99 mmol) in 5 mL of phosphoryl trichloride, PCl_5 (207 mg, 0.99 mmol) was added, under nitrogen atmosphere. The dark solution was stirred at 85°C for 18h than the solvent was removed under *vacuum* and the dark solid was used immediately in the next step without further purification and characterization.

Cavitand 8: To a solution of **7** (45 mg, 0.16 mmol) in 10 mL of dry pyridine in a sealed tube, was added, under argon, Ethyl-footed trimethylene-bridged resorcinarene **13** (50 mg, 0.08 mmol) and the solution was stirred at 60°C for 24h. The solvent was removed under *vacuum* and the crude product was dissolved in CH_2Cl_2 and washed with water. The organic layer was dried and the pure product was obtained by preparative TLC on silica gel by using ethyl acetate/Hexane (4:6*v/v*) as eluent to give isomer "in" (12 mg, 18%).

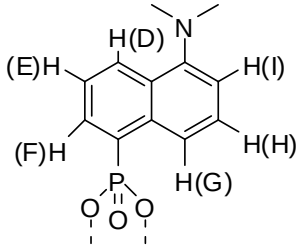

^{1}H NMR (300 MHz, acetone-d_6): 8.63 (d, 1H, H_D, J=8.0 Hz), 8.47 (d, 1H, H_G, J=8.2 Hz), 8.38 (dd, 1H, HF, J=7.0 Hz, J=17 Hz), 7.71-7.57 (m, 6H, H_E + H_H + H_d), 7.27 (d, 1H, H_I, J=7.2 Hz), 7.72 (d, 2H, H_u, J=1.9 Hz), 6.52 (s, 2H, H_u), 5.76 (d, 2H, H_{out}, J=7.4 Hz), 5.64 (d, 1H, H_{out}, J=7.5 Hz), 4.70-4.56 (m, 6H, H_{in} + Ar-C*H*-Ar), 4.25 (d, 1H, H_{in}, J=7.5 Hz), 2.87 (s, 6H, NCH_3), 2.36 (m, 2H, CH_2-CH_3), 2.27 (m, 6H, CH_2-CH_3), 0.92-0.81 (m, 12H, CH_3); **ESI-MS** *m/z* (%): 847 [M+Na^+,100].

6-bromo-N-phenylnaphthalen-2-amine (9): A mixture of 6-bromo-2-naphthol (8.2 g, 37.1 mmol), aniline (12.5 mL, 0.14 mol), xylene (12 mL), and p-toluensulfonic acid monohydrate (1.41 g, 7.41 mmol) was heated to reflux under nitrogen. A portion of xylene was distilled off to raise the reflux temperature to 190°C and the reaction temperature was maintained at 190°C for 5h. After cooling to 85°C, anhydrous sodium acetate (1.83 g, 23.3 mmol) and 50 mL of ethanol were added. The mixture was heated to reflux and the solution was cooled to 5°C. The cooled slurry mixture was filtered and the solid was washed and dried. The solid was suspended in warm water, filtered, and the resulting solid was washed with water to give the pure product (7.40 g, 67%).

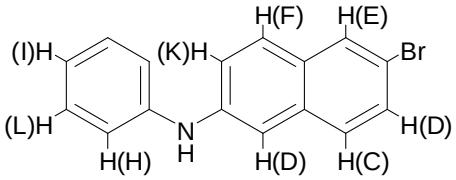

^{1}H NMR (300 MHz, $CDCl_3$): δ= 7.87 (s, 1H, H_E), 7.63 (d, 1H, H_F, J=8.8 Hz), 7.50 (d, 1H, H_C, J=8.8 Hz), 7.44 (dd, 1H, H_G, J=8.8 Hz, J=1.8 Hz), 7.37 (d, 1H, H_D), 7.32 (t, 2H, H_L, J=8.4 Hz), 7.22 (dd, 1H, H_K, J=8.8 Hz, J=2.3 Hz), 7.17 (d, 1H, H_H, J=8.6 Hz), 7.01 (t, 1H, H_I, J=7.3 Hz); **GC-MS** *m/z* (%): 297 [M^+, 100].

diethyl 6-(phenylamino)naphthalen-2-phosphonate (10): In a sealed tube, **9** (2.5 g, 8.40 mmol) was melt at 180°C and a catalytic amount of $NiCl_2$ (100 mg, 0.77 mmol) was added. Under argon atmosphere, 6 mL of triethyl phosphate was added dropwise and the reaction was stirred for 5h at 180°C. The reaction was cooled to room temperature and poured into cool water and extracted with CH_2Cl_2. The pure product (1.3 g, 43%) was obtained by column chromatography on silica gel by using Ethyl acetate/CH_2Cl_2 (7:3 v/v) as eluent and dried under *vacuum* for several hours at 150°C.

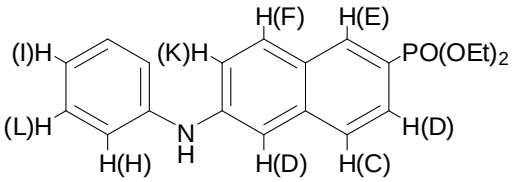

^{1}H NMR (600 MHz, $CDCl_3$): δ= 8.32 (d, 1H, H_E, J=15 Hz), 7.83 (d, 1H, H_F, J=8.4 Hz), 7.67 (m, 2H, H_C + H_G), 7.43 (d, 1H, H_D, J=1.8 Hz), 7.38 (t, 2H, H_L, J=7.8 Hz), 7.28 (d, 1H, H_K, J=1.8 Hz), 7.25 (d, 1H, H_H, J=8.4 Hz), 7.08 (t, 1H, H_I, J=7.8 Hz), 4.16 (m, 4H, OCH_2CH_3), 1.37 (m, 6H, OCH_2CH_3); **^{31}P NMR** (162 MHz, $CDCl_3$): δ= 18.3 (s, 1P); **GC-MS** *m/z* (%): 355 [M^+, 100].

6-(phenylamino)naphthalen-2-phosphonic acid (11): To a solution of **10** (550 mg, 1.64 mmol) in CH_2Cl_2, $(CH_3)_3SiBr$ (1.19 mL, 9.02 mmol) was added under argon atmosphere. The solution was stirred for 36h at room temperature, then the solvent was removed and the solid was dissolved in methanol and stirred for 30 minutes at room temperature. The solution was dried to give the pure product as white solid (570 mg, quantitative yield).

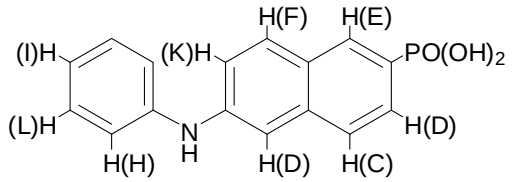

^{1}H NMR (300 MHz, CD_3OD): δ= 8.32 (d, 1H, H_E, J=15Hz), 7.83 (d, 1H, H_F, J=8.4 Hz), 7.50 (d, 1H, H_C, J=8.8 Hz), 7.44 (dd, 1H, H_G, J=8.8 Hz, J=1.8 Hz), 7.43 (bs, 1H, H_D), 7.38 (t, 2H, H_L, J=7.8 Hz), 7.28 (d, 1H, H_K, J=1.8Hz), 7.25 (d, 1H, H_J, J=8.4 Hz), 7.08 (t, 1H, H_I, J=7.8 Hz); **^{31}P NMR** (162 MHz, $CDCl_3$): δ= 19.22 (s, 1P); **ESI-MS** *m/z* (%): 301 [$M+H^+$, 100].

6-(phenylamino)naphthalen-2-ylphosphonic dichloride (12): To a solution of **11** (223 mg, 0.67 mmol) in 4 mL of phosphoryl trichloride, PCl_5 (138 mg, 0.66 mmol) was added, under nitrogen atmosphere. The dark solution was stirred at 90°C for 17h than the solvent was removed under vacuum and the dark solid was used immediately in the next step without further purification and characterization.

Ethyl-footed trimethylene-bridged resorcinarene (13): K_2CO_3 (5.67 g, 41.7 mmol) and CH_2Br_2 (0.643 mL, 9.16·mmol) were added, under nitrogen, to a solution of resorcinarene (R: C_2H_5) (2.5 g, 4.17·mmol) in 45 mL of dry DMSO. The purple mixture was stirred in a sealed tube at 80°C for 4 hours. The reaction was quenched by addition 10 % $HCl_{(aq)}$ solution and the resulting mixture filtered and washed with water. The crude product was purified by column chromatography on silica gel by using hexane/ethyl acetate (7:3 *v/v*) as eluant to give cavitand as a white solid (205 mg, 13%).
^{1}H NMR (300 MHz, $CDCl_3$): δ= 7.14 (s, 2H, Ar*H*), 7.08 (s, 2H, Ar*H*), 6.48 (s, 2H, ArH), 6.36 (s, 2H, ArH), 5.73 (d, 2H, H_{out}, J=7.2 Hz), 5.70 (d, 1H, H_{out}, J=7.2 Hz), 4.64 (t, 2H, $CHAr_2$, J=6.7 Hz), 4.58 (t, 1H, $CHAr_2$, J=8.1 Hz), 4.46 (d, 2H, CH_{in}, J=7.2 Hz), 4.35 (d, 1H, CH_{in}, J=7.2 Hz); 4.20 (t, 1H, $CHAr_2$, J=7.8 Hz), 2.23 (m, 8H, $CHCH_2CH_3$), 1.24 (t, 3H, CH_3, J=7.1 Hz), 0.90 (m, 9H, CH_3); ESI-MS m/z (%): 659 [M+Na^+,100].

Cavitands 14-in and 15-out To a solution **12** (283 mg, 0.77 mmol) in 15 mL of dry pyridine in a sealed tube, Ethyl-footed trimethylene-bridged resorcinarene (244 mg, 0.38 mmol) was added, under argon, and the solution was stirred at 60°C for 24h. The solvent was removed under *vacuum* and the crude product was dissolved in CH_2Cl_2 and washed with water. The organic layer was dried and the pure product was obtained by preparative TLC on silica gel by using ethyl acetate/CH_2Cl_2 (3:7 *v/v*) as eluant to give **14-in** (83 mg, 24%) and **15-out** (65 mg, 19%).

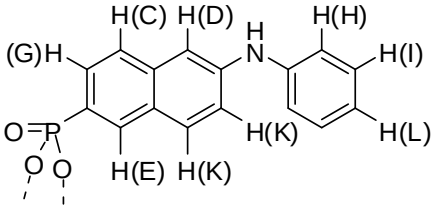

14-in

^{1}H NMR (600 MHz, acetone-d_6): δ= 8.38 (d, 2H, H_E, J=15.6 Hz), 7.87 (d, 1H, H_F, J=8.4 Hz), 7.80 (dd, 1H, H_G, J=11.4 Hz, J=8.4 Hz), 7.73 (dd, 1H, H_C, J=8.4 Hz, J=4.8 Hz), 7.55 (s, 2H, Ar-H_d), 7.49 (s, 2H, Ar-H_d), 7.45 (s, 1H, H_D), 7.31 (d, 1H, H_K, J=9.0 Hz), 7.26-7.20 (m, 4H, H_L+H_H), 6.90 (t, 1H, H_I, J=7.8 Hz), 6.60 (d, 2H, Ar-H_u, J=1.8 Hz), 6.41 (s, 2H, Ar-H_u), 5.65 (d, 2H, H_{out}, J=7.8 Hz), 5.52 (d, 1H, H_{out}, J=7.2 Hz), 4.57 (d, 2H, H_{in}, J=7.2 Hz), 4.55-4.45 (m, 4H, Ar-C*H*-Ar), 4.15 (d, 1H, H_{in}, J=7.2 Hz), 2.36 (m, 2H, CH_2-CH_3), 2.28 (m, 6H, CH_2-CH_3), 0.92-0.82 (m, 12H, CH_3); **^{31}P NMR** (162 MHz, acetone-d_6): δ= 14.4 (s, 1P); **ESI-MS** *m/z* (%): 900 [M+H^+,100], 923 [(M+Na^+,25].

15-out

^{1}H NMR (600 MHz, acetone-d_6): δ= 7.79 (s, 2H, Ar-H_d), 7.72 (s, 2H, Ar-H_d), 7.40 (t, 2H, H_L, J=7.8 Hz), 7.28 (d, 2H, H_H, J=7.8 Hz), 7.18 (s, 1H, H_D), 7.11 (dd, 1H, H_K, J=8.4Hz, J=1.8 Hz), 7.08 (t, 2H, H_I, J=7.2 Hz), 6.73 (d, 1H, H_E, J=14.4 Hz), 6.64 (dd, 1H, H_C, J=8.4 Hz, J=4.8 Hz), 6.51 (s, 2H, Ar-H_u), 6.50 (d, 1H, H_F, J=7.9 Hz), 6.27 (bdd, 1H, H_G, J=8.4 Hz), 6.12 (d, 2H, Ar-H_u, J=1.2 Hz), 5.77 (d, 1H, H_{out}, J=7.2 Hz), 5.40 (d, 2H, H_{out}, J=7.2 Hz), 4.76 (t, 1H, Ar-C*H*-Ar, J=8.4 Hz), 4.54 (m, 3H, Ar-C*H*-Ar+H_{in}), 4.26 (t, 1H, Ar-C*H*-Ar, J=7.0 Hz), 2.36 (m, 2H, CH_2-CH_3), 2.27 (m, 6H, CH_2-CH_3), 0.92-0.81 (m, 12H, CH_3); **^{31}P NMR** (162 MHz, acetone-d_6): δ= 8.5 (s, 1P); **ESI-MS** *m/z* (%): 900 [M+H^+,100], 923 [M+Na^+,25].

Cavitand TSiiii[C_2H_5, H, Ph] 16: To a solution of resorcinarene (R: C_2H_5) (1.50 g, 2.50 mmol) in 50 mL of dry pyridine, dichlorophenylphosphine (1.32 mL, 10.2 mmol) was added dropwise, under argon atmosphere. The solution was stirred at room temperature for 1 h. Sulfur (510 mg, 2.00 mmol) was added and the mixture was heated at 80°C for 5 h. The solvent was removed in vacuum and the solid was washed and sonicated with water, then filtered and dried. The pure product (1.85 g, 64%) was obtained by column chromatography on silica gel by using hexane/CH_2Cl_2 (from 4:6 to 3:7 *v/v*) as eluent.

^{1}H NMR (300 MHz, $CDCl_3$): δ= 8.17 (m, 8H, P(S)ArH_{ortho}), 7.56 (m, 4H, P(S)ArH_{para}), 7.51 (m, 8H, P(S)ArH_{meta}), 7.30 (s, 4H, ArH_d), 6.67 (s, 4H, ArH_u), 4.64 (bt, 4H, ArCH), 2.39 (m, 8H, C$H_2$$CH_3$), 1.06 (t, 12H, CH_2CH_3, J=6.8 Hz); **ESI-MS** m/z (%): 1176 [M+Na^+,100].

Resorcinarene 17: Cavitand **16** (1.00g, 0.860 mmol) was solved in dry DMF at 50°C. Catechol (100 mg, 0.910 mmol) and K_2CO_3 (1.20g, 8.67 mmol) were added and the mixture was stirred at 80°C for 5 h. The solvent was removed

under *vacuum* and the solid was washed and sonicated with water, then filtered and dried. The pure product (0.46 g, 52%) was obtained by column chromatography on silica gel by using ethanol/CH_2Cl_2 (from 1:99 to 4:6 *v/v*) as eluent.

^{1}H NMR (300 MHz, $CDCl_3$): δ= 8.17 (m, 6H, P(S)ArH_{ortho}), 7.57-7.53 (m, 9H, P(S)ArH_{para}+ P(S)ArH_{meta}), 7.32 (s, 2H, ArH_d), 7,20 (s, 2H, ArH_d), 6.68 (s, 2H, ArH_u), 6.49 (s, 2H, ArH_u), 4.64 (m, 4H, ArCH), 2.39-2.26 (m, 8H, CH_2CH$_3$), 1.06 (t, 6H, CH_2CH_3, J = 6.8 Hz), 1.00 (t, 3H, CH_2CH_3, J=6.8 Hz); **ESI-MS** m/z (%): 1016 [M+H$^+$,40], 1037 [M+Na$^+$,100], 1054 [M+K$^+$,50].

Cavitands 18-in and 19-out: To a solution of **12** (188 mg, 0.56 mmol) in 15 mL of dry pyridine in a sealed tube, was added, under argon, resorcinarene **17** (200 mg, 0.19 mmol) and the solution was stirred at 60°C for 24h. The solvent was removed under *vacuum* and the crude product was dissolved in CH_2Cl_2 and washed with water. The organic layer was dried and the pure product was obtained by preparative TLC on silica gel by using ethyl acetate/Hexane (5:5 *v/v*) as eluent to give **18-in** (30 mg, 12%) and **19-out** (26 mg, 10%).

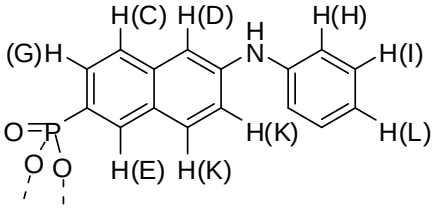

18-in

^{1}H NMR (600 MHz, Acetone-d_6): δ = 8.38 (d, 2H, H_E, J=16 Hz), 8.09 (m, 6H, P(S)Ar$_{ortho}$), 7.85-7.82 (m, 2H, H_F + H_G), 7.75 (s, 2H, ArH_d), 7.72-7.69 (m, 3H, ArH_d + H_C), 7.50 (m, 9H, P(S)ArH_{meta} + P(S)ArH_{para}), 7.43 (d, 1H, H_D, J=2.4 Hz), 7.29 (dd, 1H, H_K, J=9.0 Hz, J=2.4 Hz), 7.23-7.19 (m, 3H, H_L + H_H), 6.87 (t, 2H, H_I, J=7.8 Hz), 6.63 (s, 2H, ArH_u), 6.51 (s, 2H, ArH_u), 4.70 (t, 1H, ArCH, J=7.8 Hz), 4.60 (bt, 2H, ArCH), 4.45 (t, 1H, ArCH, J=7.8 Hz), 2.35 (m, 2H, CH_2CH$_3$), 2.28 (m, 6H, CH_2CH$_3$), 0.93- 0.80 (m, 12H, CH_3); **^{31}P NMR** (162 MHz, $CDCl_3$): δ = 78.9 (s, 1P, P=S), 77.2 (s, 2P, P=S), 8.2(s, 1P, P=O); **ESI-MS** m/z (%): 1278 [M+H$^+$, 40], 1300 [M+Na$^+$, 100].

19-out

^{1}H NMR (600 MHz, Acetone-d_6): δ = 8.16 (m, 2H, P(S)ArH_{ortho}), 8.07 (d, 1H, H_E, J = 16.0 Hz), 7.90 (m, 4H, P(S)ArH_{ortho}), 7.87 (s, 2H, ArH_d), 7.82 (s, 2H, ArH_d), 7.65 (d, 1H, HF, J = 9.0 Hz), 7.58 (m, 3H, P(S)ArH_{meta} + P(S)ArH_{para}), 7.51 (t, 2H, H_L, J=7.8 Hz), 7.41-7.38 (m, 7H, P(S)ArH_{meta} + P(S)ArH_{para} + H_H), 7.20-7.10 (m, 4H, H_D + H_K + H_I), 6.91 (m, 1H, H_C), 6.80 (t, 1H, H_G, J=8.5 Hz), 6.58 (s, 2H, ArH_u), 6.07 (s, 2H, ArH_u), 4.91 (t, 1H, ArCH, J=7.8 Hz), 4.66 (t, 1H, ArCH, J=7.8 Hz), 4.60 (bt, 2H, ArCH), 2.46-2.43 (m, 8H, C$H_2$$CH_3$), 0.97-0.90 (m, 12H, CH_3); **^{31}P NMR** (162 MHz, $CDCl_3$): δ = 77.2 (s, 1P, P=S), 76.2 (s, 2P, P=S), 3.8 (s, 1P, P=O); **ESI-MS** m/z (%): 1278 [M+H^+, 40], 1300 [M+Na^+, 100].

UV-Vis and Fluorescence Titration in solution:

To a solution of the host in a Chromasolv® grade solvent, the guest was added in several aliquots and the absorption and emission spectra were recorded.

UV-Vis titration of 5 with Ethanol: Solvent $CHCl_3$ Chromasolv®; Solution of **5** 2.02 10^{-4} M; Guest Ethanol Absolute; Absorption Spectra 250-600 nm; Guest addition in 24 aliquots 5, 10, 25, 50, 100 uL.

Fluorescence titration of 5 with Ethanol: Solvent $CHCl_3$ Chromasolv®; Solution of **5** 2.02 10^{-4} M; Guest Ethanol Absolute; Emission Spectra 350-600 nm; Excitation wavelength 340 nm; Ex and Em windows 10 nm; Em filter cut-off at 290 nm; Guest addition in 24 aliquots 5, 10, 25, 50, 100 uL.

UV-Vis titration of 8 with Ethanol: Solvent $CHCl_3$ Chromasolv®; Solution of **8** 1.07 10^{-4} M; Guest Ethanol Absolute; Absorption Spectra 250-600 nm; Guest addition in 24 aliquots 5, 10, 25, 50, 100 uL.

Fluorescence titration of 8 with Ethanol: Solvent $CHCl_3$ Chromasolv®; Solution of **8** 1.07 10^{-4} M; Guest Ethanol Absolute; Emission Spectra 350-600 nm; Excitation wavelength 340 nm; Ex and Em windows 10 nm; Em filter cut-off at 290 nm; Guest addition in 24 aliquots 5, 10, 25, 50, 100 uL.

UV-Vis titration of 10 with Ethanol: Solvent $CHCl_3$ Chromasolv®; Solution of **10** 2.09 10^{-4} M; Guest Ethanol Absolute; Absorption Spectra 250-650 nm; Guest addition in 24 aliquots 5, 10, 25, 50, 100 uL.

Fluorescence titration of 10 with Ethanol: Solvent $CHCl_3$ Chromasolv®; Solution of **10** 2.09 10^{-4} M; Guest Ethanol Absolute; Emission Spectra 350-600 nm; Excitation wavelength 305 nm; Ex and Em windows 10 nm; Em filter cut-off at 290 nm; Guest addition in 24 aliquots 5, 10, 25, 50, 100 uL.

UV-Vis titration of 10 with Ethanol: Solvent CH_3CN Chromasolv®; Solution of **10** 2.61 10^{-4} M; Guest Ethanol Absolute; Absorption Spectra 250-650 nm; Guest addition in 24 aliquots 5, 10, 25, 50, 100 uL.

Fluorescence titration of 10 with Ethanol: Solvent CH_3CN Chromasolv®; Solution of **10** 2.61 10^{-4} M; Guest Ethanol Absolute; Emission Spectra 350-600 nm; Excitation wavelength 305 nm; Ex and Em windows 10 nm; Em filter cut-off at 290 nm; Guest addition in 24 aliquots 5, 10, 25, 50, 100 uL.

UV-Vis titration of 14-in with Ethanol: Solvent $CHCl_3$ Chromasolv®; Solution of **14-in** 1.07 10^{-4} M; Guest Ethanol Absolute; Absorption Spectra 250-650 nm; Guest addition in 24 aliquots 5, 10, 25, 50, 100 uL.

Fluorescence titration of 14-in with Ethanol: Solvent $CHCl_3$ Chromasolv®; Solution of **14-in** 1.07 10^{-4} M; Guest Ethanol Absolute; Emission Spectra 350-600 nm; Excitation wavelength 305 nm; Ex and Em windows 10 nm; Em filter cut-off at 290 nm; Guest addition in 24 aliquots 5, 10, 25, 50, 100 uL.

UV-Vis titration of 14-in with Ethanol: Solvent CH_3CN Chromasolv®; Solution of **14-in** 8.50 10^{-5} M; Guest Ethanol Absolute; Absorption Spectra 250-650 nm; Guest addition in 24 aliquots 5, 10, 25, 50, 100 uL.

Fluorescence titration of 14-in with Ethanol: Solvent CH_3CN Chromasolv®; Solution of **14-in** 8.50 10^{-5} M; Guest Ethanol Absolute; Emission Spectra 350-600 nm; Excitation wavelength 305 nm; Ex and Em windows 10 nm; Em filter cut-off at 290 nm; Guest addition in 24 aliquots 5, 10, 25, 50, 100 uL.

UV-Vis titration of 15-out with Ethanol: Solvent $CHCl_3$ Chromasolv®; Solution of **15-out** 9.58 10^{-5} M; Guest Ethanol Absolute; Absorption Spectra 250-650 nm; Guest addition in 24 aliquots 5, 10, 25, 50, 100 uL.

Fluorescence titration of 15-out with Ethanol: Solvent $CHCl_3$ Chromasolv®; Solution of **15-out** 9.58 10^{-5} M; Guest Ethanol Absolute; Emission Spectra 350-600 nm; Excitation wavelength 305 nm; Ex and Em windows 10 nm; Em filter cut-off at 290 nm; Guest addition in 24 aliquots 5, 10, 25, 50, 100 uL.

UV-Vis titration of 15-out with Ethanol: Solvent CH_3CN Chromasolv®; Solution of **15-out** 9.70 10^{-5} M; Guest Ethanol Absolute; Absorption Spectra 250-650 nm; Guest addition in 24 aliquots 5, 10, 25, 50, 100 uL.

Fluorescence titration of 15-out with Ethanol: Solvent CH_3CN Chromasolv®; Solution of **15-out** 9.70 10^{-5} M; Guest Ethanol Absolute; Emission Spectra 350-600 nm; Excitation wavelength 305 nm; Ex and Em windows 10 nm; Em filter cut-off at 290 nm; Guest addition in 24 aliquots 5, 10, 25, 50, 100 uL.

UV-Vis titration of 18-in with Ethanol: Solvent $CHCl_3$ Chromasolv®; Solution of **18-in** 1.80 10^{-5} M; Guest Ethanol Absolute; Absorption Spectra 250-650 nm; Guest addition in 24 aliquots 5, 10, 25, 50, 100 uL.

Fluorescence titration of 18-in with Propanol: Solvent $CHCl_3$ Chromasolv®; Solution of **18-in** 1.80 10^{-5} M; Guest Ethanol Absolute; Emission Spectra 350-600 nm; Excitation wavelength 305 nm; Ex and Em windows 10 nm; Em filter cut-off at 290 nm; Guest addition in 24 aliquots 5, 10, 25, 50, 100 uL.

Fluorescence titration of 18-in with Butanol: Solvent $CHCl_3$ Chromasolv®; Solution of **18-in** 1.80 10^{-5} M; Guest Ethanol Absolute; Emission Spectra 350-600 nm; Excitation wavelength 305 nm; Ex and Em windows 10 nm; Em filter cut-off at 290 nm; Guest addition in 24 aliquots 5, 10, 25, 50, 100 uL.

Fluorescence titration of 19-out with Ethanol: Solvent $CHCl_3$ Chromasolv®; Solution of **19-out** 9.80 10^{-6} M; Guest Ethanol Absolute; Emission Spectra 350-600 nm; Excitation wavelength 305 nm; Ex and Em windows 10 nm; Em filter cut-off at 290 nm; Guest addition in 24 aliquots 5, 10, 25, 50, 100 uL.

FLUORESCENCE MEASURE AT THE GAS-SOLID INTERFACE

General procedure: Carrier gas: Nitrogen; Analyte: From certificate graduate cylinder; Total flux: 200 sccm.
To reach the necessary concentration, the analytes were diluted in nitrogen using two mass flow controllers.
Emission spectra: 350-600 nm; Time drive parameters: Excitations: 333 nm, Emission 460 nm, Excitations split 2-11 nm, Emission split 2-11 nm, data interval 2 s.
Certified cylinders were prepared by SAPIO S.r.l. with gravimetric procedure (ISO6142):
Methanol (C_1): 516.00 ± 0.02 ppm, 150 bar
Ethanol (C_2): 504.00 ± 0.02 ppm, 26 bar
n-Propanol (C_3): 501.40 ± 0.02 ppm, 10 bar
n-Butanol (C_4): 100.40 ± 0.02 ppm, 10 bar
n-Pentanol (C_5): 98.30 ± 0.02 ppm, 10 bar

THIN FILM DEPOSITION

Solution A: In a volumetric flask 120 mg of Low Molecular Weight PVC and 260 uL of Bis(2-ethylhexyl) sebacate were dissolved in 3 mL of distilled THF, the mixture was stirred and sonicated for 1.5h until complete solution of PVC.
Solution B: In a volumetric flask a quantity of fluorescent receptor was dissolved in 1 mL of distilled THF.
Solution C: The solution was made by mixing 500 uL of Solution A with 500 uL of Solution B.
The spin coating was made on glass substrate (1.5cm x 1.5cm) using one to five drops of Solution C.

Solution A		
Receptor	**Quantity**	**% w/w**
14-in	0.66 mg	0.1%
15-out	0.66mg	0.1%
10	1.2 mg	0.2%

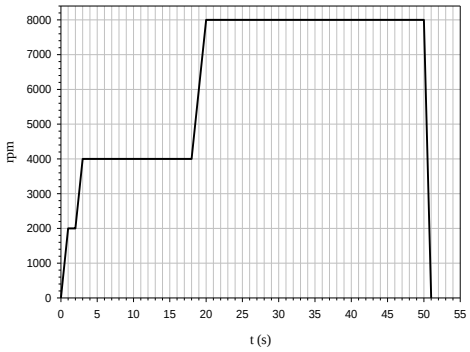

TITRATION SPECTRA

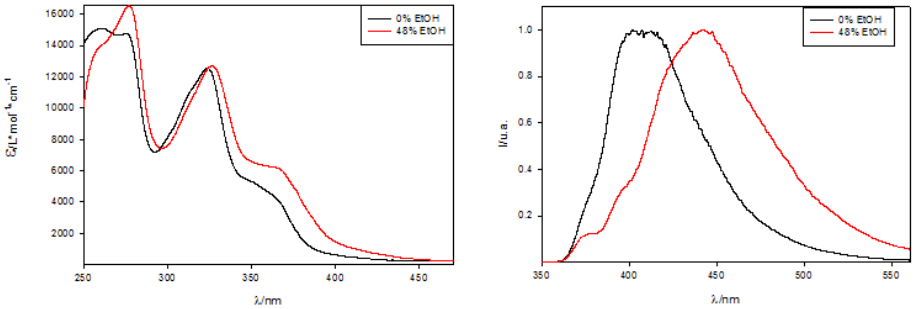

Absorption (left) and emission (right) spectra of **10** in $CHCl_3$. With 0% (black line) and 48% (red line) of abs. ethanol.

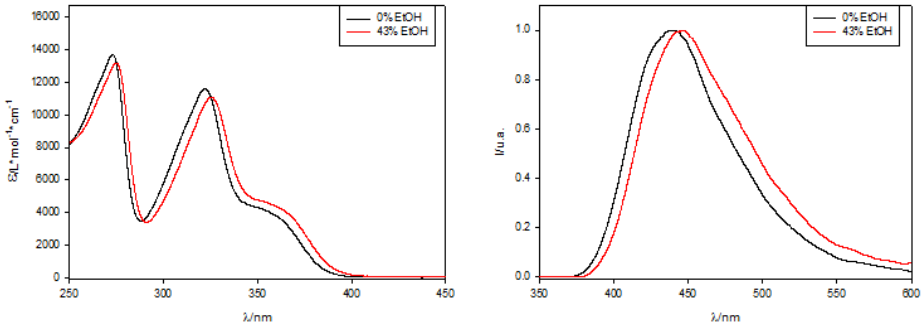

Absorption (left) and emission (right) spectra of **10** in CH_3CN. With 0% (black line) and 43% (red line) of abs. ethanol.

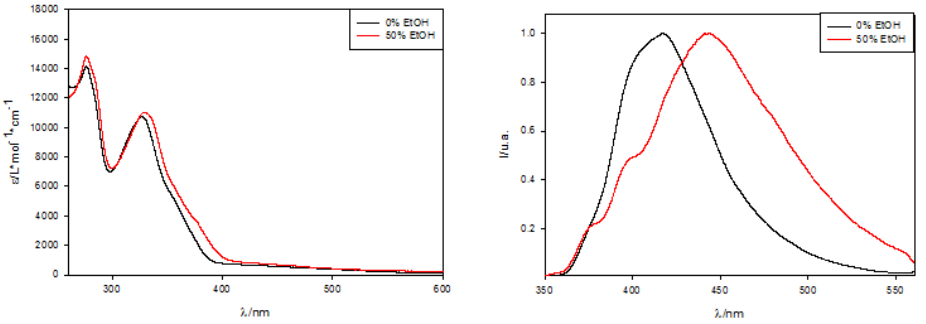

Absorption (left) and emission (right) spectra of **14-in** in $CHCl_3$. With 0% (black line) and 50% (red line) of abs. ethanol.

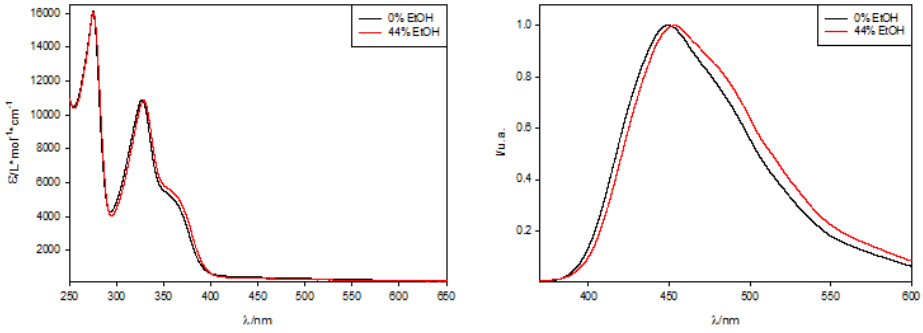

Absorption (left) and emission (right) spectra of the **14-in** in CH_3CN. With 0% (black line) and 44% (red line) of abs. ethanol.

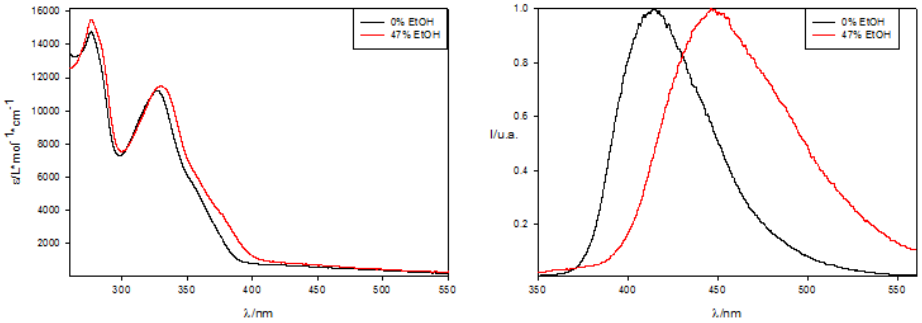

Absorption (left) and emission (right) spectra of **15-out** in $CHCl_3$. With 0% (black line) and 50% (red line) of abs. ethanol.

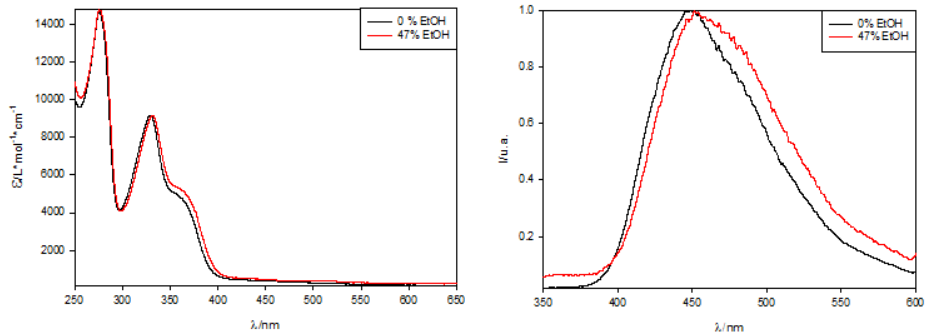

Absorption (left) and emission (right) spectra of **15-out** in CH_3CN. With 0% (black line) and 47% (red line) of abs. ethanol.

4.7 References and notes

[1] L. Prodi *New J. Chem.* **2005**, *29*, 20-31; J. R. Lakowicz *Principles of Fluorescence Spectroscopy* **1999**, Kluwer, NY.
[2] L. Fabbrizzi *Coord. Chem. Rev.* **2000**, *205*, 1.
[3] L. Fabbrizzi, A. Poggi *Chem Soc Rev* **1995**, *24*, 197.
[4] O.S. Wolfbeis, Fiber Optic Chemical Sensors and Biosensors, vols. I-II, CRC Press, Boca Raton, FL, **1991.**
[5] B. Valeur, I. Leary *Coord. Chem. Rev.* **2000**, *205*, 3.
[6] H.-G Lohr, F. Vogtle *Acc. Chem. Res.* **1985**, *18*, 65.
[7] K. Iawamoto, K. Araki, H. Fujishima, S. Shinkai *J. Chem. Soc. Perkin Trans.* **1992**, *1*, 1885.
[8] J. G. Rodriguez, J. L. Tejedor *J. Org. Chem.* **2002**, *67*, 7631.
[9] B. C. Gibb, R. G. Chapman, J. C. Sherman *J. Org. Chem.* **1996**, *61*, 1505.
[10] R. Pinalli, F.F. Nachtugall, F. Ugozzoli, E. Dalcanale *Angew. Chem. Int. Ed.* **1999**, *38*, 2377.
[11] H. Wei, S.F.Y. Li *J. Chromatogr. A.* **1998**, *800*, 333; H. Dodiuk, H. Kanety, E. M. Kosower *J. Phys. Chem.* **1979**, *83*, 515.
[12] P. Delangle, J.-C. Mulatier, B. Tinant, J.-P. Dutasta *Eur. J. Org. Chem.* **2001**, 3695-3704.
[13] B. Bibal, B. Tinant, J.-P. Declercq, J.-P. Dutasta *Chem. Commun.* **2002**, 432.
[14] M. Melegari *Ph.D. Thesis* **2008**, University of Parma, Italy.

Host-Guest complexation on Si(100) surface

5

5.1 Introduction

The synthesis of hybrid organic/inorganic systems in which organic molecules are anchored by covalent bonding on inorganic surfaces represent a key point for the development of molecular devices. The most promising architecture for this systems is represented by a dense array of molecular receptors hosted on a silicon-based microelectronic circuit.[1] In this context, the development of hybrid systems require the functionalization of the silicon surface.[2]
In the past few years, the peculiar molecular recognition proprieties of synthetic molecular receptors[3] has been transferred from solutions to surfaces leading to high selective chemical sensors. Cavitands[3] together cyclodextrins[4] and calixarenes[5] are the most used receptors for vapor sensing due to their well studied host-guest proprieties. The major reason for choosing this approach lies in the possibility to design the receptor according to the analyte to be detected, by tailoring the specific host-guest interactions responsible for molecular recognition. Among the various covalent bonding modes of organic molecules on silicon surfaces, hydrosilylation of molecule with terminal double bonds on hydrogen-terminated surfaces appears the best suited for the largest potential applications. In a previous paper we reported the direct anchoring of

quinoxaline cavitands (QxCav) having ω-decylenic feet on H-terminated Si(100) surfaces via photochemical hydrosilylation (Figure 5.1).[6]

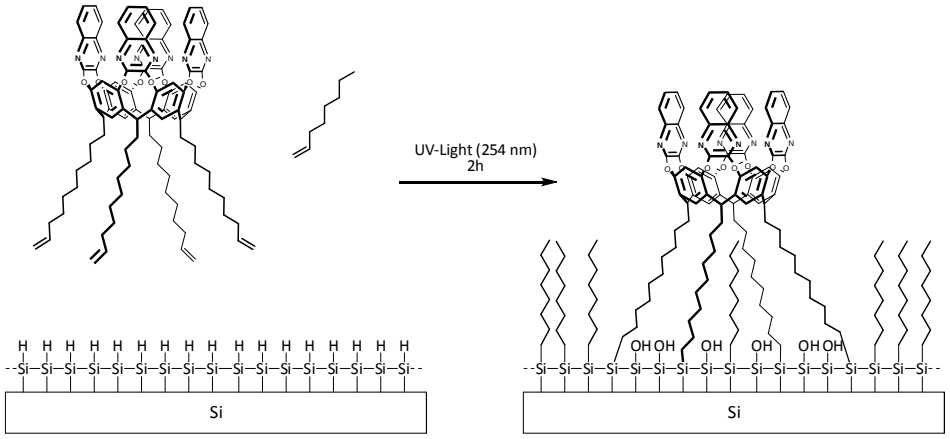

Scheme 5.1. Grafting procedure of QxCav **4** on silicon surface.

In this chapter the same procedures has been applied to the case of cavitand AcCav (Figure 5.1).
The quinoxaline cavitand, as reported in the Chapters 2 and 3 is a well studied receptor for benzene and small aromatic molecules. The two cavitands AcCav **5-in** and AcCav **6-out** and are selective receptors for the detection of organophosphorous vapors, many of them well-known as chemical warfare agents.[7]

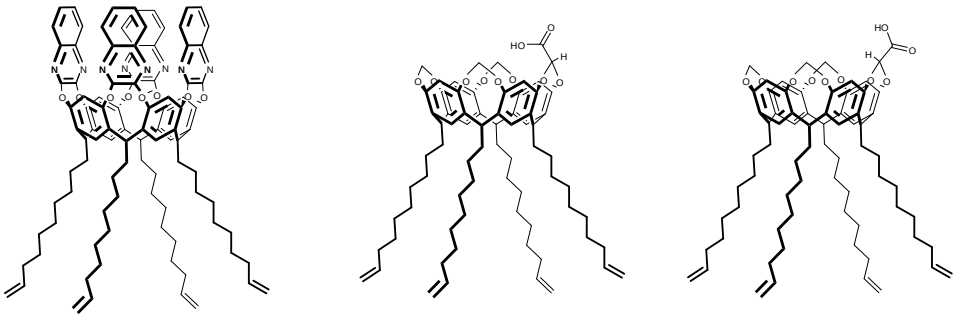

QxCav **4** AcCav **5-in** AcCav **6-out**

Figure 5.1. Cavitands receptors for molecular recognition

The complexation ability of the resulting cavitand decorated surfaces towards selected analytes were tested using angle resolved X-ray photoelectron spectroscopy (AR-XPS). X-ray photoelectron spectroscopy (XPS) proved to be an ideal tool for testing complexation event on surface.

5.2 Results and discussion

5.2.1 Molecular receptors

We chose to test two different types of receptor for two different environmental applications. The fist cavitand is a well know quinoxaline cavitand, used in Chapter 2 and 3 as sorbent material for aromatic VOCs, thanks to weak attractive host-guest interactions involving π electrons of the host, with two C-H_{guest} bonds aligned along the direction of the π orbital of the interacting C_{host} resorcinarene atoms is a perfect host for benzene and small aromatic compounds.
The second type of cavitand was designed by Dalcanale and coworkers[6] to complex a sarin nerve gas simulant, dimethylmethylphosphonate (DMMP).

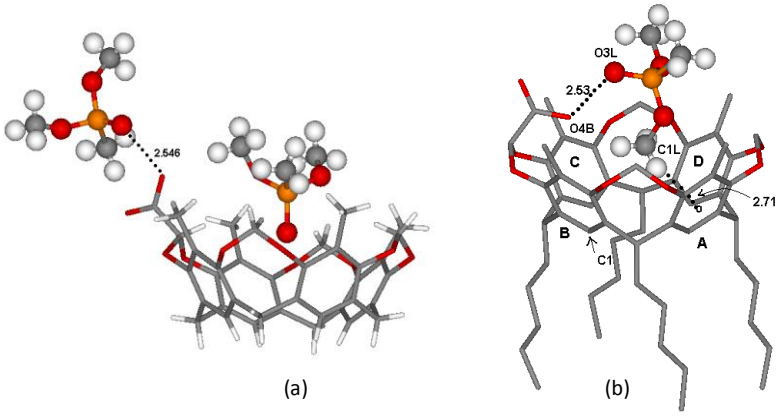

Figure 5.2. Partial stick views of AcCav-out@DMMP (a) and AcCav-in@DMMP (b) complexes. The hosts have been traced in the stick mode and the DMMPs in the ball and stick mode. Hydrogen bond contacts and CH-π interaction are shown in dashed lines. Only the hydrogen atoms of the DMMPs have been reported.

In the design they focused their attention on the P=O and OCH_3 moieties of the DMMP molecule, considering that DMMP's "acidic" methyl groups interact with the cavitand via inclusion within a π-basic cavity and DMMP's P=O group interacts with the cavitand via H-bonding with COOH H-bonding donor (Figure 5.2). The desired synergy between the two interactions is obtained by introducing the COOH group in the inward position on one of the bridging groups at the upper rim of the cavity as proved by the crystal structures of the complexes.

The QxCav used for this work is the same described in Chapter 3. The synthesis of cavitand EsCav **2-in** and EsCav **3-out** is outlined in Scheme 5.2: partial bridging of resorcinarene ($R:C_{10}H_{19}$) is obtained operating in defect of bromochloromethane, the bridging reagent of choice.

The desired carboxylic acid is then introduced in the form of ester on the remaining pair of phenolic OHs using methyl dichloroacetate as bridging reagent to give cavitand **2-in** e **3-out** after column chromatographic separation.

The configuration of in/out isomers has been assigned on the basis of the different ^{1}H-NMR chemical shifts of the protons of the OCH_3 ester group and of the corresponding hydrogen on the same bridge, according to their orientation inward or outward with respect to the cavity. Protons inside the cavity resonate at higher field with respect to their outside counterparts, a feature diagnostic of inward orientation. Hydrolysis of the ester with potassium tert-butoxide in DMSO was performed on the silicon surface after the grafting of the ester (EsCav **3-out**). For the preliminary grafting experiment the cavitand the cavitand EsCav **3-out** was chosen, because it has the $COOCH_3$ exposed out of the cavity, making its hydrolysis on surface easier.

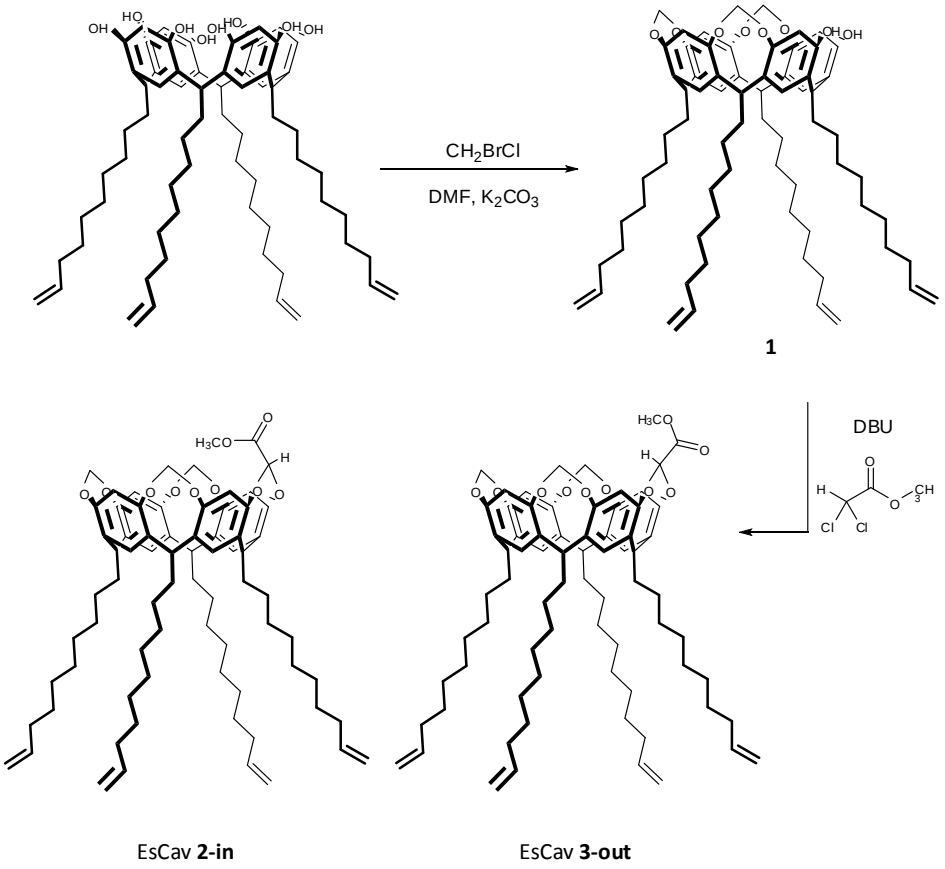

Scheme 5.2. Synthesis of EsCav **2-in** and EsCav **3-out**.

5.2.2 GRAFTING ON SILICON

The grafting of cavitand EsCav **3-out** was made by socking an etched silicon wafer, Si(100), in a mesitylene solution of **3-out** and 1-octene (for mixed monolayer). The grafting photochemical reaction was promoted by UV light irradiation (254 nm) Scheme 5.3.

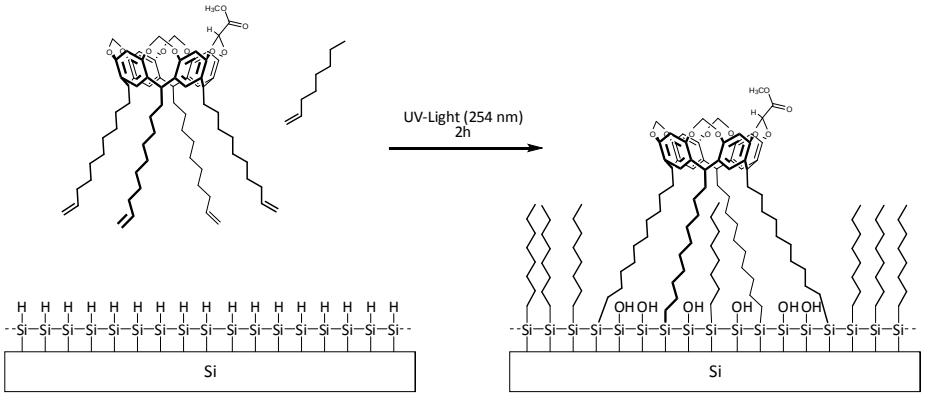

Scheme 5.3. Grafting procedure of EsCav **3-out** on Si (100).

The QxCav layers (mixed and full) were also prepared follow the procedure of reference 6.[6]

For each cavitand receptor three decorated surfaces were prepared at different molar ratio Cavitand/1-octene: 1.0, 0.5, 0.2. The efficiency of grafting process has been evaluated by XPS measurements Table 5.1 compares elemental composition of a HF freshly etched silicon surface, sample treated in pure mesitylene, and samples decorated with QxCav **4** or **3-out**. Data show that C 1s peaks are observed for both reference samples, HF freshly etched silicon and mesitylene treated surface. These C 1s signals arise from adventitious contaminant species which cannot be completely eliminated during etching and handling steps.[8] However, cavitand decorated surfaces show an evident enhancement of C 1s related signals as compared to both freshly etched silicon surface and mesitylene treated samples. This enhancement together with the observation of nitrogen for QxCav represents an indication of the presence of cavitand molecules on the silicon surface.

Atomic fraction				
	HF etched	Mes	QxCav **4**	EsCav **3-out**
Si	87.3	57.1	40.1	42.3
C	9.4	23.2	48.5	34.4
O	3.3	19.7	10.1	17.4
N	-		1.2	-

Table 5.1. XPS analysis of elemental compositions of decorated silicon surfaces.

Figure 5.2 shows the high-resolution C 1s photoelectron spectral region obtained at a takeoff angle of 45°C.

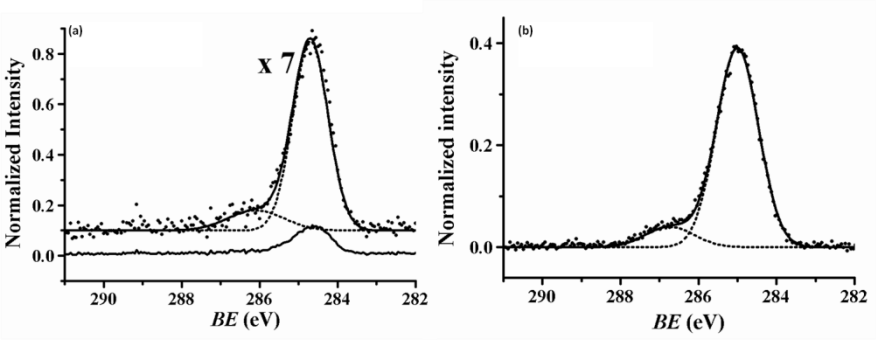

Figure 5.3. High resolution of C 1s XPS spectra (takeoff angle 45°) of HF etched Si(100) substrate (a) and of reference samples prepared by immersion of a freshly etched surface in pure mesitylene followed by the same treatments (UV exposure and sonication) adopted for cavitand decorated surfaces (b). The intensities are normalized to the total Si 2p intensity.

In both, freshly etched silicon surface (Figure 5.3 a) and samples irradiated in pure mesitylene (Figure 5.3 b), the carbon region consists of two components. The first component is centered at 285.0 eV (referred to as C^0). It represents aliphatic and aromatic hydrocarbons. The second component is centered at 286.5 eV (referred to as C^{+1}). This feature can be attributed to carbon bonded to one oxygen.[9]

Concerning the QxCav (Figure 5.4 left) , the C 1s spectrum of the grafted cavitands shows a richer structure compared to reference samples, clearly due to the presence of further bonding states. They consist of three main components: i) a C^0 component at 285.0 eV due to the aliphatic and aromatic hydrocarbon backbone; ii) a C^{+1} component at 286.3 eV due to oxidized carbon centers both in the cavitand phenyl ring bonded to one oxygen atom as well as in adventitious Si-O-C frameworks, iii) a C^{+2} component at 287.6 eV due to quinoxalinic carbons that bond both oxygen and nitrogen atom.

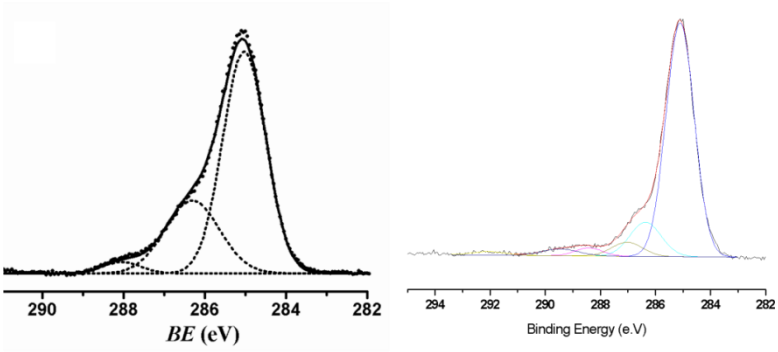

Figure 5.4. High resolution C 1s XPS spectra of Si(100) surfaces after grafting the QxCav **4** (left) and EsCav **3-out** (right).

Regarding the EsCav **3-out** (Figure 5.3 right), the C 1s spectrum come from the convolution of five components: i) a C^0 component at 285.0 eV (also observed in the previous sample) due to the aliphatic and aromatic hydrocarbon backbone, ii) C^{+1} component at 286.3 eV, due to oxidized carbon centers both in the cavitand phenyl ring bonded to one oxygen atom as well as in adventicious Si-O-C frameworks, iii) C^{+1} at 287.3 eV referred to the O-CH_3 moiety, iv) C^{+2} at 288.4 eV due to methylene groups bridging the oxygen atoms at the upper rim of the cavitand, and v) C^{+3} component at 289.3 eV owing to the carbon of the ester moiety(-O-C=O).

After the grafting the EsCav **3-out** the saponification to acid was performed directly on surface with potassium tert-butoxide in DMSO (Scheme 5.3). XPS characterization proves the disappearance of the component at 287.3 eV, referred to the O-CH_3 moiety, in high resolution C 1s spectrum.

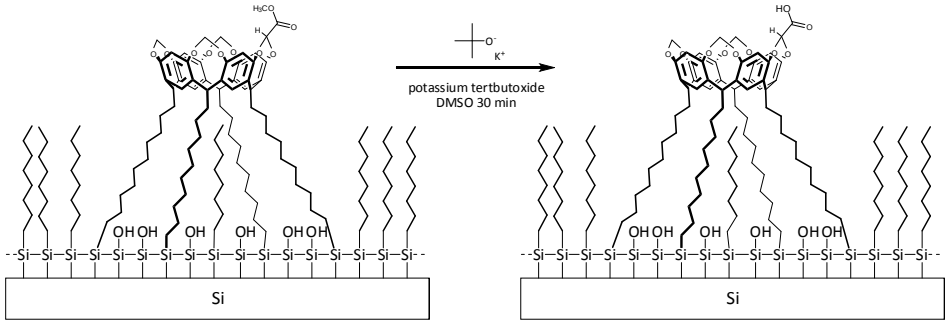

Scheme 5.4. Saponification of EsCav **3-out** to AcCav **6-out**.

5.2.3 XPS EVIDENCE OF COMPLEXATION OF QXCAV@TRIFLUOROTOLUENE

The XPS technique is useful not only for the characterization of the grafted samples but also to prove the complexation ability of the receptor grafted.
We chose to use as guest trifluorotoluene, an aromatic molecule, containing fluorine atoms which are easy to detect *via* XPS measurements. The surfaces decorated either with QxCav **4** or with 1-decene were exposed to the analyte then washed with CH_2Cl_2 and analyze with XPS. We use the 1-decene layer without molecular receptor as reference. Several high resolution F 1s plots were recorded before and after the exposition to the analyte. As reported in Figure 5.4 and in Table 5.2 after the complexation there was a enhancement of the signal of fluorine due to the presence of trifluorotoluene.

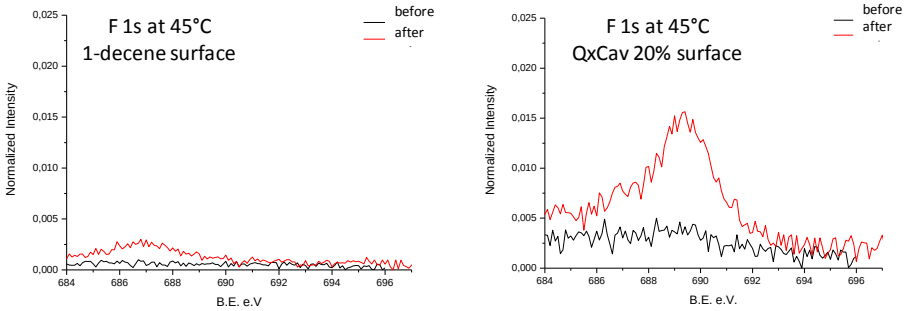

Figure 5.5. High resolution F 1s XPS spectra (takeoff angle 45°) of Si(100) decorated with QxCav **4** or with 1-decene before (black line) and after (red line) exposition to α,α,α-trifluorotoluene.

F 1s spectra is present only in the surfaces with a cavitand grafted on, and it is absent in the surface decorated with only 1-decene. This is a clear proof of complexation of the aromatic guest in the cavities of grafted QxCav.
This experiment has been performed at the solid-liquid interface, since the silicon surface has been exposed to the analyte in dichloromethane solution. Dichloromethane , also used for rinsing, is a competitive guest for QxCav inclusion, so these data underestimate the real potential of the receptor for the gas phase adsorption. Experiments at gas-solid interface are outgoing.

Atomic fraction								
	1-decene	1-decene + TFT	QxCav 100%	QxCav 100% + TFT	QxCav 50%	QxCav 50% + TFT	QxCav 20%	QxCav 20% + TFT
Si	55.08	43.58	26.33	25.05	31.47	35.29	34.11	33.23
C	3.54	25.16	36.70	38.78	26.45	24.54	29.42	28.1
O	41.36	31.08	34.00	32.49	41.22	39.08	35.43	37.03
N	-	-	2.95	3.32	0.84	0.65	1.02	1.12
F	-	0.16*	-	0.33	-	0.42	-	0.51

Table 5.2 XPS analysis of elemental compositions of decorated silicon surfaces before and after exposition to trifluorotoluene.

5.2.4 Preliminary XPS study of complexation of AcCav@DMMP

The XPS was used to evaluate the complexation capability of AcCav **6-out** toward DMMP as sarin nerve gas simulant (Figure 5.6).

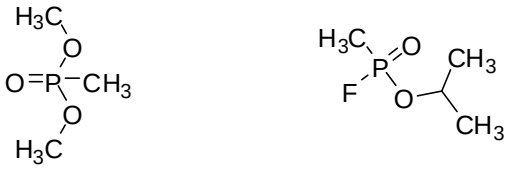

DMMP Sarin

Figure 5.6 Molecular structures of DMMP and Sarin.

In this case the P 2p spectrum of the guest is the diagnostic peak to follow to prove cavity inclusion. The surfaces decorated with EsCav **3-out** and AcCav **6-out** were exposed to 10^{-3} M DMMP in CH_2Cl_2, then washed with pure CH_2Cl_2 and analyzed with XPS to investigate the presence of phosphorous atoms. The EsCav **3-out** was used as reference since it is unable to binding the analyte via H-bonding. As reported in Figure 5.6 we did not found the proof of a complexation. The P 2p XPS signal is centered at 134 eV, this region includes three satellite peaks of Silicon spectrum, centered at 142, 140 and 133 eV due

to bulk plasmon loss. Their ponder ratio remains constant changing angle of take off whilst their intensities decreases at lower angle. At angle of take off of 10° the P 2p band should become evident but in our case no evidence of P 2p bands were found both for EsCav **3-out** and AcCav **6-out**.

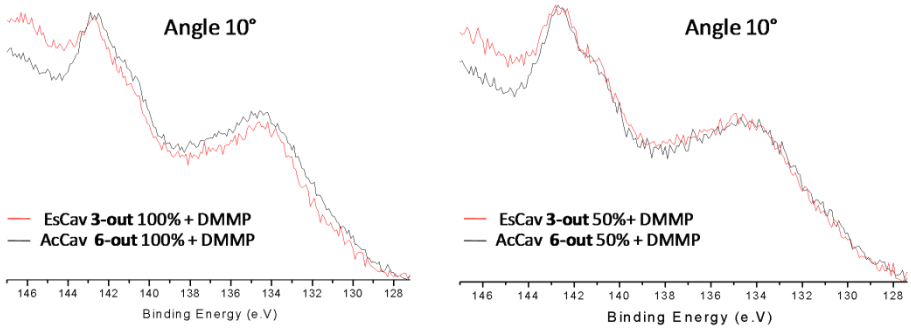

Figure 5.7 High resolution P 2p XPS spectra (takeoff angle 10°) of Si(100) decorated with EsCav **3-out** and AcCav **6-out** after exposition to DMMP.

In this case the solution expose of the cavitand grafted silicon surface is not the best procedure to highlight possible inclusion. The solvent plays a major role in AcCav solvation, inhibiting DMMP complexation. The CH_2Cl_2 washing procedure in particular is detrimental of any possible inclusion. Moreover AcCav **6-out** is not the preferred host for DMMP. The AcCav **5-in** isomer is better suited. The deposition of EsCav **2-in** is ongoing and the subsequently complexation experiments will be run with gaseous DMMP.

5.3 Conclusions

A molecular recognition event in the liquid phase, cannot be automatically transferred to vapour and gas sensing on silicon surfaces. In this Chapter the complexation capability of a monolayer of QxCav on Silicon (100) surface towards trifluorotoluene was proved by XPS analysis. Moreover a decorate silicon surface with a specific chemical warfare agents receptor was made but XPS analysis did not prove its complexation ability.

5.4 Experimental section

General metod: All commercial reagents were ACS grade. All solvents were dried over 3 Å and 4 Å molecular sieves. ^{1}H NMR spectra were recorded on a Brucker Avance 300 MHz spectrometer at 300 K and all chemical shifts were reported in parts per million (ppm) in relation to the proton resonances resulting from incomplete deuteration of the NMR solvents. Electrospray ionisation mass spectrometry (ESI-MS) experiments were performed on a Waters ZMD spectrometer equipped with an electrospray interface. Column chromatography was performed using silica gel 60 (Merck 70-230 mesh) as stationary phase. The preparation of QxCav **4** is reported in Chapter 3.

Resorcinarene 1. To a stirred solution of resorcinarene (R:$C_{10}H_{19}$) (5.00 g, 4.80 mmol) in 30 mL of dry DMF, bromochloromethane (765 µL, 12.0 mmol) and potassium carbonate (3.31 g, 24.0 mmol) were added. The reaction mixture was stirred for 16h at 70°C and then quenched in acidic water. The resulting precipitate obtained was filtered and dissolved in dichloromethane: the organic solution was washed to neutrality and then the solvent was removed under vacuum. Purification by column chromatography using Hexane/Ethyl Acetate (8:2 v/v) as eluant afforded compound **1** (671 mg, 16%).
^{1}H NMR ($CDCl_3$, 300 MHz): δ= 7.08 (s, 2H, ArH_d), 7.02 (s, 2H, ArH_d), 6.50 (s, 2H, ArH_u), 6.42 (s, 2H, ArH_u), 5.81-5.63 (m, 7H, CH_{out} + CH=CH_2), 4.95-4.85 (m, 8H, CH=CH_2), 4.67-4.57 (m, 3H, CH_{in}), 4.40 (d, 2H, C$H_{in,}$ J=7.0 Hz), 4.30 (d, 1H, C$H_{in,}$ J=7.0 Hz), 4.23 (t, 1H, CH, J=8.0 Hz), 2.24 (m, 8H, -CH_2CH=CH_2), 2.04 (m, 8H, -CH_2CHAr$_2$), 1.30 (m, 48H, -CH_2-); **ESI-MS** *m/z* (%): 1100 [M+Na$^+$, 100].

EsCav 2-in and 3-out. To a stirred solution of tri-bridged resorcinarene **1** (670 mg, 0.62 mmol) and methyl dichloroacetate (0.25 mL, 2.4 mmol) in 20 mL of dry DMF, DBU (372 µL, 2.5 mmol) was added dropwise. The mixture was heated at 80°C for 6h and then quenched in acidic water. The precipitate obtained was filtered and washed to neutrality. Purification by column chromatography using CH_2Cl_2/Hexane (8:2 v/v) as eluant afforded **2-in** (R_f=0.3, 229 mg, 31%) and **3-out** (R_f=0.4, 294 mg, 40%) as white solids.

3-out

^{1}H NMR ($CDCl_3$, 300 MHz): δ= 7.10 (s, 2H, ArH_d), 7.08 (s, 2H, ArH_d), 6.56 (s, 2H, ArH_u), 6.46 (s, 2H, ArH_u), 5.87-5.72 (m, 7H, CH_{out} + CH=CH_2), 5.01-4.94 (m, 8H, CH=CH_2), 4.78 (s, 1H, CHCOOCH_3), 4.73 (m, 4H, CH), 4.41 (d, 3H, C$H_{in,}$ J=6.9 Hz), 3.86 (s, 3H, CHCOOCH_3), 2.23 (m, 8H, -CH_2CH=CH_2), 2.03 (m, 8H, -CH_2CHAr_2), 1.31 (m, 48H, -CH_2-); **ESI-MS** *m/z* (%): 1185 [M+K^+, 100], 1170 [M+Na^+, 50].

2-in

^{1}H NMR ($CDCl_3$, 300 MHz): δ= 7.10 (s, 2H, ArH_d), 7.07 (s, 2H, ArH_d), 6.49 (s, 2H, ArH_u), 6.45 (s, 2H, ArH_u), 6.08 (s, 1H, CHCOOCH_3), 5.87-5.75 (m, 5H, CH_{out} + CH=CH_2), 5.68 (d, 2H, CH_{out}, J=7.0 Hz), 5.01-4.91 (m, 8H, CH=CH_2), 4.74-4.39 (m, 4H, CH+CH_{in}), 4.37 (d, 2H, CH_{in}, J=6.9 Hz), 3.42 (s, 3H, CHCOOCH_3), 2.24 (m, 8H, -CH_2CH=CH_2), 2.03 (m, 8H, -CH_2CHAr_2), 1.30 (m, 48H, -CH_2-); **ESI-MS** *m/z* (%): 1185 [M+K^+, 100], 1170 [M+Na^+, 50].

Hydrolysis of 3-out on silicon. A surface decorated with EsCav **3-out** was placed in a solution of 250 mM of potassium tert-butoxide in DMSO for 20 minutes at room temperature, then washed with CH_2Cl_2.

Monolayer Preparation. Various cavitand/1-octene mixtures with the following cavitand mole fractions 1.0, 0.5 and 0.2 were dissolved in mesitylene (solution concentration = 0.05 M), for grafting of pure and mixed monolayers. A total of 2.0 mL of cavitand solution was placed in a quartz cell and was deoxygenated by stirring in a dry box for at least 1 h. Subsequently, a Si(100) substrate was etched in 2.5% hydrofluoric acid for 2 min. and immediately placed in the solution. The cell remained under UV irradiation (254 nm) for two hours. The sample was then removed from the solution and sonicated in dichloromethane for 10 min.

Monolayer Characterization. The XPS spectra were run with a PHI multi-technique ESCA-Auger spectrometer equipped with a monochromated Al Kα X-ray source. The analyses were carried out at various photoelectron angles (relative to the sample surface) in the 10°-80° range with an acceptance angle of $\pm$7°. XPS binding energy (BE) scale was calibrated by centering the C 1s peak due to the hydrocarbon moieties at 285.0 eV.[10]

5.5 References and notes

[1] G. F. Cerofolini, G. Ferla *J. Nanopart. Res*. **2002**, *4*, 185-191.
[2] J. M. Buriak *Chem Rev.* **2002**, *102*, 1271-1308.
[3] D. J. Cram, J. M. Cram *Container Molecules and Their Guests* **1994**, RSC, Cambridge; L. Trembleau, J. Rebek *Science* **2003**, *301*, 1291-1220.
[4] J. Snopek, E. Stolkova-Keuemansova, T. Cserhati, K.N. Gahn, A. Stalcup *Comprehensive Supramolecular Chemistry Vol.3:Cyclodextrins* **1996**, Szejtli.
[5] C. D. Gutsche *Calixarenes* **1989**, RSC, Cambridge UK.
[6] C. G. Condorelli, A. Motta, M. Favazza, I. L. Fragalà, M. Busi, E. Menozzi, E. Dalcanale, L. Cristofolini *Langmuir* **2006**, *22*, 11126-11133.
[7] S. M. Daly, M. Grassi, D. K. Shenoy, F. Ugozzoli, E. Dalcanale *J. Mater. Chem.* **2007**, *17*, 1809-1818.
[8] G. F. Cerofolini, C. Galati, S. Lorenti, L. Renna, O. Viscuso, C. Bongiorno, V. Ranieri, C. Spinella, G. G. Condorelli, I. L. Fragalà. L. Terrasi *Appl. Phys. A* **2003**, *77*, 403-409; J. A. Haber, N. S. Lewis *J. Phys. Chem. B* **2002**, *106*, 3639-3656.
[9] G. F. Cerofolini, C. Galati, S. Reina, L. Renna, O. Viscuso, G. Condorelli, I. L. Fragalà *Mater. Sci. Eng. C* **2003**, *23*, 989-994; G. F. Cerofolini, C. Galati, S. Reina, L. Renna *Mater. Sci. Eng. C* **2003**, *23*, 253-257;G. G. Condorelli, A. Motta, I. L. Fragalà, F. Giannazzo, V. Raineri, A. Caneschi, D. Gatteschi *Angew. Chem. Int. Ed.* **2004**, *43*, 4081-4084; D. Briggs *Pratical Surfaces Analysis 2nd ed.* **1995**, WILWY-VCH, Weinheim, Germany; G. Beamson, D. Briggs *High Resolution XPS of Organic Polymers* **1992**, The Scienta ESCA300 Database Wiley & Sons.
[10] I. L. Swift *Surf. Interface Anal.* **1982**, *4*, 47-51; D. Brigg, G. Beamson *Anal. Chem* **1992**, *64*, 1729-1736.

Synthesis of partially-bridged phosphonate and thiophosphonate resorcinarenes[⊗]

6

6.1 Introduction

Cavitands are particularly attractive as host molecules owing to the wide choice of suitable bridging groups. In fact, the appropriate structural preorganization of the host in combination with the appropriate set of complementary binding sites leads to the formation of highly stable complexes with neutral and charged guests[1]. The most common bridging groups employed for cavitands are alkylenedioxy[2] and derivatives[3], dialkylsilicon[4], heterophenylene[5] and phosphoryl[6]. In particular, phosphoryl derivatives are able to form strong complexes with cationic guests, such as metal ions[7], alkali metal and ammonium cations[8] and are efficient hydrogen bond acceptors in the complexation of alcohols[9]. Owing to their high binding capabilities, P=O groups have been included in preorganized structures to increase the stability of the complexes thus formed. Dutasta and co-workers reported the synthesis and the study of the binding properties of tetrabridged phosphonated cavitands having all the inward configuration of the P=O groups[10]. To ensure

[⊗] The content of this Chapter has been published in *Supramolecular Chemistry* **2008** in press.

strong binding, the P=O groups must be oriented towards the cavity (indicated as (iiii)).

Partially-bridged thiophosphonate and phosphonate resorcinarenes (Figure 6.1) are attractive molecules as intermediates in the preparation of preorganized and multidentate cavitand ligands.

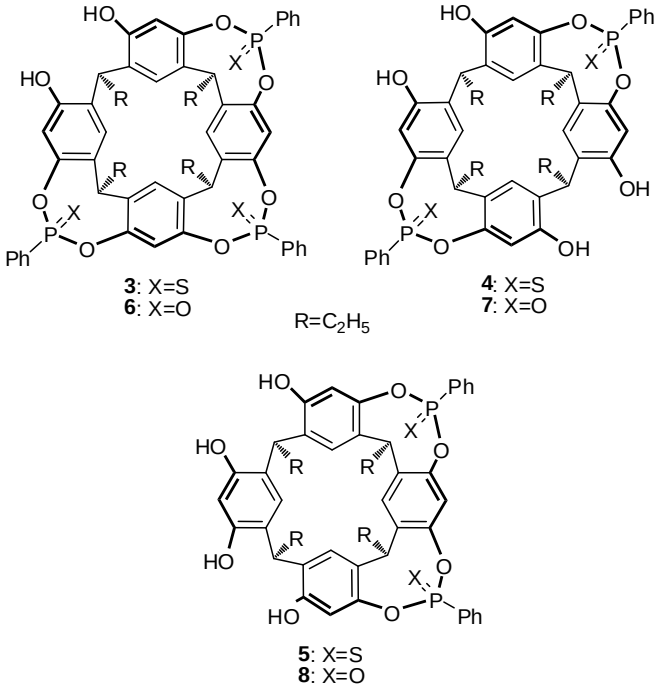

Figure 6.1. Partially-bridged thiophosphonate and phosphonate resorcinarenes: tri- and di-substituted molecules.

In particular, we are interested in AC-disubstituted resorcinarenes **4** and **7** for their potential use as ligand precursors in the self-assembly of coordination cages capable of molecular recognition. A synthetic study of these partially bridged building blocks is presented herein as well as the X-ray crystallographic investigation of the AC-dithiophosphonated resorcinarene **4**.

6.2 Results and discussion

6.2.1 Synthesis of resorcinarenes bearing two and three P=X (X=S,O) bridges at the upper rim

The starting cavitand **1** (Scheme 6.1) was prepared in good yields according to the protocols reported in the literature[7] starting from the ethyl-footed resorcinarene. Briefly, 4.05 equivalents of dichlorophenylphosphine were added to the resorcinarene solution under basic conditions to give a tetraphosphonito cavitand. The intermediate was treated with sulphur to obtain the desired tetraphosphonate cavitand **1**. This synthetic procedure allows the formation of the (iiii) stereoisomer with the four P=S groups oriented towards the molecular cavity as the major product. In order to synthesize partially bridged thiophosphonate resorcinarenes, we performed the same protocol reducing the amount of bridging agent. When 2.8 equivalents of dichlorophenylphosphine were used, cavitand **1** was obtained as the major product in low yield (14%), while the tribridged compound **3** was also formed (6%) and only traces of the AC- and AB-dibridged resorcinarenes were found (**4** and **5**). Other attempts to obtain one of the partially bridged resorcinarene in higher yields by varying the stoichiometric amount of phosphine derivative were unsuccessful. Therefore, this approach proved to be inadequate for the preparation of suitable amounts of partially bridged resorcinarenes.

A novel approach for the selective excision of one and two quinoxaline units from the tetraquinoxaline cavitand has been developed by Gutierrez-Tunstad and co-workers[11]. After the treatment of tetraquinoxaline cavitand with 1,2-dihydroxybenzene under basic conditions, they reported a overall yield of approximately 56% for triquinoxaline resorcinarene and approximately 48% for AC-diquinoxaline resorcinarene. The AB-diquinoxaline isomer was obtained in a maximum yield of 11%. Following this approach, we investigated the behavior of (iiii) tetrathiophosphonate cavitand in the presence of 1,2-dihydroxybenzene under basic conditions.

In order to prepare the (iii) trisubstituted resorcinarene **3**, the (iiii) tetrathiophosphonate cavitand **1** was reacted with **1** equivalent of 1,2-dihydroxybenzene in the presence of K_2CO_3 as base (Scheme 6.1).

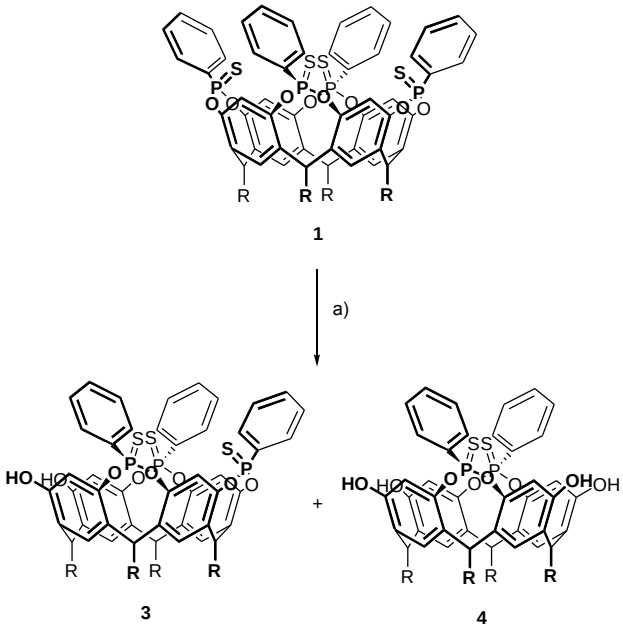

Scheme 6.1. Preparation of the (iii) tri- and the (ii) AC-dithiophosphorylated resorcinarenes. (a) 1,2-Dihydroxybenzene, K_2CO_3, dry DMF, 80°C, 5 h.

Under these conditions, we obtained (iii) trithiophosphonated resorcinarene **3** as the major product in a yield of 52%. When 2 equivalents of 1,2-dihydroxybenzene were added to the reaction, a mixture of the (iii) trithiophosphonated resorcinarene **3** (21%), the (ii) AC dithiophosphonated isomer **4** (28%) and only traces of the (ii) AB-dithiophosphonated isomer **5** were isolated. Higher yields of the desired product **4** were not achieved when the amounts of 1,2-dihydroxybenzene was increased. Moreover, during the reaction, the stereochemistry of the residual P=S groups did not change. Therefore, this synthetic route allows a good control of the product distribution between the dibridged resorcinarenes without altering the P=S stereochemistry.

The stability of phosphonate derivatives was also investigated under basic conditions in the presence of 1,2-dihydroxybenzene. Tetraphosphonate cavitand **2** is readily available following Dutasta's synthetic procedure[10]. In analogy to (iiii) tetrathiophosphonate cavitand **1**, the treatment of compound **2** with 1,2-dihydroxybenzene and K_2CO_3 in DMF led to the abstraction of a variable number of P=O bridges depending on the number of equivalents of nucleophile used (Scheme 6.2).

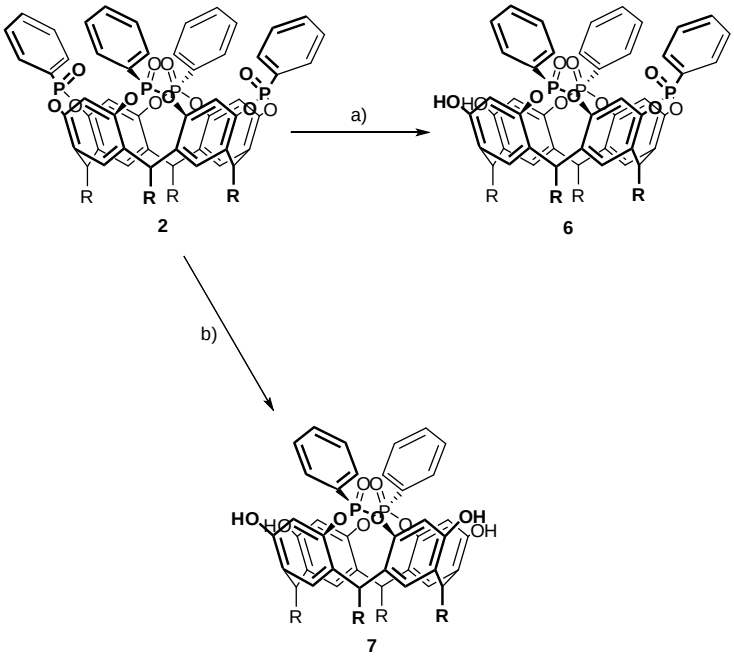

Scheme 6.2. Abstraction of one or two phosphoryl bridges from the tetraphosphonate cavitand **2**. (a) 1 eq. 1,2-dihydroxybenzene, K_2CO_3, dry DMF, 80°C, 5 h. (b) 2 eq. 1,2-dihydroxybenzene, K_2CO_3, dry DMF, 80°C, 5 h.

When 1 equivalent of 1,2-dihydroxybenzene was added to a mixture of cavitand **2** and K_2CO_3 in DMF, the (iii) triphosphonate resorcinarene **6** was obtained in good yields (65%). Under these conditions, a small amount of the (ii) AC-diphosphonate isomer **7** was isolated, but neither the corresponding (ii) AB isomer nor the starting compound were observed. Similarly, when 2 equivalents of 1,2-dihydroxybenzene were used, we obtained the (ii) AC-diphosphonate isomer **7** as the major product (62% yields) without the presence of the (ii) AB diphosphonate isomer **8**.

In comparison with (iiii) tetrathiophosphonate cavitand **1**, the selective excision of one or two phosphonate groups from (iiii) tetraphosphonate cavitand **2** is more sensitive to the amount of nucleophile used. In particular, the reaction of 2 equivalents of 1,2-dihydroxybenzene with (iiii) tetrathiophosphonate cavitand **1** leads to the formation of similar amount of (ii) and (iii) resorcinarenes, whereas that with (iiii) tetraphosphonate cavitand **2** produces exclusively the AC isomer. Also in this case, the nucleophilic attack of 1,2-dihydroxybenzene to the P=O bridges does not change the

stereochemistry of the remaining bridges. This last aspect is crucial to retain the recognition properties in the partially bridged resorcinarenes bearing P=O groups.

6.2.2 X-RAY CRYSTALLOGRAPHIC INVESTIGATION

The stereochemistry of the [ii] AC-disubstituted isomer has been confirmed also by the X-ray crystal structure of resorcinarene **4** (Figures 6.2 and 6.3)[12].

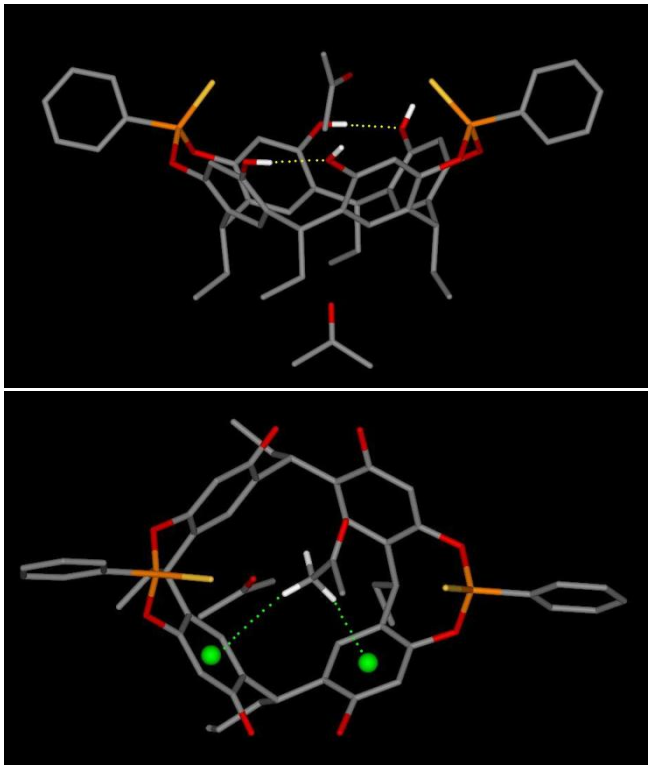

Figure 6.2. Molecular structure of resorcinarene **A** showing the intramolecular hydrogen bonds as yellow dotted lines (above) and the CH-π interactions as green dotted lines (below; only the hydrogens involved in the interactions are shown). Color code: carbon, grey; hydrogen, white; oxygen, red; phosphorus, orange; sulphur, yellow.

Crystals of **4** were obtained by slow evaporation of a solution of **4** in acetone. Compound **4** crystallizes in the space group P21/n as two independent resorcinarenes **A** and **B**. The structure of each resorcinarene shows indeed the presence of two P=S groups pointing inside the cavity and of four C_2H_5 chains at the lower rim. The cavity is stabilized by a network of intramolecular O-H···O hydrogen bonds among the OH groups on the phenyl rings at the upper rim, with the O···O distances spanning from 2.691(3) to 2.784(3) Å and the O-H···O angles going from 167.2(2)° to 175.2(2)°. Each resorcinarene crystallizes with two acetone molecules, one dispersed in the lattice and one with a CH_3 group inside the cavity, giving rise to two weak CH···π interactions (resorcinarene **A**: C···centroid distances of 3.061(2) and 3.294(3) Å, with C-H···centroid angles of 147.6(4)° and 147.6(3)° respectively; resorcinarene **B**: distances of 3.001(2) and 3.105(3) Å, with angles of 157.5(2)° and 143.1(4)° respectively, Figure 6.2).

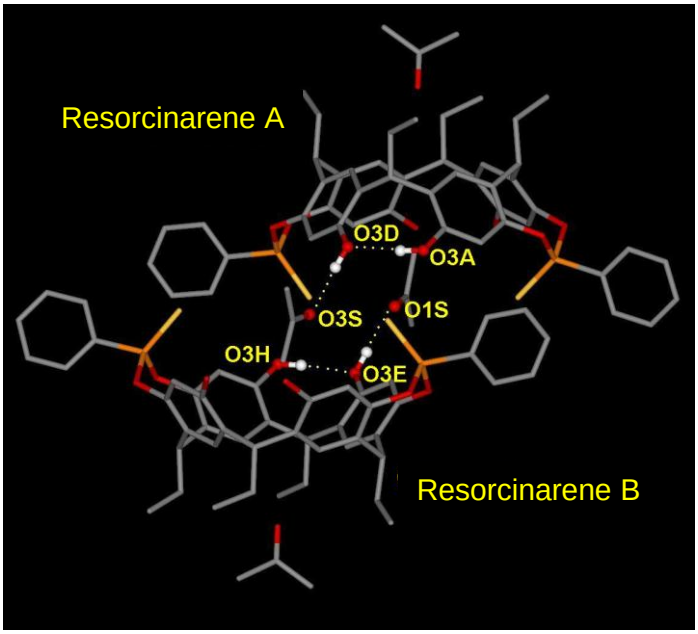

Figure 6.3. The dimer formed by resorcinarene **A** and **B** through a network of hydrogen bonds involving the acetone guests. Colour code: carbon, grey; hydrogen, white; oxygen, red; phosphorus, orange; sulphur, yellow.

In the lattice the resorcinarenes **A** and **B** face each other to give a supramolecular dimer stabilized by a network of hydrogen bonds involving the

acetone molecules inside the cavity and the OH groups at the upper rim [O3D O3S 2.675(3) Å, O3D-H3D O3S 168.8(2)°; O3E O1S 2.695(3) Å, O3E-H3E O1S 166.1(2)°] (Figure 6.3).

6.3 Conclusions

An effective protocol for the preparation of partially bridged thiophosphonate and phosphonate resorcinarenes is reported. Different amounts of 1,2-dihydroxybenzene were used to perform the abstraction of one or two P=X (X = S, O) bridges from the corresponding tetrabridged cavitands in good yields. This synthetic route allowed a good control of the product distribution producing mainly the (ii) AC-dibridged isomer and the (iii) trisubstituted resorcinarene. Moreover, during the excision of the P=X groups, the configuration of the remaining P=X (X = S, O) bridges on the molecules is retained. These compounds are useful precursors for the preparation of differently functionalized cavitands having specific molecular recognition properties[13].

6.4 Acknowledgments

We are grateful to Francesca Boccini, Carlo Nicosia, Barbara Cantadori and Chiara Massera for the precious help.

6.5 Experimental section

General method: All commercial reagents were ACS grade. All solvents were dried over 3 Å and 4 Å molecular sieves. ^{1}H NMR spectra were recorded on a Bruker Avance 300 MHz spectrometer at 300 K and all chemical shifts were reported in parts per million (ppm) in relation to the proton resonances resulting from incomplete deuteration of the NMR solvents. ^{31}P NMR spectra were recorded on a Bruker 162 MHz spectrometer and all chemical shifts were reported in ppm relative to external 85% H_3PO_4 at 0.00 ppm. Electrospray ionization mass spectrometry (ESI-MS) experiments were performed on a Waters ZMD spectrometer equipped with an electrospray interface. Column chromatography was performed using silica gel 60 (Merck 70-230 mesh) as stationary phase. Cavitands **1**[7] and **2**[10] were prepared according to the protocols reported in literature.

[iii] trithiophosphonated resorcinarene (3) and the [ii] AC-dithiophosphonated resorcinarene (4): A mixture of cavitand **1** (0.500 g, 0.43 mmol), K_2CO_3 (0.599 g, 4.34 mmol), and freshly recrystallized 1,2-dihydroxybenzene (0.095 g, 0.87 mmol) in 10 ml of dry DMF was stirred in a sealed tube at 80 °C for 5 h. The reaction mixture was then cooled and poured into ice-cold brine. The solid formed was then filtered, washed with water, and dried. The crude product was purified by column chromatography (SiO_2; CH_2Cl_2/ethyl acetate = 95/5) to give **3** in a 21% yield (0.095 g, 0.09 mmol) followed by **4** in a 28% yield (0.108 g, 0.12 mmol).

Resorcinarene 3

^{1}H NMR ($CDCl_3$, 300 MHz): δ= 8.17 (m, 6H, P-Ar*H*), 7.55 (m, 9H, P-Ar*H*), 7.32 (s, 2H, ArH_{down}), 7.20 (s, 2H, ArH_{down}), 6.68 (d, 2H, ArH_{up}, $^{4}J_{HP}$ = 2.2 Hz), 6.49 (s, 2H, ArH_{up}), 4.60 (m, 3H, ArC*H*), 4.29 (t, 1H, ArC*H*, J= 7.9 Hz), 2.40-2.23 (m, 8H, ArCH-CH_2), 1.09-0.91 (m, 12H, CH_2CH_3); **ESI-MS**: m/z 1037 $[M+Na]^+$; methanol.

Resorcinarene 4

^{1}H NMR (Acetone-d_6, 300 MHz): δ= 8.22 (dd , 4H, P-Ar*H*, $^{3}J_{PH}$ = 14.8 Hz, J_{HH} = 6.9 Hz), 7.78 (s, 4H, ArH_{down})**,** 7.75 (m, 2H, P-Ar*H*), 7.67 (m, 4H, P-Ar*H*), 6.44 (s, 4H, ArH_{up}, $^{4}J_{HP}$ = 2.2 Hz), 4.63 (t, 2H, ArC*H***,** J= 8.1 Hz), 4.34 (t, 2H, ArC*H***,** J= 8.0 Hz), 2.51 (m, 4H, ArCH-CH_2), 2.40 (m, 4H, ArCH-CH_2), 1.05 (t, 6H, CH_2CH_3, J= 7.2 Hz), 0.92 (t, 6H, CH_2CH_3, J= 7.2 Hz); **^{31}P NMR** ($CDCl_3$, 162 MHz): δ 81.2 (s, 2P); **ESI-MS**: m/z 877 $[M+H]^+$,899 $[M+Na]^+$; acetone.

Crystal structure determination of compound 4

The molecular structure of compound $C_{48}H_{46}O_8S_2P_2{\cdot}2C_3H_6O$ **4** was determined by single-crystal X-ray diffraction methods. Crystallographic and experimental details are summarized in Table 5.1.

	Resorcinarene **4**
Formula	$C_{54}H_{58}O_{10}P_2S_2$
Formula weight	993.06
Crystal system	Monoclinic
Space group	*P21/n*
a/Å	11.611(1)
b/Å	50.654(5)
c/Å	17.557(2)
β/°	97.519(1)
V/Å^3	10237(2)
Z	8
D_c/g cm^{-3}	1.289
F(000)	4192
μ/mm^{-1}	0.224
$\theta_{min,max}$/°	2.83, 26.84
Reflections collected	83251
Independent reflections	19682 (*R*int = 0.0389)
Obs. refl. [Fo>4σ(Fo)]	14100
Data / restr. / param	19682 / 0 / 1255
R indeces [Fo>4σ(Fo)][a]	R1 = 0.0558, *w*R2 = 0.1372
R indeces (all data)	R1 = 0.1848, *w*R2 = 0.1481
$\Delta\rho_{min,max}$/e Å^{-3}	-0.311, 0.232
S[b]	1.025

[a] $R_1 = \Sigma \parallel Fo|-|Fc\parallel/\Sigma|Fo|$, $wR_2 = [\Sigma\, w(Fo^2-Fc^2)^2/\, \Sigma wFo^4]^{1/2}$. [b] Goodness-of-fit S = $[\Sigma w(Fo^2-Fc^2)^2/\,(n-p)]^{1/2}$, where *n* is the number of reflections and *p* the number of parameters.

Table 6.1. Crystallographic data and refinement details for resorcinarene **4**.

Intensity data were collected using a Mo Kα radiation on a Bruker AXS Smart 1000 single-crystal diffractometer equipped with a CCD area detector at 293(2) K. The structure was solved by direct methods with the sir97 program[14] and refined on F_0^2 by full-matrix least-squares procedures with the shelxl-97 program[15].The data reduction for **4** was performed using the SAINT[16] and SADABS[17] programs. All the non-hydrogen atoms were refined with anisotropic atomic displacements. The hydrogen atoms were included in the refinement at idealized geometries (C–H 0.95 Å) and refined "riding" on the corresponding parent atoms. The weighting scheme used in the last cycle of refinement was $w = 1/ [\sigma^2 F_o^2 + (0.0695P)^2 + 4.56219P]$. Geometric calculations and molecular graphics were performed with the PARST97 program[18] and the DS ViewerPro 5.0 package. Crystallographic data (excluding structure factors) for the structure reported in this paper have been deposited with the Cambridge Crystallographic Data Centre as supplementary publications no. CCDC-655076. These data can be obtained free of charge at www.ccdc.cam.ac.uk/conts/retrieving.html [or from the Cambridge Crystallographic Data Centre, 12 Union Road, Cambridge CB2 1EZ, UK; Fax: +44-1223/336-033; E-mail:deposit@ccdc.cam.ac.uk].

[iii] triphosphonated resorcinarene (6): 66 mg (0.6 mmol) of freshly recrystallized 1,2-dihydroxybenzene were dissolved in ca. 50 mL of DMF and 828 mg of K_2CO_3 (ca. 10 eq) were added. After the addition of 650 mg (0.6 mmol) of cavitand **2** the reaction mixture was heated to 80 °C and stirred for 5 hours. The reaction mixture was then cooled to room temperature and DMF was completely evaporated in *vacuum*. The solid was dissolved in CH_2Cl_2 and three extractions with acidic water were performed. The final product was purified by silica gel chromatography with CH_2Cl_2–EtOH as eluent (90/10 v/v). The yield of the reaction was 65 % (375 mg).
^{1}H NMR ($CDCl_3$, 300 MHz): δ= 9.56 (bs, 2H, Ar-O*H*), 8.05 (m, 6H, P-Ar*H*), 7.59 (m, 9H, P-Ar*H*), 7.36 (s, 2H, ArH_{down}), 7.17 (s, 2H, ArH_{down}), 6.93 (s, 2H, ArH_{up}), 6.80 (s, 2H, ArH_{up}), 4.60 (m, 3H, ArC*H*), 4.37 (t, 1H, ArC*H***,** J= 7.9 Hz), 2.38 (m, 6H, ArCH-CH_2), 2.26 (m, 2H, ArCH-CH_2), 1.08 (t, 6H, CH_2CH_3, J=7.2 Hz), 1.00 (t, 3H, CH_2CH_3, J=7.2 Hz), 0.94 (t, 3H, CH_2CH_3, J=7.2 Hz); **ESI-MS**: m/z 989 $[M+Na]^+$; methanol.

[ii] AC-diphosphonated resorcinarene (7): K_2CO_3 (0.511 g, 3,69 mmol) and freshly recrystallized 1,2-dihydroxybenzene (0.081 g, 0.74 mmol) were added to a solution of cavitand **2** (0.402 g, 0.37 mmol) in 12 ml of dry DMF. The

reaction mixture was stirred at 80° C for 5 h, cooled at room temperature and then poured into ice-cold brine. The solid formed was filtered, washed with water, and dried. The desired product **7** (183 mg) was collected by filtration in a 62% yield after the treatment of the crude with diethyl ether.
^{1}H NMR ($CDCl_3$, 300 MHz):): δ 7.94 (m, 4H, P-Ar*H*), 7.60 (m, 2H, P-Ar*H*), 7.48 (m, 4H, P-Ar*H*), 7.01 (s, 4H, ArH_{down}), 6.37 (s, 4H, ArH_{up}), 4.40 (t, 2H, ArC*H***,** J= 7.0 Hz), 4.28 (t, 2H, ArC*H***,** J= 7.8 Hz), 2.26 (m, 4H, ArCH-CH_2), 2.17(m, 4H, ArCH-CH_2), 0.96 (t, 6H, CH_2CH_3, J= 6.9 Hz), 0.87 (t, 6H, CH_2CH_3, J= 6.9 Hz); **ESI-MS**: m/z 868 $[M+Na]^+$, 884 $[M+K]^+$; methanol.

6.5 References and notes

[1] D. J. Cram *Angew. Chem. Int. Ed. Engl* **1986**, *98*, 1041.

[2] D. J. Cram, S. Karbach, H. –E. Kim, C. B. Knobler, E. F. Maverich, J. L. Ericson, R. C. Helgeson *J. Am. Chem. Soc.* **1988**, *110*, 2229.

[3] H. Xi, C. L. D. Gibb, E. D. Stevens, B. C. Gibb *Chem Commun* **1998**, 1743.

[4] D. J. Cram, K. D. Stewart, I. Goldberg, K. N. Trueblood *J. Am. Chem. Soc.* **1985**, *107*, 2574; J. A. Tucker, C. B. Knobler, K. N. Trueblood, D. J. Cram *J. Am. Chem. Soc.* **1989**, *111*, 3688.

[5] J. R. Moran, J. L. Ericson, E. Dalcanale, J. A. Bryant, C. B. Knobler, D. J. Cram *J. Am, Chem. Soc.* **1991**, *113*, 5707; D. J. Cram, H. J. Choi, J. A. Bryant, C. B. Knobler *J. Am Chem. Soc.* **1992**, *114*, 7748.

[6] T. Lippmann, H. Wilde, E. Dalcanale, L. Mavilla, G. Mann, U. Heyer, S. Spera *J. Org. Chem.* **1995**, *60*, 235; E. Dalcanale, P. Jacopozzi, F. Ugozzoli, G. Mann *Supramol. Chem* **1998**, *9*, 305.

[7] B. Bibal, B. Tinant, J. -P Declercq, J. –P. Dutasta *Chem Commun* **2002**, 423; B. Bibal, J. -P Declercq, J. –P. Dutasta, B. Tinant, A. –G. Valade *Tetrahedron* **2003**, *59*, 5849.

[8] J. –P. Dutasta *Top. Curr. Chem.* **2004**, *232*, 55.

[9] E. Ventola, P. Vainiotalo, M. Suman, E. Dalcanale *J. Am. Soc. Mass. Spectrom* **2006**, *17*, 213; R. Pinalli, M. Suman, E. Dalcanale *Eur. J. Org. Chem.* **2004**, *3*, 451; M. Suman, M. Freddi, C. Massera, F. Ugozzoli, E. Dalcanale *J. Am. Chem. Soc.* **2003**, *125*, 12068.

[10] P. Delangle, J. –C. Mulatier, B. Tinant, J. –P Declercq, J. –P. Dutasta *Eur. J. Org. Chem.* **2001**, *16*, 3695.

[11] P. Castro, G. Zhao, G. A. Hernandez, L. M. Gutierrez-Tunstad *Organic Letter* **2004**, *6*, 333.

[12] The crystal structure of a AC-diphosphonate resorcinarene with undecyl feet has been reported by Dutasta's group: B. Dubessy, PhD thesis **2006**, École Normale Supériur de Lyon.

[13] L. Pirondini, E. Dalcanale *Chem. Soc. Rev.* **2007**, *36*, 695.

[14] A. Altomare, M.C. Burla, M. Camalli, G. L. Cascarano, C. Giacovazzo, A. Guagliardi, A.G.G Molitemi, G. Polidori, R. Spagna *J. Appl. Crystallogr.* **1999**, *32*, 115.

[15] G.M. Sheldrick *SHELXL97* **1997**. Program of Crystal Structure Refinement, Göttinghen, Germany.

[16] *SAINT, Software Users Guide 6.0* **1999**, Bruker Analytical X-ray System.

[17] G.M. Sheldrick *SADABS Area-Detector Adsorption Correction 2.03*, Göttinghen, Germany.

[18] M. Nardelli *J. Appl. Crystallogr* **1996**, *29*, 296.

7 Crystallographic description of solvent inclusion in cavitands via CH-π interactions

7.1 Introduction

Crystal structure determination represents one of the most powerful tools to understand host-guest interactions.[1] Type, number, geometry and synergy of weak interactions can be evaluated in the solid state by X-Ray crystallography. This is particularly true for very weak interactions like CH-π interactions, which are very difficult to be detected in solution, and which play an important role in supramolecular chemistry. Structural evidences for these contacts are increasing in the literature; in a recent review[2] Prof. Nishio has underlined the importance of the statistical analysis of the crystallographic data contained in the Cambridge Structural Database, to fully understand the nature of these bonds.

Another important issue which can be inferred from crystal structure determination is the orientation of a given guest within the host cavity, particularly when multiple options are possible.

In the present Chapter we hence report two examples of cavitand-guest complexes in the solid state where the above mentioned situations have been addressed. Resorcinarene-based cavitands are extremely versatile molecules for guest inclusion[3]; they provide an open rigid cavity which combines a

permanent free volume with a π-basicity. Moreover the oxygen atoms at the upper rim are also possible sites for hydrogen bonds when a suitable guest is present.

7.2 Results and Discussion

7.2.1 Crystal structure of compounds 1 and 2

Two tetramethylene bridged cavitands differently functionalized at the upper and lower rim have been dissolved in ethyl acetate and acetone respectively, to yield crystals suitable for X-Ray analysis.

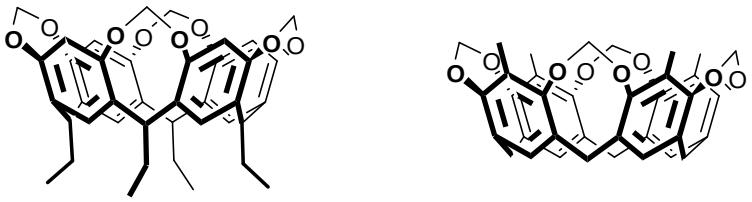

Figure 7.1. Molecular structure of cavitand **1** (left) and **2** (right).

Compound **1** consists of a 1:1 cavitand:ethyl acetate complex which crystallizes in the space group Pnma. Only half of the cavitand is independent and the other half is generated by the mirror plane which contains the solvent molecule. The ethyl acetate points with the CH_3 of the ethyl group inside the cavity forming three CH-π interactions, which are equally distributed over two different orientations related to each other by the mirror plane, giving rise to an entropically favoured situation [C-H···centroid distances of 2.740(3), 2.847(2) and 2.910(2) Å and C-H···centroid angles of 170.2(2), 143.3(4) and 138.3(4)° respectively, see Figure 7.2(a)].
The oxygen atom of the CH_3CH_2O group is involved in a weak interaction with two symmetry-related H atoms belonging to two methylene groups at the upper rim [C-H···O 2.794(2) Å, C-H···O, 156.4(2)°]. These weak interaction are

probably sterically favoured by the fact that the acetate molecule enters the cavity with the methyl group of the ester instead that with the other CH_3 (which could be expected in view of the higher acidity of its hydrogen atoms).

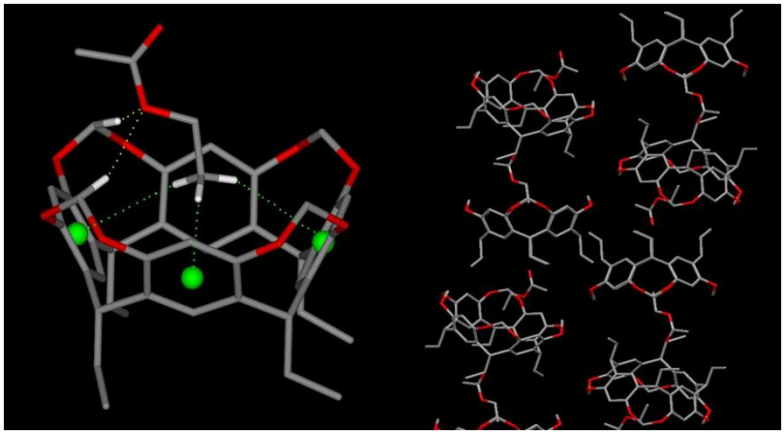

(a) **(b)**

Figure 7.2. (a) Molecular structure of **1** showing the oxygen-hydrogen interactions as yellow dotted lines and the CH-π interactions as green dotted lines (only one of the two symmetry-related orientations is shown). Hydrogens atoms are omitted for clarity with the exceptions of those involved in the interactions. Color code: carbon, grey; hydrogen, white; oxygen, red; centroid, green. (b) Crystal packing along the a axis.

The crystal packing shows that the cavitands are roughly piled in channels along the a axis, so that the ethylic CH_3 of the solvent forms CH-π interactions with one cavity and the oxygen of the C=O moiety at the other end interacts with the phenylic hydrogens of an adjacent cavitand. The asymmetric unit of compound **2** consists of two tetra-methylene-bridged cavitands and three acetone molecules, one of which is included in one of the two cavitands, while the other two fill the empty spaces in the crystal lattice (see Figure 7.3 (a)). Also here the inclusion of the solvent shows a pattern similar to the situation found for compound **1**.

The acetone molecule points with one methyl group inside the cavity giving rise to three CH-π interactions [C-H···centroid distances of 2.853(8), 2.952(7) and 2.967(7) Å and C-H···centroid angles of 170.5(2), 131.4(3) and 135.3(5)° respectively, see Figure 7.3 (b)]. At the same time the oxygen atom is involved in a weak hydrogen bond with the H atom belonging to a methylene group at the upper rim [C-H···O 2.629(7) Å, C-H···O, 168.2(5)°]. The crystal lattice is further stabilized by the presence of various O···C-H interactions.

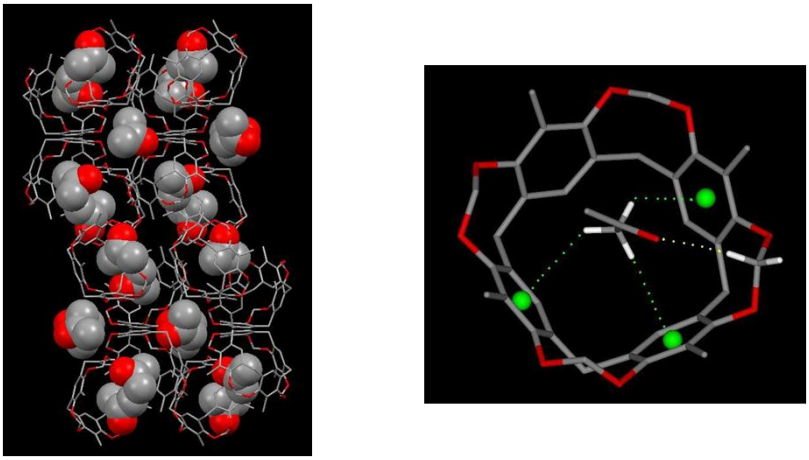

(a) (b)

Figure 7.3. (a) crystal lattice of compound **2**. (b) Molecular structure showing the intramolecular hydrogen bond as yellow dotted line and the CH-π interactions as green dotted lines (only the hydrogens involved in the interactions are shown). Color code: carbon, grey; hydrogen, white; oxygen, red; centroid, green.

7.3 Conclusions

The crystal structures of the complexes **1** and **2** here reported are a further example of the importance of the weak CH-π interactions in supramolecular chemistry, especially when cooperativity and entropic stabilization come into play. Moreover, they confirm the ability displayed by resorcinarene cavitands of acting as host for small molecules. The presence of a rigid π-basic cavity and the various possible functionalizations at the upper rim are important parameters to selectively tune the inclusion properties of these compounds, as demonstrated by previous work in our group.[4]

7.4 Acknowledgments

We are grateful to Chiara Massera for the X-ray analysis.

7.5 Experimental Section

General method: All commercial reagents were ACS reagent grade and use as received. All solvents were dried over 3Å molecular sieves. ^{1}H NMR spectra were recorded on Bruker AVANCE (300 MHz) spectrometer and all chemical shift (δ) were reported in parts per million (ppm) relative to the proton resonances resulting from incomplete deuteration of the NMR solvents. Electrospray ionization (ESI)-MS experiments were performed on a Waters ZMD spectrometer equipped with an electrospray interface. Column chromatography was performed using silica gel 60 (Merck 70-230 mesh). Resorcinarenes (R:C_2H_5[5]and R:H[6]) and cavitand **2**[7] were prepared according to literature procedures.

Cavitand 1. K_2CO_3 (11.06 g, 80·mmol) and CH_2Br_2 (2.0 mL, 36·mmol) were added, under nitrogen, to a solution of resorcinarene (R: C_2H_5) (3.0 g, 5·mmol) in 20 mL of dry DMSO. The purple mixture was stirred in a sealed tube at 90°C for 3 hours. The reaction was quenched by addition 10 % $HCl_{(aq)}$ solution and the resulting mixture was extracted with CH_2Cl_2. The organic layer was washed with water (3 x 15 mL), dried on Na_2SO_4 and evaporated. The crude product was purified by column chromatography on silica gel by using hexane/ethyl acetate (6:4 v/v) as eluant to give cavitand **1** as dark yellow solid (2.85 g, 88 %). ^{1}H NMR (300 MHz, $CDCl_3$): δ= 1.00 (t, 12H, *CH*$_3$); 2.27 (m, 8H, CH*CH*$_2$CH$_3$); 4.44 (d, 4H, C*H*$_{in}$, J=7.2 Hz); 4.67 (t, 4H, C*H*Ar$_2$, J=8.1 Hz); 5.74 (d, 4H, C*H*$_{out}$, J=7.2 Hz); 6.49 (s, 4H, Ar*H*); 7.11 (s, 4H, Ar*H*); ESI-MS: *m/z* (%): 671 [M+Na$^+$,100], 637 [MH$^+$, 80].

X-RAY CRYSTALLOGRAPHIC ANALYSIS AND DATA COLLECTION.

The molecular structure of compounds **1** and **2** was determined by single-crystal X-ray diffraction methods. Crystallographic and experimental details are summarized in Table **z**. Intensity data were collected at room temperature using a Mo K□radiation on a Bruker AXS Smart 1000 diffractometer, equipped with a CCD area detector (**1**) and on a Philips PW 1100 diffractometer (**2**). All the structures were solved by direct methods using the sir97 program[8] and

refined on F_0^2 by full-matrix least-squares procedures, using the shelxl-97 program[9]. The data reduction for **1** was performed using the SAINT[10] and SADABS[11] programs. Intensity data for **2** were corrected for Lorenz and polarization, but not for absorption. All the non-hydrogen atoms were refined with anisotropic atomic displacements, with the exclusion of one methyl group of the acetate molecule in **1** and of the acetone molecules in **2**.

	1	**2**
Formula	$C_{44}H_{48}O_{10}$	$C_{81}H_{82}O_{19}$
Formula weight	736.86	1359.52
Crystal system	Orthorhombic	Orthorhombic
Space group	*Pnma*	*Pbca*
a/Å	18.093(9)	20.502(5)
b/Å	18.955(9)	38.647(5)
c/Å	10.797(9)	17.722(5)
V/Å^3	3703(4)	14042(6)
Z	4	8
D_c/g cm^{-3}	1.322	1.286
F(000)	1568	5760
μ/mm^{-1}	0.093	0.091
$\theta_{min,max}$/°	2.15 - 225.19	3.04 - 26.01
Reflections collected	17031	13723
Independent reflections	3387 (*R*int = 0.0902)	13723 [R(int) = 0.0]
Obs. refl. [Fo>4σ(Fo)]	1846	2804
Data / restr. / param	3387 / 0 / 266	13723 / 4 / 858
R indeces [Fo>4σ(Fo)][a]	R1 = 0.0501, *w*R2 = 0.1144	R1 = 0.0856, wR2 = 0.0860
R indeces (all data)	R1 = 0.1037, *w*R2 = 0.1291	R1 = 0.3836, wR2 = 0.1189
$\Delta\rho_{min,max}$/e Å^{-3}	-0.355, 0.379	-0.351, 0.579
S[b]	1.007	0.996

[a] $R_1 = \Sigma \parallel Fo|-|Fc\parallel/\Sigma|Fo|$, $wR_2 = [\Sigma\, w(Fo^2-Fc^2)^2/\, \Sigma wFo^4]^{1/2}$. [b] Goodness-of-fit $S = [\Sigma w(Fo^2-Fc^2)^2/\,(n-p)]^{1/2}$, where *n* is the number of reflections and *p* the number of parameters.

The hydrogen atoms were included in the refinement at idealized geometries (C–H 0.95 Å) and refined "riding" on the corresponding parent atoms. The weighting scheme used in the last cycle of refinement was $w = 1/ [\sigma^2 F_o^2 + (0.0513P)^2]$ and $w = 1/ [\sigma^2 F_o^2 + (0.0103P)^2]$, where $P = (F_0^2 + 2F_c^2)/3$, for **1** and **2** respectively. Geometric calculations and molecular graphics were performed with the PARST97 program [12] and the DS ViewerPro 5.0 package. Crystallographic data (excluding structure factors) for the structures reported in this paper have been deposited with the Cambridge Crystallographic Data Centre as supplementary publications no. CCDC-658609 and -658610 for compounds **1** and **2** respectively. These data can be obtained free of charge at www.ccdc.cam.ac.uk/conts/retrieving.html [or from the Cambridge Crystallographic Data Centre, 12 Union Road, Cambridge CB2 1EZ, UK; Fax: +44-1223/336-033; E-mail:deposit@ccdc.cam.ac.uk].

7.6 References and notes

[1] G. R. Desiraju, T. Steiner *In The Weak Hydrogen Bond, IUCr Monographs on Crystallography*, Vol. 9, Oxford University Press, Oxford **1999**.
[2] M. Nishio *CrystEngComm.* **2004**, *6(27)*, 130 and references therein.
[3] D. J. Cram, J. M. Cram *Container Molecules and Their Guests* **1994**, RSC, Cambridge.
[4] L. Pirondini, E. Dalcanale *Chem. Soc. Rev.* **2007**, *36*, 695.
[5] L. Tunstad, J. A. Tucker, E. Dalcanale, J. Weiser, J. A. Bryant, J. C. Sherman, R. C. Helgeson, C. B. Knobler, D. J. Cram *J. Org. Chem.* **1989***, 54*, 1305.
[6] H. Konishi, Y. Iwasaki, T. Okano, J. Kiji *Chem Lett.* **1989**, 1815.
[7] C. Neumann, E. Romàn, C. Peinador, T. Ren, B. O. Patrick, A. E. Kaiser, J. C. Shermann *Chem. Eur. J.* **2001**, *7*, 1637.
[8] A. Altomare, M. C. Burla, M. Camalli, G. L. Cascarano, C. Giacovazzo, A. Guagliardi, A. G. G. Moliterni, G. Polidori, R. Spagna *J. Appl. Crystallogr.* **1999**, *32*, 115.
[9] G. M. Sheldrick *SHELXL97. Program for Crystal Structure Refinement* **1997**, University of Göttingen: Göttingen, Germany.
[10] *SAINT*, Software Users Guide, 6.0; Bruker Analytical X-ray Systems: **1999**.
[11] G. M. Sheldrick SADABS Area-Detector Absorption Correction, 2.03; University of Göttingen: Göttingen, Germany, **1999**.
[12] M. Nardelli *J. Appl. Crystallogr.* **1996**, *29*, 296.

The design, synthesis, and characterization of cavitand based materials for application in chemical sensing and environmental analyses are the main topic of this thesis. The thesis is organized in three main projects: (1) The development of a portable miniaturized system for environmental monitoring of benzene in outdoor air. Using quinoxaline cavitands as preconcentration unit, it is possible to detect benzene at ppb level with MOX sensors. The sensor has shown efficient performances not only in laboratory tests but also in real world measurements. (2) The development of a coating, with molecular recognition ability, for solid phase microextraction fibers (SPME) for aromatic VOCs from aqueous samples. With this coated fibers it is possible to sample and selectively desorb aromatic analytes at ppt level in presence of aliphatic interferents. (3) The design and characterization of highly specific fluorescent molecular receptors for short chain alcohols. The introduction of an appropriate fluorescent probe allows the specific detection of alcohols complexed into the cavity in the solid state.